ABSTRACT

A COMPARISON OF FINITE ELEMENT AND FINITE DIFFERENCE METHODS IN ELASTOSTATIC PROBLEMS

by Nicholas P. Dario

Four objectives of this thesis are: to compare finite element and finite difference solutions to elastostatic problems, to present an apparently different formulation of the Navier equations in finite difference form and to demonstrate their applicability, to formulate and apply the axially symmetric linear strain triangular ring stiffness matrix, and to present solutions for simple composite bodies.

For the sake of completeness, finite element stiffness matrices are derived for plane and axially symmetric problems. Both constant and linearly varying strain triangles are considered. Nodal point forces associated with boundary tractions are treated in detail. The constant and linear strain triangles as well as the constant strain triangular ring have been presented by other authors. The linear strain triangular ring has been mentioned by other writers but has apparently not been specifically presented prior to this. Furthermore, the present author is unaware of earlier published applications of this stiffness matrix.

Finite difference expressions associated with the Navier elasticity equations are derived in a more general form which allows consideration of anisotropic materials. This is done by simply replacing

amannes " atives by 😿 🛚 Missilly of miletentes. unius are : - e Etiliations. mailies. In slatica is to Walet "exact Per is also : en enci. Statute in the itite differe

et finite di: Act analysis:

fifference 35 State trians

stan triang Page aceterits

the for the y the for t

ecutions is b

derivatives by appropriate difference expressions. These are also derived by what is believed to be a different method involving the equilibrium of a material element. Inherent in the procedure is the necessity of making assumptions of the strains in terms of displacement differences. The method has the advantage that static boundary conditions are readily derived as well.

The comparison of the methods is given in terms of specific applications. Both plane stress and axially symmetric examples are included. In each category, a problem with a well-known elasticity solution is treated so that comparisons can also be made with the so-called "exact" solution. An application involving a simple composite body is also presented.

The investigation demonstrates the ability of the finite element and finite difference methods to give equally good results in displacement analysis. Agreement with elasticity solutions is excellent for each method. However, the stresses which result from the finite difference analysis and the finite element analysis using constant strain triangular elements are generally less satisfactory than those obtained in the finite element analysis which employs linearly varying strain triangular elements. This is especially true at boundary points. Displacements in simple composite bodies treated are also very comparable for the various methods. Interfacial stresses, however, were more erratic for the finite element solutions than for the corresponding finite difference solutions. The smoother variation of the difference solutions is believed to be more realistic.

PLEASE NOTE:

Some pages have small and indistinct type. Filmed as received.

University Microfilms

A COMPARISON OF FINITE ELEMENT AND FINITE DIFFERENCE METHODS IN ELASTOSTATIC PROBLEMS

Ву

Nicholas P. Dario

A THESIS

Submitted to
Michigan State University
in partial fulfillment of the requirements
for the degree of

DOCTOR OF PHILOSOPHY

Department of Metallurgy, Mechanics and Materials Science

. t

De Milliage

ATRIVATE DET

.

in vert i

reliter Millig

1148 of 40

Steplainte

Particle

Sur Hackey (c.

East pla

× ...

4-23/3

ACKNOWLEDGEMENT

The numerical work in this thesis was carried out in part at the Michigan State University Computer Center. The balance of the work was performed at General Motors Institute in its Computer Laboratory. The author takes this opportunity to thank these groups for their cooperation in this effort. I am especially indebted to Walter M. Arnston of the GMI Computer Services Department for many hours of assistance in debugging programs written for this research. Special thanks go to Mrs. Janice Walton for her patience in the preparation of numerous sets of tedious data for the computer programs.

Sincere appreciation is extended to Professor William A.

Bradley for suggesting this topic and for his guidance and assistance in all phases of this research.

Finally, I am extremely grateful to Mrs. Frances Abel for many hours of typing in the preparation of this final thesis.

35 C.D. IN FEE 157 1.1. 1.2. 1.3. II. EIXITE 2.3. 2.3. 2.5. 2.6. 2.8. 3.1. 3.2. 3.3. 3.4. 2.5. 3.6.

TABLE OF CONTENTS

	Page
CKNOWLEDGEMENT	. ii
LIST OF TABLES	. v
IST OF FIGURES	. vii
LIST OF SYMBOLS	. xii
INTRODUCTION	. 1
	• •
1.1. Remarks	
1.2. Previous Developments	
1.3. Present Investigation	. 4
II. FINITE DIFFERENCE METHOD	. 6
2.1. General Remarks	. 6
2.2. Differential Equations for Plane Stress	
2.3. Differential Equations for Plane Strain	-
2.4. Differential Equations for Axially Symmetric	
Problems	. 12
2.5. Finite Difference Equations for Plane Stress	. 15
2.6. Finite Difference Equations for Plane Strain	. 18
2.7. Axially Symmetric Finite Difference Equations .	. 19
2.8. Alternate Derivation of Plane Stress Difference	
Equations	
2.9. Alternate Derivation of Axially Symmetric Diffe	
Equations	
2.10. Finite Difference Stresses	. 48
III. FINITE ELEMENT METHOD	. 50
3.1. General Remarks	. 50
3.2. Direct Stiffness Method	. 52
3.3. Constant Strain Triangle	
3.4. Linearly Varying Strain Triangle	
3.5. Constant Strain Triangular Ring	
3.6. Linear Strain Triangular Ring	. 88

D. E18

٠..

A. I.a.

5.2

POINT.

		F	Page
IV.	PLANE S	TRESS APPLICATIONS	95
	4.1.	Cantilever Beam	95
		Elasticity Solution	97
		Finite Difference Solution	98
		CST Solution	101
		LST Solution	L06
		Further Comparisons	109
			121
	4.2.	Composite Plate	L24
		Finite Difference Solution	126
		CST Solution	L33
		LST Solution	L33
		Comparison of Solutions	L43
			L72
٧.	AXIALLY	SYMMETRIC APPLICATIONS	l 7 7
	5.1.	Thick Cylinder	178
		· · · · · · · · · · · · · · · · · · ·	178
			180
		Concluding Remarks	187
	5.2.		187
		•	191
			200
			207
			215
			232
VI.	CONCLUS	IONS AND RECOMMENDATIONS	236
	6.1.	Conclusions	236
	6.2.	Recommendations	237
BIBL	OGRAPHY.		241
APPE	NDIX A.	ADDITIONAL RESULTS	246
APPE	NDIX B.	COMPUTER PROGRAMS	259

ii.e · Bear · is the el kr ٠.;

LIST OF TABLES

Table		Page
4.1	Beam Deflections, 65 Point Configurations	110
4.2	Beam Deflections, 225 Point Configurations	111
4.3	Beam Flexural Stress, 225 Point Configurations	113
4.4	Boundary Flexural Stress, 225 Point Configurations	115
4.5	Beam Shear Stress, 225 Point Configurations	119
4.6	Beam Longitudinal Displacements, 225 Point Configurations	122
4.7	Composite Plate Top Edge v-Displacements	152
4.8	Composite Plate Top Edge u-Displacements	153
4.9	Composite Plate Horizontal Interface v-Displacements	154
4.10	Composite Plate Horizontal Interface u-Displacements	155
4.11	Composite Plate Vertical Symmetry Axis v-Displacements .	156
4.12	Composite Plate Horizontal Interface Stress, $\sigma_{\mathbf{x}}$ (Matrix).	163
4.13	Composite Plate Horizontal Interface Stress, $\sigma_{\mathbf{x}}$ (Stiffener)	164
4.14	Composite Plate Horizontal Interface Stress, $\sigma_{\mathbf{y}}$ (Matrix)	166
4.15	Composite Plate Horizontal Interface Stress, og (Stiffener)	167
4.16	Composite Plate Vertical Interface Stress, og (Matrix)	169
4.17	Composite Plate Vertical Interface Stress, $\sigma_{\mathbf{y}}$ (Stiffener)	170
4.18	Composite Plate Vertical Interface Stress, [†] xy (Matrix)	173

12.5

•.19 (.....)

:: **:**::

:: -...

53 51

i. 1.21

13 1.e.

ia si:

i. a. r.

13 gg

13 - 5 F.

lin lett. the letter

in Em

40 km

labie		Page
4.19	Composite Plate Vertical Interface Stress, τ (Stiffener)	174
5.1	Thick Cylinder Radial Displacement	183
5.2	Thick Cylinder Radial Stress	185
5.3	Thick Cylinder Circumferential Stress	188
5.4	Composite Cylinder End w-Displacement	216
5.5	Composite Cylinder Horizontal Interface w-Displacement .	218
5.6	Horizontal Interface Stress, or (Matrix)	223
5.7	Horizontal Interface Stress, $\sigma_{\mathbf{r}}$ (Stiffener)	224
5.8	Horizontal Interface Stress, $\sigma_{\mathbf{z}}$ (Matrix)	226
5.9	Horizontal Interface Stress, σ_z (Stiffener)	227
5.10	Vertical Interface Stress, σ_z (Matrix)	229
5.11	Vertical Interface Stress, σ_z (Stiffener)	230
5.12	Horizontal Interface Stress, σ_{θ} (Matrix)	233
5.13	Horizontal Interface Stress, σ_A (Stiffener)	234

.. v_e.

in Material

la us

in less

14 S. 71

13 Es. 14: 93.5

la cu

LIST OF FIGURES

Figure		Page
2.1	Rectangular Mesh	15
2.2	Mesh Point and Neighboring Points	15
2.3	Rectangular Mesh	19
2.4	Mesh Point and Neighboring Points	20
2.4	Material Region Around a Mesh Point and Associated Cartesian Stresses and Body Forces	24
2.6	Outside Corner Boundary Point	29
2.7	Vertical Boundary Point	31
2.8	Horizontal Boundary Point	32
2.9	Inside Corner Boundary Point	33
2.10	Cylindrical Volume Element	35
2.11	Circumferential Stresses	36
2.12	Circumferential Stresses	36
2.13	Material Region Around a Mesh Point and Associated Cylindrical Stresses and Body Forces	37
2.14	Composite Material Region	48
2.15	Material Region	49
3.1	Constant Strain Triangle	64
3.2	Normal Boundary Traction-CST	68
3.3	Linear Strain Triangle	70
3.4	Normal Boundary Traction-LST	76

4.19 E 7.

Figure		Page
3.5	Constant Strain Triangular Ring Segment	79
3.6	Cross Section of Ring Element	79
3.7	Axial Boundary Traction-CSTR	84
3.8	Linear Strain Triangular Ring Segment	88
3.9	Axial Boundary Traction-LSTR	94
4.1a	Cantilever Beam	96
4.1b	Cantilever Beam-LST Finite Element Configuration	96
4.2	Cantilever Beam - Finite Difference Configurations	99
4.3	Finite Difference Beam Deflections	100
4.4	Finite Difference Flexural Stress	102
4.5	Cantilever Beam-CST Finite Element Configurations	103
4.6	CST Beam Deflections	104
4.7	CST Flexural Stress	105
4.8	Alternate CST Beam Configuration	107
4.9	LST Beam Deflections	108
4.10	Beam Deflections	112
4.11	Beam Flexural Stress	114
4.12	Top Boundary Flexural Stress	116
4.13	CST Boundary Flexural Stress	118
4.14	Beam Shear Stress	120
4.15	Longitudinal Free End Displacements	123
4.16	Composite Plate	125
4.17	Composite Plate - Finite Difference Configurations	127
4.18	FD Top Edge v-Displacements	128
4.19	FD Top Edge u-Displacements	129

:::::e E -

... E.-[

u E

.3 te

... :::

-3 37

· 3.

.: :::

·11

1.3 La₁

-A. 31; - Al 127 (

·22 137

-33 U:

44 Li

SE E.

-08 - E.,

% E,

13 E.

·...

Figure		Page
4.20	FD Horizontal Interface v-Displacements	130
4.21	FD Horizontal Interface u-Displacements	131
4.22	FD Vertical Symmetry Axis v-Displacements	132
4.23	Composite Plate - CST Configurations	134
4.24	CST Top Edge v-Displacements	135
4.25	CST Top Edge u-Displacements	136
4.26	CST Horizontal Interface v-Displacements	137
4.27	CST Horizontal Interface u-Displacements	138
4.28	CST Vertical Symmetry Axis v-Displacements	139
4.29	Composite Plate - LST Configurations	140
4.30	LST Top Edge v-Displacements	141
4.31	LST Top Edge u-Displacements	142
4.32	LST Horizontal Interface v-Displacements	144
4.33	LST Horizontal Interface u-Displacements	145
4.34	LST Vertical Symmetry Axis v-Displacements	146
4.35	FD, CST, LST Top Edge v	147
4.36	FD, CST, LST Top Edge u	148
4.37	FD, CST, LST Horizontal Interface v	149
4.38	FD, CST, LST Horizontal Interface u	150
4.39	FD, CST, LST Vertical Symmetry Axis v	151
4.40	Composite Plate - FD Stress Distribution	158
4.41	Composite Plate - CST Stress Distribution	159
4.42	Composite Plate-LST Stress Distribution	160
4.43	Composite Plate Horizontal Interface $\sigma_{\mathbf{x}}$	165
4.44	Composite Plate Horizontal Interface $\sigma_{\mathbf{y}}$	168

Figure		Page
4.45	Composite Plate Vertical Interface σ_y	171
4.46	Composite Plate Vertical Interface τ_{xy}	175
5.1	Pressurized Thick Cylinder	179
5.2	Thick Cylinder, Finite Element and Finite Difference Configurations	181
5.3	Thick Cylinder Radial Displacements	184
5.4	Thick Cylinder Radial Stress	186
5.5	Thick Cylinder Circumferential Stress	189
5.6	Composite Cylinder	190
5.7	Composite Cylinder - Finite Difference Configurations	192
5.8	FD Cylinder End Axial Displacements	194
5.9	FD Horizontal Interface Axial Displacements	195
5.10	Extrapolated FD Displacements	197
5.11	Composite Cylinder - FD Stress Distribution	198
5.12	FD Corner Stresses	199
5.13	Composite Cylinder - CSTR Configurations	201
5.14	CSTR Cylinder End Axial Displacements	202
5.15	CSTR Horizontal Interface Axial Displacements	203
5.16	CSTR Extrapolated Displacements	205
5.17	Composite Cylinder - CSTR Stress Distribution	206
5.18	CSTR Corner Stresses	207
5.19	Composite Cylinder - LSTR Configurations	208
5.20	LSTR Cylinder End Axial Displacements	210
5.21	LSTR Horizontal Interface Axial Displacements	211
5.22	LSTR Extrapolated Displacements	212

i.j.ir 5.22 2 = ; 11. 127 5.25 : -: 1.12 3.27 | 1.77 5.35 0.75 5.19 E. T. Mi - :. 111 lil zir. 5/1**a** (35/12) Ath 112 squar 11: Ε. £3. F. ; €. -37: ₩. Q37**;** £, લસ્ક Æ. 45, LOTA 40. Ling EL 1578 EL. 1378

Ĩ

F. C

F. H.

E A

Q.,

Figure		Page
5.23	Composite Cylinder - LSTR Stress Distribution	213
5.24	LSTR Corner Stresses	214
5.25	Comparison of End Axial Displacements	217
5.26	Comparison of Horizontal Interface Axial Displacements .	219
5.27	Comparison of End Radial Displacements	220
5.28	Comparison of Horizontal Interface Radial Displacements.	221
5.29	Horizontal Interface σ_r	225
5.30	Horizontal Interface σ_z	228
5.31	Vertical Interface σ_z	231
5.32	Horizontal Interface $\boldsymbol{\sigma}_{\boldsymbol{\theta}}$	235
6.1a	Square Plate with a Circular Hole - Finite Difference Approximation for Present Analysis	239
6.1b	Square Plate with a Circular Hole - Possible Finite Difference Approximation	239
A1.	FD Cylinder End u-Displacements	247
A2.	FD Horizontal Interface u-Displacements	248
A3.	FD Axial Displacements	249
A4.	FD Radial Displacements	250
A5.	CSTR Cylinder End u-Displacements	251
A6.	CSTR Horizontal Interface u-Displacements	252
A7.	CSTR Axial Displacements	253
A8.	CSTR Radial Displacements	254
A9.	LSTR Cylinder End u-Displacements	255
A10.	LSTR Horizontal Interface u-Displacements	256
A11.	LSTR Axial Displacements	257
A12.	LSTR Radial Displacements	258

LIST OF SYMBOLS

x, y, z	Rectangular Cartesian coordinates
σ _x , σ _y , σ _z	Cartesian normal stress components
^τ xy, ^τ yz, ^τ zx	Cartesian shear stress components
ϵ_{x} , ϵ_{y} , ϵ_{z}	Cartesian normal strains
Y _{xy} , Y _{yz} , Y _{zx}	Cartesian shear strains
u, v, w	Cartesian displacements
X, Y, Z	Cartesian body force components
X , Y , Z	Cartesian boundary traction resultants
r, θ, z	Polar cylindrical coordinates
σ _r , σ _θ , σ _z	Cylindrical normal stress components
^τ rθ, ^τ θz, ^τ zr	Cylindrical shear stress components
$\epsilon_{\mathbf{r}}, \ \epsilon_{\theta}, \ \epsilon_{\mathbf{z}}$	Cylindrical normal strains
γ _{rθ} , γ _{θz} , γ _{zr}	Cylindrical shear strains
u, v, w	Cylindrical displacements
R, Z	Cylindrical body force components
R, Z	Cylindrical boundary traction resultants
Е	Modulus of elasticity (Young's modulus)
ν	Poisson's ratio
G	Shear modulus
C _{ij} i,j = 1,4	General elastic constants
h, k, r	Mesh dimensions for difference approximations
N, S, E, W	North, south, east, and west designation

NE Northeast

NW Northwest

SW Southwest

SE Southeast

U, V Displacement functions

α Generalized displacements

β Generalized forces

W Work

[k] Element stiffness matrix

 $[k_{\alpha}]$ Generalized element stiffness matrix

[K], [K] Overall structural stiffness matrix

p, q Boundary traction

[f] Matrix of element nodal point forces, or force

intensities

dV Element of volume

da Element of surface area

ds Element of arc length

[F], [F] Matrix of overall structural modal point force

or force intensities

M, N Weighting functions

at asserble

exert of p

I. INTRODUCTION

1.1 Remarks

A fundamental problem of mechanics of deformable bodies is the determination of the state of stress and deformation in arbitrary three dimensional solids. Of particular importance are two dimensional situations involving plane stress or plane strain. The literature of the classical theory of elasticity contains exact solutions to many of these problems. These are restricted for the most part to two dimensional problems involving simple geometry and boundary conditions. In more complicated problems, it is necessary to resort to approximate methods of solution.

Two approximate procedures which have found widespread application in recent years are finite difference and finite element methods. Finite difference methods involve mathematical approximations. The governing differential equations and related boundary conditions are replaced by difference expressions. These relate discrete values of approximating functions at a finite number of points. The result is a system of linear algebraic equations which is solved by standard numerical procedures. Finite element methods refer to a class of approximate procedures in which the actual body or structure is replaced by an assemblage of carefully chosen elements connected at a finite number of points called nodal points. In the stiffness method for example, an assumption of the strain distribution in the element is

more with st Equilibrium

more of for

finite diffe

Expectal man

relate modal

Expectation

Fraid equation

Extracours.

... Previo

The classification of the control of

iterative pro

differences i

is and his s

The : Structural pr

eltotaft stro

Methods of st

lasteriko e Lasteriko e Biolioge made with strains related to the displacements of element nodal points. Equilibrium conditions are then satisfied at the nodal points. There is no need for approximating the governing equations as is the case with finite difference methods. The approximation, on the contrary, is of a physical nature. The procedure results in systems of equations which relate nodal point displacements to nodal point forces through stiffness or flexibility influence coefficient matrices. These are linear algebraic equations which are likewise solved by standard numerical procedures.

1.2 Previous Developments

The first application of finite difference methods is apparently due to C. Runge [1]². He used the method in the analysis of torsion problems. L. F. Richardson [2] made further progress by applying an iterative procedure to obtain the stress distribution in dams.

H. Marcus [3] and later H. Hencky [4] were successful in applying finite differences in the analysis of plate bending problems. R. V. Southwell [5] and his students are responsible for many applications in recent times.

The finite element methods are a generalization of well known structural procedures which were originally developed in conjunction with aircraft structural problems. They are related to the so called "matrix methods of structural analysis" advanced by Langefors [6] and Argyris [7].

¹Timoshenko and Goodier, "Theory of Elasticity," Page 461.

The numbers in square brackets refer to references listed in the Bibliography.

li fedell 114 mer struct. 221 15 11.5e generally gre læ 10 mrenni miles is v Elements. To cur Parian # Top [11] SILLA MILLE its elerent De displace estelsively courted dur. Philietent : किक्षेति ty c: 2 21:411 (C.Z. Relative des initial stra. to the to is Gladratic. Epils (17, 1 the products |

The f

At s

Σę

Je, e

In recent times, application of these methods to continuum problems and other structures has been extensive. Their increasing use and development is closely related to progress made in digital computation and generally greater availability of digital computers themselves.

The first achievement in the area of finite element methods is due to Hrennikoff [8]. He developed a framework analogy for plane stress problems in which the actual body is replaced by a lattice of beam elements. The procedure was subsequently improved by McHenry [9] after which Parikh and Norris [10] generalized the method by including bending.

A most sifnigicant achievement is due to Turner, Clough, Martin, and Topp [11]. They presented a triangular plate element stiffness matrix which could be used in the analysis of plane stress problems.

This element is assumed to be in a homogeneous state of strain and the displacement field is a linear one. This matrix has been used extensively and is directly responsible for many advances which have occurred during the past ten years. Argyris [12] has given this matrix a different form, one which he calls the natural or invariant stiffness.

The original work of Argyris and Kelsey [7,13] demonstrates the capability of the methods to account for initial strains of a thermal or misalignment nature. Turner, Dill, Martin, and Melosh [14] consider the large deformation of heated structures. Argyris [15] discusses initial strains due to plasticity and thermal effects.

DeVeubeke [16] introduced a plane stress triangle plate element for which the strain variation is linear and thus the displacement field is quadratic. This element has been used by some writers including Argyris [17, 15] and Felippa [18]. It has proven to be very useful for problems involving stress concentration. Felippa [18] has discussed

oper refler upir raci mi stell ;: Elin [1] ages (... modes as . Willies for aed a tettu 44 a a . Resident in various of equipment dent it is il the Age ^{ख्र}ात • क्र. iationality ! Rose Ed mattsons an ases it was stations to j ^{ध्रु} सक्ता_{स्यह} । terits of sev

•

Tie.

other refinements to these stiffness matrices involving quadratic and higher order strain variation.

Finite elements have also been used in the analysis of plate and shell problems. Among the many contributors in this regard are Melosh [19], Argyris [20], Schmit [21], Clough [22] and Zienkiewicz [23]. Argyris [24] has demonstrated the applicability to large displacement problems as well. Wilson [25] and Rashid [26] have worked out stiffness matrices for axially symmetric ring elements. Argyris [24, 27] has used a tetrahedron element in the analysis of three dimensional problems. A number of writers have discussed the dynamic problems involving the determination of natural frequencies and natural modes of oscillation for various systems [28, 29, 30]. Felippa [18] gives a detailed account of nonlinear analysis including the formulation and solution of elastoplastic problems. Chang and Taylor [31, 32] demonstrate the usefulness of the method in linear viscoelastic problems which arise in nuclear reactor work.

1.3 Present Investigation

The objective of this present work is to compare solutions of elastostatic problems obtained by finite element and finite difference methods. Included are some examples which have known solutions. Thus, comparisons are also made with the exact elasticity solution in these cases. It was of primary interest in this dissertation to obtain solutions to problems involving composite materials. Exact solutions to such problems are not generally available. In these situations, the results of several approximate solutions are compared with one another.

ifference af

mi mially

entain to ;

dest for

SMain elen-

ASSISTED !

AUT the Los

the maily six

Included in this investigation are formulations of the finite difference and finite element methods for plane stress or plane strain and axially symmetric elastostatic problems. Particular applications pertain to plane stress and axially symmetric problems only. Finite element formulations are given for both constant and linearly varying strain elements. Finite difference problems are formulated in terms of displacement (Navier) equations of equilibrium. This is in contrast with the usual stress function approach which has been used so often in the analysis of plane problems.

Klations an

stations to

inite time,

the frequen

afference k

if these eq.

miecure.

Electively .

Activate se

ieal with th

leuss ellait

lt i

he of these

≋itelate:

etytessions.

II. FINITE DIFFERENCE METHOD

2.1 General Remarks

The analysis of elastostatic problems by finite difference methods is a two step procedure. The first step involves obtaining finite difference expressions for the governing partial differential equations and associated boundary conditions. These difference equations relate discrete values of an approximating function at a finite number of points. A mesh of lines is then superimposed over the domain of the boundary value problem forming a set of nodal points. A finite system of linear algebraic equations is obtained by writing difference equations for each nodal point of the system. The solution of these equations comprises the second step in the finite difference procedure. The equations are characterized by the existence of a relatively small number of non-zero coefficients. The coefficient matrix is said to be sparsely populated. It is therefore possible to deal with truly large systems involving as many as 1000 equations. The solution can be obtained by iterative procedures or by a modified Gauss elimination technique.

It is possible to achieve the first step in a number of ways.

One of these is to simply replace the governing differential equations and related boundary conditions by appropriate finite difference expressions. This would be the most direct approach if boundary

animal primit
difference for
any value respondings or
approach insommers
directorated
in stresses
a finite don'

milling at

Constant for

Realism)

ietis - z' - y sitess is ta

is completel

∷e

:: :x

The te y and

E_E

Stips are su

conditions are known in advance. A second approach involves a variational principle whereby potential energy is expressed in finite difference form. Letting the total potential energy take on a stationary value results in both governing equations and associated boundary conditions in the form of finite difference expressions. Still another approach involves writing equilibrium equations for material regions corresponding to interior and boundary points. Approximate expressions for stresses are used along with any externally applied loads resulting in finite difference expressions for both interior and boundary points.

2.2. Differential Equations for Plane Stress

Consider first the state of stress in a thin plate loaded by boundary forces which are applied parallel to the plane of the plate and are uniformly distributed over the thickness. For convenience, the midplane of the plate is taken to be the x-y plane. If the stress components σ_z , τ_{yz} , and τ_{zx} are zero at every point in the body, the state of stress is called plane stress. Thus, the state of stress in such a body is completely specified by the stress components σ_x , σ_y , and τ_{xy} .

The equilibrium of the force system is expressed by the equations

$$\frac{\partial \sigma}{\partial x} + \frac{\partial \tau}{\partial y} + X = 0$$

$$\frac{\partial \sigma}{\partial y} + \frac{\partial \tau}{\partial x} + Y = 0$$
(2.1)

where X and Y are body force components reckoned per unit of volume.

For most applications, the orthotropic constitutive relationships are sufficiently general. For the case of plane stress these become

$$\sigma_{\mathbf{x}} = C_{11} \varepsilon_{\mathbf{x}} + C_{12} \varepsilon_{\mathbf{y}}$$

$$\sigma_{\mathbf{y}} = C_{21} \varepsilon_{\mathbf{x}} + C_{22} \varepsilon_{\mathbf{y}}$$

$$\tau_{\mathbf{xy}} = C_{33} \gamma_{\mathbf{xy}}$$
(2.2)

In the case of isotropic behavior, the elastic constants are

$$C_{11} = C_{22} = \frac{E}{1 - v^2}$$

$$C_{12} = C_{21} = \frac{vE}{1 - v^2}$$

$$C_{33} = \frac{E}{2(1 + v)}$$
(2.3)

with E the modulus of elasticity and ν Poisson's ratio.

The strain-displacement relationships are

$$\varepsilon_{\mathbf{x}} = \frac{\partial \mathbf{u}}{\partial \mathbf{x}}$$

$$\varepsilon_{\mathbf{y}} = \frac{\partial \mathbf{v}}{\partial \mathbf{y}}$$

$$\gamma_{\mathbf{x}\mathbf{y}} = \frac{\partial \mathbf{u}}{\partial \mathbf{y}} + \frac{\partial \mathbf{v}}{\partial \mathbf{x}}$$
(2.4)

where u and v are continuous displacement functions in the x and y directions respectively. The three strain components ε_x , ε_y , γ_{xy} cannot be specified independently since they depend on two functions u and v. By differentiating the equations (2.4) it is possible to show that the strain components must satisfy the equation

- <u>x</u>

cur is call

stiffe: 12

Ten

field is expr

d strains :

£ . .

· . .

li is and p

Matthon 12

٠.

E-822-15 (2)

is they because

tipitessions

$$\frac{\partial^2 \varepsilon}{\partial \mathbf{v}^2} + \frac{\partial^2 \varepsilon}{\partial \mathbf{x}^2} = \frac{\partial^2 \gamma}{\partial \mathbf{x} \partial \mathbf{y}}$$
 (2.5)

which is called the compatibility equation. Thus if a stress or displacement field is assumed, it is necessary that equation (2.5) be satisfied in order to assure continuity of deformation.

Then at each point in the body, the equilibrium of the stress field is expressed by equations (2.1). These can be expressed in terms of strains by introducing equations (2.2). Thus

$$C_{11} \frac{\partial \varepsilon_{\mathbf{x}}}{\partial \mathbf{x}} + C_{12} \frac{\partial \varepsilon_{\mathbf{y}}}{\partial \mathbf{x}} + C_{33} \frac{\partial \gamma_{\mathbf{x}\mathbf{y}}}{\partial \mathbf{y}} + X = 0$$

$$C_{21} \frac{\partial \varepsilon_{x}}{\partial y} + C_{22} \frac{\partial \varepsilon_{y}}{\partial y} + C_{33} \frac{\partial \gamma_{xy}}{\partial x} + Y = 0$$

It is now possible to eliminate strains through the strain-displacement relationships (2.4). The result is

$$C_{11} \frac{\partial^{2} u}{\partial x^{2}} + C_{33} \frac{\partial^{2} u}{\partial y^{2}} + (C_{12} + C_{33}) \frac{\partial^{2} v}{\partial x \partial y} + X = 0$$

$$C_{22} \frac{\partial^{2} v}{\partial y^{2}} + C_{33} \frac{\partial^{2} v}{\partial x^{2}} + (C_{21} + C_{33}) \frac{\partial^{2} u}{\partial x \partial y} + Y = 0$$
(2.6)

Equations (2.6) are a generalization of the Navier plane stress equations. They reduce to the Navier equations for isotropic materials. It is only necessary to replace the constants C_{11} , C_{12} , C_{21} , C_{33} by expressions (2.3). The result is

<u>:</u>

<u>:</u>

Tose last a

The firmlites

-1.913.1

Paterect :

Ristally,

H APPROXICE

Capter.

A1;

ation of a

man ;

ad if the

Tus, the t

u =

Vz

٠

$$\frac{E}{1 - v^2} \frac{\partial^2 u}{\partial x^2} + \frac{E}{2(1 + v)} \frac{\partial^2 u}{\partial y^2} + \frac{E}{2(1 - v)} \frac{\partial^2 v}{\partial x \partial y} + X = 0$$

$$\frac{E}{1 - v^2} \frac{\partial^2 v}{\partial y^2} + \frac{E}{2(1 + v)} \frac{\partial^2 v}{\partial x^2} + \frac{E}{2(1 - v)} \frac{\partial^2 u}{\partial x \partial y} + Y = 0$$
(2.7)

These last equations are also presented by Sokolnikoff [33] in the indicial notation and in terms of the Lamé coefficients.

Thus it is seen that the plane stress elasticity problem can be formulated in terms of two second order partial differential equations in displacements. In principle, one would hope to be able to find displacement functions u and v which satisfy equations (2.6) or (2.7). Generally, this is a formidable problem so that one is forced to resort to approximate methods of solution. Finite difference expressions for these equations will be presented in a subsequent section of this chapter.

2.3 Differential Equations for Plane Strain

Although very different in principle, the plane strain formulation closely resembles that for plane stress. A body is said to be in a state of plane strain parallel to the x-y plane if the displacement component perpendicular to this plane is zero for all points in the body and if the remaining displacements are independent of the z coordinate. Thus, the relationships

$$u = u(x,y)$$

$$v = v(x,y)$$

$$w = 0$$
(2.8)

teithe the

mit felati

• 2

'y:

2)

De pin-ses The

> . X

> > ÿ ~ ,

χv

The two rem

c . .

C.:

Ç.,

is likewise

define the state of plane strain. It follows from the strain-displacement relationships that

$$\varepsilon_{\mathbf{z}} = \frac{\partial \mathbf{w}}{\partial \mathbf{z}} = 0$$

$$\gamma_{\mathbf{yz}} = \frac{\partial \mathbf{w}}{\partial \mathbf{y}} + \frac{\partial \mathbf{v}}{\partial \mathbf{z}} = 0$$

$$\gamma_{\mathbf{zx}} = \frac{\partial \mathbf{u}}{\partial \mathbf{z}} + \frac{\partial \mathbf{w}}{\partial \mathbf{x}} = 0$$
(2.9)

The non-zero strain components are ϵ_x , ϵ_y , and γ_{xy} .

The orthotropic constitutive relationships for plane strain are

$$\sigma_{\mathbf{x}} = C_{11} \varepsilon_{\mathbf{x}} + C_{12} \varepsilon_{\mathbf{y}}$$

$$\sigma_{\mathbf{y}} = C_{21} \varepsilon_{\mathbf{x}} + C_{22} \varepsilon_{\mathbf{y}}$$

$$\sigma_{\mathbf{z}} = C_{31} \varepsilon_{\mathbf{x}} + C_{32} \varepsilon_{\mathbf{y}}$$

$$\tau_{\mathbf{xy}} = C_{44} \gamma_{\mathbf{xy}}$$
(2.10)

The two remaining shear stresses vanish throughout the body in view of equations (2.9). For isotropic materials, the elastic constants are

$$C_{11} = C_{22} = \frac{(1 - v)E}{(1 + v)(1 - 2v)}$$

$$C_{12} = C_{21} = C_{13} = C_{31} = \frac{vE}{(1 + v)(1 - 2v)}$$

$$C_{44} = \frac{E}{2(1 + v)}$$
(2.11)

The equilibrium of the force system for the case of plane strain is likewise expressed by relationships (2.1). Using the strain-

mstlatebent

give, equi.

mannes ..

2.

lit sattaja

/: - :

Relationer a

a jigga.

144 1441) 551

2655 (S.T. ...)

Maria:

ere express

ء ئا

٧į

displacement relationships and the constitutive relationships, (2.10) above, equilibrium equations in terms of displacements similar to equations (2.6) can be written for the case of plane strain:

$$C_{11} \frac{\partial^{2} u}{\partial x^{2}} + C_{44} \frac{\partial^{2} u}{\partial y^{2}} + (C_{12} + C_{44}) \frac{\partial^{2} v}{\partial x \partial y} + X = 0$$

$$C_{22} \frac{\partial^{2} v}{\partial y^{2}} + C_{44} \frac{\partial^{2} v}{\partial x^{2}} + (C_{21} + C_{44}) \frac{\partial^{2} u}{\partial x \partial y} + Y = 0$$
(2.12)

For isotropic materials these become

$$\frac{(1-v)E}{(1+v)(1-2v)} \frac{\partial^{2}u}{\partial x^{2}} + \frac{E}{2(1+v)} \frac{\partial^{2}u}{\partial y^{2}} + \frac{E}{2(1+v)(1-2v)} \frac{\partial^{2}v}{\partial x \partial y} + X = 0$$

$$\frac{(1-v)E}{(1+v)(1-2v)} \frac{\partial^{2}v}{\partial y^{2}} + \frac{E}{2(1+v)} \frac{\partial^{2}v}{\partial x^{2}} + \frac{E}{2(1+v)(1-2v)} \frac{\partial^{2}u}{\partial x \partial y} + Y = 0$$
(2.13)

The above are the Navier equations for plane strain. They are likewise presented by Sokolnikoff [33] in indicial notation.

2.4 Differential Equations for Axially Symmetric Problems

The state of deformation in a solid of revolution is called axially symmetric if the displacements are the same in all planes which pass through the axis of revolution. Thus, the circumferential displacement vanishes at each point in the body and the remaining displacement components depend only on the radial and axial coordinates. These ideas are expressed by the relationships

$$u = u(r, z)$$

 $w = w(r, z)$ (2.14)
 $v = 0$

en i mi •

...

::::le18 87

· _:

···:

Vitte R and

Rait 7.

sularie a

Z

. ::

Te elasti in the plan

: -4.

C .

7:.

Here u and w are the radial and axial displacements respectively.

The stress-equations of equilibrium for axially symmetric problems are

$$\frac{\partial \sigma}{\partial \mathbf{r}} + \frac{\partial \tau}{\partial \mathbf{z}} + \frac{\sigma}{\mathbf{r}} - \frac{\sigma}{\theta} + R = 0$$

$$\frac{\partial \tau}{\partial \mathbf{r}} + \frac{\partial \sigma}{\partial \mathbf{z}} + \frac{\tau}{\mathbf{r}} + Z = 0$$
(2.15)

where R and Z are the radial and axial components of body forces reckoned per unit volume.

Once again, the orthotropic constitutive relationships are of suitable generality for most problems.

$$\sigma_{\mathbf{r}} = C_{11} \varepsilon_{\mathbf{r}} + C_{12} \varepsilon_{\mathbf{z}} + C_{13} \varepsilon_{\theta}$$

$$\sigma_{\mathbf{z}} = C_{12} \varepsilon_{\mathbf{r}} + C_{22} \varepsilon_{\mathbf{z}} + C_{23} \varepsilon_{\theta}$$

$$\sigma_{\theta} = C_{13} \varepsilon_{\mathbf{r}} + C_{23} \varepsilon_{\mathbf{z}} + C_{33} \varepsilon_{\theta}$$

$$\tau_{\mathbf{rz}} = C_{44} \varepsilon_{\mathbf{rz}}$$

$$(2.16)$$

The elastic constants for isotropic materials are much the same as those in the plane strain formulation.

$$C_{11} = C_{22} = C_{33} = \frac{(1 - \nu)E}{(1 + \nu)(1 - 2\nu)}$$

$$C_{12} = C_{21} = C_{23} = C_{32} = C_{13} = C_{31} = \frac{\nu E}{(1 + \nu)(1 - 2\nu)}$$

$$C_{44} = \frac{E}{2(1 + \nu)}$$
(2.17)

The strain-displacement relations in cylindrical components

zillei ti

.

.

::

és equations

.

c*′

in lateria

ol113ec

)(1

applied to the axially symmetric case become

$$\varepsilon_{\mathbf{r}} = \frac{\partial \mathbf{u}}{\partial \mathbf{r}}$$

$$\varepsilon_{\mathbf{z}} = \frac{\partial \mathbf{w}}{\partial \mathbf{z}}$$

$$\varepsilon_{\theta} = \frac{\mathbf{u}}{\mathbf{r}}$$

$$\gamma_{\mathbf{r}\mathbf{z}} = \frac{\partial \mathbf{u}}{\partial \mathbf{z}} + \frac{\partial \mathbf{w}}{\partial \mathbf{r}}$$
(2.18)

When equations (2.18) and (2.16) are introduced into equations (2.15), a set of equilibrium equations is obtained in displacement components.

$$C_{11} \left(\frac{\partial^{2} u}{\partial r^{2}} + \frac{1}{r} \frac{\partial u}{\partial r} \right) + C_{44} \frac{\partial^{2} u}{\partial z^{2}} - C_{33} \frac{u}{r^{2}} + (C_{12} + C_{44}) \frac{\partial^{2} w}{\partial r \partial z} + (C_{12} - C_{23}) \frac{1}{r} \frac{\partial w}{\partial z} + R = 0$$

$$C_{44} \left(\frac{\partial^{2} w}{\partial r^{2}} + \frac{1}{r} \frac{\partial w}{\partial r} \right) + C_{22} \frac{\partial^{2} w}{\partial z^{2}} + (C_{12} + C_{44}) \frac{\partial^{2} u}{\partial r \partial z} + C_{44} \right) \frac{\partial^{2} u}{\partial r \partial z} + (C_{23} + C_{44}) \frac{1}{r} \frac{\partial u}{\partial z} + Z = 0$$

$$(2.19)$$

For materials which display isotropic behavior, these become the axially symmetric Navier equations.

$$\frac{(1-v)E}{(1+v)(1-2v)} \left(\frac{\partial^{2}u}{\partial r^{2}} + \frac{1}{r} \frac{\partial u}{\partial r}\right) + \frac{E}{2(1+v)} \frac{\partial^{2}u}{\partial z^{2}} - \frac{(1-v)E}{(1+v)(1-2v)} \frac{u}{r^{2}} + \frac{E}{2(1+v)(1-2v)} \frac{\partial^{2}w}{\partial r\partial z} + R = 0 \qquad (2.20)$$

$$\frac{E}{2(1+v)} \left(\frac{\partial^{2}w}{\partial r^{2}} + \frac{1}{r} \frac{\partial w}{\partial r}\right) + \frac{(1-v)E}{(1+v)(1-2v)} \frac{\partial^{2}w}{\partial z^{2}} + \frac{E}{2(1+v)(1-2v)} \frac{\partial^{2}u}{\partial r\partial z} + \frac{E}{2(1+v)} \frac{\partial^{2}u}{\partial r\partial z} + \frac{E}{2(1+v)} \frac{\partial^{2}u}{\partial r\partial z} +$$

ARBELL.

litalit are

Te plants

M tillej

सम्बद्धाः हत्।

Clettines.

Hilletett χ

Saint is

the where

150 DBR 01

ttel--at :

allin spa

::

Et Tistal .

ateriate v

≆so point

(e.g.

2.5 Finite Difference Equations for Plane Stress

Consider the arbitrary domain of
Figure 2.1 corresponding to the plane of
plane stress or plane strain. A mesh
(rectangular in this case) is superimposed
over the actual domain. The points of
intersection of these lines within the
domain are called mesh (nodal) points.
The points of intersection with the boundary
are called boundary points. It is

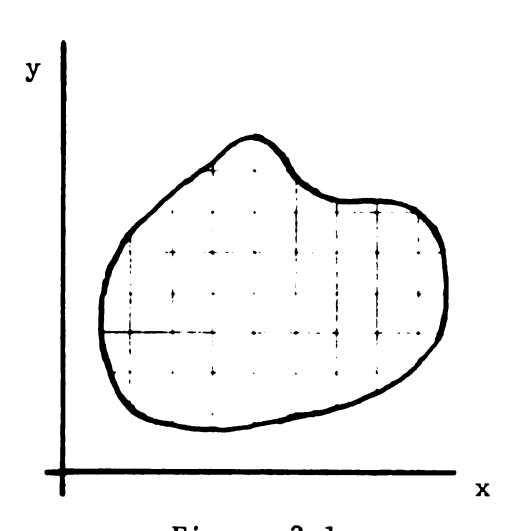
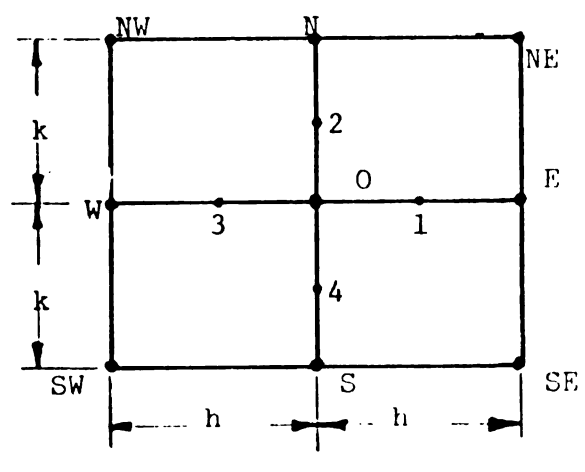


Figure 2.1
Rectangular Mesh

usually convenient to use a uniform spacing with equal magnitudes in both directions. However, in certain cases it is desirable to select a different x and y spacing, while in still other instances, a nonuniform spacing is useful. The latter is particularly

true where stress concentration is involved or in the neighborhood of irregular boundaries. Only uniform spacing is treated in this work.

In Figure 2.2, let the x and y spacing be h and k respectively. The mesh or boundary points in the immediate vicinity of an arbitrary mesh point 0 are shown.



Mesh Point and Neighboring
Points

Figure 2.2

Some formulations may dictate the use of other mesh configurations (e.g. oblique, polar, or arbitrary curvilinear meshes).

ur te app

_

la live -

... t..

Sourse Sourse

Mult 3, 21 Writative

the approxi

.

de ficie

*47 is

Partial d

EC 1. 1

The partial derivative with respect to x of a function u(x, y) can be approximated at the point 0 by the first divided difference

$$\frac{\partial \mathbf{u}}{\partial \mathbf{x}} = \frac{\mathbf{u}_{\mathbf{E}} - \mathbf{u}_{\mathbf{W}}}{2\mathbf{h}} \tag{2.21}$$

In a like manner

$$\frac{\partial \mathbf{u}}{\partial \mathbf{y}} = \frac{\mathbf{u}_{N} - \mathbf{u}_{S}}{2\mathbf{k}} \tag{2.22}$$

Approximations to second derivatives can be established in much the same way. At the point 1, midway between 0 and E, $\frac{\partial u}{\partial x} \simeq \frac{u_E - u_O}{h}$ and at the point 3, midway between 0 and W, $\frac{\partial u}{\partial x} \simeq \frac{u_O - u_W}{h}$. Thus the second partial derivative of u with respect to x can be approximated by differences in the approximate first partial derivatives.

$$\frac{\partial^2 \mathbf{u}}{\partial \mathbf{x}^2} = \frac{\frac{\partial \mathbf{u}}{\partial \mathbf{x}_1} - \frac{\partial \mathbf{u}}{\partial \mathbf{x}_3}}{h} = \frac{\mathbf{u}_E - 2\mathbf{u}_0 + \mathbf{u}_W}{h^2}$$
 (2.23)

The finite difference approximation to $\frac{\partial^2 u}{\partial y^2}$ obtained in much the same way is

$$\frac{\partial^2 u}{\partial y^2} \simeq \frac{u_N - 2u_0 + u_S}{k^2}$$
 (2.24)

To obtain the second mixed partial derivative $\frac{\partial^2 u}{\partial x \partial y}$, the first partial derivative of u with respect to y is approximated at points E and W. That is

:... :<u>;</u>

$$\frac{\partial \mathbf{u}}{\partial \mathbf{y}}_{E} = \frac{\mathbf{u}_{NE} - \mathbf{u}_{SE}}{2\mathbf{k}}$$

$$\frac{\partial \mathbf{u}}{\partial \mathbf{y}} = \frac{\mathbf{u}_{NW} - \mathbf{u}_{SW}}{2\mathbf{k}}$$

Then

$$\frac{\partial^{2} \mathbf{u}}{\partial \mathbf{x} \partial \mathbf{y}} = \frac{\partial}{\partial \mathbf{x}} \left(\frac{\partial \mathbf{u}}{\partial \mathbf{y}} \right)_{0}^{2} = \frac{\frac{\partial \mathbf{u}}{\partial \mathbf{y}}}{2h} = \frac{\mathbf{u}_{NE} - \mathbf{u}_{SE} - \mathbf{u}_{NW} + \mathbf{u}_{SW}}{4hk}$$
 (2.25)

When equations (2.23), (2.24), and (2.25) are introduced into the governing second order partial differential equations, the finite difference expressions are obtained. Corresponding to (2.6) for plane stress are

$$\left(\frac{2C_{11}}{h^2} + 2\frac{C_{33}}{k^2}\right) u_0 - \frac{C_{11}}{h^2} (u_E + u_W) - \frac{C_{33}}{k^2} (u_N + u_S)
+ \left(\frac{C_{12} + C_{33}}{4hk}\right) (v_{NE} - v_{NW} - v_{SE} + v_{SW}) = X_0$$
(2.26)

$$\left(\frac{2c_{33}}{h^2} + \frac{2c_{22}}{k^2}\right) v_0 - \frac{c_{33}}{h^2} (v_E + v_W) - \frac{c_{22}}{k^2} (v_N + v_S)$$
$$- \frac{c_{21} + c_{33}}{4hk} (u_{NE} - u_{NW} - u_{SE} + u_{SW}) = Y_0$$

Here X_0 and Y_0 are body force components applied at the mesh point 0.

If the same spacing is taken in the x and y directions (2.26)

become

$$8(C_{11} + C_{33}) u_0 - 4C_{11}(u_E + u_W) - 4C_{33}(u_N + u_S)$$

$$- (C_{12} + C_{33})(v_{NE} - v_{NW} - v_{SE} + v_{SW}) = h^2X_0$$
 (2.27)

(2.24), an

this is is is the x a

$$8(C_{22} + C_{33}) v_0 - 4C_{33}(v_E + v_W) - 4C_{22}(v_N + v_S)$$
$$- (C_{21} + C_{33})(u_{NE} - u_{NW} - u_{SE} + u_{SW}) = h^2 Y_0$$

These same equations for isotropic materials become

$$8(3 - v)u_{0} - 8(u_{E} + u_{W}) - 4(1 - v)(u_{N} + u_{S})$$

$$- (1 + v)(v_{NE} - v_{NW} - v_{SE} + v_{SW}) = 8 \frac{1 - v^{2}}{E} h^{2}X_{0} \qquad (2.28)$$

$$8(3 - v)v_{0} - 4(1 - v)(v_{E} + v_{W}) - 8(v_{N} + v_{S})$$

$$- (1 + v)(u_{NE} - u_{NW} - u_{SE} + u_{SW}) = 8 \frac{1 - v^{2}}{E} h^{2}Y_{0}$$

The relative magnitudes of the coefficients in the above equations becomes more apparent when a particular value of Poisson's ratio is assigned. Taking $v = \frac{1}{4}$ in equations (2.28) one obtains

$$88u_{0} - 32(u_{E} + u_{W}) - 12(u_{N} + u_{S}) - 5(v_{NE} - v_{NW} - v_{SE} + v_{SW}) = \frac{30h^{2}X_{0}}{E}$$

$$88v_{0} - 12(v_{E} + v_{W}) - 32(v_{N} + v_{S}) - 5(u_{NE} - u_{NW} - u_{SE} + u_{SW}) = \frac{30h^{2}X_{0}}{E}$$

2.6 Finite Difference Equations for Plane Strain

The development of finite difference equations for the case of plane strain involves the same concepts presented in the previous section. One simply introduces the partial derivative approximations (2.23), (2.24), and (2.25) into the appropriate differential equations. When this is done for the isotropic relations (2.13) with equal spacing, h, in the x and y directions, the result is

$$8(3 - 4v) u_{0} - 8(1 - v)(u_{E} + u_{W}) - 4(1 - 2v)(u_{N} + u_{S})$$

$$- (v_{NE} - v_{NW} - v_{SE} + v_{SW}) = \frac{8(1 + v)(1 - 2v)}{E} h^{2}X_{0}$$

$$(2.30)$$

$$8(3 - 4v)v_{0} - 4(1 - 2v)(v_{E} + v_{W}) - 8(1 - v)(v_{N} + v_{S})$$

$$- (u_{NE} - u_{NW} - u_{SE} + u_{SW}) = \frac{8(1 + v)(1 - 2v)}{E} h^{2}Y_{0}$$

These results are more readily compared with corresponding plane stress equations for a particular choice of Poisson's ratio. Again using $\nu = \frac{1}{4} \text{ one obtains}$

$$96u_{0} - 36(u_{E} + u_{W}) - 12(u_{N} + u_{S}) - 6(v_{NE} - v_{NW} - v_{SE} + v_{SW}) = \frac{30h^{2}X_{0}}{E}$$

$$(2.31)$$

$$96v_{0} - 12(v_{E} + v_{W}) - 36(v_{N} + v_{S}) - 6(u_{NE} - u_{NW} - u_{SE} + u_{SW}) = \frac{30h^{2}Y_{0}}{E}$$

2.7 Axially Symmetric Finite Difference Equations

The development of

finite difference equations for

axially symmetric problems is

quite similar to that for plane

stress or plane strain. Figure 2.3

represents one quarter of the cross

section of a solid of revolution. The

z axis is the axis of symmetry. A

rectangular mesh has been superimposed

over the region.

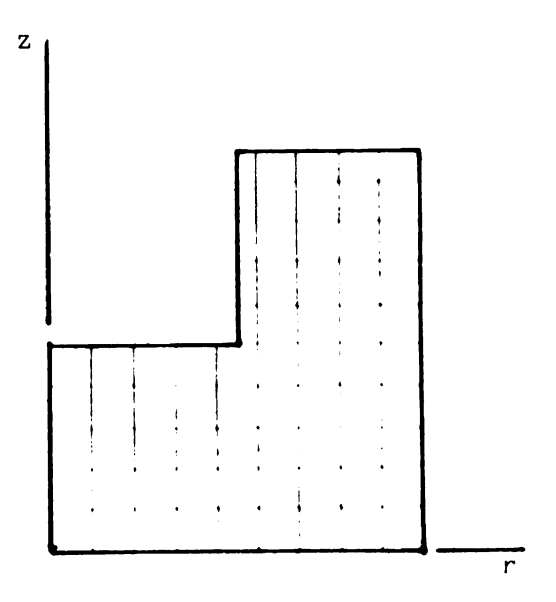


Figure 2.3
Rectangular Mesh

A.

nii wsi

meinte.

Equa I...

if a fizit

er mili:

epitate (

ufference |

Tese (in)

+ (c_{..}

A typical mesh point 0
with mesh or boundary points
immediately around it is shown in
Figure 2.4. Partial derivatives
of a function u(r,z) up to
and including the second order are
approximated by the following
difference expressions:

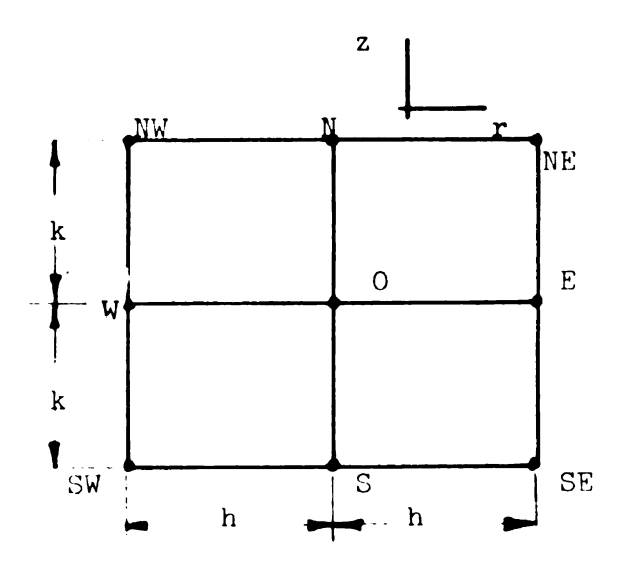


Figure 2.4

Mesh Point and Neighboring Points

$$\frac{\partial \mathbf{u}}{\partial \mathbf{r}} = \frac{\mathbf{U}_{\mathbf{E}} - \mathbf{u}_{\mathbf{W}}}{2\mathbf{h}} \tag{2.32}$$

$$\frac{\partial \mathbf{u}}{\partial \mathbf{z}} = \frac{\mathbf{U}_{\mathbf{N}} - \mathbf{u}_{\mathbf{S}}}{2\mathbf{k}} \tag{2.33}$$

$$\frac{\partial^2 \mathbf{u}}{\partial \mathbf{r}^2} \simeq \frac{\mathbf{U}_{\mathbf{E}} - 2\mathbf{u}_{\mathbf{0}} + \mathbf{u}_{\mathbf{W}}}{\mathbf{h}^2} \tag{2.34}$$

$$\frac{\partial^2 \mathbf{u}}{\partial \mathbf{r} \partial \mathbf{z}} = \frac{\mathbf{u}_{NE} - \mathbf{u}_{NW} - \mathbf{u}_{SE} + \mathbf{u}_{SW}}{4hk}$$
 (2.35)

$$\frac{\partial^2 \mathbf{u}}{\partial \mathbf{z}^2} \simeq \frac{\mathbf{u}_{N} - 2\mathbf{u}_{0} + \mathbf{u}_{S}}{\mathbf{k}^2}$$
 (2.36)

These finite difference approximations are introduced into the differential equations (2.18).

$$C_{11} \frac{(u_{E} - 2u_{O} + u_{W})}{h^{2}} + \frac{C_{11}}{r_{O}} \frac{(u_{E} - u_{W})}{2h} + C_{44} \frac{(u_{N} - 2u_{O} + u_{S})}{k^{2}} - C_{33} \frac{u_{O}}{r_{O}^{2}}$$

+
$$(C_{11} + C_{44}) \frac{(w_{NE} - w_{NW} - w_{SE} + w_{SW})}{4hk} + \frac{C_{12} - C_{23}}{r_0} \frac{(w_{N} - w_{S})}{2k} + R_0 = 0$$

: " -		
• :		
ine sie		
:•		
-		
٠.		
↓		
•		
Med e Maid		
3:a		

$$C_{44} \frac{(w_{E} - 2w_{O} + w_{W})}{h^{2}} + \frac{C_{44}}{r_{O}} \frac{(w_{E} - w_{W})}{2h} + C_{22} \frac{(w_{N} - 2w_{O} + w_{S})}{k^{2}}$$

$$+ (C_{12} + C_{44}) \frac{(u_{NE} - u_{NW} - u_{SE} + u_{SW})}{4hk} + \frac{C_{23} + C_{44}}{r_{O}} \frac{(u_{N} - u_{S})}{2k} + Z_{O} = 0$$

Upon simplification, the above reduce to

$$(2C_{11} + 2C_{44} \frac{h^{2}}{k^{2}} + C_{33} \frac{h^{2}}{r_{0}^{2}}) u_{0} - C_{11} (1 + \frac{h}{2r_{0}}) u_{E} - C_{11} (1 - \frac{h}{2r_{0}}) u_{W}$$

$$- C_{44} \frac{h^{2}}{k^{2}} (u_{N} + u_{S}) - \frac{C_{12} + C_{44}}{4} \frac{h}{k} (w_{NE} - w_{NW} - w_{SE} + w_{SW})$$

$$- \frac{C_{12} - C_{23}}{2} \frac{h}{k} \frac{h}{r_{0}} (w_{N} - w_{S}) = h^{2}R_{0}$$

$$(2.37)$$

$$2(C_{22} + C_{44} \frac{h^{2}}{k^{2}}) w_{0} - C_{44} (1 + \frac{h}{2r_{0}}) w_{E} - C_{44} (1 - \frac{h}{2r_{0}}) w_{W}$$

$$- C_{22} \frac{h^{2}}{k^{2}} (w_{N} + w_{S}) - \frac{C_{12} + C_{44}}{4} \frac{h}{k} (u_{NE} - u_{NW} - u_{SE} + u_{SW})$$

$$- \frac{C_{23} + C_{44}}{2} \frac{h}{k} \frac{h}{r_{0}} (u_{N} - u_{S}) = h^{2}Z_{0}$$

When equal spacing is taken for the r and z directions, k = h, one obtains

$$(2C_{11} + 2C_{44} + C_{33} \frac{h^{2}}{r_{0}^{2}}) u_{0} - C_{11} (1 + \frac{h}{2r_{0}}) u_{E} - C_{11} (1 - \frac{h}{2r_{0}}) u_{W}$$

$$- C_{44} (u_{N} + u_{S}) - \frac{C_{12} + C_{44}}{4} (w_{NE} - w_{NW} - w_{SE} + w_{NW})$$

$$- \frac{C_{12} - C_{33}}{2} \frac{h}{r_{0}} (w_{N} - w_{S}) = h^{2}R_{0}$$
(2.38)

:: (::).

- C. .

But the case of

P quatritis

13- ...

- • 1

33-4.7 W

411

Bally for

tese beco

$$2(C_{22} + C_{44}) w_{0} - C_{44}(1 + \frac{h}{2r_{0}}) w_{E} - C_{44}(1 - \frac{h}{2r_{0}}) w_{W}$$

$$- C_{22}(w_{N} + w_{S}) - \frac{C_{12} + C_{44}}{4} (u_{NE} - u_{NW} - u_{SE} + u_{SW})$$

$$- \frac{C_{23} + C_{44}}{2} \frac{h}{r_{0}} (u_{N} - u_{S}) = h^{2}Z_{0}$$

For the case of isotropic elasticity, the coefficients C_{ij} are given by equations (2.17). The resulting finite difference relationships are

$$8[(3-4\nu) + (1-\nu)\frac{h^2}{r_0^2}] u_0 - 4(1-\nu)(2+\frac{h}{r_0}) u_E - 4(1-\nu)(2-\frac{h}{r_0}) u_W$$

$$- 4(1-2\nu)(u_N + u_S) - (w_{NE} - w_{NW} - w_{SE} + w_{SW})$$

$$= 8(1+\nu)(1-2\nu)\frac{h^2}{E} R_0$$
(2.39)

$$8(3 - 4v) w_{0} - 2(1 - 2v)(2 + \frac{h}{r_{0}}) w_{E} - 2(1 - 2v)(2 - \frac{h}{r_{0}}) w_{W}$$

$$-8(1 - v)(w_{N} + w_{S}) - 2 \frac{h}{r_{0}} (u_{N} - u_{S}) - (u_{NE} - u_{NW} - u_{SE} + u_{SW})$$

$$= 8(1 + v)(1 - 2v) \frac{h^{2}}{E} Z_{0}$$

Finally for the specific case in which Poisson's ratio is taken as $\frac{1}{4}$ these become

$$(16 + 6 \frac{h^2}{r_0^2}) u_0 - 3(2 + \frac{h}{r_0}) u_E - 3(2 - \frac{h}{r_0}) u_W - 2(u_N + u_S)$$

$$- (w_{NE} - w_{NW} - w_{SE} + w_{SW}) = 5 \frac{h^2}{E} R_0$$
(2.40)

$$16w_{0} - (2 + \frac{h}{r_{0}}) w_{E} - (2 - \frac{h}{r_{0}}) w_{W} - 6(w_{N} + w_{S}) - 2 \frac{h}{r_{0}} (u_{N} - u_{S})$$
$$- (u_{NE} - u_{NW} - u_{SE} + u_{SW}) = 5 \frac{h^{2}}{E} Z_{0}$$

2.8 Alternate Derivation of Plane Stress Difference Equations

Finite difference equations corresponding to the previously mentioned situations can also be derived from the equilibrium of a material element in the neighborhood of an arbitrary mesh point 0. This method has the advantage that boundary conditions can be derived in exactly the same way. This is important in the case of certain questionable situations such as corners where boundary conditions are not immediately apparent.

Inherent in this procedure is the need to make assumptions regarding the strain approximations to be used. Corresponding to different choices for these strain approximations are somewhat different finite difference equations.

Figure 2.5, on Page 24 illustrates the rectangular region around the mesh point 0. The x and y dimensions are h and k respectively. X_{0} and Y_{0} are body force components per unit volume assumed to act at the point 0. In the case of boundary points, to be discussed later, X_{0} and Y_{0} may be components of the static resultant of boundary tractions. The normal and shear stresses are designated in the usual way and sign

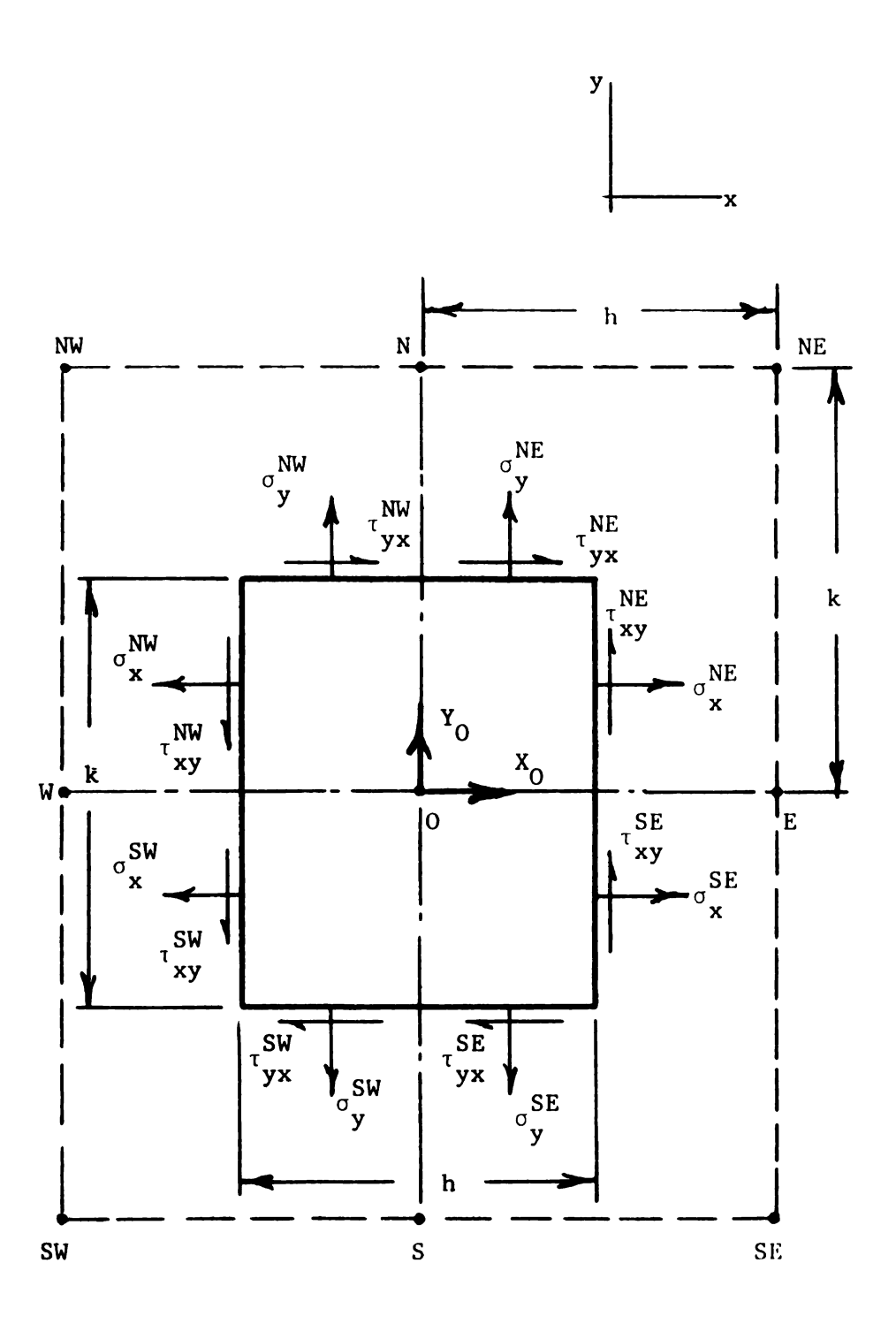


Figure 2.5

Material Region Around a Mesh Point and Associated Cartesian Stresses and Body Forces

::DVellills

mai the 🖘

west, and so

seeffing count

these region

previously po

la de

terms of the

springere .

Constitutive

i.i) and str

ху

• Ух

The distinct

Parious Ways

conventions of classical elasticity are employed. The four quadrants around the mesh point 0 are designated as northeast, northwest, southwest, and southeast beginning in the upper right hand corner and proceeding counterclockwise. Normal and shear stresses corresponding to these regions are given superscripts accordingly.

In deriving finite difference expressions corresponding to previously presented results, it is necessary to express stresses in terms of displacements through the constitutive relationships and approximate expressions for strains. For the isotropic materials, the constitutive relationships (2.2), with isotropic elastic coefficients (2.3) and strain-displacement relationships (2.4) become

$$\sigma_{\mathbf{x}} = \frac{E}{1 - v^2} \left(\frac{\partial \mathbf{u}}{\partial \mathbf{x}} + v \frac{\partial \mathbf{v}}{\partial \mathbf{y}} \right)$$

$$\sigma_{\mathbf{y}} = \frac{E}{1 - v^2} \left(\frac{\partial \mathbf{v}}{\partial \mathbf{y}} + v \frac{\partial \mathbf{u}}{\partial \mathbf{x}} \right)$$

$$\tau_{\mathbf{xy}} = \frac{E}{2(1 + v)} \left(\frac{\partial \mathbf{v}}{\partial \mathbf{x}} + \frac{\partial \mathbf{u}}{\partial \mathbf{y}} \right)$$

$$\tau_{\mathbf{yx}} = \frac{E}{2(1 + v)} \left(\frac{\partial \mathbf{u}}{\partial \mathbf{y}} + \frac{\partial \mathbf{v}}{\partial \mathbf{x}} \right)$$
(2.41)

The displacement gradients in equations (2.41) are approximated in various ways to give the following stress expressions:

$$\sigma_{x}^{NE} = \frac{E}{1 - v^{2}} \left(\frac{u_{E} - u_{O}}{h} + v \frac{v_{NE} - v_{E} + v_{N} - v_{O}}{2k} \right)$$

$$\sigma_{y}^{NE} = \frac{E}{1 - v^{2}} \left(\frac{v_{N} - v_{O}}{k} + \frac{u_{NE} - u_{N} + u_{E} - u_{O}}{2h} \right)$$

$$\tau_{xy}^{NE} = \frac{E}{2(1 + v)} \left(\frac{v_{E} - v_{O}}{h} + \frac{u_{NE} - u_{E} + u_{N} - u_{O}}{2k} \right)$$

$$\tau_{xy}^{NE} = \frac{E}{2(1 + v)} \left(\frac{u_{N} - u_{O}}{k} + \frac{v_{NE} - v_{N} + v_{E} - v_{O}}{2h} \right)$$

$$\sigma_{x}^{NW} = \frac{E}{1 - v^{2}} \left(\frac{u_{O} - u_{W}}{h} + v \frac{v_{N} - v_{O} + v_{NW} - v_{W}}{2k} \right)$$

$$\sigma_{y}^{NW} = \frac{E}{2(1 + v)} \left(\frac{v_{N} - v_{O}}{k} + v \frac{u_{N} - u_{NW} + u_{O} - u_{W}}{2k} \right)$$

$$\tau_{xy}^{NW} = \frac{E}{2(1 + v)} \left(\frac{v_{O} - v_{W}}{h} + \frac{u_{N} - u_{O} + u_{NW} - u_{W}}{2k} \right)$$

$$\sigma_{x}^{NW} = \frac{E}{2(1 + v)} \left(\frac{u_{N} - u_{O}}{h} + v \frac{v_{N} - v_{NW} + v_{O} - v_{W}}{2h} \right)$$

$$\sigma_{x}^{SW} = \frac{E}{1 - v^{2}} \left(\frac{u_{O} - u_{W}}{h} + v \frac{v_{O} - v_{S} + v_{W} - v_{SW}}{2h} \right)$$

$$\sigma_{xy}^{SW} = \frac{E}{1 - v^{2}} \left(\frac{v_{O} - v_{S}}{k} + v \frac{u_{O} - u_{W} + u_{S} - u_{SW}}{2h} \right)$$

$$\tau_{xy}^{SW} = \frac{E}{2(1 + v)} \left(\frac{v_{O} - v_{S}}{h} + v \frac{u_{O} - u_{W} + u_{S} - u_{SW}}{2h} \right)$$

$$\tau_{xy}^{SW} = \frac{E}{2(1 + v)} \left(\frac{v_{O} - v_{W}}{h} + \frac{u_{O} - u_{W} + u_{S} - u_{SW}}{2h} \right)$$

$$\tau_{yy}^{SW} = \frac{E}{2(1 + v)} \left(\frac{v_{O} - v_{W}}{h} + \frac{v_{O} - v_{W} + v_{S} - v_{SW}}{2h} \right)$$

JSE yx Te equilibr If the elemen The stresses (2.46) and as

$$\sigma_{\mathbf{x}}^{SE} = \frac{E}{1 - v^{2}} \left(\frac{u_{E} - u_{O}}{h} + v \frac{v_{E} - v_{SE} + v_{O} - v_{S}}{2k} \right)$$

$$\sigma_{\mathbf{y}}^{SE} = \frac{E}{1 - v^{2}} \left(\frac{v_{O} - v_{S}}{k} + v \frac{u_{E} - u_{O} + u_{SE} - u_{S}}{2h} \right)$$

$$\tau_{\mathbf{xy}}^{SE} = \frac{E}{2(1 + v)} \left(\frac{v_{E} - v_{O}}{h} + \frac{u_{E} - u_{SE} + u_{O} - u_{S}}{2k} \right)$$

$$\tau_{\mathbf{yx}}^{SE} = \frac{E}{2(1 + v)} \left(\frac{u_{O} - u_{S}}{k} + \frac{v_{E} - v_{O} + v_{SE} - v_{S}}{2h} \right)$$

The equilibrium of an arbitrary element requires that

$$\Sigma \mathbf{F}_{\mathbf{x}} = 0$$

$$\Sigma \mathbf{F}_{\mathbf{y}} = \mathbf{0}$$

If the element is of thickness t, these equations become

$$t \frac{k}{2} \sigma_{x}^{NE} - t \frac{k}{2} \sigma_{x}^{NW} - t \frac{k}{2} \sigma_{x}^{SW} + t \frac{k}{2} \sigma_{x}^{SE}$$

$$+ t \frac{h}{2} \tau_{yx}^{NE} + t \frac{h}{2} \tau_{yx}^{NW} - t \frac{h}{2} \tau_{yx}^{SW} - t \frac{h}{2} \tau_{yx}^{SE} + thk X_{0} = 0$$

$$t \frac{h}{2} \sigma_{y}^{NE} + t \frac{h}{2} \sigma_{y}^{NW} - t \frac{h}{2} \sigma_{y}^{SW} - t \frac{h}{2} \sigma_{y}^{SE}$$

$$+ t \frac{k}{2} \tau_{xy}^{NE} - t \frac{k}{2} \tau_{xy}^{NW} - t \frac{k}{2} \tau_{xy}^{SW} + t \frac{k}{2} \tau_{xy}^{SE} + thk Y_{0} = 0$$

$$(2.46)$$

The stresses (2.41) through (2.45) are next substituted into equations (2.46) and after some simplification with k = h one obtains

$$\begin{split} \frac{E}{1-v^2} & \left[4(u_0 - u_E) + 2v(v_0 + v_E - v_N - v_{NE}) + 2(1-v)(u_0 - u_N) \right. \\ & + (1-v)(v_0 + v_N - v_E - v_{NE}) \right] \\ & + \frac{E}{1-v^2} \left[4(u_0 - u_E) + 2v(v_S + v_{SE} - v_0 - v_E) + 2(1-v)(u_0 - u_S) \right. \\ & + (1-v)(v_E + v_{SE} - v_0 - v_S) \right] \\ & + \frac{E}{1-v^2} \left[4(u_0 - u_W) + 2v(v_W + v_0 - v_S - v_{SW}) + 2(1-v)(u_0 - u_S) \right. \\ & + (1-v)(v_0 + v_S - v_W - v_{SW}) \right] \\ & + \frac{E}{1-v^2} \left[4(u_0 - u_W) + 2v(v_N + v_{NW} - v_0 - v_W) + 2(1-v)(u_0 - u_N) \right. \\ & + (1-v)(v_{NW} + v_W - v_N - v_0) \right] = 8h^2 X_0 \qquad (2.47) \\ & \frac{E}{1-v^2} \left[4(v_0 - v_N) + 2v(u_N + u_0 - u_E - u_{NE}) + 2(1-v)(v_0 - v_E) \right. \\ & + (1-v)(u_0 + u_E - u_N - u_{NE}) \right] \\ & + \frac{E}{1-v^2} \left[4(v_0 - v_S) + 2v(u_E + u_{SE} - u_0 - u_S) + 2(1-v)(v_0 - v_E) \right. \\ & + (1-v)(u_S + u_{SE} - u_0 - u_E) \right] \\ & + \frac{E}{1-v^2} \left[4(v_0 - v_S) + 2v(u_0 + u_S - u_W - u_{SW}) + 2(1-v)(v_0 - v_W) \right. \\ & + (1-v)(u_W + u_0 - u_{SW} - u_S) \right] \\ & + \frac{E}{1-v^2} \left[4(v_0 - v_N) + 2v(u_W + u_{NW} - u_0 - u_N) + 2(1-v)(v_0 - v_W) \right. \\ & + (1-v)(u_W + u_0 - u_{SW} - u_S) \right] \\ & + \frac{E}{1-v^2} \left[4(v_0 - v_N) + 2v(u_W + u_{NW} - u_0 - u_N) + 2(1-v)(v_0 - v_W) \right. \\ & + (1-v)(u_W + u_0 - u_{SW} - u_S) \right] \\ & + \frac{E}{1-v^2} \left[4(v_0 - v_N) + 2v(u_W + u_{NW} - u_0 - u_N) + 2(1-v)(v_0 - v_W) \right. \\ & + (1-v)(u_W + u_0 - u_0 - u_N) + 2(1-v)(v_0 - v_W) \right. \\ & + (1-v)(u_W + u_0 - u_0 - u_N) + 2(1-v)(v_0 - v_W) \right. \\ & + (1-v)(u_W + u_0 - u_0 - u_N) + 2(1-v)(v_0 - v_W) \right. \\ & + (1-v)(u_W + u_0 - u_0 - u_N) + 2(1-v)(v_0 - v_W) \right. \\ & + (1-v)(u_W + u_0 - u_0 - u_N) + 2(1-v)(v_0 - v_W) \right. \\ & + (1-v)(u_W + u_0 - u_0 - u_N) + 2(1-v)(v_0 - v_W) \right. \\ & + (1-v)(u_W + u_0 - u_0 - u_N) + 2(1-v)(v_0 - v_W) \right. \\ & + (1-v)(u_W + u_0 - u_0 - u_N) + 2(1-v)(v_0 - v_W) \right. \\ & + (1-v)(u_W + u_0 - u_0 - u_N) + 2(1-v)(v_0 - v_W) \right. \\ & + (1-v)(u_W + u_0 - u_0 - u_N) + 2(1-v)(v_0 - v_W) \right. \\ & + (1-v)(u_W + u_0 - u_0 - u_N) + 2(1-v)(v_0 - v_W) \right.$$

Equations (2) societions to considerable following:

63 - J (4₃)

\$3-0) v.

Dese resul:

Ei latelej

boundary ou

to restanga

Mas, one :

ither bound

wied using

here is the

Figure 2.6

Print for vertical a

suffaces.

Equations (2.47) are expressed in a form which allows certain boundary conditions to be derived. These will be discussed subsequently. After considerable simplification, equations (2.47) can be reduced to the following:

$$8(3 - v) u_{0} - 8(u_{E} + u_{W}) - 4(1 - v)(u_{N} + u_{S})$$

$$- (1 + v)(v_{NE} - v_{NW} - v_{SE} + v_{SW}) = 8 \frac{1 - v^{2}}{E} h^{2}X_{0}$$

$$8(3 - v) v_{0} - 4(1 - v)(v_{E} + v_{W}) - 8(v_{N} + v_{S})$$

$$- (1 + v)(u_{NE} - u_{NW} - u_{SE} + u_{NW}) = 8 \frac{1 - v^{2}}{E} h^{2}Y_{0}$$

These results are identical to those which were obtained in section 2.6 and labeled equations (2.28).

Next, consideration is given to the development of static boundary conditions. Boundary expressions treated here are restricted to rectangular boundaries which are parallel to the coordinate axes. Thus, one is able to deal with points on vertical or horizontal boundary surfaces as well as 90° corners.

Other boundary conditions can be approximated using sufficiently small spacing.

The first situation treated here is the 90° outside corner. In Figure 2.6, point 0 is such a corner point formed by the intersection of vertical and horizontal boundary surfaces. The x and y spacings are

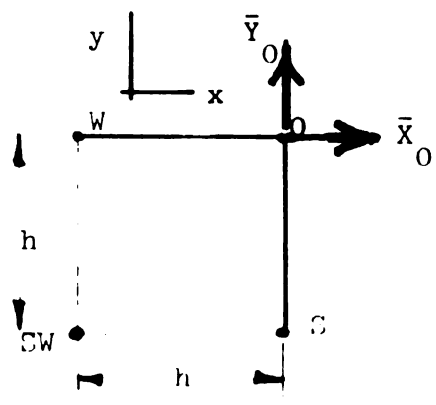


Figure 2.6

Outside Corner Boundary Point

nit t. İg

tratticos.

The

menately

tems of the

EDTESSION 1

De result :

 $\frac{1}{1+\frac{1}{2}}\left(\cdot \cdot \cdot \cdot \right)$

\frac{1}{12.5} \left[\frac{1}{2.5} \cdot \fra

ar simpli:

13 - Hu -

²⁽³ - ·)v₀ -

hen for the

12u - 16u

²²y - 6y -

both h. \bar{X}_0 and \bar{Y}_0 are the components of the resultant of boundary tractions.

The finite differences expressions for such a point follow immediately from equations (2.47). One need only use the left hand side terms of these equations which pertain to the southwest corner. The expression in the third bracket in each of equations (2.47) is pertinent. The result is

$$\frac{E}{1 - v^2} \left[4(u_0 - u_W) + 2v(v_W + v_0 - v_S - v_{SW}) + 2(1 - v)(u_0 - u_S) + (1 - v)(v_0 + v_S - v_W - v_{SW}) \right] = 8\bar{X}_0$$

$$\frac{E}{1 - v^2} \left[4(v_0 - v_S) + 2v(u_0 + u_S - u_W - u_{SW}) + 2(1 - v)(v_0 - v_W) + (1 - v)(u_W + u_0 - u_{SW} - u_S) \right] = 8\overline{Y}_0$$

Upon simplification, the above become

$$2(3 - v)u_{0} - 4u_{W} - 2(1 - v)u_{S} + (1 + v)v_{0} - (1 - 3)v_{W}$$

$$+ (1 - 3v)v_{S} - (1 + v)v_{SW} = 8 \frac{1 - v^{2}}{E} \bar{X}_{0}$$
(2.48)

$$2(3 - v)v_{0} - 2(1 - v)v_{W} - 4v_{S} + (1 + v)u_{0} + (1 - 3v)u_{W}$$
$$- (1 - 3v)u_{S} - (1 + v)u_{SW} = 8 \frac{1 - v^{2}}{E} \overline{Y}_{0}$$

Then for the special case with $v = \frac{1}{4}$ one obtains

$$22u_{0} - 16u_{W} - 6u_{S} + 5v_{O} - v_{W} + v_{S} - 5v_{SW} = \frac{30\overline{X}_{O}}{E}$$

$$22v_{0} - 6v_{W} - 16v_{S} + 5u_{O} + u_{W} - u_{S} - 5u_{SW} = \frac{30\overline{Y}_{O}}{E}$$
(2.49)

Can-

a mertical b

point is ill

Ince again 3

of the resul

Mattions.

punts is h

₹.e

Man print

and southwell

expressions

tegi.ns are

South Brack

to obtain th

Pertain to t

Tiese can t

Consider next a point 0 on a vertical boundary surface. Such a point is illustrated in Figure 2.7. Once again \overline{X}_0 and \overline{Y}_0 denote components of the resultant of boundary tractions. The spacing of mesh points is h for both directions.

The material around the

mesh point 0 includes the northwest

and southwest regions. The

expressions which correspond to these

regions are obtained from the third and

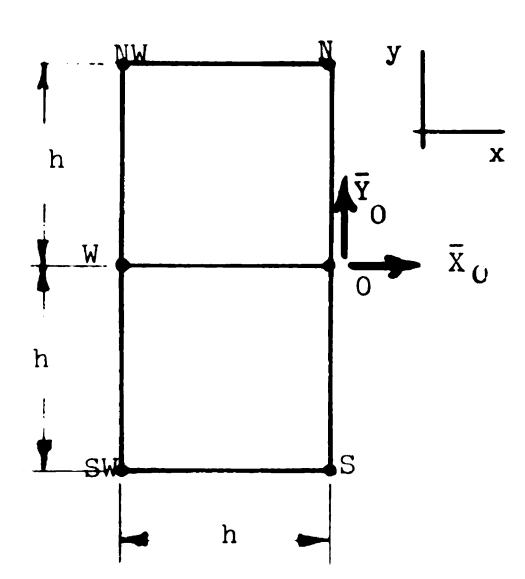


Figure 2.7

Vertical Boundary Point

fourth bracketed terms in equations (2.47). These terms must be added to obtain the left hand sides of finite difference equations which pertain to the boundary point 0. When this is done the result is

$$\frac{E}{1-v^2} \left[8(u_0 - u_W) + 2v(v_N - v_S + v_{NW} - v_{SW}) + 2(1-v)(2u_0 - u_N - u_S) + (1-v)(v_S - v_N + v_{NW} - v_{SW}) \right] = 8\bar{X}_0$$

$$\frac{E}{1-v^2} \left[4(2v_0 - v_N - v_S) + 2v(u_S - u_N + u_{NW} - u_{SW}) + 4(1-v)(v_0 - v_W) + (1-v)(u_N - u_S + u_{NW} + u_{SW}) \right] = 8\bar{Y}_0$$

These can be simplified to some extent and upon doing so one obtains

.3 - ./u₃ -

-:-., **v**g

Tem for cas

-- "j - 11."

...e

in almost e

the preced:

illustrate

actation i

Previously

pomgati 1

o bawas

godepeast

these are

expressi

$$4(3 - v)u_{0} - 8u_{W} - 2(1 - v)(u_{N} + u_{S}) - (1 - 3v)v_{N} + (1 - 3v)v_{S}$$

$$+ (1 + v)v_{NW} - (1 + v)v_{SW} = 8 \frac{1 - v^{2}}{E} \bar{x}_{0}$$

$$4(3 - v)v_{0} - 4(1 - v)v_{W} - 4(v_{N} + v_{S}) + (1 - 3v)u_{N} - (1 - 3v)u_{S}$$

$$+ (1 + v)u_{NW} - (1 + v)u_{SW} = 8 \frac{1 - v^{2}}{E} \bar{x}_{0}$$

$$(2.51)$$

Then for cases where Poisson's ratio is taken to be $\frac{1}{4}$, these become

$$44u_{0} - 32u_{W} - 6(u_{N} + u_{S}) - v_{N} + v_{S} + 5v_{NW} - 5v_{SW} = \frac{30X_{0}}{E}$$

$$44v_{0} - 12v_{W} - 16(v_{N} + v_{S}) + u_{N} - u_{S} + 5u_{NW} - 5u_{SW} = \frac{30\overline{Y}_{0}}{E}$$

$$(2.52)$$

The case of a point 0 on a horizontal boundary surface is treated in almost exactly the same manner as the preceding. This situation is illustrated in Figure 2.8. The notation is identical to that used previously with regard to other boundary points.

In this case, the material around 0 is in the southwest and southeast regions. Corresponding to these are the second and third bracketed expressions of equations (2.47). The

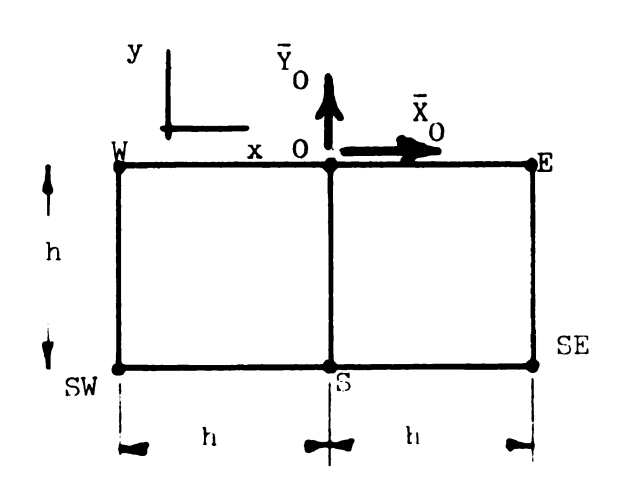
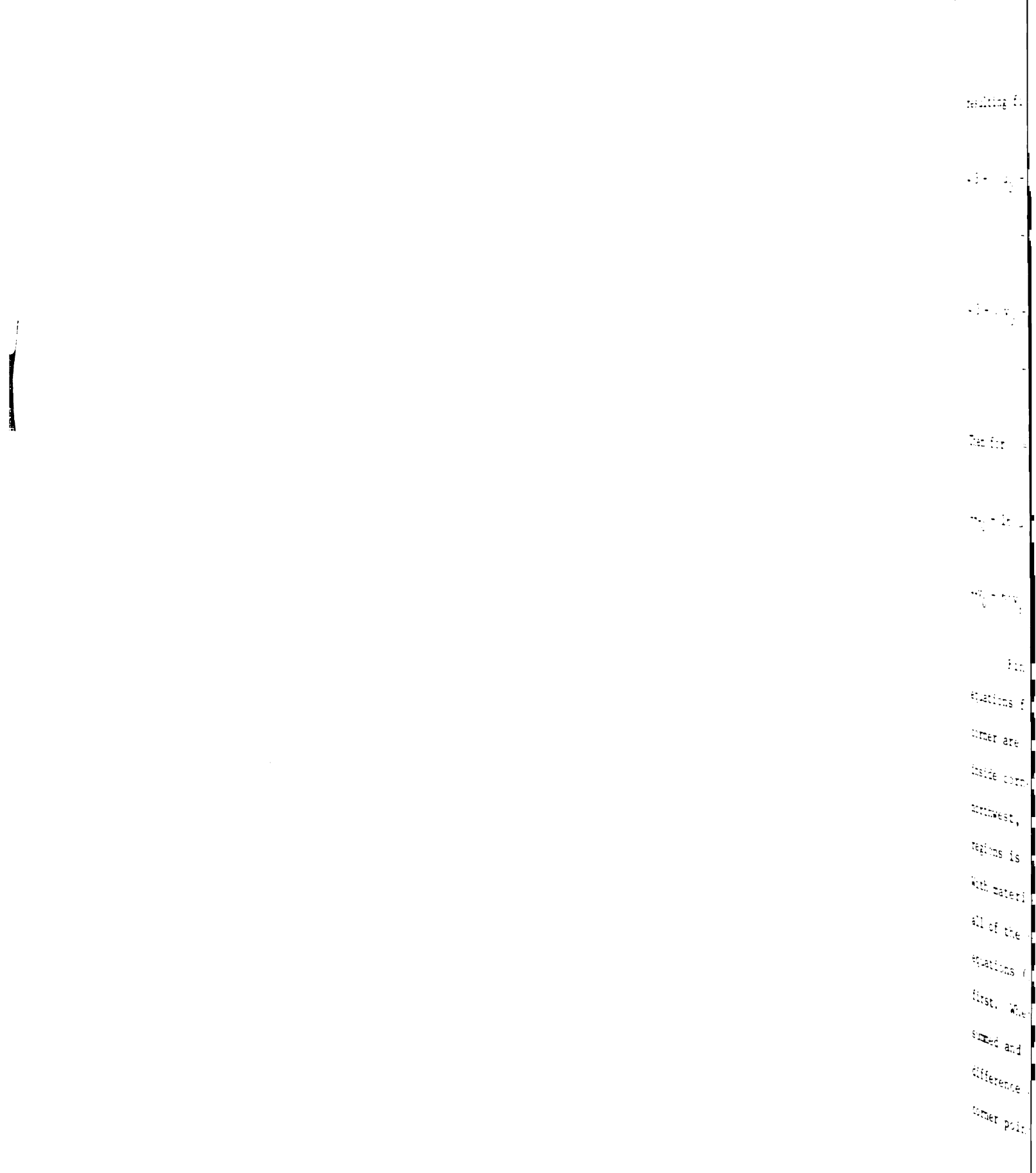


Figure 2.8
Horizontal Boundary
Point



resulting finite difference equations for such boundary points are

$$4(3 - v)u_{0} - 4(u_{E} + u_{W}) - 4(1 - v)u_{S} + (1 - 3v)v_{E} - (1 - 3v)v_{W}$$

$$- (1 + v)v_{SW} + (1 + v)v_{SE} = 8 \frac{1 - v^{2}}{E} \bar{X}_{0}$$

$$(2.53)$$

$$4(3 - v)v_{0} - 2(1 - v)(v_{E} + v_{W}) - 8v_{S} - (1 - 3v)u_{E} + (1 - 3v)u_{W}$$

$$- (1 + v)u_{SW} + (1 + v)u_{SE} = 8 \frac{1 - v^{2}}{E} \bar{Y}_{0}$$

Then for $v = \frac{1}{4}$ equations (2.53) become

$$44u_{0} - 16(u_{E} + u_{W}) - 12u_{S} + v_{E} - v_{W} - 5v_{SW} + 5v_{SE} = \frac{30\overline{X}_{0}}{E}$$

$$44v_{0} - 6(v_{E} + v_{W}) - 32v_{S} - u_{E} + u_{W} - 5u_{SW} + 5u_{SE} = \frac{30\overline{Y}_{0}}{E}$$

$$(2.54)$$

Finally, the finite difference equations for a typical 90° inside corner are discussed below. An inside corner with material in the northwest, southwest, and southeast regions is illustrated in Figure 2.9. With material in these three regions, all of the bracketed expressions in equations (2.47) are used except the first. When these expressions are summed and simplified, finite difference equations for a typical corner point are obtained.

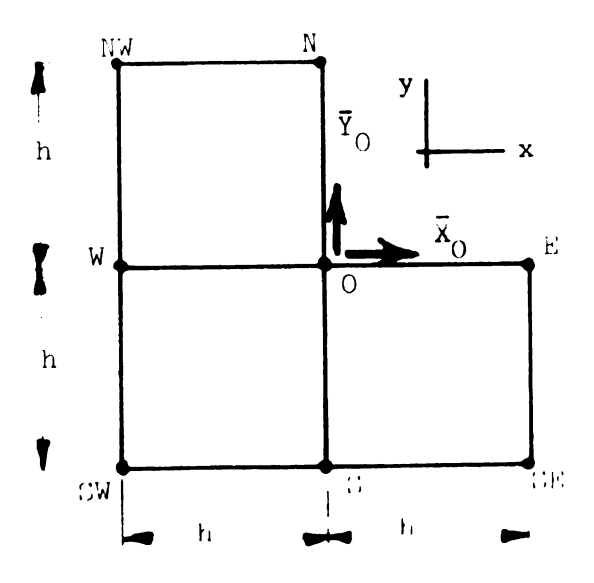


Figure 2.9
Inside Corner Boundary
Point

<u>::] - . .</u>. t3-. v Rep . = 1 u tinit, Partery eath Fil ior inte tesuit: T. K.T. Care they a

Cer. 12.

$$6(3 - v)u_{0} - 4u_{E} - 8u_{W} - 2(1 - v)(u_{N} + 2u_{S}) - (1 + v)v_{0} + (1 - 3v)v_{E}$$

$$- (1 - 3v)v_{N} + (1 + v)(v_{NW} - v_{SW} + v_{SE}) = 8 \frac{1 - v^{2}}{E} \overline{X}_{0}$$

$$(2.55)$$

$$6(3 - v)v_{0} - 2(1 - v)(v_{E} + 2v_{W}) - 4v_{N} - 8v_{S} - (1 + v)u_{0} - (1 - 3v)u_{E}$$

$$+ (1 - 3v)u_{N} + (1 + v)(u_{NW} - u_{SW} + u_{SE}) = 8 \frac{1 - v^{2}}{E} \overline{Y}_{0}$$

When $v = \frac{1}{4}$ these become

$$66u_{0} - 16(u_{E} + 2u_{W}) - 6(u_{N} + 2u_{S}) - 5v_{O} + v_{E} - v_{N}$$

$$+ 5(v_{NW} - v_{SW} + v_{SE}) = \frac{30\overline{X}_{O}}{E}$$

$$66v_{O} - 6(v_{E} + 2v_{W}) - 16(v_{N} + 2v_{S}) - 5u_{O} - u_{E} + u_{N}$$

$$+ 5(u_{NW} - u_{SW} + u_{SE}) = \frac{30\overline{Y}_{O}}{E}$$

$$(2.56)$$

Equations (2.29), (2.48), (2.51), (2.53), and (2.55) form a set of finite difference expressions which can be used to treat a wide variety of plane stress problems. Equations of this type are written for each point in the domain of the physical problem. Equations (2.29) are for interior points whereas the others pertain to boundary points. The resulting system of linear algebraic equations is then solved for the unknown displacements.

These equations are not without restrictions. As formulated, they assume the material to be homogeneous and isotropic. Anisotropy can be considered by reformulating the various equations in terms of

interior ; morgede. is ampasites . attiz lishe - Teal ds With regard 13 Altern

me proper

?:::-4.5

Weiri:

48 convent

Elebent. little e

situati. are car.

شه وب

कार्य_य itores

τ, =,

3=13

ā, e

the proper elastic coefficients, as done for example with regard to interior point equations in section 2.2. The ability to handle non-homogeneous materials in general and specifically the case of material composites was of main interest in this investigation. This can be accomplished by simply allowing for different elastic properties in the 4 regions around an arbitrary point. This idea is discussed further with regard to axially symmetric problems (page 48).

2.9 Alternate Derivation of Difference Equations for Axially Symmetric Problems

As was true for the plane stress (or plane strain) problem, it is convenient to derive finite difference equations for the axially symmetric problem by applying equilibrium considerations to a material element. Boundary conditions can be worked out at the same time with little extra effort.

The axially symmetric problem is generally a three dimensional situation insofar as stress and strain are concerned. Figure 2.10 displays the typical element of volume in cylindrical coordinates. The increments in the coordinates r, θ , and z are taken as h, $\Delta\theta$, and k respectively.

The cylindrical stress components are σ_r , σ_θ , σ_z and τ_{rz} . The shear stresses $\tau_{r\theta}$ and $\tau_{\theta z}$ are identically zero in view of

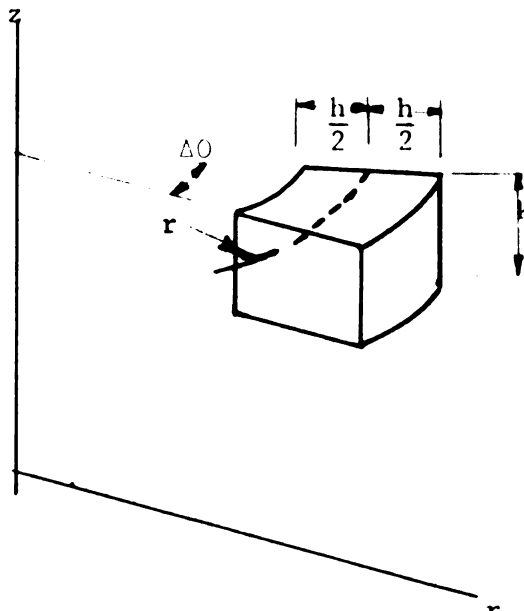


Figure 2.10

Cylindrical Volume

Element

tate compa emstenie : reactly of [illustrati | Por example ∷, is a vi Figure 2.17 manal-awa क्षां उन्हें क्षा are apain The street Wese Te, 31007.51m Stresses Dese a the for ās siyo Est va

the axist of

اهن و جمعرون محورون

the axial symmetry. The development of finite difference equations is quite comparable to the work involved in the plane stress problem. The existence of a third normal stress, namely σ_A , is a major difference.

The stresses are more readily displayed in several illustrations for this case. For example, Figure 2.13, page 35, is a view of the element of Figure 2.10 corresponding to the radial-axial plane. The regions around an arbitrary mesh point 0 are again denoted by northeast, northwest, southwest and southeast. The stress components acting in these regions are superscripted accordingly. The circumferential stresses are displayed in Figure 2.11 These are generally different in the four regions around 0. However, as shown in Figure 2.12 these do not vary with θ .

The stress-strain
law for axially symmetric
problems was presented in
section 2.4. It is repeated
here for the isotropic case.

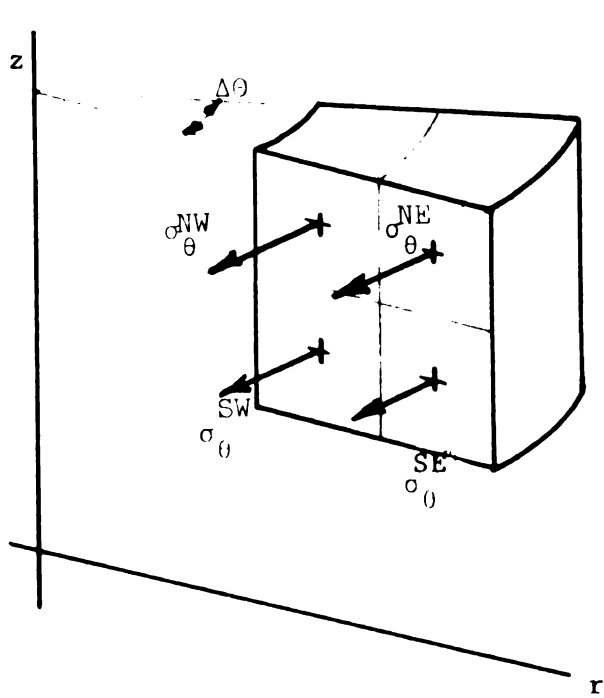


Figure 2.11
Circumferential Stresses

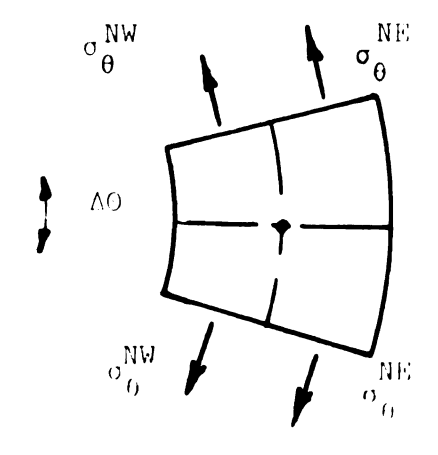


Figure 2.12
Circumferential Stresses

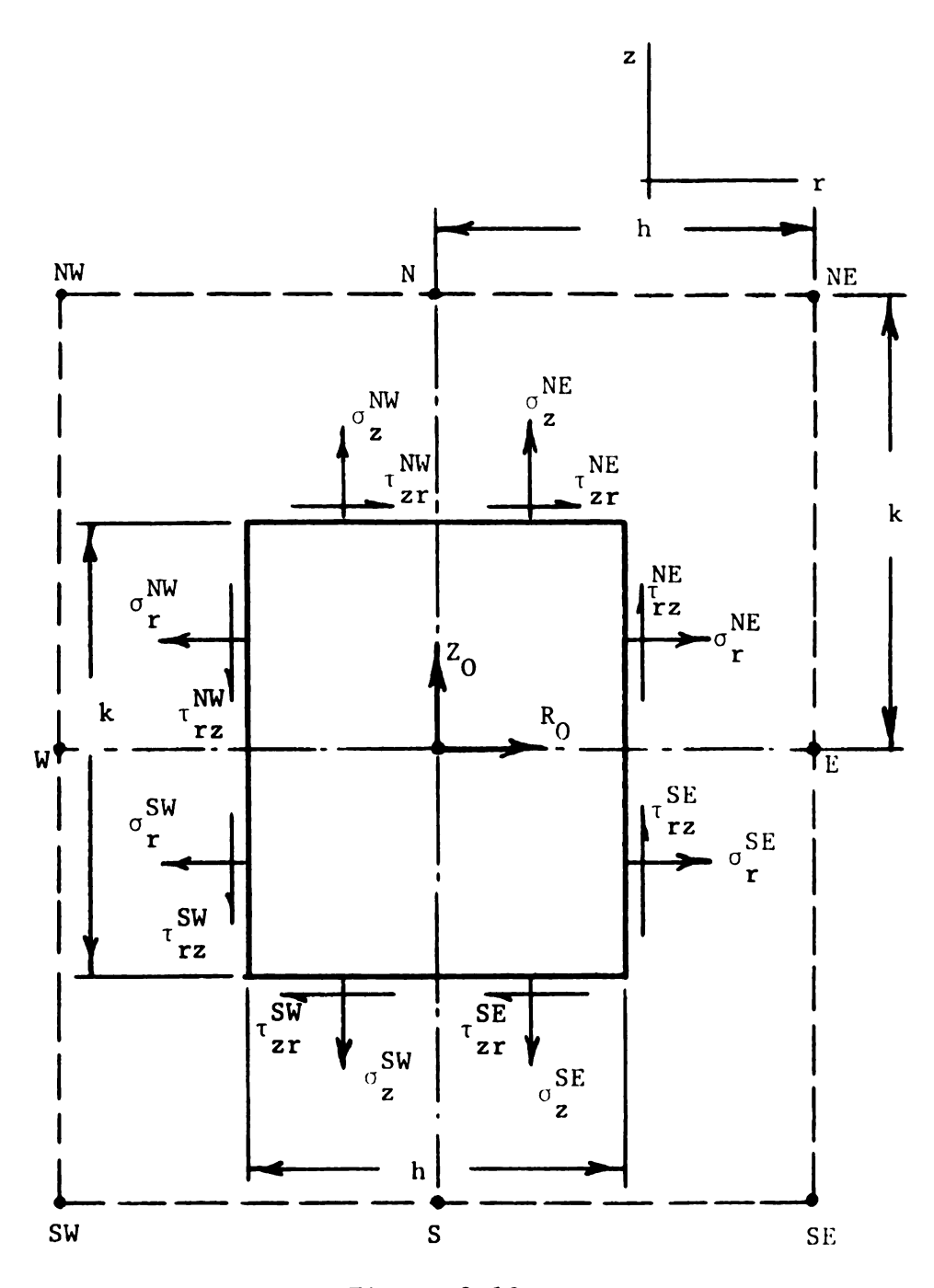


Figure 2.13

Material Region Around a Mesh Point and Associated Cylindrical Stresses and Body Forces

$$\sigma_{\mathbf{r}} = \frac{E}{(1+\nu)(1-2\nu)} [(1-\nu)\varepsilon_{\mathbf{r}} + \nu(\varepsilon_{\theta} + \varepsilon_{\mathbf{z}})]$$

$$\sigma_{\theta} = \frac{E}{(1+\nu)(1-2\nu)} [(1-\nu)\varepsilon_{\theta} + \nu(\varepsilon_{\mathbf{z}} + \varepsilon_{\mathbf{r}})]$$

$$\sigma_{\mathbf{z}} = \frac{E}{(1+\nu)(1-2\nu)} [(1-\nu)\varepsilon_{\mathbf{z}} + \nu(\varepsilon_{\mathbf{r}} + \varepsilon_{\theta})]$$

$$\tau_{\mathbf{rz}} = \frac{E}{2(1+\nu)} \gamma_{\mathbf{rz}}$$
(2.57)

Introducing the strain-displacement relationships, (2.5), these become

$$\sigma_{\mathbf{r}} = \frac{E}{(1+v)(1-2v)} \left[(1-v) \frac{\partial u}{\partial r} + v \frac{u}{r} + v \frac{\partial w}{\partial z} \right]$$

$$\sigma_{\theta} = \frac{E}{(1+v)(1-2v)} \left[(1-v) \frac{u}{r} + v \frac{\partial u}{\partial r} + v \frac{\partial w}{\partial z} \right]$$

$$\sigma_{\mathbf{z}} = \frac{E}{(1+v)(1-2v)} \left[(1-v) \frac{\partial w}{\partial z} + v \frac{\partial u}{\partial r} + v \frac{u}{r} \right]$$

$$\tau_{\mathbf{rz}} = \frac{E}{2(1+v)} \left[\frac{\partial w}{\partial r} + \frac{\partial u}{\partial z} \right]$$

$$\tau_{\mathbf{zr}} = \frac{E}{2(1+v)} \left[\frac{\partial u}{\partial z} + \frac{\partial w}{\partial r} \right]$$

Proceeding in much the same way as was done for the plane stress problem, the following approximations for stresses are used:

£: Æ . Œ .º⊑ ::: ii. §:<u>t</u> tas :as Į; ેંુડુ.

$$\sigma_{\mathbf{r}}^{NE} = \frac{E}{(1+\nu)(1-2\nu)} \left[(1-\nu) \frac{u_{E} - u_{O}}{h} + \nu \frac{u_{E} + u_{O}}{2(r_{O} + \frac{h}{2})} + \nu \frac{w_{N} - w_{O} + w_{NE} - w_{E}}{2k} \right]$$

$$\sigma_{\theta}^{NE} = \frac{E}{(1+\nu)(1-2\nu)} \left[(1-\nu) \frac{u_0}{r_0} + \nu \frac{u_E - u_0}{h} + \nu \frac{w_N - w_0}{k} \right]$$
 (2.59)

$$\sigma_{\mathbf{z}}^{\text{NE}} = \frac{E}{(1+\nu)(1-2\nu)} \left[(1-\nu) \frac{w_{\text{N}}-w_{\text{O}}}{k} + \nu \frac{u_{\text{NE}}-u_{\text{N}}+u_{\text{E}}-u_{\text{O}}}{2h} \right]$$

$$+ v \frac{u_{NE} + u_{N} + u_{E} + u_{O}}{4(r_{O} + \frac{h}{4})}$$

$$\tau_{rz}^{NE} = \frac{E}{2(1 + v)} \left[\frac{w_E - w_O}{h} + \frac{u_{NE} - u_E + u_N - u_O}{2k} \right]$$

$$\tau_{zr}^{NE} = \frac{E}{2(1+v)} \left[\frac{u_N - u_O}{k} + \frac{w_{NE} - w_N + w_E - w_O}{2h} \right]$$

Similar sets of stresses exist for the northwest, southwest, and southeast regions.

The pertinent equilibrium equations for the axially symmetric case are

$$\Sigma F_{\mathbf{r}} = 0$$

$$\Sigma F_{\mathbf{z}} = 0 \tag{2.60}$$

It is significant that the σ_{θ} stresses have a radial component and hence must be accounted for in the radial force equation. In this connection,

me approx.

XE + SE r r

Σ . S. z.

De quanti

* 1 · ...

Nest print

into equat

· 201 + .

(1+.)

11

the approximation $\sin \frac{\Delta \theta}{2} \simeq \frac{\Delta \theta}{2}$ is used.

$$(\sigma_{\mathbf{r}}^{NE} + \sigma_{\mathbf{r}}^{SE}) \frac{k}{2} (\mathbf{r}_{0} + \frac{h}{2}) \Delta \theta - (\sigma_{\mathbf{r}}^{NW} + \sigma_{\mathbf{r}}^{SW}) \frac{k}{2} (\mathbf{r}_{0} - \frac{h}{2}) \Delta \theta$$

$$+ (\tau_{\mathbf{zr}}^{NE} - \tau_{\mathbf{zr}}^{SE}) \frac{h}{2} (\mathbf{r}_{0} + \frac{h}{4}) \Delta \theta + (\tau_{\mathbf{zr}}^{NW} - \tau_{\mathbf{zr}}^{SW}) \frac{h}{2} (\mathbf{r}_{0} - \frac{h}{4}) \Delta \theta$$

$$- 2(\sigma_{\theta}^{NE} + \sigma_{\theta}^{NW} + \sigma_{\theta}^{SW} + \sigma_{\theta}^{SE}) \frac{h}{2} \frac{k}{2} \frac{\Delta \theta}{2} + R_{0} \mathbf{r}_{0} \Delta \theta \mathbf{h} \mathbf{k} = 0$$

$$(\sigma_{\mathbf{z}}^{NE} - \sigma_{\mathbf{z}}^{SE}) \frac{h}{2} (\mathbf{r}_{0} + \frac{h}{4}) \Delta \theta + (\sigma_{\mathbf{z}}^{NW} - \sigma_{\mathbf{z}}^{SW}) \frac{h}{2} (\mathbf{r}_{0} - \frac{h}{4}) \Delta \theta$$

$$+ (\tau_{\mathbf{rz}}^{NE} + \tau_{\mathbf{rz}}^{SE}) \frac{k}{2} (\mathbf{r}_{0} + \frac{h}{2}) \Delta \theta - (\tau_{\mathbf{rz}}^{NW} + \tau_{\mathbf{rz}}^{SW}) \frac{k}{2} (\mathbf{r}_{0} - \frac{h}{2}) \Delta \theta + Z_{0} \mathbf{r}_{0}^{\Delta} \theta h k = 0$$

$$(2.61)$$

The quantities R_0 and Z_0 are body force components assumed to act at the mesh point 0. Introducing the stress approximations of the form (2.59) into equations (2.61) yields

$$\begin{split} \frac{E}{(1+\nu)(1-2\nu)} & \left[(1-\nu) \, \frac{u_E - u_O}{h} + \nu \, \frac{u_E + u_O}{2(r_O + \frac{h}{2})} \right] \\ & + \nu \, \frac{w_N - w_O + w_{NE} - w_E}{2k} \, \left] \frac{k}{2} \, \left(r_O + \frac{h}{2} \right) \\ & + \frac{E}{2(1+\nu)} \left[\frac{u_N - u_O}{k} + \frac{w_{NE} - w_N + w_E - w_O}{2h} \, \right] \, \frac{h}{2} \, \left(r_O + \frac{h}{4} \right) \\ & - \frac{E}{(1+\nu)(1-2\nu)} \left[\, (1-\nu) \, \frac{u_O}{r_O} + \nu \, \frac{u_E - u_O}{h} + \nu \, \frac{w_N - w_O}{k} \, \right] \frac{hk}{4} \\ & - \frac{E}{(1+\nu)(1-2\nu)} \left[\, (1-\nu) \, \frac{u_O - u_W}{h} + \nu \, \frac{u_O + u_W}{2(r_O - \frac{h}{2})} \right] \\ & + \nu \, \frac{w_N - w_O + w_{NW} - w_W}{2k} \, \left[\frac{k}{2} \, \left(r_O - \frac{h}{2} \right) \right] \end{split}$$

· 11 · 1

E 271 +

$$\begin{split} &+\frac{E}{2(1+\nu)}\left[\frac{u_{N}-u_{0}}{k}+\frac{w_{0}-w_{W}+w_{N}-w_{NW}}{2h}\right]\frac{h}{2}\left(r_{0}-\frac{h}{4}\right) \\ &-\frac{E}{(1+\nu)\left(1-2\nu\right)}\left[\left(1-\nu\right)\frac{u_{0}}{r_{0}}+\nu\frac{u_{0}-u_{W}}{h}+\nu\frac{w_{N}-w_{0}}{k}\right]\frac{hk}{4} \\ &-\frac{E}{(1+\nu)\left(1-2\nu\right)}\left[\left(1-\nu\right)\frac{u_{0}-u_{W}}{h}+\nu\frac{u_{0}+u_{W}}{2\left(r_{0}-\frac{h}{2}\right)}\right] \\ &+\nu\frac{w_{0}-w_{S}+v_{W}-w_{SW}}{2k}\right]\frac{k}{2}\left(r_{0}-\frac{h}{2}\right) \\ &-\frac{E}{2(1+\nu)}\left[\frac{u_{0}-u_{S}}{k}+\frac{w_{0}-w_{W}+w_{S}-w_{SW}}{2h}\right]\frac{h}{2}\left(r_{0}-\frac{h}{4}\right) \\ &-\frac{E}{(1+\nu)\left(1-2\nu\right)}\left[\left(1-\nu\right)\frac{u_{0}}{r_{0}}+\nu\frac{u_{0}-u_{W}}{h}+\nu\frac{w_{0}-w_{S}}{k}\right]\frac{hk}{4} \\ &+\frac{E}{(1+\nu)\left(1-2\nu\right)}\left[\left(1-\nu\right)\frac{u_{E}-u_{0}}{h}+\nu\frac{u_{E}+u_{0}}{2\left(r_{0}+\frac{h}{2}\right)} \\ &+\nu\frac{w_{0}-w_{S}+w_{E}-w_{SE}}{2k}\right]\frac{k}{2}\left(r_{0}+\frac{h}{2}\right) \\ &-\frac{E}{2\left(1+\nu\right)}\left[\frac{u_{0}-u_{S}}{k}+\frac{w_{E}-w_{0}+w_{SE}-w_{S}}{2h}\right]\frac{h}{2}\left(r_{0}+\frac{h}{4}\right) \\ &-\frac{E}{(1+\nu)\left(1-2\nu\right)}\left[\left(1-\nu\right)\frac{u_{0}}{r_{0}}+\nu\frac{u_{E}-u_{0}}{h}+\nu\frac{w_{0}-w_{S}}{k}\right]\frac{hk}{4}+R_{0}r_{0}hk=0 \end{split}$$

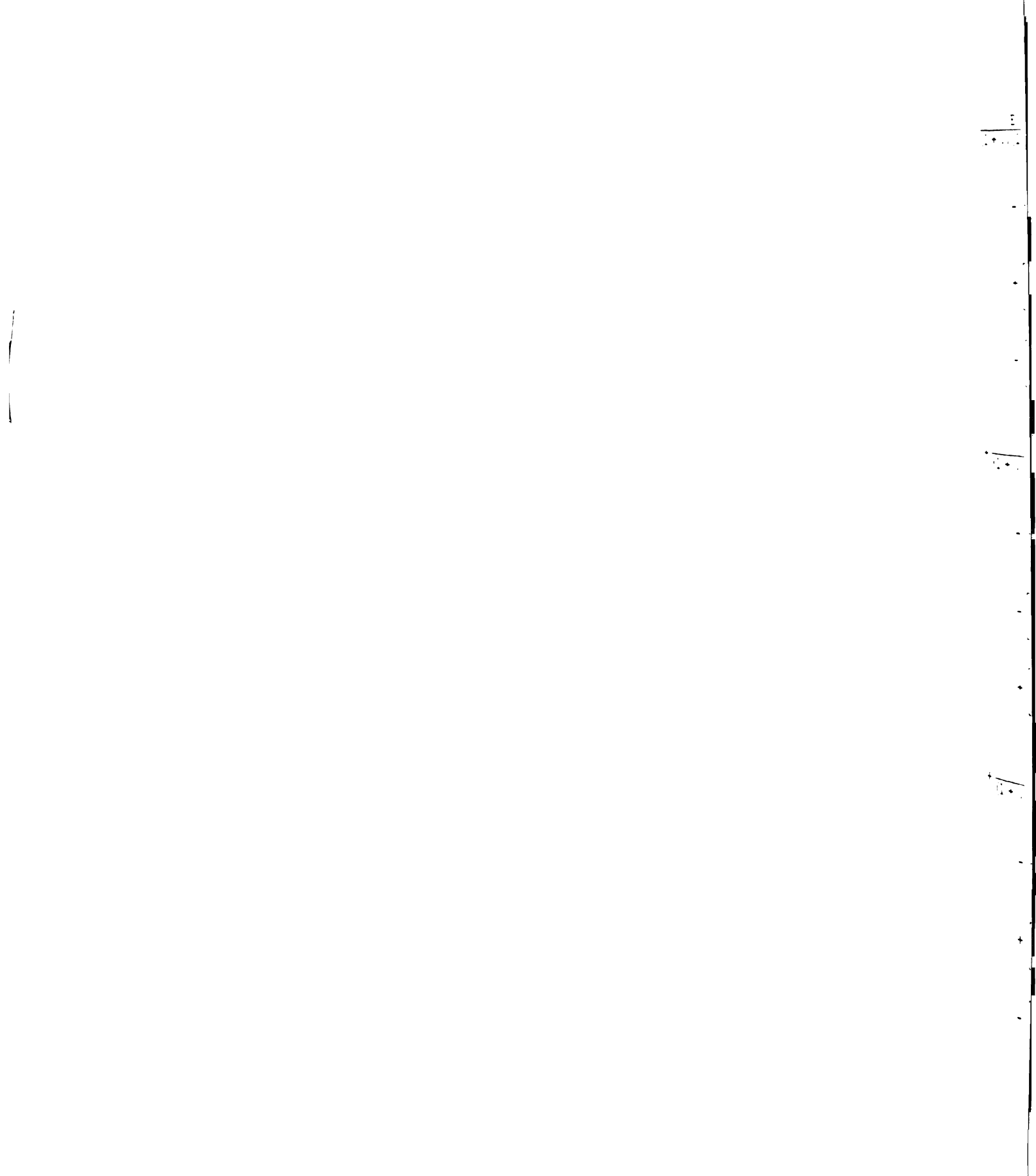
$$\frac{E}{(1+\nu)(1-2\nu)} \left[(1-\nu) \frac{w_N - w_O}{k} + \nu \frac{u_{NE} - u_N + u_E - u_O}{2h} + \nu \frac{u_{NE} + u_N + u_E + u_O}{4(r_O + \frac{h}{4})} \right] \frac{h}{2} (r_O + \frac{h}{4})$$

• :::• • ----- <u>:</u> • • : - -

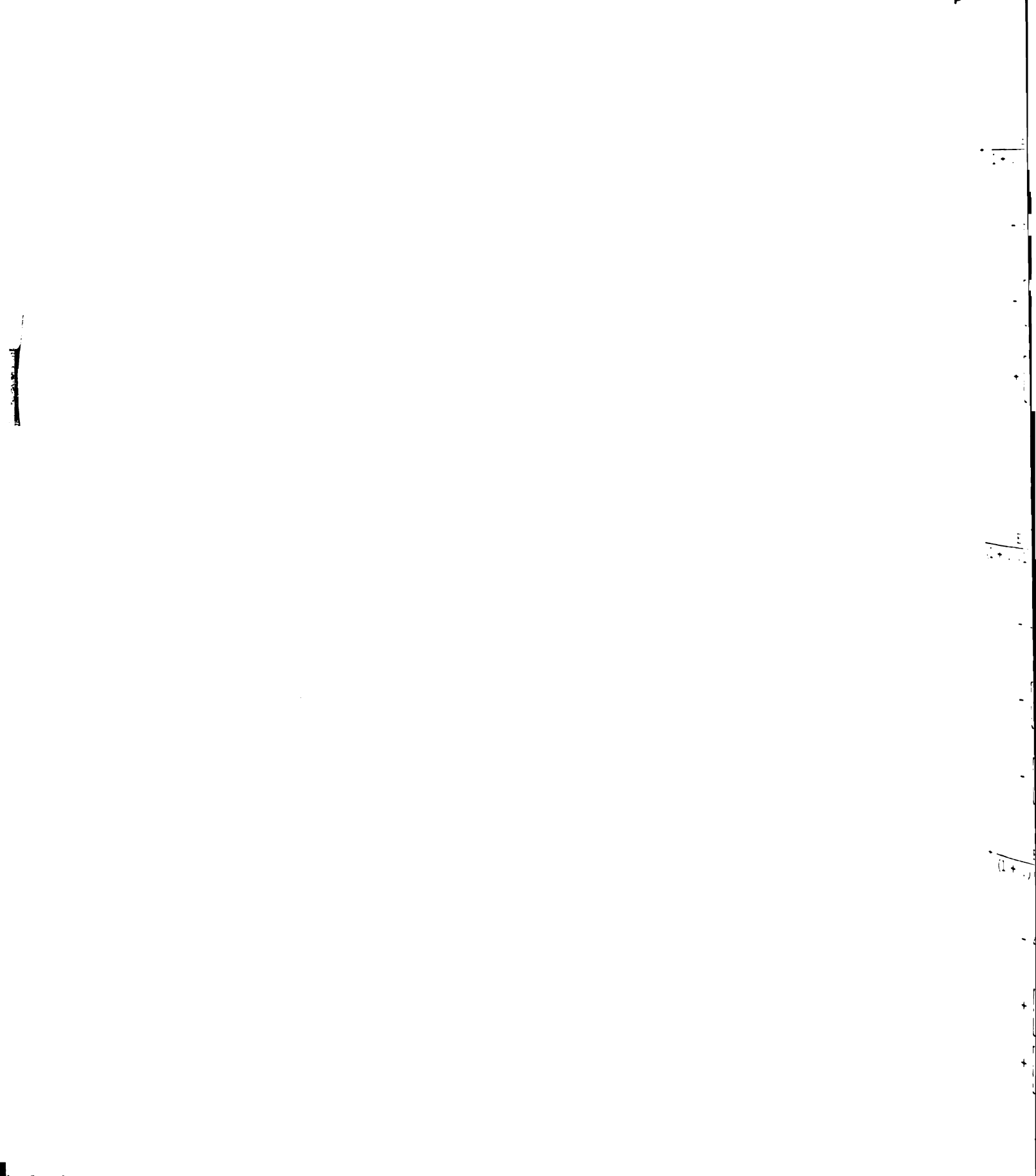
$$\begin{split} &+\frac{E}{2(1+\nu)} \left[\frac{w_E - w_O}{h} + \frac{u_{NE} - u_E + u_N - u_O}{2k} \right] \frac{k}{2} (r_O + \frac{h}{2}) \\ &+ \frac{E}{(1+\nu)(1-2\nu)} \left[(1-\nu) \frac{w_N - w_O}{k} + \nu \frac{u_N - u_{NW} + u_O - u_W}{2h} \right. \\ &+ \nu \frac{u_{NW} + u_N + u_W + u_O}{4(r_O - \frac{h}{4})} \right] \frac{h}{2} (r_O - \frac{h}{4}) \\ &- \frac{E}{2(1+\nu)} \left[\frac{w_O - w_W}{h} + \frac{u_N - u_O + u_{NW} - u_W}{2k} \right] \frac{k}{2} (r_O - \frac{h}{2}) \\ &- \frac{E}{(1+\nu)(1-2\nu)} \left[(1-\nu) \frac{w_O - w_S}{k} + \nu \frac{u_O - u_W + u_S - u_{SW}}{2h} \right. \\ &+ \nu \frac{u_{SW} + u_S + u_W + u_O}{4(r_O - \frac{h}{4})} \right] \frac{h}{2} (r_O - \frac{h}{4}) \\ &- \frac{E}{(1+\nu)(1-2\nu)} \left[(1-\nu) \frac{w_O - w_S}{k} + \nu \frac{u_E - u_O + u_{SE} - u_S}{2h} \right. \\ &+ \frac{u_{SE} + u_S + u_E + u_O}{4(r_O + \frac{h}{4})} \right] \frac{h}{2} (r_O + \frac{h}{4}) \\ &+ \frac{E}{2(1+\nu)} \left[\frac{w_E - w_O}{h} + \frac{u_E - u_{SE} + u_O - u_S}{2k} \right] \frac{k}{2} (r_O + \frac{h}{2}) + z_O r_O hk = 0 \end{split}$$

Once again the terms corresponding to the 4 regions around 0 have been kept together to facilitate the consideration of boundary conditions and the governing equations for fiber reinforced composites.

With k = h and a considerable amount of rearranging, equations (2.62) can be expressed in the following way:



$$\begin{split} &\frac{E}{(1+\nu)(1-2\nu)} \left\{ \left[8(3-4\nu) + 2(5-14\nu) \, \frac{h}{r_0} + 8(1-\nu) \, \frac{h^2}{r_0^2} \right] u_0 \right. \\ &- 8(1-\nu)(2+\frac{h}{r_0}) \, u_E - 2(1-2\nu)(4+\frac{h}{r_0}) \, u_N \\ &+ \left[4+(1-6\nu) \, \frac{h}{r_0} \right] w_0 - \left[4+(1+2\nu) \, \frac{h}{r_0} \right] w_{NE} \\ &- \left[4(1-4\nu) + (1-6\nu) \, \frac{h}{r_0} \right] w_E + \left[4(1-4\nu) + (1+2\nu) \, \frac{h}{r_0} \right] w_N \right\} \\ &+ \frac{E}{(1+\nu)(1-2\nu)} \left\{ \left[8(3-4\nu) - 2(5-14\nu) \, \frac{h}{r_0} + 8(1-\nu) \, \frac{h^2}{r_0^2} \right] u_0 \\ &- 8(1-\nu)(2-\frac{h}{r_0}) \, u_W - 2(1-2\nu)(4-\frac{h}{r_0}) \, u_N \\ &- \left[4-(1-6\nu) \, \frac{h}{r_0} \right] w_0 + \left[4-(1+2\nu) \, \frac{h}{r_0} \right] w_{NW} \\ &+ \left[4(1-4\nu) - (1-6\nu) \, \frac{h}{r_0} \right] w_W - \left[4(1-4\nu) - (1+2\nu) \, \frac{h}{r_0} \right] w_N \right\} \\ &+ \frac{E}{(1+\nu)(1-2\nu)} \left\{ \left[8(3-4\nu) - 2(5-14\nu) \, \frac{h}{r_0} + 8(1-\nu) \, \frac{h^2}{r_0^2} \right] u_0 \\ &- 8(1-\nu)(2-\frac{h}{r_0}) \, u_W - 2(1-2\nu)(4-\frac{h}{r_0}) \, u_S \\ &+ \left[4-(1-6\nu) \, \frac{h}{r_0} \right] w_0 - \left[4-(1+2\nu) \, \frac{h}{r_0} \right] w_{SW} \\ &- \left[4(1-4\nu) - (1-6\nu) \, \frac{h}{r_0} \right] w_W + \left[4(1-4\nu) - (1+2\nu) \, \frac{h}{r_0} \right] w_S \right\} \end{split}$$



$$+ \frac{E}{(1+v)(1-2v)} \left\{ \left[8(3-4v) + 2(5-14v) \frac{h}{r_0} + 8(1-v) \frac{h^2}{r_0^2} \right] u_0 \right.$$

$$- 8(1-v)(2+\frac{h}{r_0}) u_E - 2(1-2v)(4+\frac{h}{r_0}) u_S$$

$$- \left[(4+(1-6v) \frac{h}{r_0} \right] w_0 + \left[4+(1+2v) \frac{h}{r_0} \right] w_{SE}$$

$$+ \left[4(1-4v) + (1-6v) \frac{h}{r_0} \right] w_E - \left[4(1-4v) + (1+2v) \frac{h}{r_0} \right] w_S \right\}$$

$$= 32h^2 R_0$$

$$(2.63)$$

$$\begin{split} \frac{E}{(1+\nu)(1-2\nu)} & \left\{ \left[8(3-4\nu) + 4(2-3\nu) \, \frac{h}{r_0} \right] w_0 - 4(1-2\nu)(2+\frac{h}{r_0}) \, w_E \right. \\ & \left. - 4(1-\nu)(4+\frac{h}{r_0}) \, w_N + \left[4+2(1-3\nu) \, \frac{h}{r_0} \right] u_0 \right. \\ & \left. - \left[4+2(1+\nu) \, \frac{h}{r_0} \right] u_{NE} + \left[4(1-4\nu) + 2(1-5\nu) \, \frac{h}{r_0} \right] \, u_E \right. \\ & \left. - \left[4(1-4\nu) + 2(1-\nu) \, \frac{h}{r_0} \right] u_N \right\} \\ & + \frac{E}{(1+\nu)(1-2\nu)} \left\{ \left[8(3-4\nu) - 4(2-3\nu) \, \frac{h}{r_0} \right] w_0 - 4(1-2\nu)(2-\frac{h}{r_0}) \, w_W \right. \\ & \left. - 4(1-\nu)(4-\frac{h}{r_0}) w_N - \left[4-2(1-3\nu) \, \frac{h}{r_0} \right] u_0 \right. \\ & \left. + \left[4-2(1+\nu) \, \frac{h}{r_0} \right] u_{NW} - \left[4(1-4\nu) - 2(1-5\nu) \, \frac{h}{r_0} \right] u_W \\ & \left. + \left[4(1-4\nu) - 2(1-\nu) \, \frac{h}{r_0} \right] u_N \right\} \end{split}$$

• : • ., • icr an or: of equation

$$\begin{split} &+ \frac{E}{(1+\nu)(1-2\nu)} \left\{ \left[8(3-4\nu) - 4(2-3\nu) \, \frac{h}{r_0} \right] w_0 - 4(1-2\nu)(2-\frac{h}{r_0}) \, w_W \right. \\ &- 4(1-\nu)(4-\frac{h}{r_0}) \, w_S + \left[4-2(1-\nu) \, \frac{h}{r_0} \right] u_0 \\ &- \left[4-2(1+\nu) \, \frac{h}{r_0} \right] u_{SW} + \left[4(1-4\nu) - 2(1-5\nu) \, \frac{h}{r_0} \right] u_W \\ &- \left[4(1-\nu) - 2(1-\nu) \, \frac{h}{r_0} \right] u_S \right\} \\ &+ \frac{E}{(1+\nu)(1-2\nu)} \left\{ \left[8(3-4\nu) + 4(2-3\nu) \, \frac{h}{r_0} \right] w_0 - 4(1-2\nu)(2+\frac{h}{r_0}) \, w_E \right. \\ &- 4(1-\nu)(4+\frac{h}{r_0}) \, w_S - \left[4+2(1-3\nu) \, \frac{h}{r_0} \right] u_0 \\ &+ \left[4+2(1+\nu) \, \frac{h}{r_0} \right] u_{SE} - \left[4(1-4\nu) + 2(1-5\nu) \, \frac{h}{r_0} \right] u_E \\ &+ \left[4(1-4\nu) + 2(1-\nu) \, \frac{h}{r_0} \right] u_S \right\} = 32h^2 Z_0 \end{split}$$

For an ordinary mesh point the bracketed terms on the right hand sides of equations (2.63) can be added to obtain a more simplified form.

$$32\left[\left(3-4\nu\right)+\left(1-\nu\right)\frac{h^{2}}{r_{0}^{2}}\right]u_{0}-16\left(1-\nu\right)\left(2+\frac{h}{r_{0}}\right)u_{E}-16\left(1-\nu\right)\left(2-\frac{h}{r_{0}}\right)u_{W}$$

$$-16\left(1-2\nu\right)\left(u_{N}+u_{S}\right)+2\left(1+2\nu\right)\frac{h}{r_{0}}\left(w_{N}-w_{S}\right)-\left[4+\left(1+2\nu\right)\frac{h}{r_{0}}\right]w_{NE}$$

$$+\left[4-\left(1+2\nu\right)\frac{h}{r_{0}}\right]w_{NW}-\left[4-\left(1+2\nu\right)\frac{h}{r_{0}}\right]w_{SW}$$

$$+\left[4+\left(1+2\nu\right)\frac{h}{r_{0}}\right]w_{SE}=32\frac{\left(1+\nu\right)\left(1-2\nu\right)}{E}h^{2}R_{0} \qquad (2.65)$$

11.3 - 4.

-32+1

ί.

Er a part

3 - , 3

15w₀ - (2

1.7 it be

Enveyer,

$$32(3 - 4v) w_{0} - 8(1 - 2v)(2 + \frac{h}{r_{0}}) w_{E} - 8(1 - 2v)(2 - \frac{h}{r_{0}}) w_{W}$$

$$-32(1 - v)(w_{N} + w_{S}) - 4(1 - v) \frac{h}{r_{0}} (u_{N} - u_{S}) - \left[4 + 2(1 + v)\frac{h}{r_{0}}\right] u_{NE}$$

$$+ \left[4 - 2(1 + v) \frac{h}{r_{0}}\right] u_{NW} - \left[4 - 2(1 + v) \frac{h}{r_{0}}\right] u_{SW}$$

$$+ \left[4 + 2(1 + v) \frac{h}{r_{0}}\right] u_{SE} = 32 \frac{(1 + v)(1 - 2v)}{E} h^{2} Z_{0}$$

For a particular choice of Poisson's ratio, say $v = \frac{1}{4}$, one obtains

$$(16 + 6 \frac{h^2}{r_0^2}) u_0 - 3(2 + \frac{h}{r_0}) u_E - 3(2 - \frac{h}{r_0}) u_W - 2(u_N + u_S)$$

$$+ \frac{3}{4} \frac{h}{r_0} (w_N - w_S) - (1 + \frac{3}{8} \frac{h}{r_0}) w_{NE} + (1 - \frac{3}{8} \frac{h}{r_0}) w_{NW}$$

$$- (1 - \frac{3}{8} \frac{h}{r_0}) w_{SW} + (1 + \frac{3}{8} \frac{h}{r_0}) w_{SE} = 5 \frac{h^2}{E} R_0$$
(2.66)

$$16w_{0} - (2 + \frac{h}{r_{0}}) w_{E} - (2 - \frac{h}{r_{0}}) w_{W} - 6(w_{N} + w_{S})$$

$$- \frac{3}{4} \frac{h}{r_{0}} (u_{N} - u_{S}) - (1 + \frac{5}{8} \frac{h}{r_{0}}) u_{NE} + (1 - \frac{5}{8} \frac{h}{r_{0}}) u_{NW}$$

$$- (1 - \frac{5}{8} \frac{h}{r_{0}}) u_{SW} + (1 + \frac{5}{8} \frac{h}{r_{0}}) u_{SE} = 5 \frac{h^{2}}{E} Z_{0}$$

Now comparing these equations with equations (2.40) in section

2.7 it becomes apparent that the two sets of equations are not identical.

However, if one makes the additional assumptions that

equations

Stainer Mis, No.

slightly equally

the grant

ā lērtā

tions.

bowdan

elasti Puter

วัญ_{นักตัด}

gra<u>t</u>,

ior

Priat

¥1.(0

$$u_N = \frac{u_{NE} + u_{NW}}{2}$$

$$u_S = \frac{u_{SE} + u_{SW}}{2}$$

$$w_N = \frac{w_{NE} + w_{NW}}{2}$$

$$w_S = \frac{w_{SE} + w_{SW}}{2}$$

equations (2.66) can be shown to be identical to the previous results obtained from the equations of elasticity. It is unnecessary to do this, however, since equations (2.65) or (2.66) simply represent a slightly different set of finite difference equations which should give equally good results. These equations have been used exclusively throughout this investigation.

In the previous section which dealt with plane stress problems, a certain amount of detail was included with regard to boundary conditions. It is possible to do much the same thing here for points on boundary surfaces of the solid under consideration. However, as these equations have become more involved, it is advantageous to let the computer do the calculations rather than derive explicit expressions for boundary points. Thus equations (2.63) or their equivalent are programmed with each bracketed term a subroutine. Equations for the interior and boundary points of the problem are generated by calling appropriate subroutines. For example, for a point on an outside corner, only the first bracketed terms are required in the two equations (2.63) to form the left hand side of such relationships. Thus only the subroutine which computes the coefficients corresponding to the first bracketed

ಚಿತ್ರಕ್ಕು 1211.111 Matrele. ti trest fint in atizi a 522 **a** 1. \$0.000 dilleten. i print i DE 1 5.1 itove but the 4 dis-Mest part io e the alter

and bound

Points of

expressed

exercise

terms would be called. In the case of a typical mesh point, each of 4 subroutines must be called to generate the coefficients since all bracketed terms of equations (2.63) are involved.

In a like manner, one is able to treat composite materials. As shown in Figure 2.14, the region around a particular mesh point in such a composite may consist of two different materials. Finite difference equations for such a point are obtained by calling the 4 subroutines discussed above but in this case using the appropriate elastic constants for the 4 different regions around the mesh point 0.

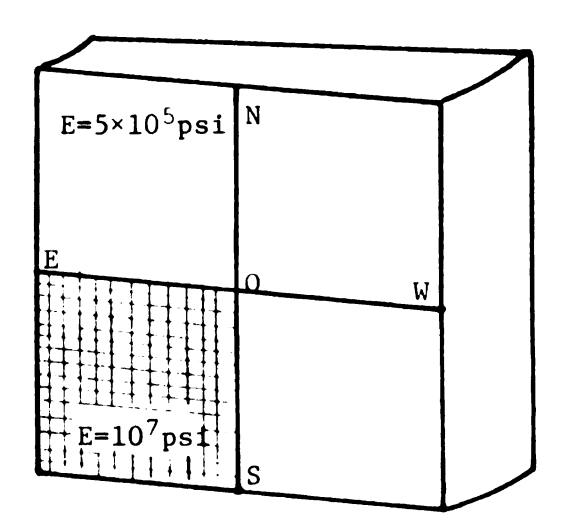


Figure 2.14
Composite Material Region

2.10 Finite Difference Stresses

As discussed earlier, the finite difference equations derived by the alternate method were used exclusively in this work. The interior and boundary point equations form a system of equations which is solved by standard numerical procedures to yield the displacements for the mesh points of the problem.

The stresses corresponding to this alternate procedure are expressed by equations (2.42) through (2.45) for plane stress problems and equations (2.59) for axially symmetric problems. It is necessary to exercise care in the interpretation of these stresses. The reason for

mis rest

given Teg.

mi • ii

umeşir.

pertains

test point

tie tater.

15 817...;

fir part

min 1,

zi the y

Hiller :

the test

the mater

Sat this

iut perha

this rests with the fact that a given region is generally associated with 4 different sets of stresses corresponding to the fact that it pertains to as many as 4 different mesh points. Thus for example, the material region in Figure 2.15 is simultaneously the NE region for point 1, the NW region for point 2, the SW corner for point 3, and the SE corner for point 4.

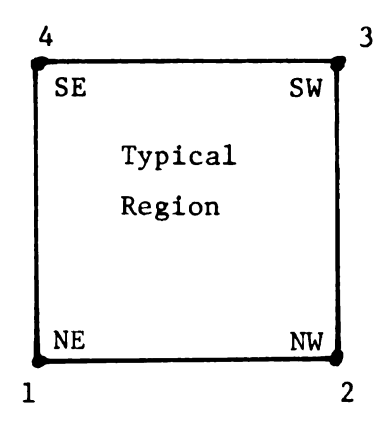


Figure 2.15
Material Region

It is, therefore, suggested that a set of mesh point stresses be defined in terms of these material element stresses. For this purpose, the mesh point stresses are assumed to be the average of the stresses in the material regions around the point. Previous experience suggests that this averaging technique would give good results at interior points but perhaps less satisfactory results for boundary points.

j.: <u>Geor</u>

inteilre.

malacing

fizite pur

finite na

13517451

*:::.s.

in of e

Wiel is

tiz eje

¥: 35

\$\$ c.=

ié ié .

are: ye

€eqe_{ta}

if the

t_{esed}

^{३०} ्द

ie:

III. FINITE ELEMENT METHOD

3.1 General Remarks

Finite element methods represent a large class of approximate procedures in structural mechanics. Basically, these methods involve replacing the actual structure or continua by a model consisting of a finite number of carefully selected elements which are connected at a finite number of points. The approximation is thus a physical one in constrast to the mathematical approximations of finite difference methods.

Finite element methods can be classified according to the behavior of elements in the model. A compatible element or a displacement model is one satisfying compatibility but not equilibrium. An equilibrium element or equilibrium model is one which satisfies equilibrium but not compatibility. A mixed model is one satisfying neither equilibrium nor compatibility. These classifications are discussed in detail by de Veubeke [34].

One of the chief purposes of finite element methods in structural analysis is to develop relationships between generalized loads and generalized displacements through the elastic and geometric properties of the element. A second classification of finite element methods is based on these relationships. In one approach, this is done through the so called flexibility matrix by which generalized displacements are derived from generalized forces. The other approach derives the

generalic priately

¥:::i:::

a Tan

A ii)ei mi some

Pathags :

¥Cos.

treats :

the $\kappa_{\Delta\gamma}$

itz tte

Placeme:

the ove

eler

if tran

itwes:

ïSed e

fizite

beet . descr

disca

trian

- 4

Matik

generalized forces from the generalized displacements through the appropriately named stiffness matrix.

A third classification of finite element methods is based on the method of solution. The matrix displacement method treats displacements as unknowns whereas the matrix force method treats forces as unknowns.

A mixed method of solution is also possible with some unknown forces and some unknown displacements.

As pointed out by Felippa [18], the direct stiffness method is perhaps the most powerful and fully developed of the finite element methods. The direct stiffness method employs a displacement model and treats displacements as unknowns. The word direct is used to indicate the way in which the overall structural stiffness matrix is assembled from the individual element stiffness matrices prior to imposing displacement boundary conditions. Thus in the direct stiffness method, the overall stiffness matrix is obtained by a simple systematic addition of element stiffnesses. Argyris [27] and others accomplish this by means of transformations involving location or "Boolean" matrices. The latter procedure seems to be less efficient and thus has been avoided by many investigators.

In the present investigation, the direct stiffness method is used exclusively. Thus no further reference will be made to other finite element methods. Furthermore, the philosophy of the method has been thoroughly treated by a number of writers [35] so that only a brief description of the basic steps will be presented here. The specific discussion and examples will relate to two dimensional problems and triangular elements. It is a relatively simple matter to extend the work to three dimensional situations.

1.1 <u>11:14</u>

be approx

of carefu

Tese zaj

elements .

Eletents

Simual co

truly co-

Martin 1

Enlity Hazetes

Vásá su

aldal p

toordin

²€ { };;

tėnt

eybte

3.2 Direct Stiffness Method

The behavior of the actual structure or continua is assumed to be approximated by a discretized structure consisting of an assemblage of carefully chosen elements connected at a finite number of points.

These may be beam elements in the case of frames, triangular plane stress elements for certain two dimensional continua, quadrilateral plate elements for plate flexure, or tetrahedra in the case of three dimensional continua. Other physical problems may dictate use of still different elements or possibly combinations of these elements for truly complex structures.

Inherent in the procedure is the assumption of element displacement modes. These displacement modes must satisfy internal compatibility and should insofar as possible maintain compatibility of displacements across element boundaries. The number of displacement modes used must agree with the number of degrees of freedom of the element nodal point system. Thus for a plane problem in rectangular Cartesian coordinates, with n nodal points, the equations

$$\mathbf{u}(\mathbf{x},\mathbf{y}) = \sum_{i=1}^{2n} \mathbf{U}_{i}(\mathbf{x},\mathbf{y}) \alpha_{i}$$

$$\mathbf{v}(\mathbf{x},\mathbf{y}) = \sum_{i=1}^{2n} \mathbf{V}_{i}(\mathbf{x},\mathbf{y}) \alpha_{i}$$
(3.1)

define the assumed displacement field in terms of independent displacement functions $\mathbf{U_i}$ and $\mathbf{V_i}$ and generalized displacements α_i . These can be expressed in matrix notation as well.

$$u(x,y) = [U(x,y)]^{t} [\alpha]$$

$$v(x,y) = [V(x,y)]^{t} [\alpha]$$
(3.2)

As stated above, the dimension of $[\alpha]$ is 2n and it agrees with the number of degrees of freedom for the element nodal point system.

The next step is to express the nodal point displacements in terms of the generalized displacements. This is done by evaluating (3.1) or (3.2) at the nodal point coordinates.

$$u_{j} = \sum_{i=1}^{2n} U_{i}(x_{j}, y_{j}) \alpha_{i}$$

$$y_{j} = \sum_{i=1}^{2n} V_{i}(x_{j}, y_{j}) \alpha_{i}$$

$$j = 1, 2, ... n \qquad (3.3)$$

The matrix notation is more compact and allows the 2n equations of (3.3) to be written as

$$[u] = [A][\alpha] \tag{3.4}$$

where [u] and $[\alpha]$ are column matrices defined by

$$[\mathbf{u}]^{\mathsf{t}} = \langle \mathbf{u}_1 \mathbf{u}_2 \dots \mathbf{u}_n \mathbf{v}_1 \mathbf{v}_2 \dots \mathbf{v}_n \rangle \tag{3.5}$$

$$[\alpha]^{t} = \langle \alpha_{1} \alpha_{2} \dots \alpha_{n} \alpha_{n+1} \dots \alpha_{2n} \rangle$$
 (3.6)

The matrix [A] is a square matrix whose rows are formed by evaluating the assumed displacement functions at the nodal point coordinates. Thus

i e De gere Point di le stra

Were [

$$[A] = \begin{bmatrix} U_{1}(x_{1}, y_{1}) & U_{2}(x_{1}, y_{1}) & \dots & U_{2n}(x_{1}, y_{1}) \\ U_{1}(x_{2}, y_{2}) & U_{2}(x_{2}, y_{2}) & \dots & U_{2n}(x_{2}, y_{2}) \\ \vdots & \vdots & \vdots & \vdots & \vdots \\ U_{1}(x_{n}, y_{n}) & U_{2}(x_{n}, y_{n}) & \dots & U_{2n}(x_{n}, y_{n}) \\ V_{1}(x_{1}, y_{1}) & V_{2}(x_{1}, y_{1}) & \dots & V_{2n}(x_{1}, y_{1}) \\ \vdots & \vdots & \vdots & \vdots & \vdots \\ V_{1}(x_{n}, y_{n}) & V_{2}(x_{n}, y_{n}) & \dots & V_{2n}(x_{n}, y_{n}) \end{bmatrix}$$

$$(3.7)$$

The generalized displacements are then expressed in terms of the nodal point displacements. This is simply an inversion of equation (3.4).

$$[\alpha] = [A^{-1}][u] \tag{3.8}$$

In the next phase, the strains and stresses are evaluated. The strains are given by the matrix relationship

$$[\varepsilon(x,y)] = [D(x,y)][\alpha]$$
 (3.9)

where $[\varepsilon(x,y)]$ is a column matrix defined by

mi the r

or plane

 $[\mathbb{C}[x_i]^{r_i}]$

le stres

or in vi

ia the ;

 $\mathbb{P}(\mathbf{x},y)$

$$[\varepsilon(x,y)]^{t} = \langle \varepsilon_{x}(x,y) \quad \varepsilon_{y}(x,y) \quad \gamma_{xy}(x,y) \rangle$$
 (3.10)

and the matrix [D] is formed by appropriate differentiation of the displacement functions $\mathbf{U_i}$ and $\mathbf{V_i}$. For example, in the case of plane stress or plane strain

$$\begin{bmatrix} \frac{\partial U_1}{\partial x} & \frac{\partial U_2}{\partial x} & \cdots & \frac{\partial U_{2n}}{\partial x} \\ \frac{\partial V_1}{\partial y} & \frac{\partial V_2}{\partial y} & \frac{\partial V_{2n}}{\partial y} \\ \frac{\partial U_1}{\partial y} + \frac{\partial V_1}{\partial x} & \frac{\partial U_2}{\partial y} + \frac{\partial V_2}{\partial x} & \frac{\partial U_{2n}}{\partial y} + \frac{\partial V_{2n}}{\partial x} \end{bmatrix}$$
(3.11)

The stresses arise from the constitutive relationships and can be written in matrix notation as

$$[\sigma(\mathbf{x},\mathbf{y})] = [C][\varepsilon(\mathbf{x},\mathbf{y})] \tag{3.12}$$

or in view of equation (3.9)

$$[\sigma(x,y)] = [C][D(x,y)][\alpha]$$
(3.13)

In the above, the matrix [C] is the matrix of material properties and $[\sigma(x,y)]$ is the matrix of stress components given by

$$[\sigma(\mathbf{x},\mathbf{y})]^{\mathsf{t}} = \langle \sigma_{\mathbf{x}}(\mathbf{x},\mathbf{y}) \quad \sigma_{\mathbf{y}}(\mathbf{x},\mathbf{y}) \quad \tau_{\mathbf{x}\mathbf{y}}(\mathbf{x},\mathbf{y}) \rangle$$
(3.14)

it is qui incluir

place so

tiere :

from the

ā set j

 $\mathbb{H}_{\mathbf{x},y}$

ine elem

ċ

Tsizz :

į

Mete |

āsscoia

AST TOP

It is quite possible to treat very general material characteristics including orthotropic elasticity and elasto-plasticity. For isotropic plane stress the matrix [C] becomes

$$[C] = \frac{E}{1 - v^2} \begin{bmatrix} 1 & v & 0 \\ v & 1 & 0 \\ 0 & 0 & \frac{1 - v}{2} \end{bmatrix}$$
 (3.15)

where E is the modulus of elasticity and v is Poisson's ratio.

A generalized coordinate stiffness matrix, $[k_{\alpha}]$, is derived from the principle of virtual displacements. It is necessary to equate the virtual external work to the virtual internal work. Associated with a set of virtual displacements $\delta u(x,y)$ and $\delta v(x,y)$ are virtual strains $[\delta \epsilon(x,y)]$. The virtual internal work for a differential volume, dV, in the element is

$$d(\delta W_{\underline{i}}) = [\delta \varepsilon(x,y)]^{t} [\sigma(x,y)] dV$$
 (3.16)

Using relationships (3.13) and (3.9) this last result becomes

$$d(\delta W_i) = [\delta \alpha]^t [D]^t [C][D][\alpha] dV$$

where $[\delta\alpha]$ is the column matrix of virtual generalized displacements associated with $\delta u(x,y)$ and $\delta v(x,y)$. The total internal work is the volume integral of the above expression

$$\delta W_{i} = \int_{VOI} [\delta \alpha]^{t} [D]^{t} [C][D][\alpha] dV$$

Since (2

jezera..

the gen-

viik is

POTE CUI

Eoweye:

With the

ेंद्र स

one may

Since $[\alpha]$ is independent of position

$$\delta W_{i} = [\delta \alpha]^{t} \int_{Vol} [D]^{t} [C][D] dV [\alpha]$$
 (3.17)

Now associated with the generalized displacements $[\alpha]$ are generalized forces $[\beta]$; the product of the generalized displacements and the generalized forces yields external work. Thus the virtual external work is

$$\delta W_{\beta} = [\delta \alpha]^{t} [\beta]$$
 (3.18)

Since the virtual internal work equals the virtual external work during any virtual displacement, it follows that

$$[\delta\alpha]^{t}$$
 $[\beta] = [\delta\alpha]^{t}$ $\int_{vol}^{t} [C][D] dV [\alpha]$

However, virtual displacements are arbitrary displacements consistent with the kinematic constraints. Thus the above equation implies

$$[\beta] = \int_{\text{vol}} [D]^{t} [C][D] dV [\alpha]$$
 (3.19)

From the definition of the stiffness matrix $[{\bf k}_{\alpha}^{}]$, that is

$$[\beta] = [k_{\alpha}][\alpha] \tag{3.20}$$

one may conclude that

$$\begin{bmatrix} k_{\alpha} \end{bmatrix} = \int_{VO}^{t} [D]^{t} [C][D] dV$$
 (3.21)

to océal is ieri: 1885 lai Detal. unie;: icial ; isplace a spenii ii corre Plat a tiezts d H(1) itrutu: it allow stiffae :**ant** ac: POP:141 اعتره المراد 77et[20] ::e{{{t}_C}

cotota.

The nodal point stiffness matrix [k] relates nodal point forces to nodal point displacements. In view of equation (3.8), the matrix [k] is derived from $[k_{\alpha}]$ by a standard coordinate transformation.

$$[k] = [A^{-1}]^{t} [k_{\alpha}][A^{-1}]$$
 (3.22)

Having given a general procedure for working out element stiffness matrices, attention is next given to the problem of assembling the overall stiffness matrix of the discretized structure. In the direct stiffness method this is a fairly routine procedure. Involved is the concept that the overall stiffness matrix relates applied loads at the nodal point of the assembled structure to the resulting nodal point displacements. A particular coefficient of this matrix associated with a specific nodal point of the complete structure is the algebraic sum of corresponding stiffness coefficients of elements which have this same point a nodal point of the element. In other words, stiffness coefficients of the complete structure are obtained by summing the stiffness coefficients of elements surrounding a particular point of the complete structure. This is an essential feature of the direct stiffness method. It allows the structural analyst to identify and store only the non-zero stiffness coefficients of the complete structure. This is a significant achievement since stiffness matrices are generally very sparsely populated. By storing only the non-zero coefficients, one is able to consider much finer discretizations of the actual system. Not to be overlooked, however, is that prior to adding these element stiffness coefficients they must all have been referred to the same global coordinate system.

mial :

arising

mi sur:

these, i

stati;

fatte:

Tus it

te 531

ಯಕ್ಕುವ

Z: (18

Vir._{la}

¥.÷

::::

The next part of the analysis is the determination of element nodal point forces. These are generally the result of internal stresses arising from temperature changes or perhaps imperfections, body forces, and surface tractions. Although it is possible to account for each of these, for example as in reference [25], only the nodal point loads arising from surface tractions are considered here.

As pointed out by Archer [36], these forces must not only be statically equivalent to the distributed boundary forces but they must furthermore be kinematically consistent with the assumed displacement field corresponding to elements on the loaded portion of the boundary. Thus it is required that the virtual work done by the actual loads, be the same as that done by the nodal point forces.

For convenience, the boundary tractions are considered to have components in the coordinate directions. These are designated by p(s) and q(s) with p(s) the x component and q(s) the y component. It is assumed that these have been integrated over the thickness. During a virtual displacement, the work done by the actual force system is

$$\delta W_{1} = \int_{B} [p(s) \delta u_{B} + q(s) \delta v_{B}] ds \qquad (3.23)$$

where \mathbf{u}_{B} and \mathbf{v}_{B} are boundary displacement components of the loaded portion of the element. In view of equations (3.2) these boundary displacements are

$$\mathbf{u}_{\mathbf{B}} = [\mathbf{U}_{\mathbf{B}}][\alpha]$$

$$\mathbf{v}_{\mathbf{B}} = [\mathbf{V}_{\mathbf{B}}][\alpha]$$
(3.24)

where

tave te

de de

Mails :

stati.

ccial

l: is

1.67

ēŗė

ie : {

where $[V_B]$ and $[V_B]$ are row matrices of displacement functions which have been evaluated on the loaded boundary. Thus equation (3.23) becomes

$$\delta W_1 = \int_B (p(s) [U_B] + q(s) [V_B]) ds [\delta \alpha]$$

But the generalized displacements $[\alpha]$ are related to nodal point displacements by equation (3.8). Writing the above virtual work accordingly

$$\delta W_{1} = \int_{B} (p(s) [U_{B}] + q(s) [V_{B}]) ds [A^{-1}][\delta u]$$
 (3.25)

It is required that equation (3.25) be equal to the virtual work of the statically equivalent nodal point forces acting through the same virtual nodal point displacements. The work of the external nodal point forces is

$$\delta W_2 = [f]^{t} [\delta u]$$
 (3.26)

where

$$[f]^{t} = \langle f_{1_{\mathbf{x}}} f_{2_{\mathbf{x}}} \dots f_{n_{\mathbf{x}}} f_{1_{\mathbf{y}}} f_{2_{\mathbf{y}}} \dots f_{n_{\mathbf{y}}} \rangle$$

is the matrix of nodal point loads. Finally when (3.26) and (3.25) are equated, the required nodal point forces become

$$[f]^{t} = [A^{-1}]^{t} \int_{B} (p(s) [U_{B}]^{t} + q(s) [V_{B}]^{t}) ds$$
 (3.27)

A more direct approach to obtaining these loads is to express the boundary displacements in terms of nodal point displacements.

li genera

is the

Where

€

e L

:

,

In general

$$u(x,y) = [M(x,y)]^{t} [u_{x}]$$

$$v(x,y) = [N(x,y)]^{t} [u_{y}]$$
(3.28)

On the boundary

$$u_{B} = [M_{B}]^{t} [u_{x}]$$

$$v_{B} = [N_{B}]^{t} [u_{y}]$$
(3.29)

where

$$[u_x]^t = \langle u_1 \ u_2 \ \dots \ u_n \rangle$$

$$[u_y]^t = \langle v_1 \ v_2 \ \dots \ v_n \rangle$$
(3.30)

The matrices [M] and [N] consist of weighting functions which relate element displacements to nodal point displacements. As used in (3.29), these weighting functions have been evaluated on the loaded boundary.

The virtual work of the boundary traction is then

$$\delta W_1 = \int_B p(s) \left[M_B\right]^t \left[\delta u_x\right] ds + \int_B q(s) \left[N_B\right]^t \left[\delta u_y\right] ds \qquad (3.30)$$

Furthermore, the virtual work of the nodal point forces is

$$\delta W_2 = [f_x]^t [\delta u_x] + [f_y]^t [\delta u_y]$$

where

[:

Equating (

the algeb

elements elements

the compi

and the p

in equation

(š) is to

inversion

structur. kinemati

exterma:

$$[f] = \begin{bmatrix} f_x \\ f_y \end{bmatrix}$$

Equating δW_1 and δW_2 and noting that $[\delta u_x]$ and $[\delta u_y]$ are arbitrary, one obtains

$$[f_x] = \int_B p(s)[M_B] ds$$

$$[f_y] = \int_B q(s)[N_B] ds$$
(3.31)

The nodal point forces for the complete structure are clearly the algebraic summations of element nodal point forces. Thus if several elements join at a boundary point j, the nodal point forces of these elements which correspond to j are added to obtain the nodal force of the complete structure.

Having assembled the complete structural stiffness matrix $[\tilde{K}]$ and the nodal force vector $[\tilde{F}]$ one is led to the matrix relationship

$$[\tilde{\mathbf{F}}] = [\tilde{\mathbf{K}}][\tilde{\mathbf{s}}] \tag{3.32}$$

In equation (3.32) $[\tilde{s}]$ is a column matrix of nodal point displacements of the complete structure. In two dimensional problems the dimension of $[\tilde{s}]$ is twice the number of nodal points of the assembled structure. The object now is to determine these displacements. This requires the inversion of equation (3.32). Since $[\tilde{K}]$ pertains to the unrestrained structure, it is a singular matrix and thus cannot be inverted until kinematic constraints have been imposed. This renders the structure externally stable and has the effect of reducing the size of the

11111

Tere

27.1

}a_

•

ti

3

matrices in (3.32). One may then write

$$[F] = [K][s]$$
 (3.33)

where [K] is non-singular. The solution is

$$[s] = [K]^{-1} [F]$$
 (3.34)

and it is obtainable by various inversion techniques. The use of the Gauss Seidel successive over-relaxation technique is discussed by Clough [35]. A modification of this procedure has been used throughout this investigation. A simplification of Gauss elimination applicable to band matrices has been discussed by Tocher [37].

The final step in the analysis involves the calculation of stresses. As indicated by de Veubeke [34], the best stresses in a displacement model analysis are those derived from the displacement field. In the case of linear displacement fields, however, care must be exercised in interpreting element stresses. Wilson [38] has proposed an averaging technique which appears to give fairly good results.

Accordingly, the stresses follow from equation (3.13). That is

$$[\sigma(x,y)] = [C][D(x,y)][\alpha]$$

The generalized displacements $[\alpha]$ are eliminated using equation (3.8). Thus element stresses are expressed by the relationship

$$[\sigma(x,y)] = [C][D(x,y)][A^{-1}][u]$$
 (3.35)

Equation (

set of not

at the nod

3.3 Const

strain tri

Turner et

element is

figure 3.1

of general

the local

laxer at : point syst

of the thr

T: a linear o

relations:

ν(

The 1 are

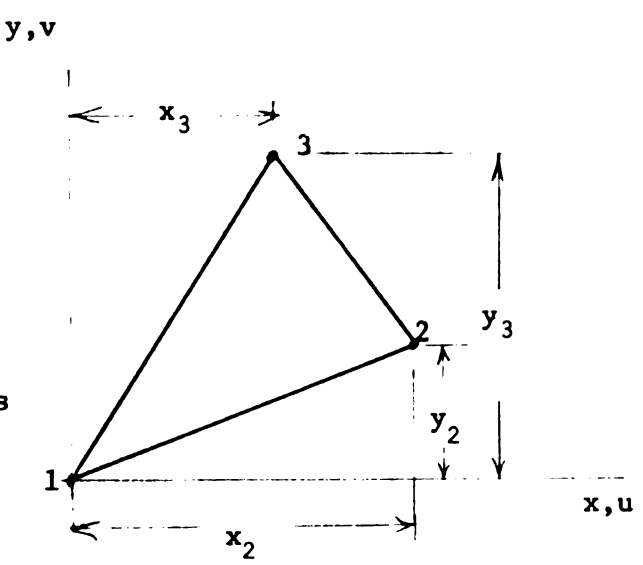
telations:

Equation (3.35) gives the stress components throughout the element. A set of nodal point stresses can be derived by evaluating equation (3.35) at the nodal point coordinates.

3.3 Constant Strain Triangle

The simplest 2 dimensional displacement model is the constant strain triangle proposed by Turner et al [11]. Such an element is displayed in Figure 3.1. There is no loss of generality if the origin of the local coordinate system is taken at point 1. The nodal point system for this case consists of the three triangle vertices.

The displacement field is a linear one expressed by the relationships



Constant Strain Triangle

Figure 3.1

$$\mathbf{u}(\mathbf{x},\mathbf{y}) = \alpha_1 + \alpha_2 \mathbf{x} + \alpha_3 \mathbf{y}$$

$$\mathbf{v}(\mathbf{x},\mathbf{y}) = \alpha_4 + \alpha_5 \mathbf{x} + \alpha_6 \mathbf{y}$$
(3.36)

The $\alpha_{_{\mbox{\scriptsize 1}}}$ are the generalized displacements of equations (3.1). The matrix relationships (3.2) for this case become

Evaluatin,
of equatio

ζĮ

The inver

$$\mathbf{u}(\mathbf{x},\mathbf{y}) = \left[\mathbf{U}_{(\mathbf{x},\mathbf{y})}\right]^{\mathsf{t}} \left[\alpha\right] = \left\langle 1 \times \mathbf{y} \ 0 \ 0 \ 0 \right\rangle \left\{ \begin{array}{c} \alpha_1 \\ \alpha_2 \\ \vdots \\ \alpha_6 \end{array} \right\}$$

$$(3.37)$$

$$\mathbf{v}(\mathbf{x},\mathbf{y}) = \left[\mathbf{v}_{(\mathbf{x},\mathbf{y})}\right]^{\mathsf{t}} \left[\alpha\right] = \left\langle 0\ 0\ 0\ 1\ \mathbf{x}\ \mathbf{y} \right\rangle \left\{ \begin{array}{c} \alpha_1 \\ \alpha_2 \\ \cdot \\ \cdot \\ \alpha_6 \end{array} \right\}$$

Evaluating these at the nodal point coordinates gives the specific form of equation (3.4).

$$\left\{
 \begin{array}{c}
 u_1 \\
 u_2 \\
 u_3 \\
 v_1 \\
 v_2
 \end{array}
 \right\} =
 \left\{
 \begin{array}{c}
 1 & 0 & 0 & 0 & 0 & 0 \\
 1 & x_2 & y_2 & 0 & 0 & 0 \\
 1 & x_3 & y_3 & 0 & 0 & 0 \\
 0 & 0 & 0 & 1 & 0 & 0 \\
 0 & 0 & 0 & 1 & x_2 & y_2 \\
 0 & 0 & 0 & 1 & x_3 & y_3
 \end{array}
 \right\}
 \left\{
 \begin{array}{c}
 \alpha_1 \\
 \alpha_2 \\
 \alpha_3 \\
 \alpha_4 \\
 \alpha_5 \\
 0 & 0 & 0 & 1 & x_3 & y_3
 \end{array}
 \right\}$$

$$(3.38)$$

or

$$[u] = [A][\alpha]$$

The inverse of [A] is easily obtained by partitioning the matrix. Thus

 $(\overline{x}^{-1}) = \overline{x}$

The matrix

 $\{ f(x,y) \} =$

and thous

The matrix

$$[A^{-1}] = \frac{1}{x_2 y_3 - x_3 y_2} \begin{bmatrix} x_2 y_3 - x_3 y_2 & 0 & 0 & 0 & 0 & 0 \\ y_2 - y_3 & y_3 & -y_2 & 0 & 0 & 0 \\ x_3 - x_2 & -x_3 & x_2 & 0 & 0 & 0 \\ 0 & 0 & 0 & x_2 y_3 - x_3 y_2 & 0 & 0 \\ 0 & 0 & 0 & y_2 - y_3 & y_3 & -y_2 \\ 0 & 0 & 0 & x_3 - x_2 & -x_3 & x_2 \end{bmatrix}$$
 (3.39)

The matrix of strains (3.9) is

$$\begin{bmatrix} \varepsilon(\mathbf{x},\mathbf{y}) \end{bmatrix} = \begin{bmatrix} \frac{\partial \mathbf{u}}{\partial \mathbf{x}} \\ \frac{\partial \mathbf{v}}{\partial \mathbf{y}} \\ \frac{\partial \mathbf{u}}{\partial \mathbf{y}} + \frac{\partial \mathbf{v}}{\partial \mathbf{x}} \end{bmatrix} = \begin{bmatrix} 0 & 1 & 0 & 0 & 0 & 0 \\ 0 & 0 & 0 & 0 & 0 & 1 \\ 0 & 0 & 1 & 0 & 1 & 0 \end{bmatrix} \begin{bmatrix} \alpha_1 \\ \alpha_2 \\ \vdots \\ \alpha_6 \end{bmatrix}$$

and thus

$$[D(x,y)] = \begin{bmatrix} 0 & 1 & 0 & 0 & 0 & 0 \\ 0 & 0 & 0 & 0 & 0 & 1 \\ 0 & 0 & 1 & 0 & 1 & 0 \end{bmatrix}$$
(3.40)

The matrix [C] of elastic properties is (3.15) for plane stress problems. For plane strain problems

[C] =
$$\frac{E}{(1+v)(1-2v)}$$
 $\begin{bmatrix} 1-v & v & 0 \\ v & 1-v & 0 \\ 0 & 0 & \frac{1-2v}{2} \end{bmatrix}$ (3.41)

and since

[k] = [I

in the ab

average :

[i] • ___

With the

elements o

ic refere

displaces.

Perform t

boundary Shown in

traction

boundary are

ate invo

The generalized coordinate stiffness matrix becomes

$$[k_{\alpha}] = \int_{\text{vol}} [D]^{t} [C][D] dV$$

and since [D] and [C] are independent of position

$$[k_{\alpha}] = [D]^{t} [C][D] \int_{\text{vol}} dV = \frac{|x_{2}y_{3} - x_{3}y_{2}|h}{2} [D]^{t} [C][D]$$

In the above, $\frac{1}{2} | x_2 y_3 - x_3 y_2 |$ is the area of the triangle and h its average thickness.

The nodal point stiffness matrix is

$$[k] = \frac{|x_2y_3 - x_3y_2|}{2} h [A^{-1}]^t [D]^t [C][D][A^{-1}]$$
 (3.42)

with the required matrices given by equations (3.39) and (3.40). The elements of [k] can be written out explicitly from (3.42) without too much effort. The final result involving 36 coefficients is presented in reference [14]. In other situations involving more complicated displacement fields this becomes impractical. In some cases it is preferable to work out the matrices of (3.42) or its equivalent and to the perform the matrix multiplication on the computer.

As an example of nodal force calculations determined from boundary tractions consider the situation illustrated in Figure 3.2. Shown in the figure is a portion of the curved boundary with a normal traction p(y). The triangular element 1-2-3 can only approximate the boundary along 1-2. Clearly, only x-components of nodal point forces are involved in this example. The first equation of (3.31) is

...

viere (M.) of weight:

m the bo.

functions equations

:(x,y) =

The bounc

Tous

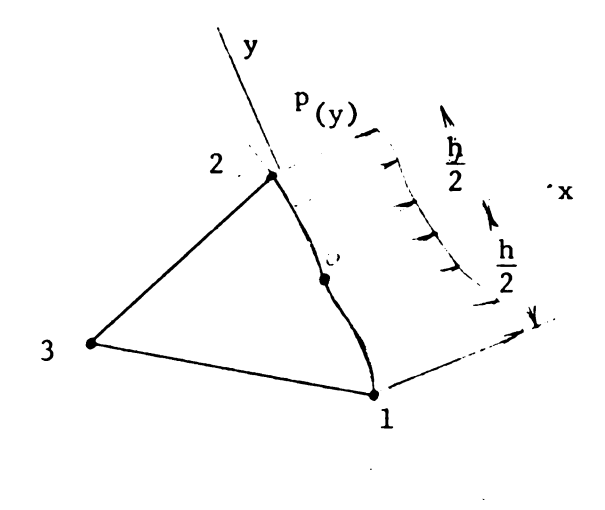
Paluatio

;

Tiese las

$$[f_x] = \int_B p(y) [M_B] ds$$

where $[M_B]$ is the column matrix of weighting functions evaluated on the boundary. To obtain these functions consider the first of equations (3.36).



$$u(x,y) = \alpha_1 + \alpha_2 x + \alpha_3 y$$

Figure 3.2

Normal Boundary Traction-CST

The boundary here is identified by the equation x = 0.

Thus

$$u_{R} = u(0,y) = \alpha_{1} + \alpha_{3}y$$
 (3.43)

Evaluating the latter at points 1 and 2 on the boundary gives

$$u_1 = \alpha_1 + \alpha_3(\frac{-h}{2})$$

$$u_2 = \alpha_1 + \alpha_3 \left(\frac{h}{2}\right)$$

These last equations can be solved for $\boldsymbol{\alpha}_1$ and $\boldsymbol{\alpha}_3$ to give

$$\alpha_1 = \frac{u_1 + u_2}{2}$$

$$\alpha_3 = \frac{\mathbf{u}_2 - \mathbf{u}_1}{\mathbf{h}}$$

Equation

De patri

..ez

and the r

For the

Also, i

Equation (3.43) can then be written as

$$u_B = (\frac{1}{2} - \frac{y}{h}) u_1 + (\frac{1}{2} + \frac{y}{h}) u_2$$
 (3.44)

The matrix of weighting functions is

$$\left[M_{\rm B}\right]^{\rm t} = \left\langle \frac{1}{2} - \frac{y}{h} \qquad \frac{1}{2} + \frac{y}{h} \qquad 0 \right\rangle \tag{3.45}$$

Then

$$[f_x]^t = \int_1^2 p(y) [M_B]^t ds = \int_{-\frac{h}{2}}^{\frac{h}{2}} p(y) \langle \frac{1}{2} - \frac{y}{h} \frac{1}{2} + \frac{y}{h} = 0 \rangle dy$$

and the result is

$$f_{1x} = \int_{-\frac{h}{2}}^{\frac{h}{2}} \left(\frac{1}{2} - \frac{y}{h}\right) p(y) dy$$

$$f_{2x} = \int_{-\frac{h}{2}}^{\frac{h}{2}} \left(\frac{1}{2} + \frac{y}{h}\right) p(y) dy$$

$$f_{3x} = 0$$
(3.46)

For the special case p(y) = p, a constant

$$f_{1_{\mathbf{X}}} = \frac{ph}{2}$$

$$f_{2_{\mathbf{X}}} = \frac{ph}{2}$$

$$(3.47)$$

Also, if p(y) is a linear variation expressed by

Finally,

?ૄis the

3.4 Line

elements de Teube

general:

displace

a ejeze

figure 3

coordina

with no

$$p(y) = \frac{P_2 + P_1}{2} + \frac{P_2 - P_1}{h}$$
 y one obtains

$$f_{1_{x}} = \frac{h}{6}(p_{2} + 2p_{1})$$

$$f_{2_{x}} = \frac{h}{6}(2p_{2} + p_{1})$$
(3.48)

y, if p(y) is quadratic with the form

$$p(y) = p_0 + \frac{p_2 - p_1}{h} + \frac{p_1 + p_2 - 2p_0}{\frac{h^2}{2}} y^2$$
 where

the load intensity at the origin

$$f_{1x} = \frac{h}{6} (2p_{4} + p_{1})$$

$$f_{2x} = \frac{h}{6} (2p_{4} + p_{2})$$
(3.49)

inearly Varying Strain Triangle

In order to maintain compatibility between triangular plate ts and beam segments,

oeke [34] introduced a

lized plane stress element

invol<mark>ves a quadrati</mark>c

ement field. Such

nent is displayed in

3.3. The origin of

nates is placed at point 1

) loss of generality.

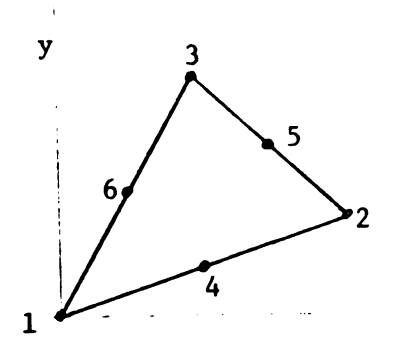


Figure 3.3
Linear Strain Triangle

X

The modal

of the tro

De modal

stained

De latte

÷ere

lal point system includes the triangle vertices and the midpoints triangle sides.

The quadratic displacement field is expressed by the relationships

$$u(x,y) = \alpha_{1} + \alpha_{2}x + \alpha_{3}y + \alpha_{4}x^{2} + \alpha_{5}xy + \alpha_{6}y^{2}$$

$$v(x,y) = \alpha_{7} + \alpha_{8}x + \alpha_{9}y + \alpha_{10}x^{2} + \alpha_{11}xy + \alpha_{12}y^{2}$$
(3.50)

dal point displacements follow from the matrix equation

$$[\mathbf{u}] = [\mathbf{A}][\alpha]$$

ed by evaluating equations (3.50) at the nodal point coordinates.

tter can be written as

$$\begin{bmatrix} \mathbf{u}_{\mathbf{x}} \\ \mathbf{u}_{\mathbf{y}} \end{bmatrix} = \begin{bmatrix} \mathbf{A}_{11} & \mathbf{0} \\ \mathbf{0} & \mathbf{A}_{22} \end{bmatrix} \begin{bmatrix} \mathbf{\alpha}_{\mathbf{x}} \\ \mathbf{\alpha}_{\mathbf{y}} \end{bmatrix}$$
(3.51)

$$[u_x]^t = \langle u_1 u_2 u_3 u_4 u_5 u_6 \rangle$$

$$[u_{\mathbf{v}}]^{\mathsf{t}} = \langle v_1 v_2 v_3 v_4 v_5 v_6 \rangle$$

$$\left[\alpha_{\mathbf{x}}\right]^{\mathsf{t}} = \left\langle \alpha_{1} \alpha_{2} \ldots \alpha_{6} \right\rangle$$

$$\left[\alpha_{\mathbf{v}}\right]^{\mathsf{t}} = \left\langle \alpha_{7} \alpha_{8} \dots \alpha_{12} \right\rangle$$

Also [A

[ā...] =

The inver

it is not The matri

program (

alternati

component

Placemen

to write

ħε ₩_i,

reader i

Also $[A_{22}] = [A_{11}]$ with

$$\begin{bmatrix} \mathbf{A}_{11} \end{bmatrix} = \begin{bmatrix} 1 & 0 & 0 & 0 & 0 & 0 & 0 \\ 1 & \mathbf{x}_2 & \mathbf{y}_2 & \mathbf{x}_2^2 & \mathbf{x}_2 \mathbf{y}_2 & \mathbf{y}_2^2 \\ 1 & \mathbf{x}_3 & \mathbf{y}_3 & \mathbf{x}_3^2 & \mathbf{x}_3 \mathbf{y}_3 & \mathbf{y}_3^2 \\ 1 & \frac{\mathbf{x}_2}{2} & \frac{\mathbf{y}_2}{2} & \frac{\mathbf{x}_2^2}{4} & \frac{\mathbf{x}_2 \mathbf{y}_2}{4} & \frac{\mathbf{y}_2^2}{4} \\ 1 & \frac{\mathbf{x}_3 - \mathbf{x}_2}{2} & \frac{\mathbf{y}_3 - \mathbf{y}_2}{2} & \frac{(\mathbf{x}_3 - \mathbf{x}_2)^2}{4} & \frac{(\mathbf{x}_3 - \mathbf{x}_2)(\mathbf{y}_3 - \mathbf{y}_2)}{4} & \frac{(\mathbf{y}_3 - \mathbf{y}_2)^2}{4} \\ 1 & \frac{\mathbf{x}_3}{2} & \frac{\mathbf{y}_3}{2} & \frac{(\mathbf{y}_3 - \mathbf{y}_2)^2}{4} & \frac{\mathbf{x}_3 \mathbf{y}_3}{4} & \frac{\mathbf{y}_3^2}{4} \end{bmatrix}$$

The inverse relationship of (3.51) is

$$\begin{bmatrix} \alpha_{\mathbf{x}} \\ \alpha_{\mathbf{y}} \end{bmatrix} = \begin{bmatrix} A_{11}^{-1} \mid 0 \\ 0 \mid A_{22}^{-1} \end{bmatrix} \begin{bmatrix} u_{\mathbf{x}} \\ u_{\mathbf{y}} \end{bmatrix}$$
(3.53)

It is not suggested that an explicit expression for $[A^{-1}]$ be worked out. The matrix $[A^{-1}]$ can be determined numerically within the computer program by simply calling a matrix inversion subroutine. Another alternative is suggested by de Veubeke [34] whereby displacement components u(x,y) and v(x,y) are expressed in terms of nodal point displacements through a set of 6 weighting functions. Thus it is possible to write

$$\mathbf{u(x,y)} = \mathbf{u_1} \mathbf{W_1} + \mathbf{u_2} \mathbf{W_2} + \mathbf{u_3} \mathbf{W_3} + \mathbf{u_4} \mathbf{W_4} + \mathbf{u_5} \mathbf{W_5} + \mathbf{u_6} \mathbf{W_6}$$

$$\mathbf{v(x,y)} = \mathbf{v_1} \mathbf{W_1} + \mathbf{v_2} \mathbf{W_2} + \mathbf{v_3} \mathbf{W_3} + \mathbf{v_4} \mathbf{W_4} + \mathbf{v_5} \mathbf{W_5} + \mathbf{v_6} \mathbf{W_6}$$

The W_1 , i = 1, 6, are functions of x and y. For further details, the reader is referred to reference [34].

ierivat.

[c(**x,y**)]

and the

 $[\mathfrak{I}(\mathbf{x},\mathbf{y})]$

The tat

stress

Howeve equati

Point

daced.

allows

The matrix of strain components follows from the partial derivatives of equations (3.50). Thus

and the matrix [D(x,y)] corresponding to (3.11) is

The matrices of elastic properties are (3.15) and (3.41) for plane stress and plane strain respectively.

The generalized coordinate stiffness is

$$[k_{\alpha}] = \int_{VOI} [D]^{T} [C][D] dV \qquad (3.55)$$

However, in this case, the integrand is a function of position, as in equation (3.54). The calculations thus become rather involved. At this point a more general matrix of linearly elastic properties is introduced. Thus

$$\begin{bmatrix} \mathbf{C} \end{bmatrix} = \begin{bmatrix} \mathbf{C}_{11} & \mathbf{C}_{12} & \mathbf{C}_{13} \\ \mathbf{C}_{21} & \mathbf{C}_{22} & \mathbf{C}_{23} \\ \mathbf{C}_{31} & \mathbf{C}_{32} & \mathbf{C}_{33} \end{bmatrix}$$
(3.56)

allows arbitrary anisotropy for the two dimensional case. With this

value of

viere

. •

•

lo_{ti}.

value of [C], the integrand in equation (3.55) can be written as

$$[D]^{T} [C][D] = \begin{bmatrix} Q_{11} & Q_{12} \\ Q_{21} & Q_{22} \end{bmatrix}$$
 (3.57)

where

$$\begin{bmatrix} \mathbf{Q}_{22} \end{bmatrix} = \begin{bmatrix} \mathbf{0} & \mathbf{0} \\ \mathbf{0} & \mathbf{C}_{33} & \mathbf{C}_{32} & 2\mathbf{x}\mathbf{C}_{33} & \mathbf{x}\mathbf{C}_{32} + \mathbf{y}\mathbf{C}_{33} & 2\mathbf{y}\mathbf{C}_{32} \\ \mathbf{0} & \mathbf{C}_{23} & \mathbf{C}_{22} & 2\mathbf{x}\mathbf{C}_{23} & \mathbf{x}\mathbf{C}_{22} + \mathbf{y}\mathbf{C}_{23} & 2\mathbf{y}\mathbf{C}_{22} \\ \mathbf{0} & 2\mathbf{x}\mathbf{C}_{33} & 2\mathbf{x}\mathbf{C}_{32} & 4\mathbf{x}^2\mathbf{C}_{33} & 2\mathbf{x}^2\mathbf{C}_{32} + 2\mathbf{x}\mathbf{y}\mathbf{C}_{33} & 4\mathbf{x}\mathbf{y}\mathbf{C}_{32} \\ \mathbf{0} & \mathbf{x}\mathbf{C}_{23} + \mathbf{y}\mathbf{C}_{33} & \mathbf{x}\mathbf{C}_{22} + \mathbf{y}\mathbf{C}_{32} & 2\mathbf{x}^2\mathbf{C}_{23} + 2\mathbf{x}\mathbf{y}\mathbf{C}_{31} & \mathbf{x}^2\mathbf{C}_{22} + \mathbf{x}\mathbf{y}(\mathbf{C}_{23} + \mathbf{C}_{32}) + \mathbf{y}^2\mathbf{C}_{34} & 2\mathbf{x}\mathbf{y}\mathbf{C}_{22} + 2\mathbf{y}^2\mathbf{C}_{42} \\ \mathbf{0} & 2\mathbf{y}\mathbf{C}_{23} & 2\mathbf{y}\mathbf{C}_{22} & 4\mathbf{x}\mathbf{y}\mathbf{C}_{21} & 2\mathbf{x}\mathbf{y}\mathbf{C}_{22} + 2\mathbf{y}^2\mathbf{C}_{23} & 4\mathbf{y}^2\mathbf{C}_{22} \end{bmatrix}$$

Lach of

mat and

seez. the foll

Ratrix

[k] =

transf

Each of these coefficients must be integrated over the element volume.

What appears to be a very formidable problem is not as bad as it would seem. Actually there are only 6 different integrals involved. These are the following:

$$\int dV = Ah = \frac{x_2 y_3 - x_3 y_2}{2} h$$

$$\int x dV = h \int x dA = \frac{A}{3} (x_2 + x_3)h$$

$$\int y dV = h \int y dA = \frac{A}{3} (y_2 + y_3)h$$

$$\int x^2 dV = h \int x^2 dA = \frac{A}{12} [x_2^2 + x_3^2 + (x_2 + x_3)^2] h$$

$$\int xy dV = h \int xy dA = \frac{A}{12} [x_2 x_3 + y_2 y_3 + (x_2 + x_3)(y_2 + y_3)] h$$

$$\int y^2 dV = h \int y^2 dA = \frac{A}{12} [y_2^2 + y_3^2 + (y_2 + y_3)^2] h$$

In each of these expressions, h represents the average thickness of the triangular element and A is its area. Thus the generalized stiffness matrix is of the form

$$[k_{\alpha}] = \int_{\text{vol}} \left[\frac{Q_{11}}{Q_{21}} + \frac{Q_{12}}{Q_{22}} - \right] dV = \left[\frac{\int Q_{11} dV}{\int Q_{21} dV} - \frac{\int Q_{12} dV}{\int Q_{22} dV} - \right]$$

The nodal point stiffness matrix is obtained by the coordinate transformation (3.22). Thus

cerives

ocráin

the app

and con

topside

illust:

a distr

The tri

t only

boundar

is the

of (3.5

The bot

$$[k] = [A^{-1}]^{t} \left[\frac{\int Q_{11} dV}{\int A_{21} dV} \right] \left[\frac{\int Q_{12} dV}{\int A_{22} dV} \right] [A^{-1}]$$

This same matrix is presented by Fellippa [18]. derives the matrix in a very elegant way using the novel idea of area coordinates. It can be expressed in an integrated form as a result of the approach taken. Its form is readily adapted to computer programming and consequently was used by the present author in this investigation.

A typical example of the determination of nodal point forces is considered next. The situation is illustrated in Figure 3.4 where a distributed load or traction acts normal to the boundary. The triangle side 1-4-2 of length h only approximates the curved boundary. The origin of coordinates is the mid point of this side.

From the first equation of (3.50)

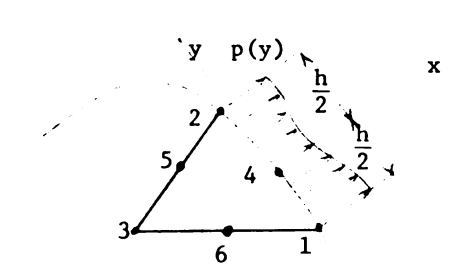


Figure 3.4 Normal Boundary Traction-LST

$$u(x,y) = \alpha_1 + \alpha_2 x + \alpha_3 y + \alpha_4 x^2 + \alpha_5 xy + \alpha_6 y^2$$

The boundary in question is characterized by x = 0. Thus

$$u_{B} = \alpha_{1} + \alpha_{3}y + \alpha_{6}y^{2}$$
 (3.61)

The boun

Stiving

The state of the s

latei.

١

 $\mathbb{R}_{\text{us tl}}$

 $[\underline{v}_{\underline{b}}]^{t}$

Then f

The boundary nodal point displacements are

$$u_{1} = \alpha_{1} + \alpha_{3} \left(\frac{-h}{2}\right) + \alpha_{6} \left(\frac{-h}{2}\right)^{2}$$

$$u_{4} = \alpha_{1}$$

$$u_{2} = \alpha_{1} + \alpha_{3} \left(\frac{h}{2}\right) + \alpha_{6} \left(\frac{h}{2}\right)^{2}$$

Solving these equations for $\alpha_1^{}$, $\alpha_3^{}$, and $\alpha_6^{}$ one obtains

$$\alpha_{1} = u_{4}$$

$$\alpha_{3} = \frac{u_{2} - u_{1}}{h}$$

$$\alpha_{6} = \frac{u_{1} + u_{2} - 2u_{4}}{\frac{h^{2}}{2}}$$

Introducing these results into equation (3.61) yields

$$u_{B} = \left(\frac{2y^{2}}{h^{2}} - \frac{y}{h}\right)u_{1} + \left(1 - \frac{4y^{2}}{h^{2}}\right)u_{4} + \left(\frac{2y^{2}}{h^{2}} + \frac{y}{h}\right)u_{2}$$
 (3.62)

Thus the matrix of weighting functions is

$$[M_B]^t = \langle \frac{2y^2}{h^2} - \frac{y}{h} \qquad \frac{2y^2}{h^2} + \frac{y}{h} \quad 0 \quad 1 - \frac{4y^2}{h^2} \quad 0 \quad 0 \rangle$$
 (3.63)

Then from the first of equations (3.31)

$$[f_x]^t = \int_R p(y) [M_B]^t ds$$

one obtains

$$f_{1_{x}} = \int_{-\frac{h}{2}}^{\frac{h}{2}} p(y) \left(\frac{2y^{2}}{h^{2}} - \frac{y}{h}\right) dy$$

$$f_{2_{x}} = \int_{-\frac{h}{2}}^{\frac{h}{2}} p(y) \left(\frac{2y^{2}}{h} + \frac{y}{h}\right) dy$$

$$f_{4_{x}} = \int_{-\frac{h}{2}}^{\frac{h}{2}} p(y) \left(1 - \frac{4y^{2}}{h^{2}}\right) dy$$

$$f_{3_{x}} = f_{5_{x}} = f_{6_{x}} = 0$$
(3.64)

If p(y) = p, a constant

$$f_{1_{x}} = f_{2_{x}} = \frac{ph}{6}$$

$$f_{4_{x}} = \frac{2}{3} ph$$
(3.65)

Then for a linearly varying load, $p(y) = \frac{p_2 + p_1}{2} + \frac{p_2 - p_1}{h}$ y

$$f_{1_{x}} = \frac{p_{1}h}{6}$$

$$f_{2_{x}} = \frac{p_{2}h}{6}$$

$$f_{4_{y}} = \frac{1}{3} (p_{1} + p_{2}) h$$
(3.66)

Finally for a parabolic load
$$p(y) = p_0 + \frac{p_2 - p_1}{h} y + \frac{p_1 + p_2 - 2p_4}{\frac{h^2}{2}} y^2$$

$$f_{1_{x}} = \frac{h}{30} (4p_{1} - p_{2} + 2p_{4})$$

$$f_{2_{x}} = \frac{h}{30} (-p_{1} + 4p_{2} + 2p_{4})$$

$$f_{4_{y}} = \frac{h}{15} (p_{1} + p_{2} + 8p_{4})$$
(3.67)

3.5 Constant Strain Triangular Ring

The finite element for axisymmetric solids is a circular ring with arbitrary cross sectional geometry. The particular case considered here involves a triangle as shown in Figure 3.5. In view of the axial symmetry, only a segment subtended by an angle $\Delta\theta$ need be shown. The triangle 1-2-3 is shown in an arbitrary position in the r-z plane.

The cross section is re-drawn in Figure 3.6. As shown, the nodal point system which has been selected Consists of the three triangle Vertices. The radial and axial displacement components are u and w respectively. They are independent of θ in view of the axial symmetry. Furthermore, the C1 Cumferential displacement component, v, is identically zero.

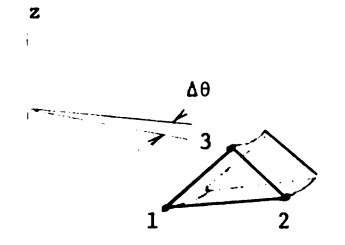


Figure 3.5 Constant Strain Triangular Ring Segment

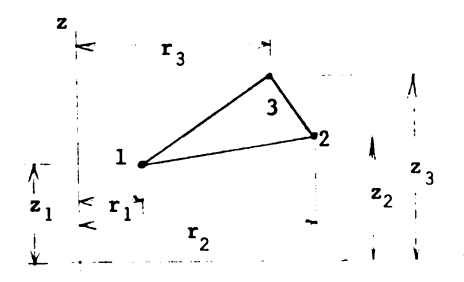


Figure 3.6 Cross Section of Ring Element

The linear displacement field is represented by the equations

$$\mathbf{u}(\mathbf{r}, \mathbf{z}) = \alpha_1 + \alpha_2 \mathbf{r} + \alpha_3 \mathbf{z}$$

$$\mathbf{w}(\mathbf{r}, \mathbf{z}) = \alpha_4 + \alpha_5 \mathbf{r} + \alpha_6 \mathbf{z}$$
(3.67)

e are evaluated at the nodal point coordinates to obtain

$$\begin{vmatrix}
\mathbf{1}_{1} \\
\mathbf{1}_{2} \\
\mathbf{1}_{3} \\
\mathbf{2}_{13} \\
\mathbf{3}_{1} \\
\mathbf{3}_{2}
\end{vmatrix} = \begin{bmatrix}
1 & \mathbf{r}_{1} & \mathbf{z}_{1} & 0 & 0 & 0 \\
1 & \mathbf{r}_{2} & \mathbf{z}_{2} & 0 & 0 & 0 \\
1 & \mathbf{r}_{3} & \mathbf{z}_{3} & 0 & 0 & 0 \\
0 & 0 & 0 & 1 & \mathbf{r}_{1} & \mathbf{z}_{1} \\
0 & 0 & 0 & 1 & \mathbf{r}_{2} & \mathbf{z}_{2} \\
0 & 0 & 0 & 1 & \mathbf{r}_{3} & \mathbf{z}_{3}
\end{bmatrix}
\begin{pmatrix}
\alpha_{1} \\
\alpha_{2} \\
\alpha_{3} \\
\alpha_{4} \\
\alpha_{5} \\
\alpha_{6}
\end{pmatrix}$$
(3.68)

latter may be written

$$[u] = [A][\alpha]$$

inverse transformation is

$$[\alpha] = [A^{-1}] [u] = \begin{bmatrix} A_{11}^{-1} & 0 \\ 0 & A_{22}^{-1} \end{bmatrix}$$

e

$$] = [A_{22}^{-1}] = \frac{1}{\lambda} \begin{bmatrix} r_2 z_3 - r_3 z_2 & r_3 z_1 - r_1 z_3 & r_1 z_2 - r_2 z_1 \\ z_2 - z_3 & z_3 - z_1 & z_1 - z_2 \\ r_3 - r_2 & r_1 - r_3 & r_2 - r_1 \end{bmatrix}$$
 (3.69)

the constant in the denominator is

$$\lambda = r_1(z_2 - z_3) + r_2(z_3 - z_1) + r_3(z_1 - z_2)$$
 (3.70)

matrix of strains is

$$\begin{bmatrix} \varepsilon (\mathbf{r}, \mathbf{z}) \end{bmatrix} = \begin{pmatrix} \varepsilon \\ \mathbf{r} \\ \varepsilon \\ \mathbf{z} \\ \end{pmatrix} = \begin{pmatrix} \frac{\partial \mathbf{u}}{\partial \mathbf{r}} \\ \frac{\partial \mathbf{w}}{\partial \mathbf{z}} \\ \frac{\mathbf{u}}{\mathbf{r}} \\ \frac{\partial \mathbf{u}}{\partial \mathbf{z}} + \frac{\partial \mathbf{w}}{\partial \mathbf{r}} \end{pmatrix}$$

differentiating equations (3.67) one obtains

latrix of displacement function gradients is accordingly

$$[D(\mathbf{r},\mathbf{z})] = \begin{bmatrix} 0 & 1 & 0 & 0 & 0 & 0 \\ 0 & 0 & 0 & 0 & 0 & 1 \\ \frac{1}{\mathbf{r}} & 1 & \frac{\mathbf{z}}{\mathbf{r}} & 0 & 0 & 0 \\ 0 & 0 & 1 & 0 & 1 & 0 \end{bmatrix}$$
(3.71)

The orthotropic stress-strain law is sufficiently general for most situations. In the axially symmetric case, it is expressed by

$$\begin{pmatrix} \sigma_{\mathbf{r}} \\ \sigma_{\mathbf{z}} \\ \sigma_{\theta} \\ \tau_{\mathbf{rz}} \end{pmatrix} = \begin{pmatrix} c_{11} & c_{12} & c_{13} & 0 \\ c_{12} & c_{22} & c_{23} & 0 \\ c_{13} & c_{23} & c_{33} & 0 \\ 0 & 0 & 0 & c_{44} \end{pmatrix} \begin{pmatrix} \varepsilon_{\mathbf{r}} \\ \varepsilon_{\mathbf{z}} \\ \varepsilon_{\theta} \\ \gamma_{\mathbf{rz}} \end{pmatrix}$$
(3.72)

or
$$[\sigma(r,z)] = [C][\varepsilon(r,z)]$$

For isotropic materials the constants are

$$C_{11} = C_{22} = C_{33} = \frac{(1 - v) E}{(1 + v)(1 - 2v)}$$

$$C_{12} = C_{13} = \frac{v E}{(1 + v)(1 - 2v)}$$

$$C_{44} = \frac{E}{2(1 + v)}$$
(3.73)

The generalized stiffness matrix is

$$[k_{\alpha}] = \int_{VO^1} [D]^t [C][D] dV$$

The in:

It is

equati. os bot

the in

i g

T. 15

area

inte

can

J

The integrand is independent of θ so that

$$[k_{\alpha}] = 2\pi \int_{\text{area}} [D]^{t} [C][D] r dr dz$$
 (3.74)

It is possible to ignore the numerical factor 2π in (3.74). In the equation [F] = [K][s] for the assembled structure, the factor 2π appears on both sides and can than be cancelled. The matrix multiplication under the integral results in

$$[D]^{t}[C][D]r =$$

$$\begin{bmatrix} \mathbf{C}_{33}/\mathbf{r} & (\mathbf{C}_{13}+\mathbf{C}_{33}) & \mathbf{C}_{33}\mathbf{z}/\mathbf{r} & \mathbf{0} & \mathbf{0} & \mathbf{C}_{23} \\ (\mathbf{C}_{13}+\mathbf{C}_{33}) & (\mathbf{C}_{11}+2\mathbf{C}_{13}+\mathbf{C}_{33})\mathbf{r} & (\mathbf{C}_{13}+\mathbf{C}_{33})\mathbf{z} & \mathbf{0} & \mathbf{0} & (\mathbf{C}_{12}+\mathbf{C}_{23})\mathbf{r} \\ \mathbf{C}_{33}\mathbf{z}/\mathbf{r} & (\mathbf{C}_{13}+\mathbf{C}_{33})\mathbf{z} & \mathbf{C}_{44}\mathbf{r}+\mathbf{C}_{33}\mathbf{z}^2/\mathbf{r} & \mathbf{0} & \mathbf{C}_{44}\mathbf{r} & \mathbf{C}_{23}\mathbf{z} \\ \mathbf{0} & \mathbf{0} & \mathbf{0} & \mathbf{0} & \mathbf{0} & \mathbf{0} \\ \mathbf{0} & \mathbf{0} & \mathbf{C}_{44}\mathbf{r} & \mathbf{0} & \mathbf{C}_{44}\mathbf{r} & \mathbf{0} \\ \mathbf{C}_{23} & (\mathbf{C}_{12}+\mathbf{C}_{23})\mathbf{r} & \mathbf{C}_{23}\mathbf{z} & \mathbf{0} & \mathbf{0} & \mathbf{C}_{22}\mathbf{r} \end{bmatrix}$$

Thus the expressions in (3.75) must be integrated over the cross sectional area of the ring. This can be done quite easily by means of numerical integration formulas. After doing this, the nodal point stiffness matrix can be evaluated from the formula

$$[k] = [A^{-1}]^{t} \int_{\text{area}} [D]^{t} [C][D] r dr dz [A^{-1}]$$
 (3.76)

Note, the constant 2π as mentioned earlier is not included here.

Since the elements employed here are circular rings, the concept nodal point force must be generalized. It is convenient in this d to speak of nodal circle forces. These are then forces on circles dius equal to the nodal point radius. Thus the problem of replacing ary tractions by nodal forces involves determining nodal circle loads. of the general aspects of the problem are considered here.

For convenience, consider e 3.7 where a traction q(r) is assumed t normal to the area shown. s 1 and 2 are on one side of

indary element. Again for nience, the line 1-2 is taken horizontal.

The work of the applied ng during a virtual displacement

is

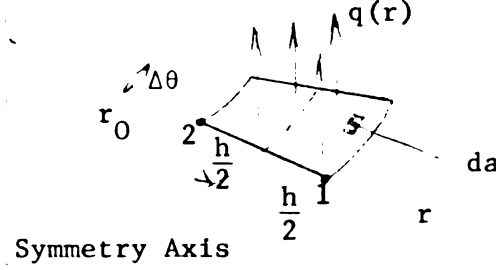


Figure 3.7

Axial Boundary Traction-CSTR

$$\delta W_1 = \int_{B} \delta w \ q(r) \ da \tag{3.77}$$

isplacement w(r,z) can be related to nodal point displacements through rix of weighting functions as was done in equations (3.28). Thus

$$w(r,z) = [N(r,z)]^{t} [u_{z}]$$
 (3.78)

$$\left[\mathbf{u}_{\mathbf{z}}\right]^{\mathsf{t}} = \left\langle \mathbf{w}_{1} \mathbf{w}_{2} \dots \mathbf{w}_{n} \right\rangle \tag{3.79}$$

e last expression n represents the number of nodal points for the ent.

Eval

i n

ž

λε tá

intens

Now th

the co

An e_{λ_1}

Evaluation of (3.78) on the boundary leads to

$$\mathbf{w}_{\mathbf{B}} = [\mathbf{N}_{\mathbf{B}}]^{\mathsf{t}} [\mathbf{u}_{\mathbf{z}}] \tag{3.80}$$

In view of (3.80), equation (3.77) can be written as

$$\delta W_{1} = \int_{R} q(r) \left[N_{B}\right]^{t} da \left[\delta u_{z}\right]$$
 (3.81)

The work done by a set of nodal circle forces with intensities $\mathbf{f_{i_{2}}} \quad \text{is} \quad$

$$\delta W_2 = 2\pi \left[rf_2 \right]^{t} \left[\delta u_2 \right] \tag{3.82}$$

The matrix $[rf_z]$ is a column matrix of products of nodal circle force intensities and their corresponding radii. It has the form

$$[rf_z]^t = \langle r_1 f_1, r_2 f_2, \dots, r_n f_n \rangle$$
 (3.83)

Now the $[\delta u_z]$ are arbitrary nodal point displacements consistent with the constraints in the problem. Thus when δW_1 is equated to δW_2 one obtains

$$2\pi \left[rf_{z}\right]^{t} = \int_{R} q(r) \left[N_{B}\right]^{t} da \qquad (3.84)$$

An example will illustrate the procedure.

From the second equation of (3.67)

$$w(r,0) = \alpha_4 + \alpha_5 r \tag{3.85}$$

Evaluating this expression at points 1 and 2 leads to

$$w_{1} = \alpha_{4} + \alpha_{5}(r_{0} + \frac{h}{2})$$

$$w_{2} = \alpha_{4} + \alpha_{5}(r_{0} - \frac{h}{2})$$
(3.86)

It should be observed in Figure 3.7 that r_1 and r_2 are taken as $r_0 + \frac{h}{2}$ and $r_0 - \frac{h}{2}$ respectively. Equations (3.86) are readily solved for α_4 and α_5 and when these are introduced into (3.85) the result is

$$w(r,o) = (\frac{1}{2} - \frac{r_0}{h} + \frac{r}{h}) w_1 + (\frac{1}{2} + \frac{r_0}{h} - \frac{r}{h}) w_2$$
 (3.87)

Thus the matrix of weighting functions is

$$[N_B]^t = \left\langle (\frac{1}{2} - \frac{r_0}{h} + \frac{r}{h}) + (\frac{1}{2} + \frac{r_0}{h} - \frac{r}{h}) \right\rangle$$

The components of equation (3.84) are then

$$2\pi \left(r_{0} + \frac{h}{2}\right) f_{1z} = \int_{B} q(r) \left(\frac{1}{2} - \frac{r_{0}}{h} + \frac{r}{h}\right) da$$

$$2\pi \left(r_{0} - \frac{h}{2}\right) f_{2z} = \int_{B} q(r) \left(\frac{1}{2} - \frac{r_{0}}{h} + \frac{r}{h}\right) da$$

$$(3.88)$$

$$f_{3z} = 0$$

If q(r) is a constant of magnitude q,

For a 1

Undecess
(3.90).

total ::

Tais cor

since the

of the as

Where [F]

intensiti.

of [F] by

$$f_{1z} = \frac{qh}{2} \left(\frac{r_0 + \frac{h}{6}}{r_0 + \frac{h}{2}} \right)$$

$$f_{2z} = \frac{qh}{2} \left(\frac{r_0 - \frac{h}{6}}{r_0 + \frac{h}{2}} \right)$$
(3.89)

a linearly varying load, $q(r) = q_1 + \frac{q_1 - q_2}{h} (r - r_0 - \frac{h}{2})$

$$f_{1_{\mathbf{z}}} = \frac{\frac{q_{1}^{h}}{3} (r_{0} + \frac{h}{4}) + \frac{q_{2}r_{0}^{h}}{6}}{r_{0} + \frac{h}{2}}$$
(3.90)

$$f_{2} = \frac{\frac{q_{1}r_{0}h}{6} + \frac{q_{2}h}{3} (r_{0} - \frac{h}{4})}{r_{0} - \frac{h}{2}}$$

In assembling the overall structural load vector, it is
essary to perform the division indicated in equations (3.89) and

The form of (3.88) can be adhered to by defining a structural
circle load as the total load on a circle of the prescribed radius.
corresponds to the left hand sides of equations (3.88). However,
the numerical factor 2π also appears in the generalized stiffness
tit can be cancelled as indicated previously. Thus, the behavior
essembled structure is characterized by the equation

$$[rF] = [K][s]$$

$$(3.91)$$

[F] is the column matrix of assembled structure nodal circle force

Sities. The elements of [rF] are obtained by multiplying the elements

] by the corresponding nodal circle radii.

3.6 <u>Line</u>

•

notal for the previ

treated

ring ele

of the p

the fin

shire i

Mial p

consist

vertice of its

Point :

functi

evalu

tadia

3.6 Linear Strain Triangular Ring

The procedure for developing the stiffness matrix and associated nodal force vector for such an element has been essentially covered in the previous articles. The notion of a quadratic strain variation was treated in article 3.4. The important aspects of an axially symmetric ring element were discussed in article 3.5. Consequently only a few of the pertinent results are included here.

A portion of
the finite element is
shown in Figure 3.8. The
nodal point system
consists of the triangle
vertices and the midpoints
of its sides. The nodal
point coordinates are



$$r_j$$
 $j = 1,2,...6$
 z_j $j = 1,2,...6$

The assumed displacement

functions are

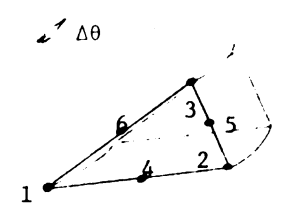


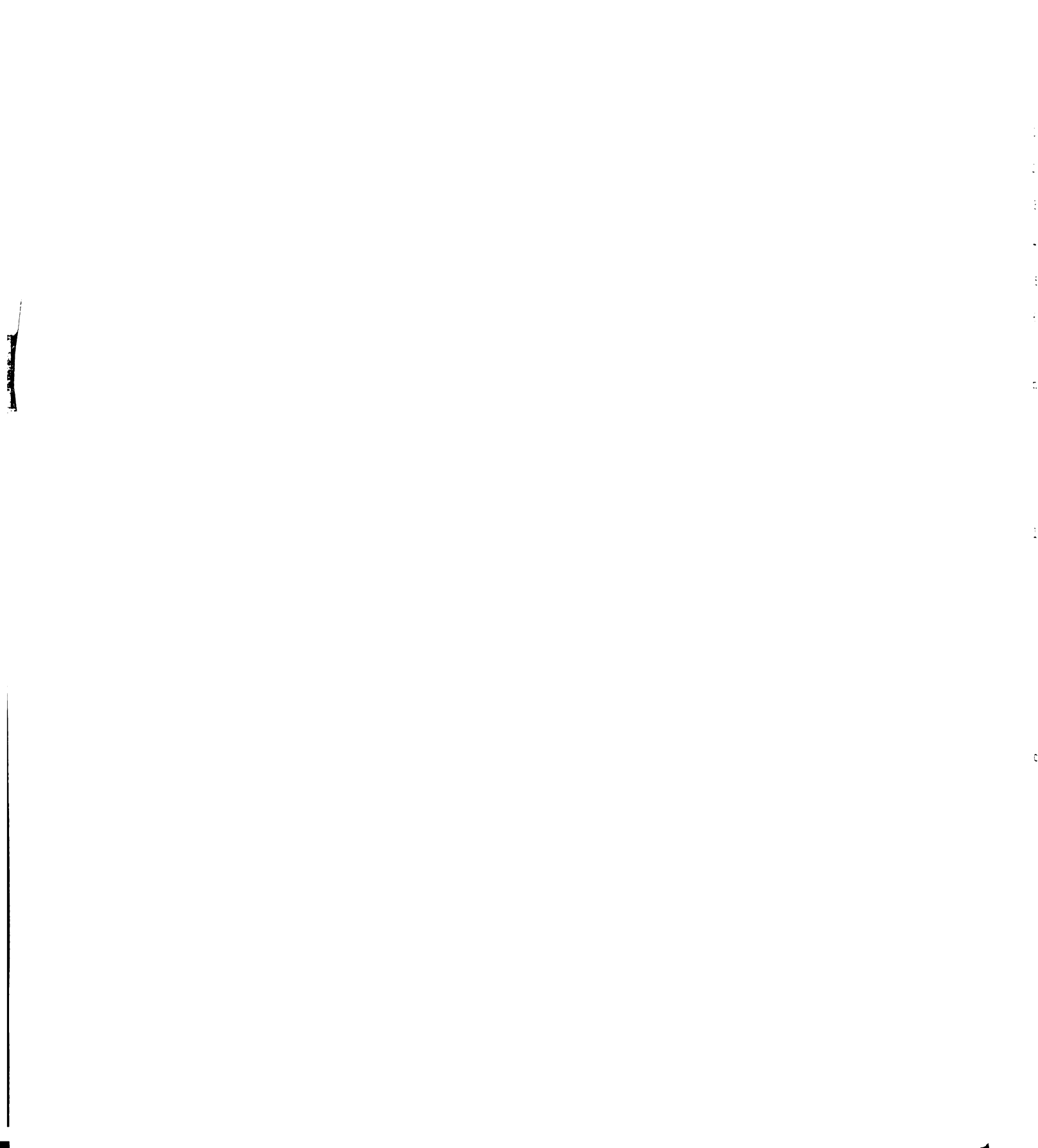
Figure 3.8
Linear Strain Triangular
Ring Segment

r

$$u(r,z) = \alpha_1 + \alpha_2 r + \alpha_3 z + \alpha_4 r^2 + \alpha_5 rz + \alpha_6 z^2$$

$$w(r,z) = \alpha_7 + \alpha_8 r + \alpha_9 z + \alpha_{10} r^2 + \alpha_{11} rz + \alpha_{12} z^2$$
(3.92)

The nodal point displacements follow when equations (3.92) are evaluated at the coordinates (r_j, z_j) . For example, the column matrix of radial displacements is



$$\begin{pmatrix}
\mathbf{u}_{1} \\
\mathbf{u}_{2} \\
\mathbf{u}_{3} \\
\mathbf{u}_{4} \\
\mathbf{u}_{5}
\end{pmatrix} = \begin{bmatrix}
1 & \mathbf{r}_{1} & \mathbf{z}_{1} & \mathbf{r}_{1}^{2} & \mathbf{r}_{1}\mathbf{z}_{1} & \mathbf{z}_{1}^{2} \\
1 & \mathbf{r}_{2} & \mathbf{z}_{2} & \mathbf{r}_{2}^{2} & \mathbf{r}_{2}\mathbf{z}_{2} & \mathbf{z}_{2}^{2} \\
1 & \mathbf{r}_{3} & \mathbf{z}_{3} & \mathbf{r}_{3}^{2} & \mathbf{r}_{3}\mathbf{z}_{3} & \mathbf{z}_{3}^{2} \\
1 & \mathbf{r}_{4} & \mathbf{z}_{4} & \mathbf{r}_{4}^{2} & \mathbf{r}_{4}\mathbf{z}_{4} & \mathbf{z}_{4}^{2} \\
1 & \mathbf{r}_{5} & \mathbf{z}_{5} & \mathbf{r}_{5}^{2} & \mathbf{r}_{5}\mathbf{z}_{5} & \mathbf{z}_{5}^{2} \\
1 & \mathbf{r}_{6} & \mathbf{z}_{6} & \mathbf{r}_{6}^{2} & \mathbf{r}_{6}\mathbf{z}_{6} & \mathbf{z}_{6}^{2}
\end{bmatrix}$$

$$\begin{pmatrix}
\alpha_{1} \\
\alpha_{2} \\
\alpha_{3} \\
\alpha_{4} \\
\alpha_{5} \\
\alpha_{6}
\end{pmatrix}$$

$$(3.92)$$

or in short

$$[u_r] = [A_{11}] [\alpha_r]$$

Similarly

$$[\mathbf{u}_{\mathbf{z}}] = [\mathbf{A}_{22}][\alpha_{\mathbf{z}}]$$

and

$$[A_{22}] = [A_{11}]$$

The column matrices in the above relationships are

$$[u_{r}]^{t} = \langle u_{1} u_{2} u_{3} u_{4} u_{5} u_{6} \rangle$$

$$[u_{z}]^{t} = \langle w_{1} w_{2} w_{3} w_{4} w_{5} w_{6} \rangle$$
(3.94)

$$\left[\alpha_{\mathbf{r}}\right]^{\mathsf{t}} = \left\langle \alpha_{1} \alpha_{2} \alpha_{3} \alpha_{4} \alpha_{5} \alpha_{6} \right\rangle \tag{3.95}$$

$$\left[\alpha_{z}\right]^{t} = \left\langle \alpha_{7} \alpha_{8} \alpha_{9} \alpha_{10} \alpha_{11} \alpha_{12} \right\rangle$$

Then

The inver

vith

It is ag

The stra

Tae Ia

net1%ec

Then

$$[\mathbf{u}] = [\mathbf{A}][\alpha] = \begin{bmatrix} \mathbf{A}_{11} & \mathbf{A}_{22} \\ \mathbf{A}_{22} & \mathbf{A}_{22} \end{bmatrix} \begin{bmatrix} \alpha_{\mathbf{r}} \\ \alpha_{\mathbf{z}} \end{bmatrix}$$
(3.96)

The inverse transformation is

$$[\alpha] = \begin{bmatrix} A_{11}^{-1} & 0 \\ 0 & A_{22}^{-1} \end{bmatrix} \begin{bmatrix} u_r \\ u_z \end{bmatrix}$$
 (3.97)

with

$$[A_{22}^{-1}] = [A_{11}^{-1}]$$

It is again desirable to compute the inverse matrix numerically.

The strains are given by

$$\varepsilon (\mathbf{r}, \mathbf{z}) = \begin{pmatrix} \frac{\partial \mathbf{u}}{\partial \mathbf{r}} \\ \frac{\partial \mathbf{w}}{\partial \mathbf{z}} \\ \frac{\mathbf{u}}{\mathbf{r}} \\ \frac{\partial \mathbf{u}}{\partial \mathbf{z}} + \frac{\partial \mathbf{v}}{\partial \mathbf{r}} \end{pmatrix} = [\mathbf{D}(\mathbf{r}, \mathbf{z})][\alpha]$$

The matrix [D(r,z)] consists of displacement function gradients and is derived from equations (3.92).

P(r,z) =

relation

The inte

The Tati

(3.98)

The stresses are related to strains through the constitutive relationships (3.72). The generalized stiffness matrix is

$$[k_{\alpha}] = \int_{VO^1} [D]^t [C][D] dV$$

The integrand is of the form

$$[D]^{t} [C][D] = \begin{bmatrix} Q_{11} & Q_{12} \\ -- & Q_{21} & Q_{22} \end{bmatrix}$$

The matrices $[Q_{ij}]$ i, j = 1, 2 are presented on the following page.

$$\begin{bmatrix} c_{11} & c_{11} + c_{12} & c_{11} z \\ \hline r^2 & \frac{c_{11} z}{r^2} & \frac{c_{11} z}{r^2} & 2c_{12} + c_{11} & (c_{11} + c_{12}) \frac{z}{r} & c_{11} \frac{z^2}{r^2} \\ & 2(c_{11} + c_{12}) & (c_{11} + c_{12}) \frac{z}{r} & 3(c_{11} + c_{12}) r & 2(c_{11} + c_{12}) & (c_{11} + c_{12}) \frac{z^2}{r} \\ & c_{11} \frac{z^2}{r^2} + c_{44} & (2c_{12} + c_{11}) z & (c_{11} + c_{12}) \frac{z}{r} + c_{44} r & c_{11} \frac{z^3}{r^2} + 2c_{44} z \\ & (5c_{11} + 4c_{12}) r^2 & 3(c_{11} + c_{12}) rz & (2c_{12} + c_{11}) z^2 \\ & 2(c_{11} + c_{12}) z^2 + c_{44} r^2 & (c_{11} + c_{12}) \frac{z^3}{r} + 2c_{44} rz \\ & (\text{Symmetric}) & c_{11} \frac{z^2}{r^2} + 4c_{44} z^2 \end{bmatrix}$$

$$[Q_{12}] = [Q_{21}] \tag{3.99}$$

$$\begin{bmatrix} Q_{21} \end{bmatrix} = \begin{bmatrix} 0 & 0 & \frac{C_{12}}{r} & 0 & C_{12} & 2C_{12} \frac{z}{r} \\ 0 & 0 & 2C_{12} & 0 & 2C_{12}r & 4C_{12}z \\ 0 & C_{44} & C_{12} \frac{z}{r} & 2C_{44}r & (C_{12} + C_{44})z & 2C_{12} \frac{z^2}{r} \\ 0 & 0 & 3C_{12}r & 0 & 3C_{12}r^2 & 6C_{12}rz \\ 0 & C_{44}r & 2C_{12}z & 2C_{44}r^2 & (2C_{12} + C_{44})rz & 4C_{12}z^2 \\ 0 & 2C_{44}r & C_{12}\frac{z^2}{r} & 4C_{44}rz & (C_{12} + 2C_{44})z^2 & 2C_{12}\frac{z^3}{r} \end{bmatrix}$$

$$\begin{bmatrix} Q_{22} \end{bmatrix} = \begin{bmatrix} 0 & 0 & 0 & 0 & 0 & 0 & 0 \\ & C_{uu} & 0 & 2C_{uu}r & C_{uu}z & 0 & & \\ & & C_{11} & 0 & C_{11}r & 2C_{11}r & & \\ & & & 4C_{uu}r^2 & 2C_{uu}rz & 0 & & \\ & & & & C_{11}r^2 + C_{uu}z^2 & 2C_{11}rz & \\ & & & & 4C_{11}z^2 & & \\ \end{bmatrix}$$

These expressions assume orthotropic behavior which is identified by the matrix of elastic properties in equation (3.72).

the coef

nlane. over th

intei

kõed t äλes,

the di

ir :

in te

To completely formulate the generalized stiffness matrix, $[k_{\alpha}]$, the coefficients of equations (3.99) must be integrated over the element volume. The axial symmetry quickly reduces this to an area integration over the triangular cross section. The latter is most efficiently performed by numerical integration formulas.

The nodal point stiffness matrix is

$$[k] = [A^{-1}]^T [k_{\alpha}][A^{-1}]$$

When these element matrices are referred to the same global coordinate axes, the overall structural stiffness matrix is easily assembled by the direct stiffness approach.

Nodal circle force intensities are determined as in article 3.5 for the constant strain ring. From the second of equations (3.92)

$$w(r,0) = \alpha_7 + \alpha_8 r + \alpha_{10} r^2$$
 (3.100)

In terms of nodal point displacements w_1 , w_2 and w_4 this becomes

$$\mathbf{w}(\mathbf{r},0) = \left[\left(-\frac{\mathbf{r}_0}{2h} + \frac{\mathbf{r}_0^2}{2h^2} \right) + \left(\frac{1}{2h} - \frac{\mathbf{r}_0}{h^2} \right) \mathbf{r} + \frac{1}{2h^2} \mathbf{r}^2 \right] \mathbf{w}_1$$

$$+ \left[\left(\frac{\mathbf{r}_0}{2h} + \frac{\mathbf{r}_0^2}{2h^2} \right) + \left(-\frac{1}{2h} - \frac{\mathbf{r}_0}{h^2} \right) \mathbf{r} + \frac{1}{2h^2} \mathbf{r}^2 \right] \mathbf{w}_2$$

$$+ \left[\left(1 - \frac{\mathbf{r}_0^2}{h^2} \right) + \frac{2\mathbf{r}_0^2}{h^2} \mathbf{r} - \frac{1}{h^2} \mathbf{r}^2 \right] \mathbf{w}_4$$

man of

circle

r, ani

i Test

article

fille.

Q (1) =

The notation here is of Figure 3.9. The nodal le radii are $r_0 + \frac{h}{2}$, and $r_0 - \frac{h}{2}$ for r_1 , r_4 , and espectively.

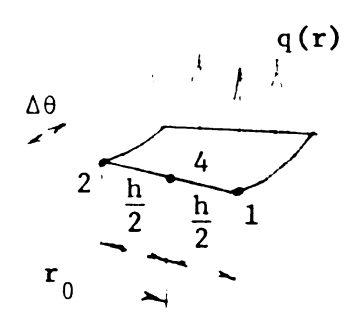
Using the procedure of ele 3.5, one is led to the owing nodal circle force esities for the case = q, a constant:

$$\mathbf{f}_{1_{\mathbf{Z}}} = \frac{1}{6} \, \mathbf{qh}$$

$$f_4 = \frac{2}{3} qh$$

$$f_{2z} = \frac{1}{6} qh$$

Z

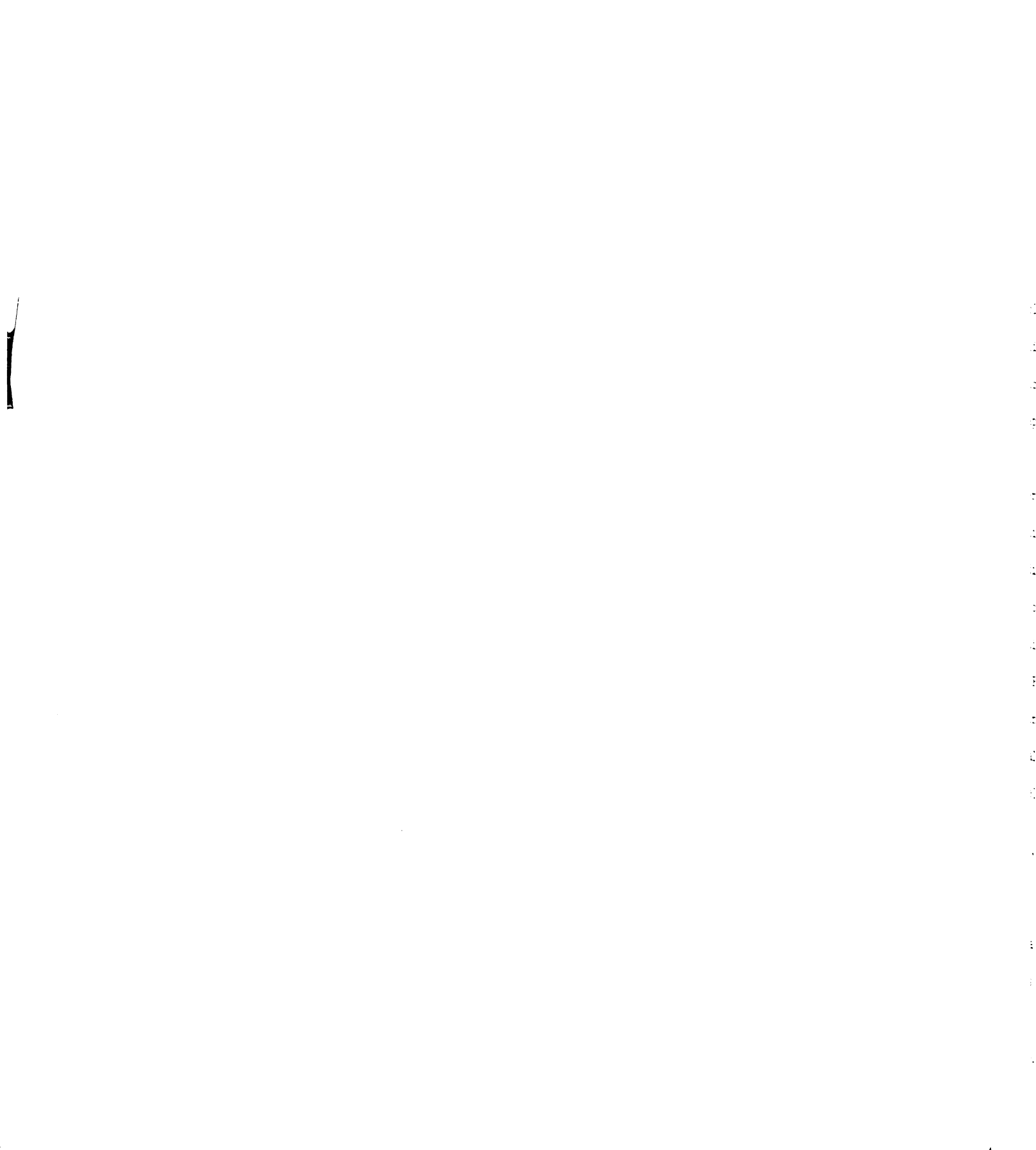


r

Figure 3.9

Axial Boundary Traction-LSTR

(3.102)



IV. PLANE STRESS APPLICATIONS

The various finite element methods have been widely applied to plane problems in continuum mechanics. Finite difference methods have likewise proved to be extremely useful in plane stress analysis; however, most of the applications have involved the stress function approach.

Treated first are several plane stress applications. The emphasis is placed on the comparison of the methods involved. Two finite element solutions are presented in each case. These involve the direct stiffness method using linear strain triangles (LST) in the one solution and constant strain triangles (CST) in the other. One finite difference solution is given as obtained by the displacement formulation (FD). Hereafter, the abbreviations LST, CST, and FD will be used to indicate such solutions. In some examples, the elasticity solution is also available. The designation "exact" when used will refer to the elasticity solution.

4.1 Cantilever Beam

As a first example, consider the cantilever beam of Figure 4.1-a, Page 96. The beam carries a parabolic load on its end whose resultant is 1000 pounds. Its dimensions in inches include a length of 6, a depth of 2, and a thickness of 1/2. The assumed material properties are:

Young's modulue $E = 10^7$ psi and Poisson's ratio $v = \frac{1}{4}$.

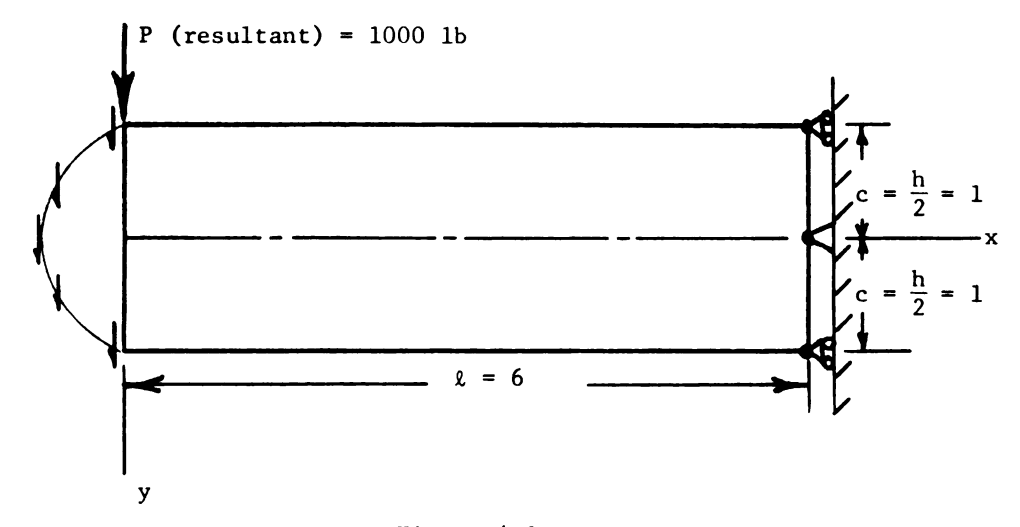


Figure 4.la

Cantilever Beam

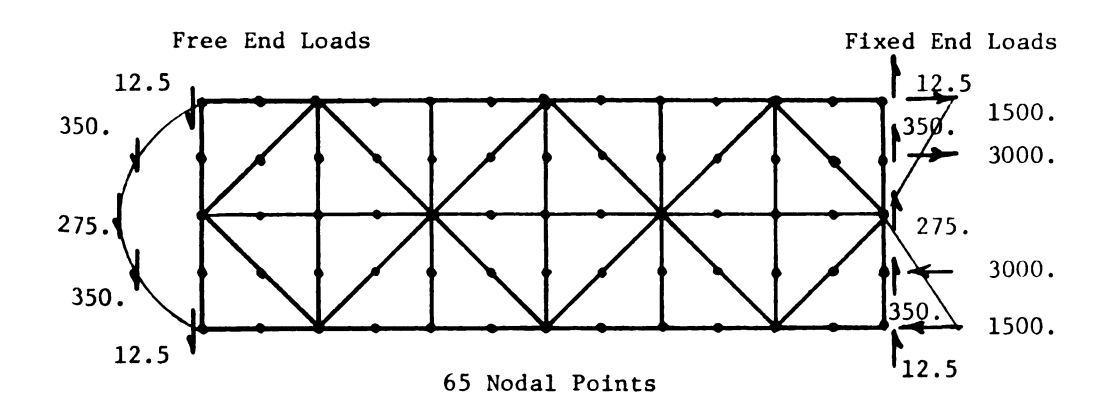


Figure 4.1-b

Cantilever Beam - LST Finite Element Configuration

This same problem, with somewhat different properties, was dealt with in a paper by Argyris [15]. The author compares the end deflection obtained from LST and CST solutions with the exact solution. He concludes that the CST solution is unsuitable for this situation.

Elasticity Solution. The cantilever beam is a classical problem of the theory of elasticity. Its solution may be found in any of the popular texts. For example, Timoshenko and Goodier present the solution for two different sets of displacement boundary conditions. The boundary conditions of the present problem have been chosen so as to allow free warping of the supported end. Thus in Figure 4.1-a, it can be observed that $u(\ell, 0) = v(\ell, 0) = 0$ and $u(\ell, c) = u(\ell, -c) = 0$. The latter prevent rigid body rotation. Following the approach of Timoshenko [39], the stresses

$$\sigma_{x} = -\frac{Pxy}{I}$$

$$\sigma_{y} = 0$$

$$\tau_{xy} = -\frac{P}{2I} (c^{2} - y^{2})$$

are valid at points sufficiently distant from the supported end. The displacements are

$$u(x,y) = -\frac{Px^{2}y}{2EI} - \frac{Py^{3}}{6EI} + \frac{Py^{3}}{6IG} - (\frac{Pc^{2}}{6IG} - \frac{P\ell^{2}}{2EI} - v \frac{Pc^{2}}{6EI}) y$$

$$v(x,y) = \frac{Pxy^{2}}{2EI} + \frac{Px^{3}}{6EI} - (\frac{Pc^{2}}{3IG} + v \frac{Pc^{2}}{6EI} + \frac{P\ell^{2}}{2EI}) x$$

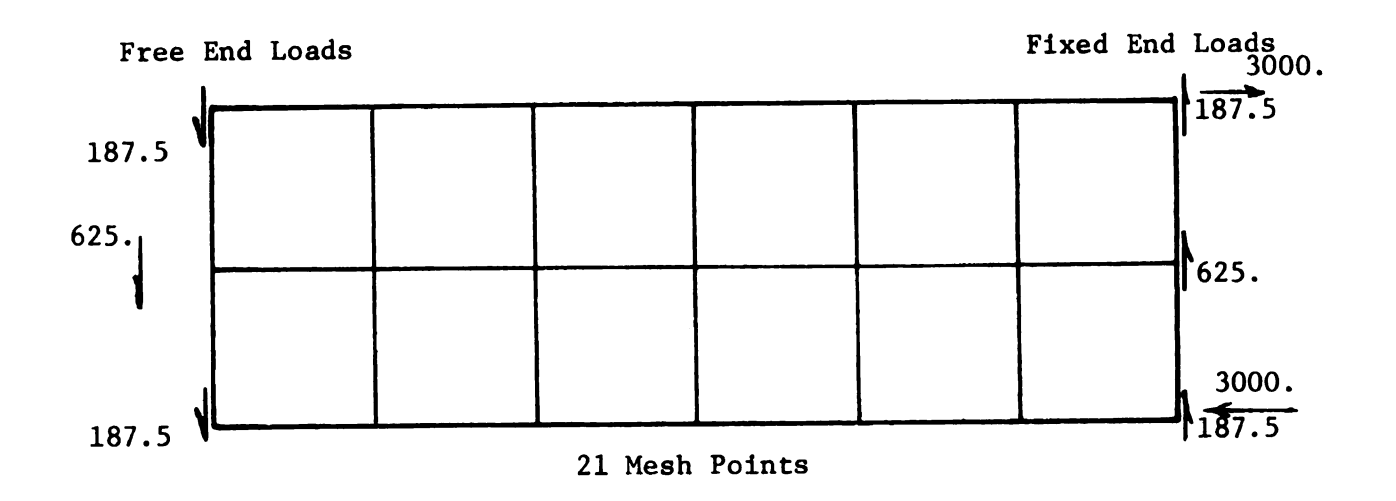
$$+ (\frac{P\ell^{2}c}{3IG} + v \frac{P\ell^{2}c}{6EI} + \frac{P\ell^{3}}{3EI})$$

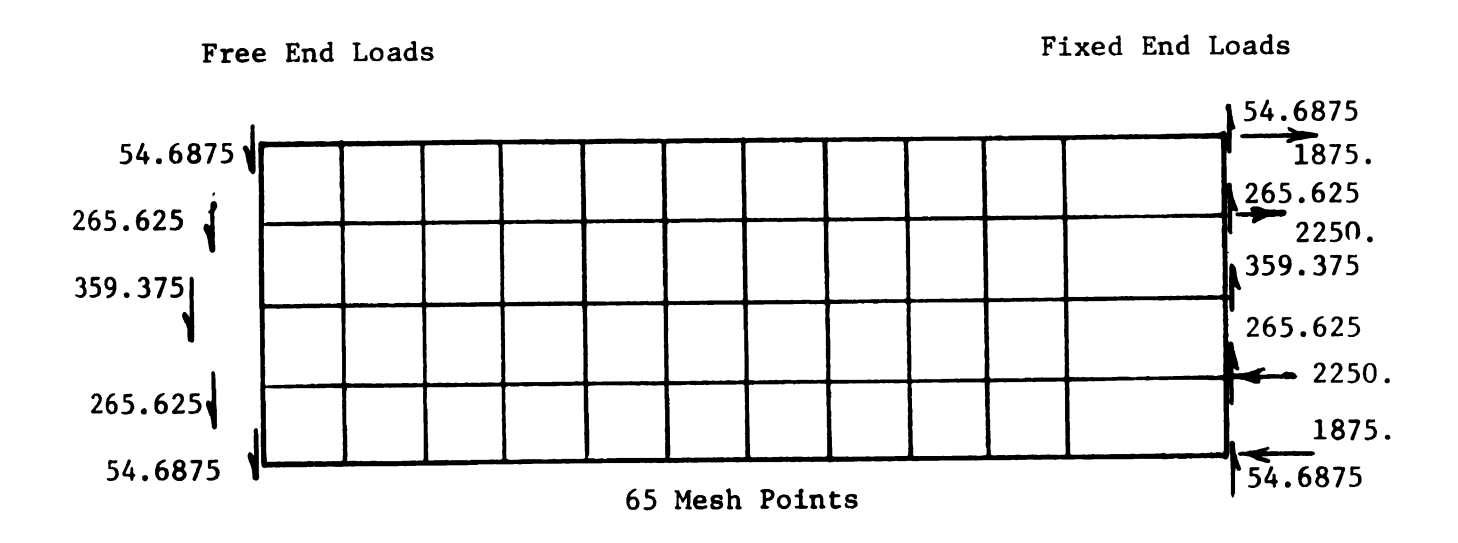
where I represents the area moment of inertia of the beam cross section and G is the shear modulus.

It is clear that the above stresses are strictly correct only when the load is distributed parabolically over the free end. However, any statically equivalent end load will produce these stresses at points sufficiently distant from the free end. In the finite element and finite difference methods, distributed loads are replaced by suitable concentrated forces. Thus in Figure 4.1-b, a set of end loads corresponding to parabolic loading on LST elements is shown. Similarly, fixed end loads are imposed corresponding to parabolic transverse loading and linear longitudinal loading. The presence of these loads insures the validity of the above stresses throughout the beam.

Finite Difference Solution. The finite difference solution was worked out for 3 mesh point systems. This was done to give some indication of the convergence to the exact solution as the number of mesh points is increased. The three configurations chosen for this purpose are shown in Figure 4.2. The mesh point spacing has been successively reduced by a factor of 2. Accordingly, the mesh point systems consist of 21, 65, and 225 mesh points respectively. The end loads are also shown.

Figure 4.3, displays the beam deflections obtained using these three approximations. As would be expected, the results are not Particularly good until a large number of mesh points is used. Thus the 225 mesh point approximation gives a maximum deflection of 2.237 × 10⁻² in. The error here is 3.47%. It is apparent that conversences to the exact solution occurs from below.





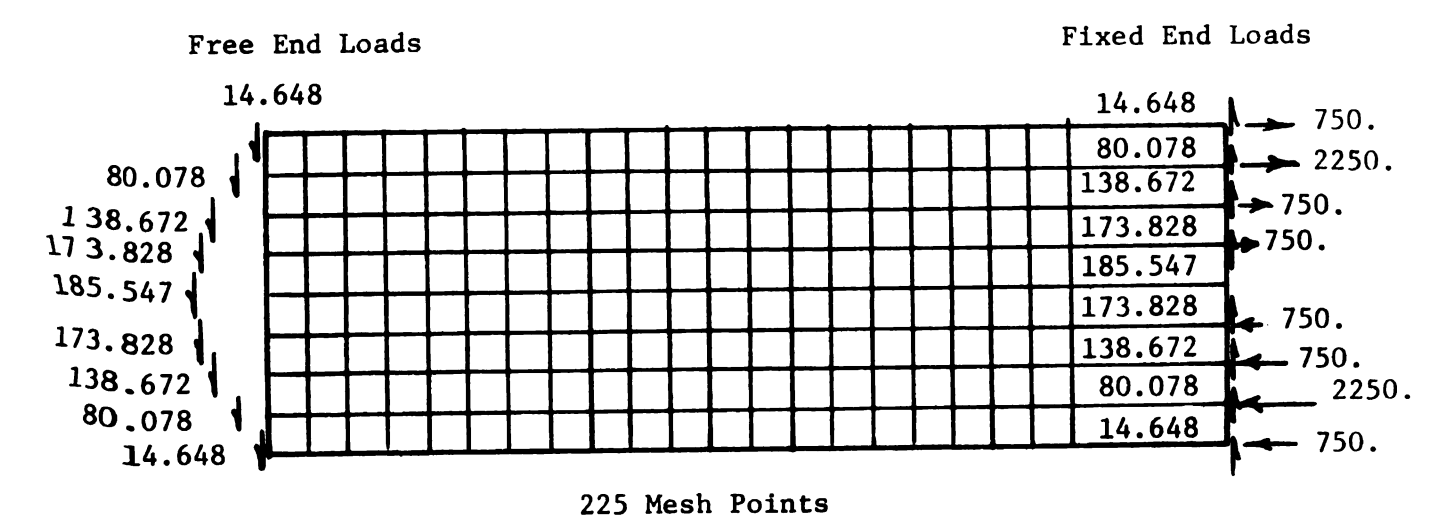


Figure 4.2

Cantilever Beam Finite Difference Configurations

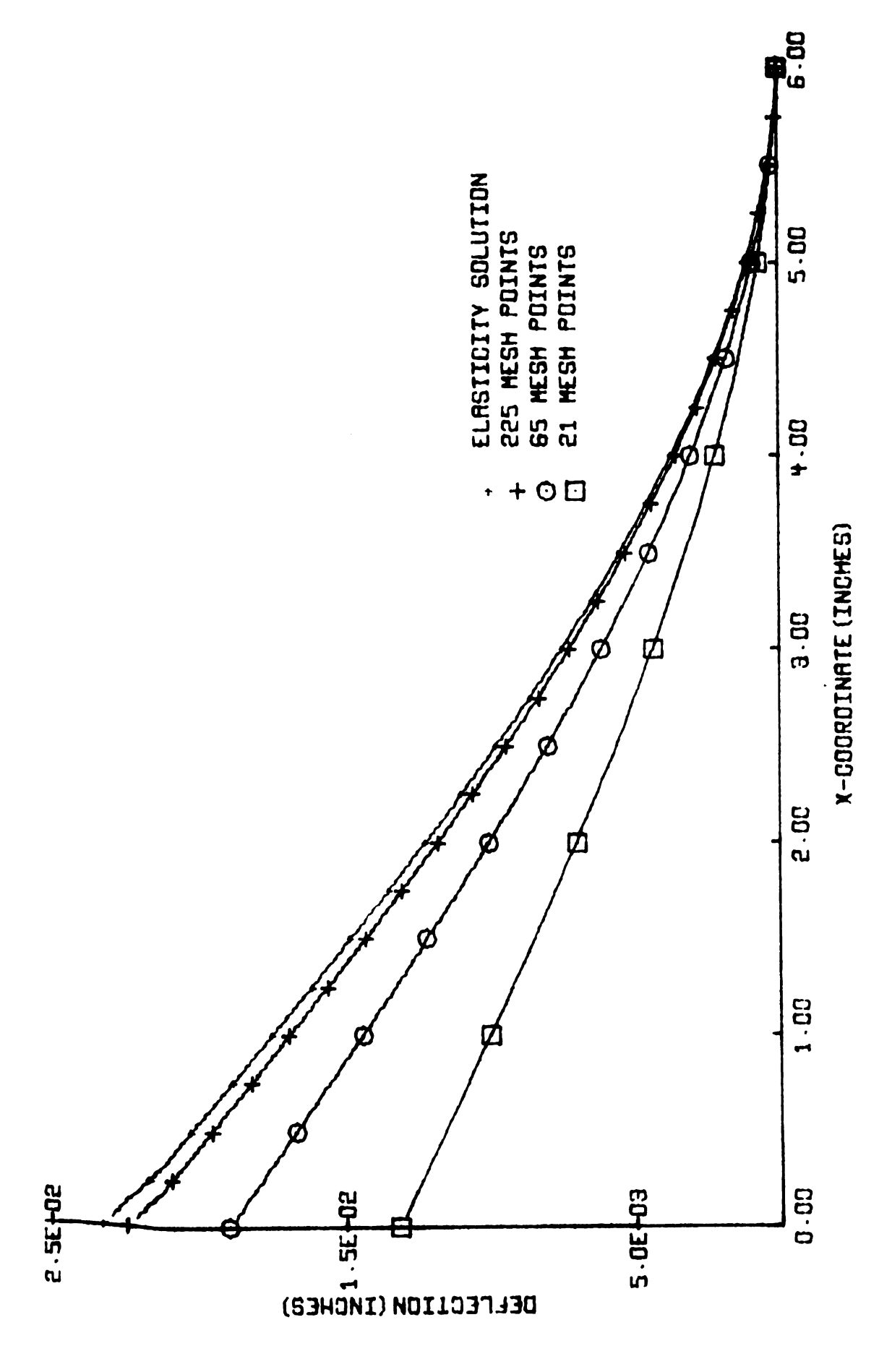


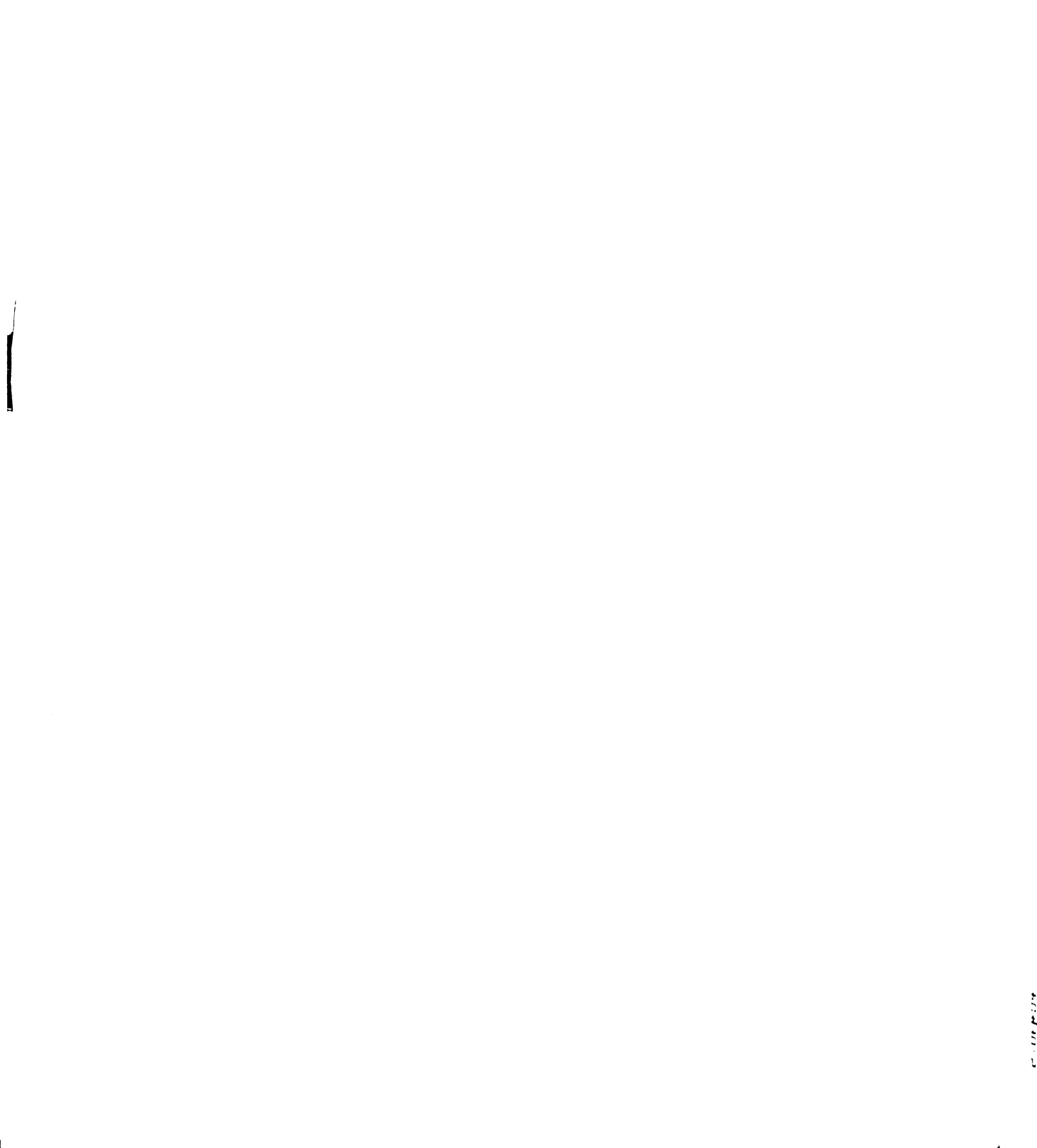
Figure 4.3, Finite Difference Beam Deflections

The flexural stress variation on the particular cross section $x = \frac{5}{6} \, \ell$ is shown in Figure 4.4, page 102. The pattern here is quite comparable to that which occurred for deflections. Very good stresses are obtained using the 225 mesh point approximation. The variation is essentially linear with a maximum value of 14,620 psi. This last result is 2.54% lower than the exact stress of 15,000 psi.

CST Solution. The finite element solution using constant strain triangles (CST) was carried through using the 3 configurations of Figure 4.5. These include 21 nodal points with 24 elements, 65 nodal points with 96 elements, and 225 nodal points with 384 elements. The locations of nodal points corresponds identically with the locations of mesh points for the previous finite difference solutions. The nodal point loads are the same as those for the finite difference solutions.

The deflection curves for these three approximations are plotted in Figure 4.6, page 104. The results compare quite closely with those obtained using the finite difference method. The lower order approximations are somewhat of an improvement over the corresponding FD solutions. The 225 point solution, however, is slightly worse. Thus for example, the end deflection is found to be 2.219×10^{-2} in. for the 225 point configuration. This is less than the exact value 2.3175×10^{-2} in. by 4.26%

The flexural stresses, obtained by averaging element stresses, are displayed in Figure 4.7 on page 105. They are generally comparable to FD stresses at interior points but are poorer indications of the true state of stress along boundaries, particularly at the lower order approximations. Even the 225 nodal point approximation gives rather



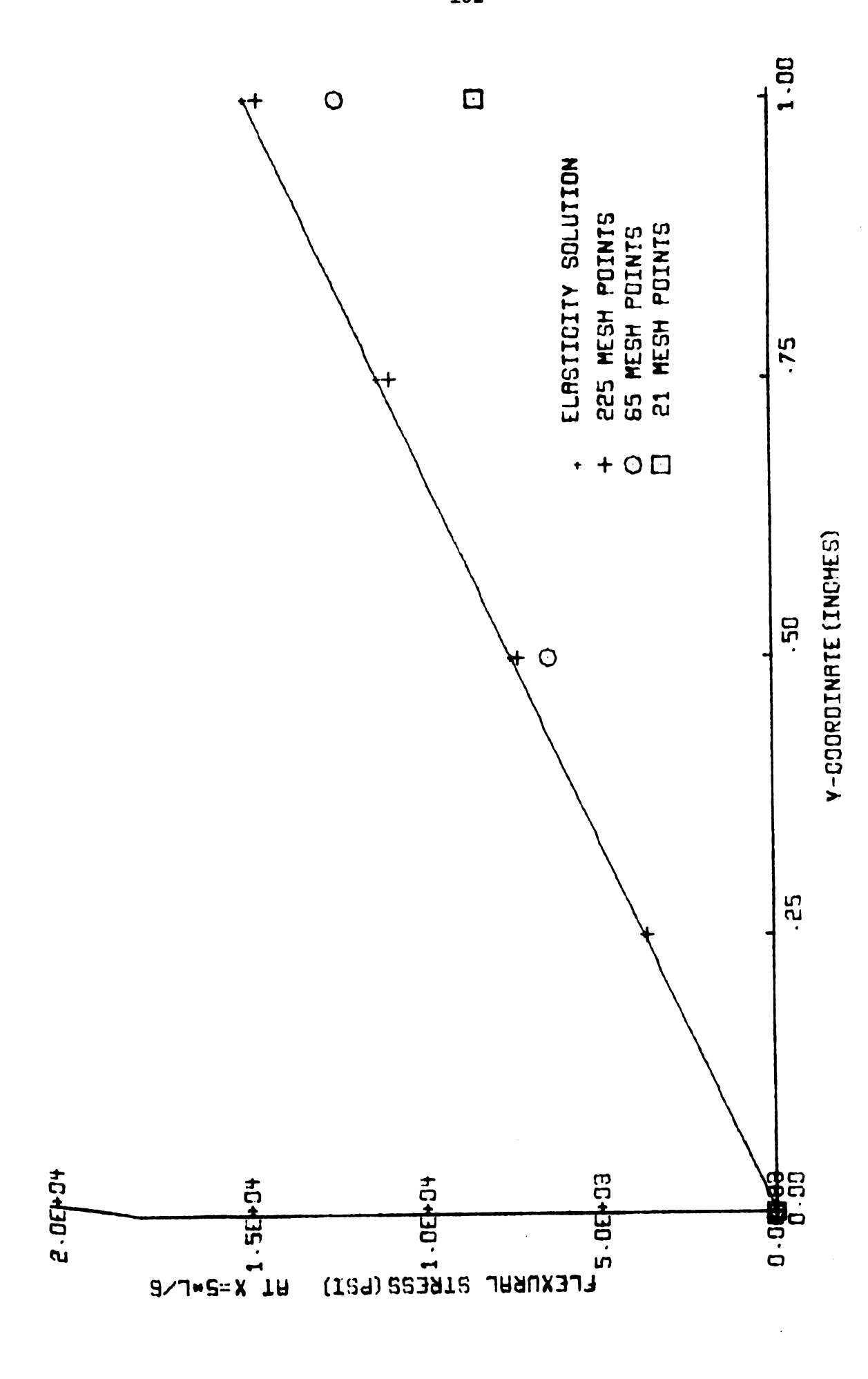
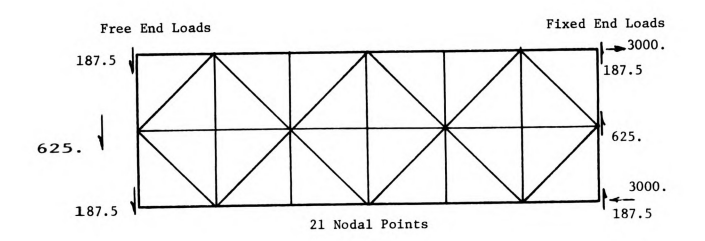
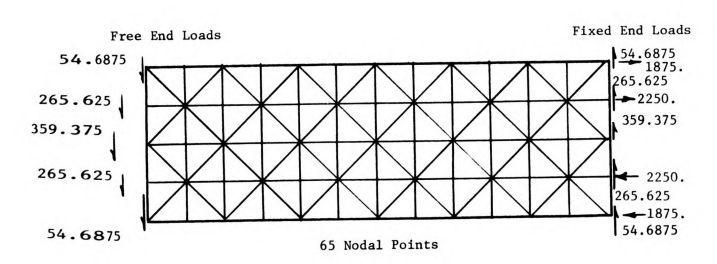


Figure 4.4, Finite Difference Flexural Stress





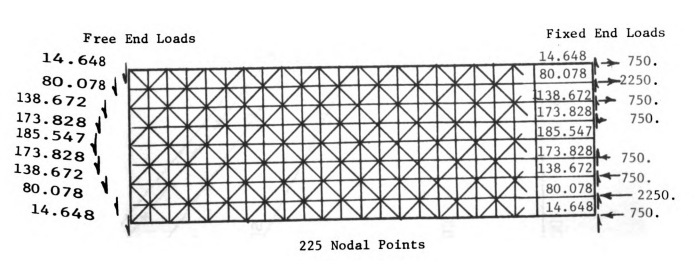


Figure 4.5

Cantilever Beam - CST Finite Element Configurations

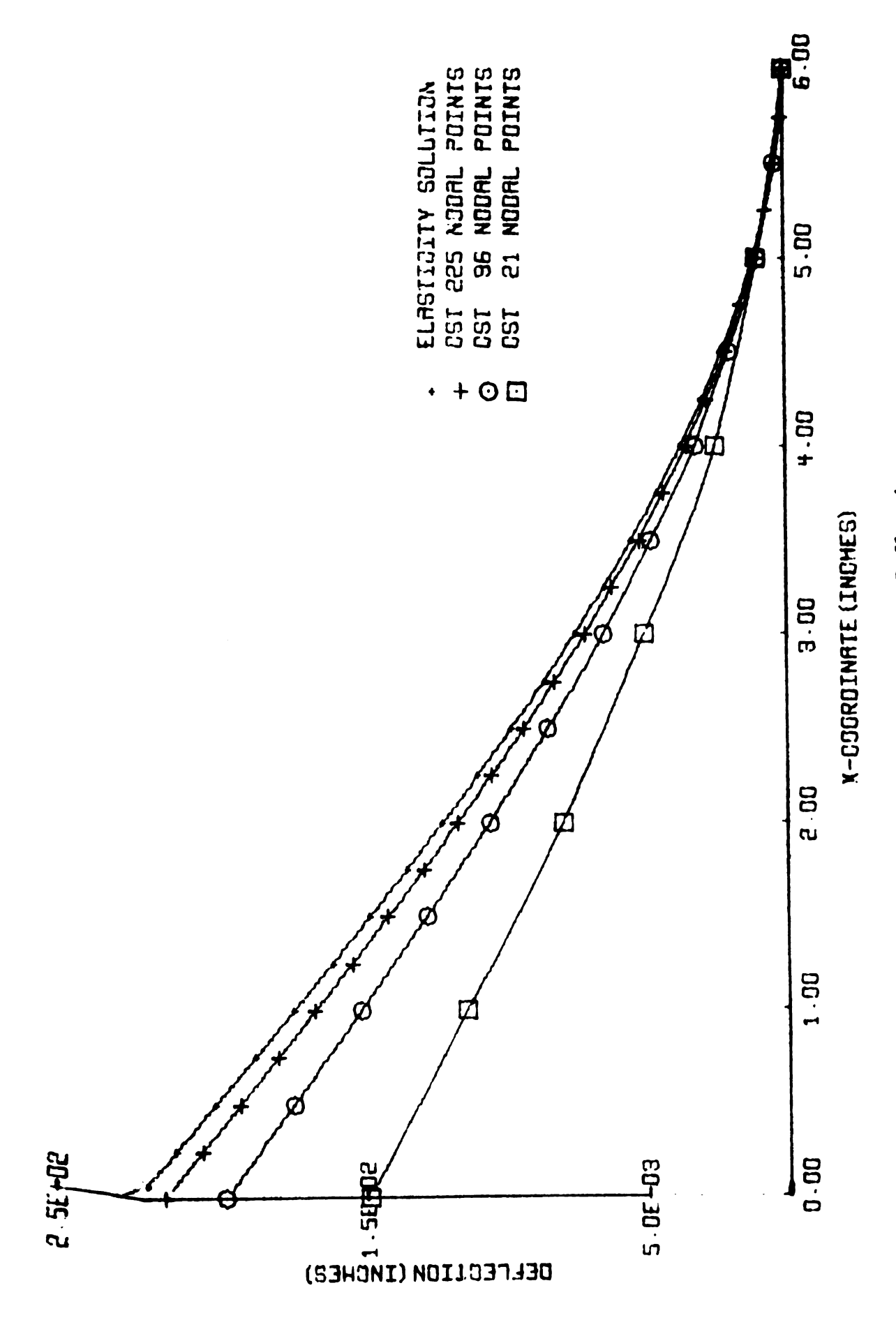


Figure 4.6, CST Beam Deflections

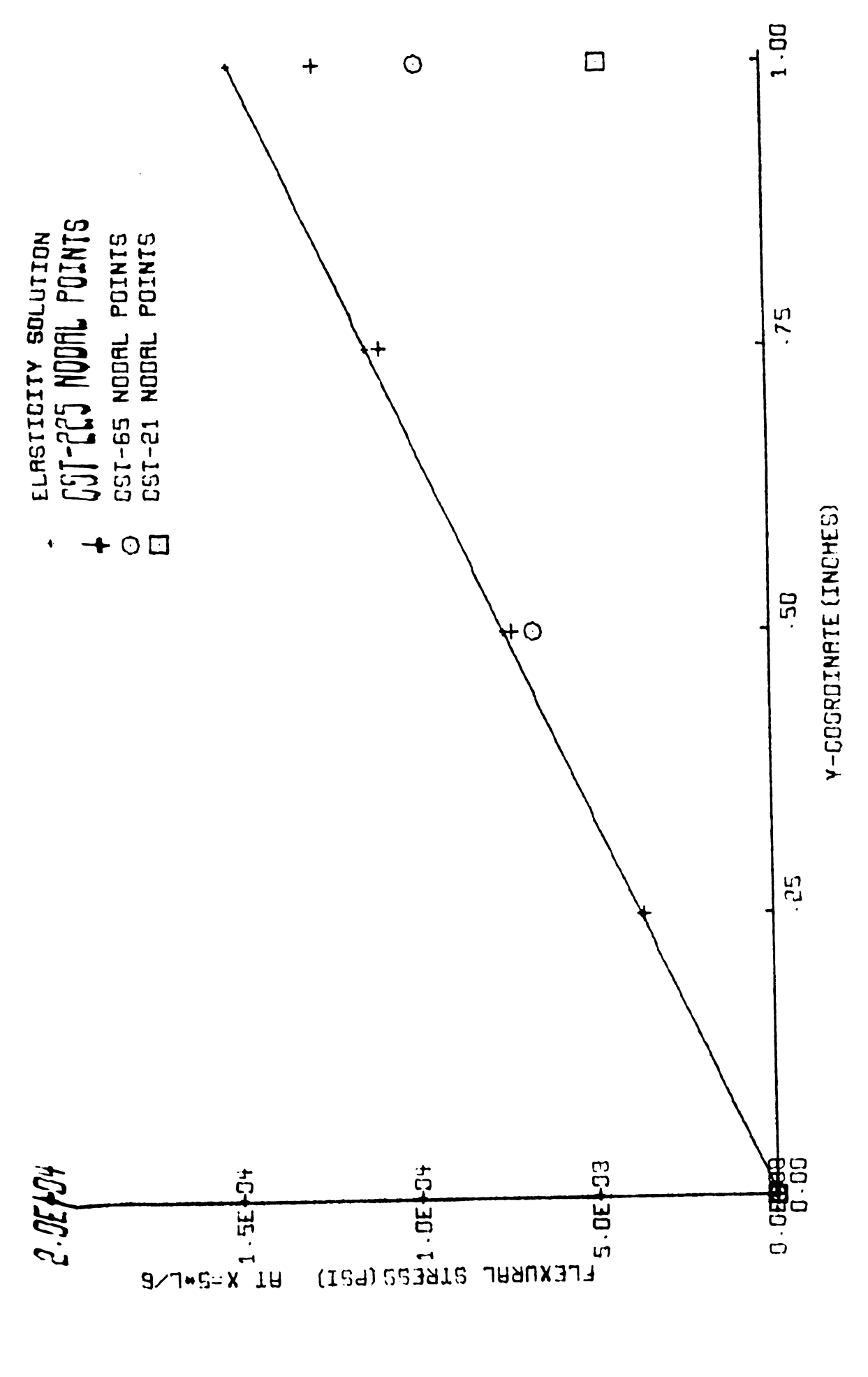


Figure 4.7, CST Flexural Stress

poor boundary stresses. For example, on the cross section $x = \frac{5}{6} \ell$ the maximum stress is 12,625 psi, some 15.8% less than the exact value. It should be mentioned, however, that the element layout affects the results to some extent. Thus for example, the layout of Figure 4.8 on page 107 gives somewhat better boundary stresses but less satisfactory interior stresses and deflections. The maximum stress on the section $x = \frac{5}{6} \ell$ is 13,912 psi compared to 12,625 for the former layout. The end deflections are 2.2004 × 10⁻² in. and 2.219 × 10⁻² in. respectively.

It should also be emphasized that in some cases it may be preferable to derive boundary stresses by extrapolation rather than by averaging element stresses. This last point is a subject in itself.

It will not be pursued further in this work.

LST Solution. Only a single solution involving linear strain triangles (LST) is considered in detail. The element layout and corresponding nodal point loads are seen in Figure 4.1-b on page 96.

Very excellent flexural stresses and deflections are obtained for this configuration. In Figure 4.9, page 108, deflections are seen to be nearly identical to the exact deflections. In fact, the end deflection is 2.319×10^{-2} in. or just .065% higher than the elasticity solution. The higher value results from the fact that it is not possible to exactly represent the prescribed distributed forces.

The theoretical stress variation is a linear one with respect to both x and y coordinates. Thus in using the linear strain triangles, one would expect to obtain stresses which are nearly exact. As seen in Table 4.3, page 113, this is precisely the case. There is essentially no difference between the LST and the exact stresses on the

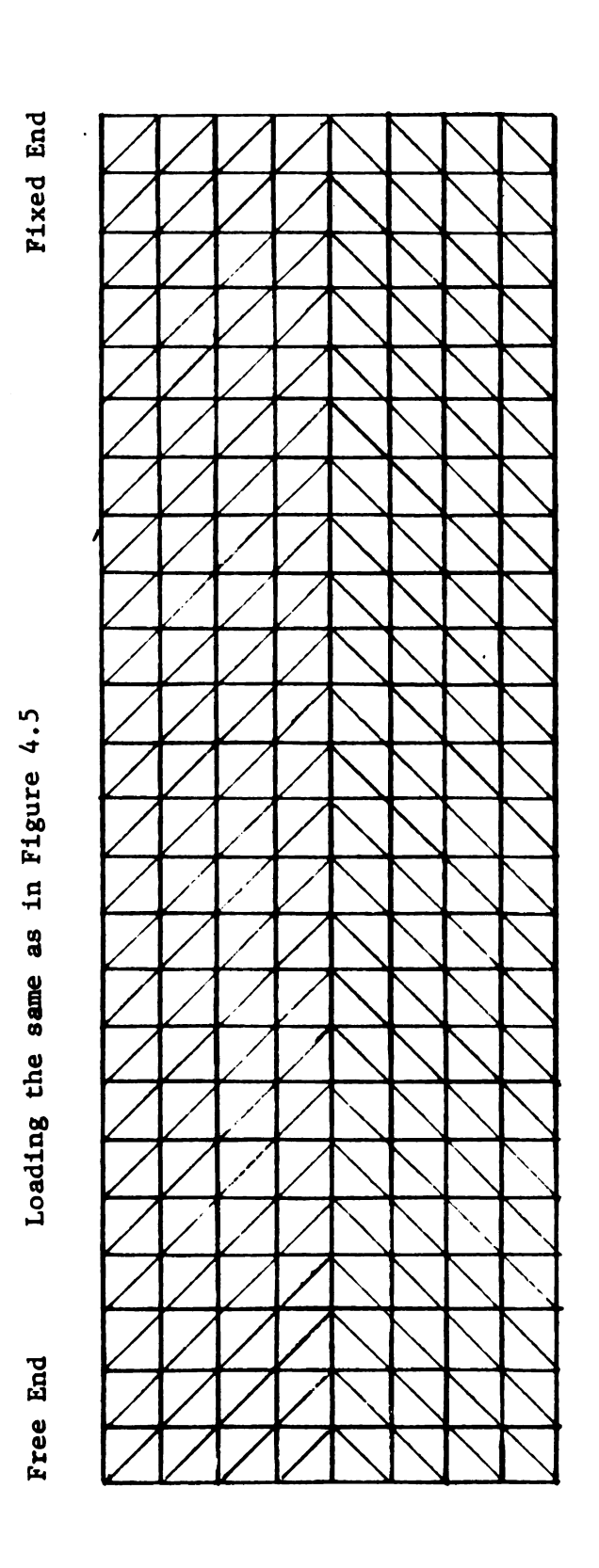


Figure 4.8, Alternate CST Beam Configuration

225 Nodal Points

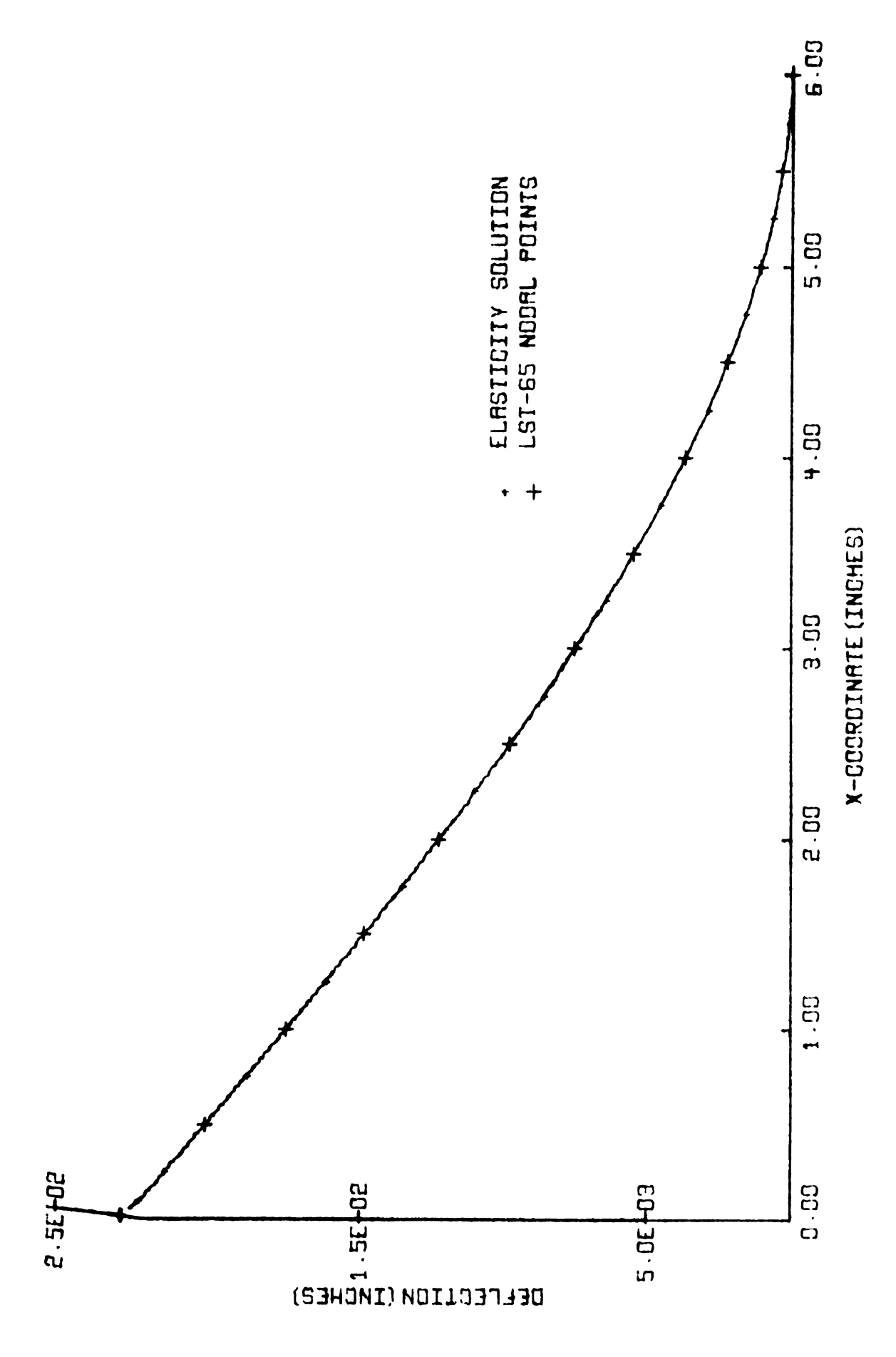


Figure 4.9, LST Beam Deflections

cross section $x = \frac{5}{6} \ell$. The only noticeable deviations from the exact theory occur near the supported and free ends.

Further Comparisons. In order to facilitate comparison of the three approximate solutions discussed above, the previous results are tabulated and plotted in a different form. Other results including shear stresses and longitudinal displacements are presented as well.

Starting with deflections, Tables 4.1 and 4.2 on pages 110 and 111 list deflections corresponding to the 65 and 225 point configurations respectively. In Table 4.1, it may be observed that CST deflections are somewhat better than FD deflections at the lower order approximations. In Table 4.2, the reverse is seen to be the case at the higher order approximation. The results in Table 4.2 are graphically illustrated in Figure 4.10. Clearly, the LST solution using only 65 nodal points is superior to CST and FD solutions involving almost 4 times as many points.

The flexural stresses on several cross sections near the fixed end are presented in Table 4.3, page 113. It is evident that the LST solution is best in each case. The FD solution is more satisfactory then the CST solution for this configuration. The stresses for the cross section $x = \frac{5}{6} \, \ell$ are also presented in graphical form on page 114. It is instructive to study the stress distribution on a free boundary. For example, the theoretical tensile stress on the top of the beam varies linearly with the horizontal coordinate x. The corresponding approximate results are listed on page 115 and plotted on the page which follows. It is clear that none of the solutions is exceptionally good everywhere on the boundary surface. The LST solution is excellent for

Table 4.1

Beam Deflections

65 Point Configurations

X-Coord.	Finite Diff.	C.S.T.	Elasticity	L.S.T.
0.	.01905	.02001	.023175	.02319
.5	.01673	.01758	.020350	.02035
1.0	.01443	.01517	.017562	.01757
1.5	.01220	.01285	.014850	.01486
2.0	.01006	.01058	.012250	.01226
2.5	.00805	.00850	.009806	.00980
3.0	.00619	.00651	.007537	.00757
3.5	.00452	.00481	.005500	.00551
4.0	.00306	.00322	.003725	.00373
4.5	.00185	.00202	.002250	.00225
5.0	.00091	.00097	.001112	.00112
5.5	.00028	.00039	.000350	.00036
6.0	.00000	.00000	.00000	.00000

Table 4.2

Beam Deflections

225 Point Configurations

X-Coord.	Finite Diff.	C.S.T.	Elasticity	L.S.T.*
0.	.02237	.02219	.023175	.02319
0.25	.02101	.02083	.021760	
0.50	.01965	.01948	.020350	.02035
0.75	.01830	.01814	.018949	
1.00	.01696	.01680	.017562	.01757
1.25	.01564	.01550	.016194	
1.50	.01434	.01420	.014850	.01486
1.75	.01307	.01295	.013533	
2.00	.01183	.01171	.012250	.01226
2.25	.01063	.01052	.011003	
2.50	.00947	.00936	.009800	.00980
2.75	.00835	.00826	.008642	
3.00	.00728	.00719	.007537	.00757
3.25	.00629	.00620	.006488	
3.50	.00531	.00524	.005500	.00551
3.75	.00443	.00437	.004577	
4.00	.00360	.00354	.003725	.00373
4.25	.00285	.00282	.002947	
4.50	.00217	.00213	.002250	.00225
4.75	.00158	.00157	.001636	
5.00	.00108	.00105	.001112	.00112
5.25	.00066	.00066	.000682	
5.50	.00034	.00032	.000350	.00036
5.75	.00012	.00013	.000121	
6.00	.00000	.00000	.000000	.00000

*65 Point Configuration

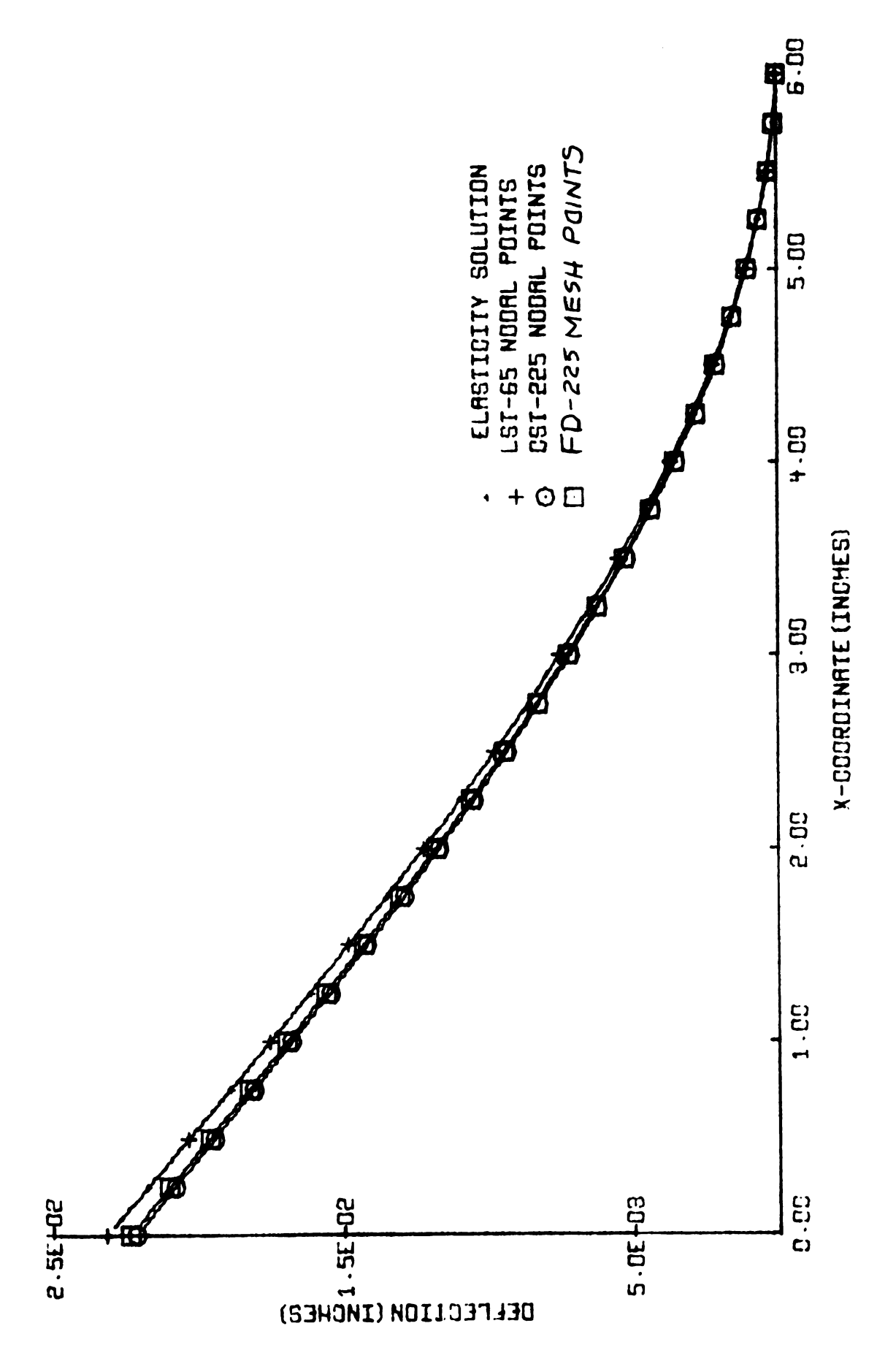


Figure 4.10, Beam Deflections

Table 4.3

Beam Flexural Stress

225 Point Configurations

x	=	$\frac{5}{6}$	l
---	---	---------------	---

y-coord.	Finite Diff.	C.S.T.	Elasticity	L.S.T.*
0.	- 6.4	6	0.	3
25	3650.	3643.	3750.	3748. **
50	7293.	7251.	7500.	7495.
75	10906.	10840.	11250.	11250. **
-1.00	14620.	12625.	15000.	15004.
		$x = \frac{11}{12} \ell$		
y-Coord.	Finite Diff.	C.S.T.	Elasticity	L.S.T.*
0.	- 10.	8	0.	6
25	4062.	4082.	4125.	3962. **
50	8111.	8063.	8250.	7926.
75	12057.	11987.	12375.	12240. **
- 1.00	15926.	13803.	16500.	16554.
		x = l		
y-Coord.	Finite Diff.	C.S.T.	Elasticity	L.S.T.*
0.	- 19.	- 1.	0.	3
25	4386.	4395.	4500.	4604. **
50	8773.	8765.	9000.	9207.
75	13039.	12981.	13500.	13487. **
- 1.00	16684.	14595.	18000.	17767.

^{* 65} Point Configuration** Interpolated Result

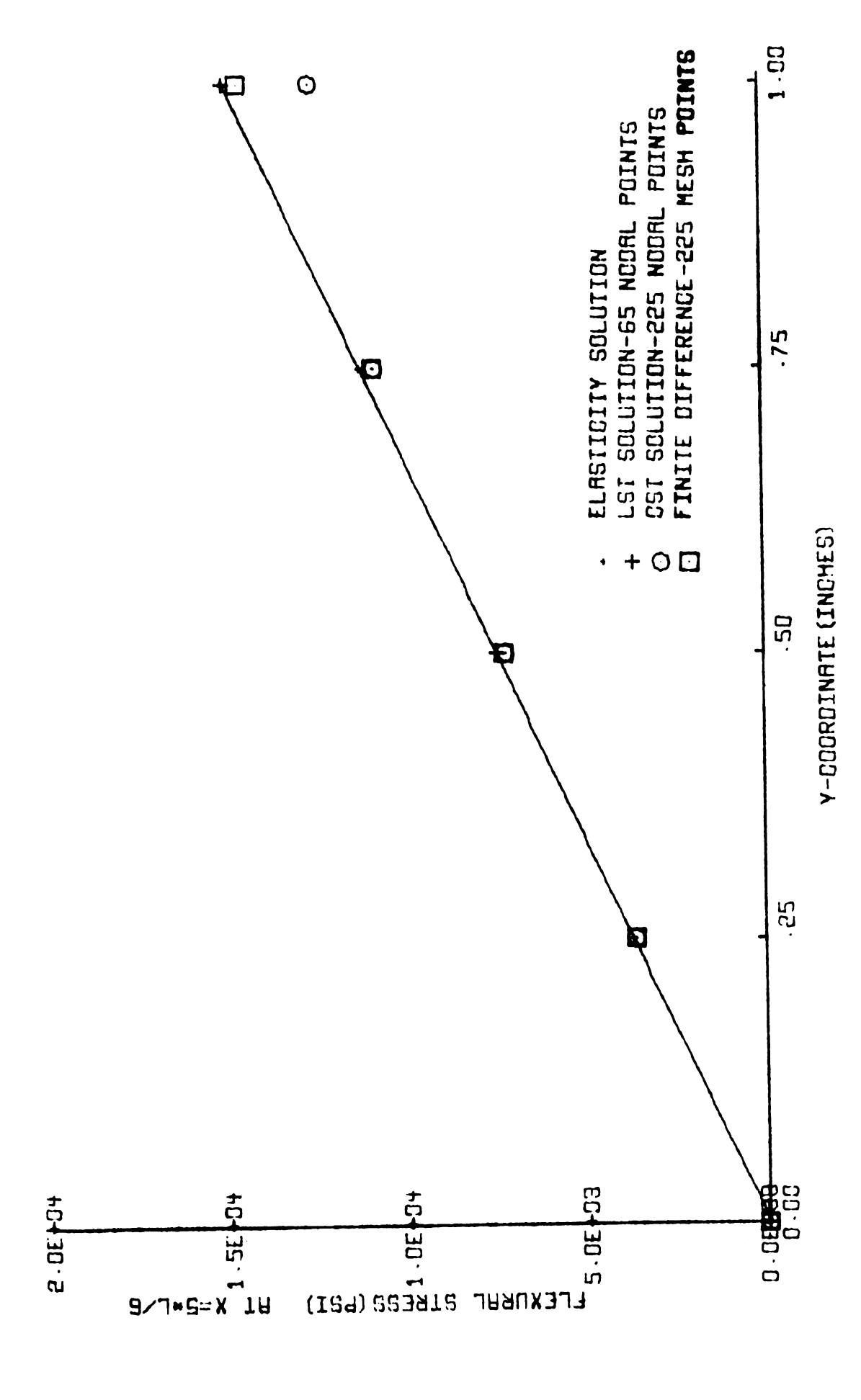


Figure 4.11, Beam Flexural Stress

Table 4.4 **Boundary Flexural Stress** 225 Point Configurations

 $y = \frac{h}{2} = c$

x-Coord.	Finite Diff.	C.S.T.	Elasticity	L.S.T.*
0.	365.	317.	0.	246.
.25	722.	711.	750.	852. **
.50	1441.	1260.	1500.	1458.
.75	2166.	2147.	2250.	2232. **
1.00	2893.	2527.	3000.	3005.
1.25	3621.	3586.	3750.	3765.
1.50	4351.	3792.	4500.	4524.
1.75	5081.	5022.	5250.	5263. **
2.00	5813.	5056.	6000.	6002.
2.25	6546.	6457.	6750.	6739. **
2.50	7280.	6322.	7500.	7475.
2.75	8015.	7893.	8250.	8240. **
3.00	8751.	7587.	9000.	9004.
3.25	9488.	9329.	9750.	9768. **
3.50	10225.	8852.	10500.	10532.
3.75	10964.	10766.	11250.	11269. **
4.00	11702.	10117.	12000.	12005.
4.25	12440.	12201.	12750.	12745. **
4.50	13175.	11379.	13500.	13484.
4.75	13905.	13621.	14250.	14244. **
5.00	14620.	12625.	15000.	15004.
5.25	15304.	14952.	15750.	15779. **
5.50	15926.	13803.	16500.	16554.
5.75	16450.	15957.	17250.	17161. **
6.00	16684.	14595.	18000.	17767.

^{* 65} Point Configuration
** Interpolated Result



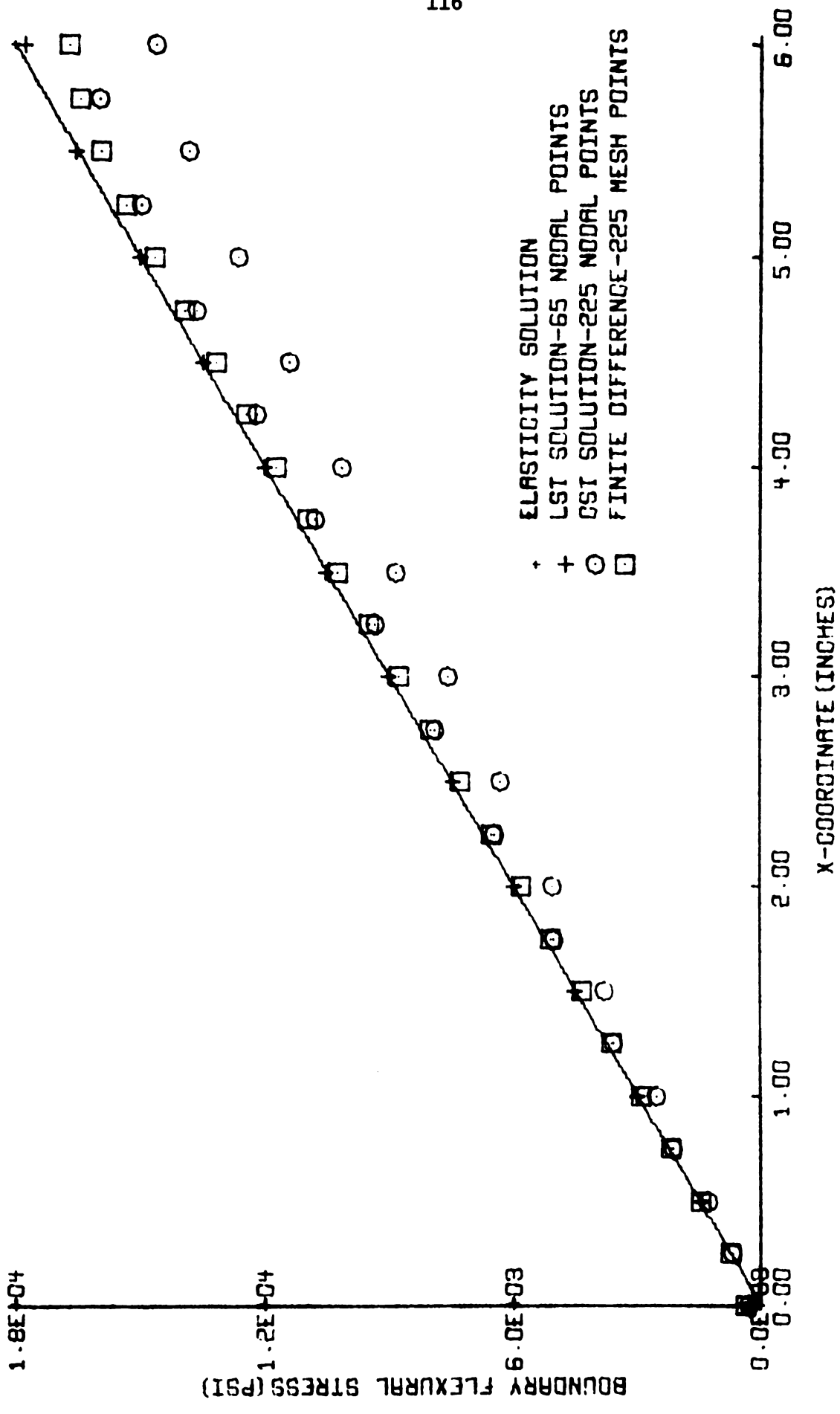


Figure 4.12, Top Boundary Flexural Stress

consistently lower than the exact solution (except at the free end). Its variation is essentially linear. The CST solution is very erratic, at times decreasing with increasing x. This is essentially the result of the choice for an element layout. As mentioned earlier, the configuration of Figure 4.8 gives somewhat better boundary stresses. In Figure 4.13 it is apparent that the stress variation using this alternate arrangement of triangles is less erratic. The former arrangement is clearly scattered on either side of the latter. Apparently a best fit curve is a better indication of the actual stress variation for CST configurations. Again it should be kept in mind that these are not the best boundary stresses. For truly accurate results, one would resort to extrapolation.

Further insight into the relative merits of the methods discussed is gained by examining the shear stress distribution. The exact shear stress varies parabolically with y and is independent of x. Shear stresses corresponding to the various approximations are tabulated on page 119 and graphically presented in Figure 4.14. None of the shear stresses conform very closely with the exact theory. Particularly poor results occur on the free top and bottom boundaries. Certainly some of this difficulty arises from the use of constant and linearly varying strain elements in a parabolic stress field. More satisfactory results would certainly be obtained if the element size was further reduced.

The FD solution is consistently better than either the LST or CST solutions. The LST solution is poor because only one element is placed above and below the neutral surface in this configuration. In doing this, one is trying to approximate a parabola by a single straight line. The use of more points in the 225 point CST and FD solutions allows for



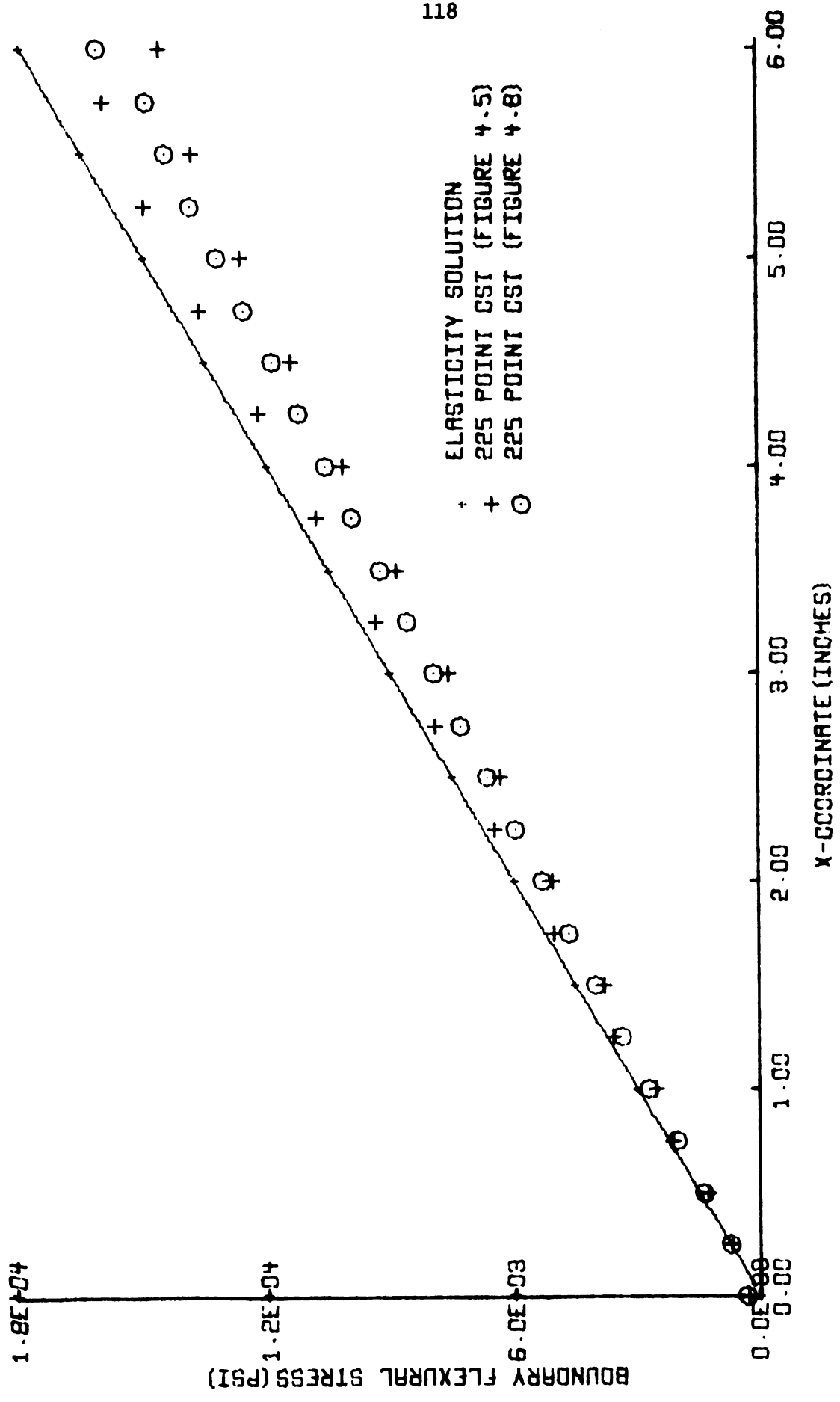


Figure 4.13, CST Boundary Flexural Stress

Table 4.5
Beam Shear Stress

225 Point Configurations

 $x = \frac{5}{6} \ell$

y-Coord.	Finite Diff.	C.S.T.	Elasticity	L.S.T.*
0.	1508.	1487.	1500.	1788.
25	1409.	1378.	1406.25	
50	1115.	1088.	1125.	1055.
75	641.	611.	656.75	
- 1.00	344.	345.	0.	240.
		$x = \frac{11}{12} \ell$		
y-Coord.	Finite Diff.	C.S.T.	Elasticity	L.S.T.*
0.	1559.	1560.	1500.	1 715.
25	1453.	1432.	1406.25	
50	1128.	1099.	1125.	993.
75	599.	560.	656.25	
- 1.00	275.	249.	0.	207.
y-Coord.	Finite Diff.	C.S.T.	Elasticity	L.S.T.*
0.	2053.	1570.	1500.	1747.
25	1932.	1952.	1406.25	
50	1599.	1172.	1125.	1048.
75	962.	946.	656.25	
- 1.00	531.	93.	0.	247.

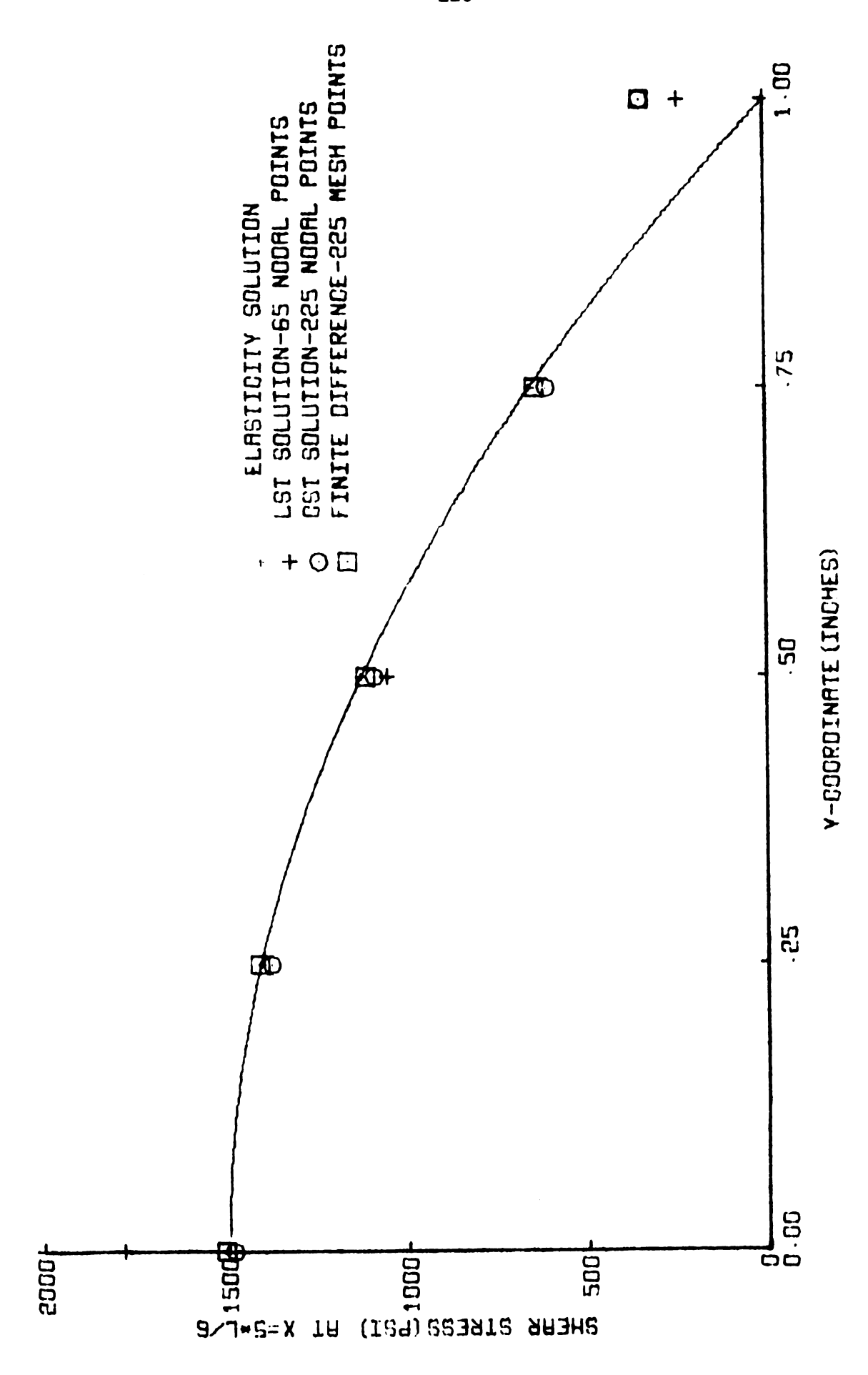


Figure 4.14, Beam Shear Stress

a better approximation to such a function. Additional analysis using more nodal points in an LST solution has shown this to be the case.

Further examination of the results in Table 4.5 indicate that the end stresses are also poor. This is additional evidence of the fact that care must be exercised in interpreting such results. Extrapolation would certainly be advisable in view of the relatively good interior stresses for the CST and FD solutions.

The last results presented here involve the longitudinal displacements (u) for points on the free end of the beam. These are presented on pages 122 and 123. They differ little in pattern from already presented transverse displacements. The FD displacements are slightly better than the CST displacements, but both fall short of the exact values. The LST results are very close to the elasticity solution.

Concluding Remarks. The preceding work demonstrates the superiority of the LST element in the presence of non-uniform stress states. It is possible to derive much more acceptable results using fewer nodal Points. The LST analysis is also superior to the particular FD method employed in this work. However, the present work seems to demonstrate a Potential for the FD method to give equally good and perhaps even better stress and displacement results than the CST analysis. This in the authors opinion is a significant point since programming the FD method is to a degree less involved and requires less memory capability.

Table 4.6

Beam Longitudinal Displacements

225 Point Configuration

(Free End)

y-Coord.	Finite Diff.	C.S.T.	Elasticity	L.S.T.*
-1.	005194	005167	005400	005403
75	003860	003840	004013	
5	002557	002544	002657	002681
25	001273	001266	001323	
Ο.	.000000	.00000	.000000	.000000
.25	.001275	.001267	.001323	
.50	.002559	.002544	.002657	.002661
.75	.003862	.003840	.004013	
1.0	.005195	.005167	.005400	.005403

^{* 65} Point Configuration

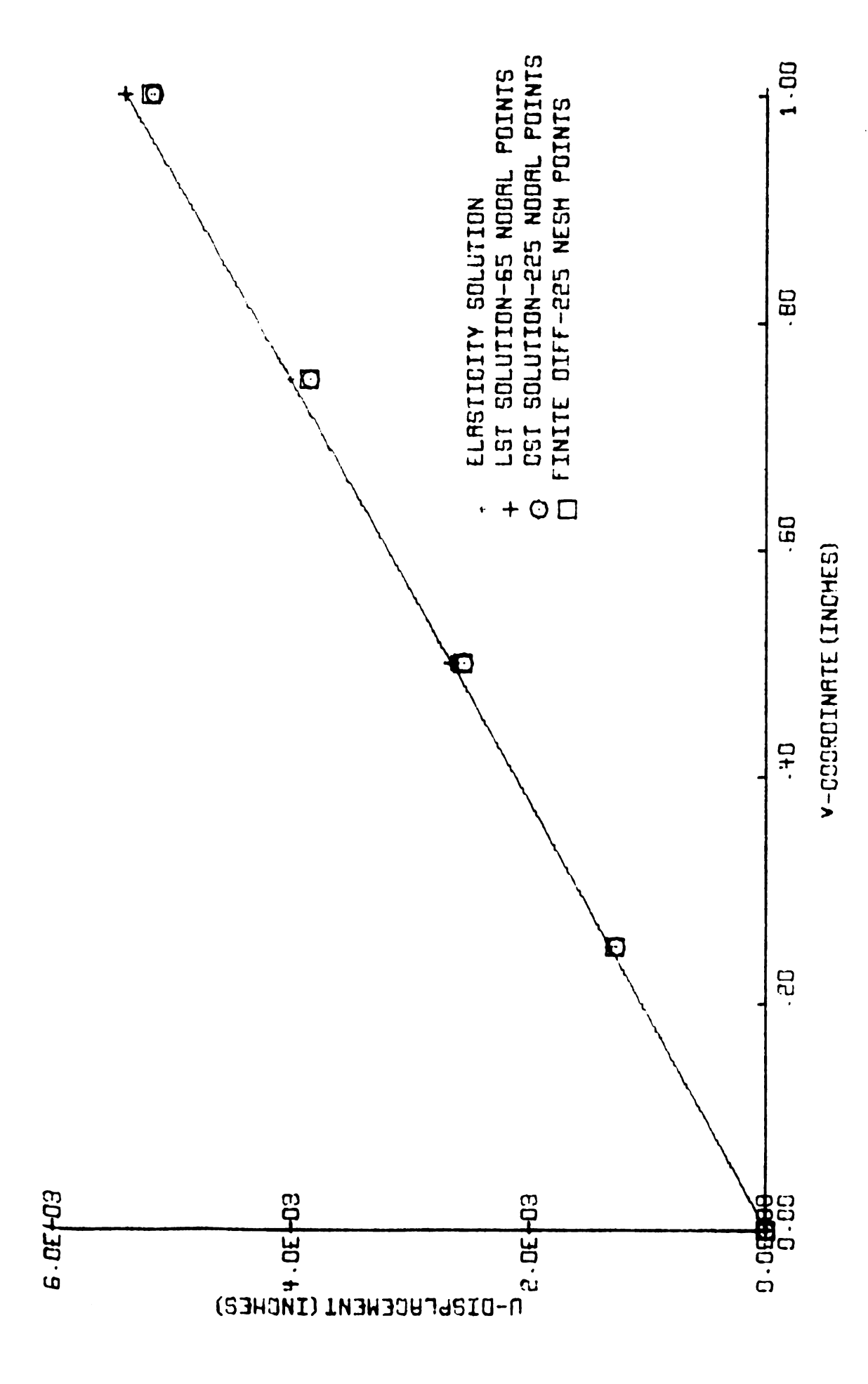


Figure 4.15, Longitudinal Free End Displacements

4.2 Composite Plate

The second numerical example considered here is that of a composite plate. One quarter of the symmetrical arrangement is shown in Figure 4.16 on the page which follows. The plate has a length of 4 in., a width of 2 in. and is of unit thickness. A uniformly distributed load of 1200 psi acts on the top and bottom ends.

As shown in the figure, the plate consists primarily of a rather flexible material (perhaps plastic) molded around a rather large rectangular stiffener (perhaps aluminum). The ratio of elastic moduli is taken to be 20. Throughout the analysis, the continuity of displacements across the material interfaces is assumed. A more ambitious and realistic example allows the stiffener (inclusion) to be more fiber like and thus completely surrounded by the matrix. Many such fibers could conceivably be present. This would of course involve a three dimensional or axially symmetric analysis. A more practical example is treated in Chapter V of this thesis. Involved is a reinforced cylinder which is analyzed using axially symmetric programs.

In the present example, the solution is carried out using two finite element models and the finite difference method. Several displacement curves are plotted corresponding to each method to demonstrate convergence of the approximate solutions to the true solution. Of primary interest is the stress distribution along the interface of the two materials, as it occurs in both the matrix and the inclusion.

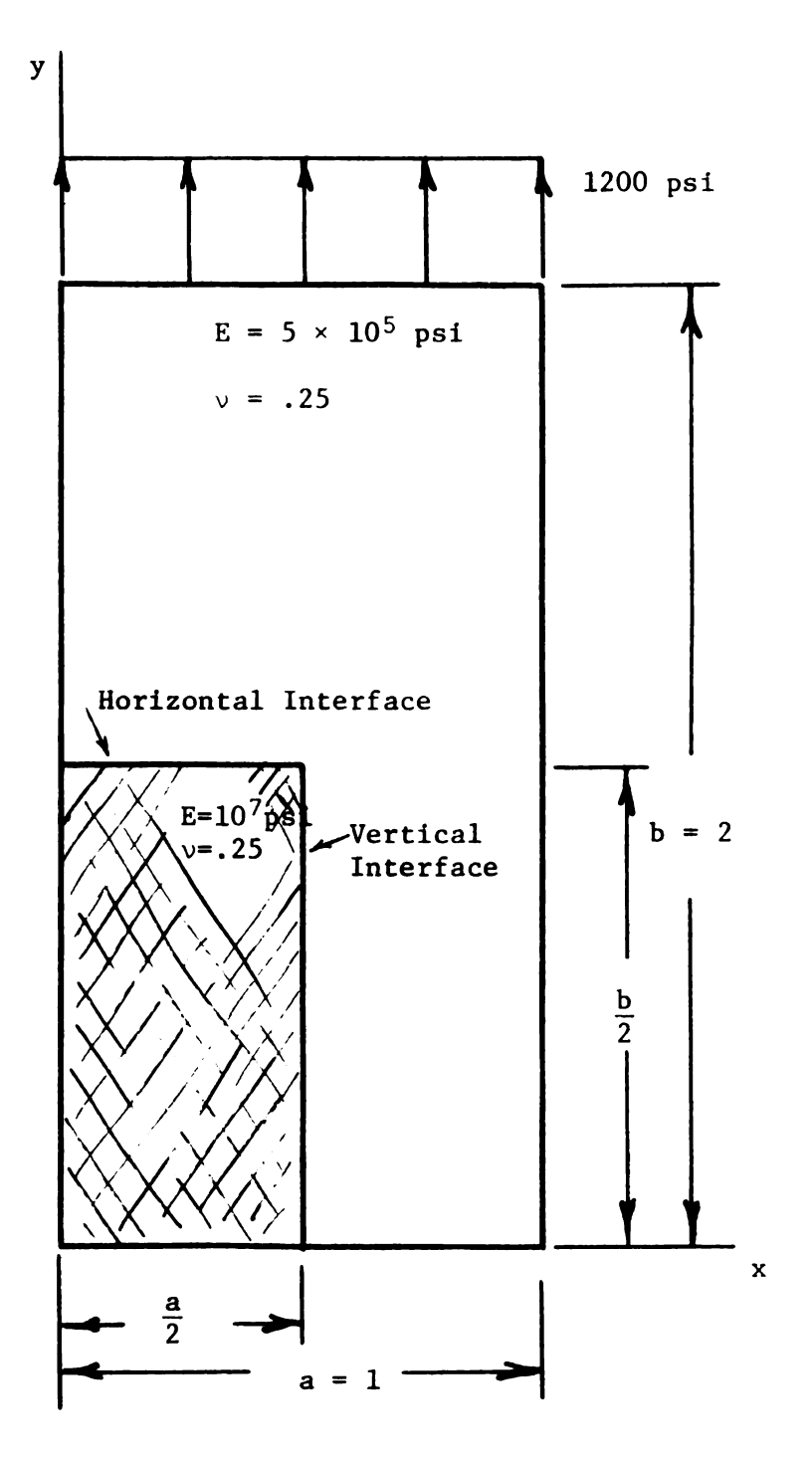


Figure 4.16
Composite Plate

<u>Finite Difference Solution</u>. The FD analysis employed here consisted of 4 different mesh arrangements ranging from a 45 mesh point configuration to a 231 mesh point configuration. These 4 mesh arrangements are identified in Figure 4.17, page 127.

It is of particular importance in situations of this kind to know what deformations occur. One might ask for example how the total maximum extension compares with that which would occur if no stiffener were present at all. In Figure 4.18, page 128, the vertical displacement of the top edge is plotted for the 4 configurations mentioned above. Clearly, displacement convergence is very rapid. Since no exact solution is available, one can only make comparisons with problems for which solutions are available. Thus the maximum displacement of 3.26×10^{-3} in. derived from the 231 point configuration seems very reasonable when compared with the value 4.8×10^{-3} in. which occurs in a homogeneous solid plate having E equal to 5×10^{5} psi.

The horizontal displacement of this same edge is shown in Figure 4.19. Again, very rapid convergence is displayed. It is evident from both Figures that relatively good displacements are obtained with even a very course mesh spacing. Additional evidence of the nature of the displacement solution is given by Figures 4.20 and 4.21 on pages 130 and 131 respectively. These are plots of the displacements of points on the horizontal interface. It is interesting to note that displacements are generally overestimated in the stiffener and underestimated in the matrix. A final set of curves is plotted in Figure 4.22. These involve vertical displacements of points on the vertical symmetry axis. Once again the excellence of the displacement solution is displayed, even at the crudest approximation.

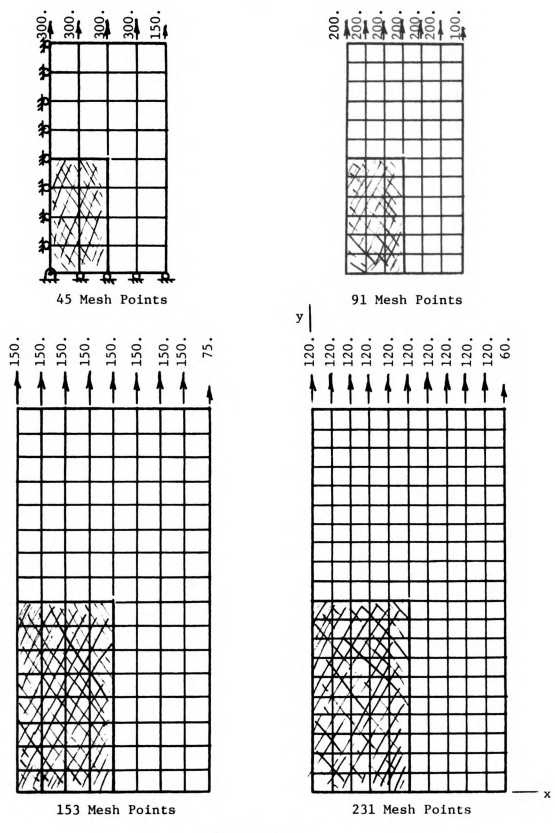


Figure 4.17

Composite Plate - Finite Difference Configurations

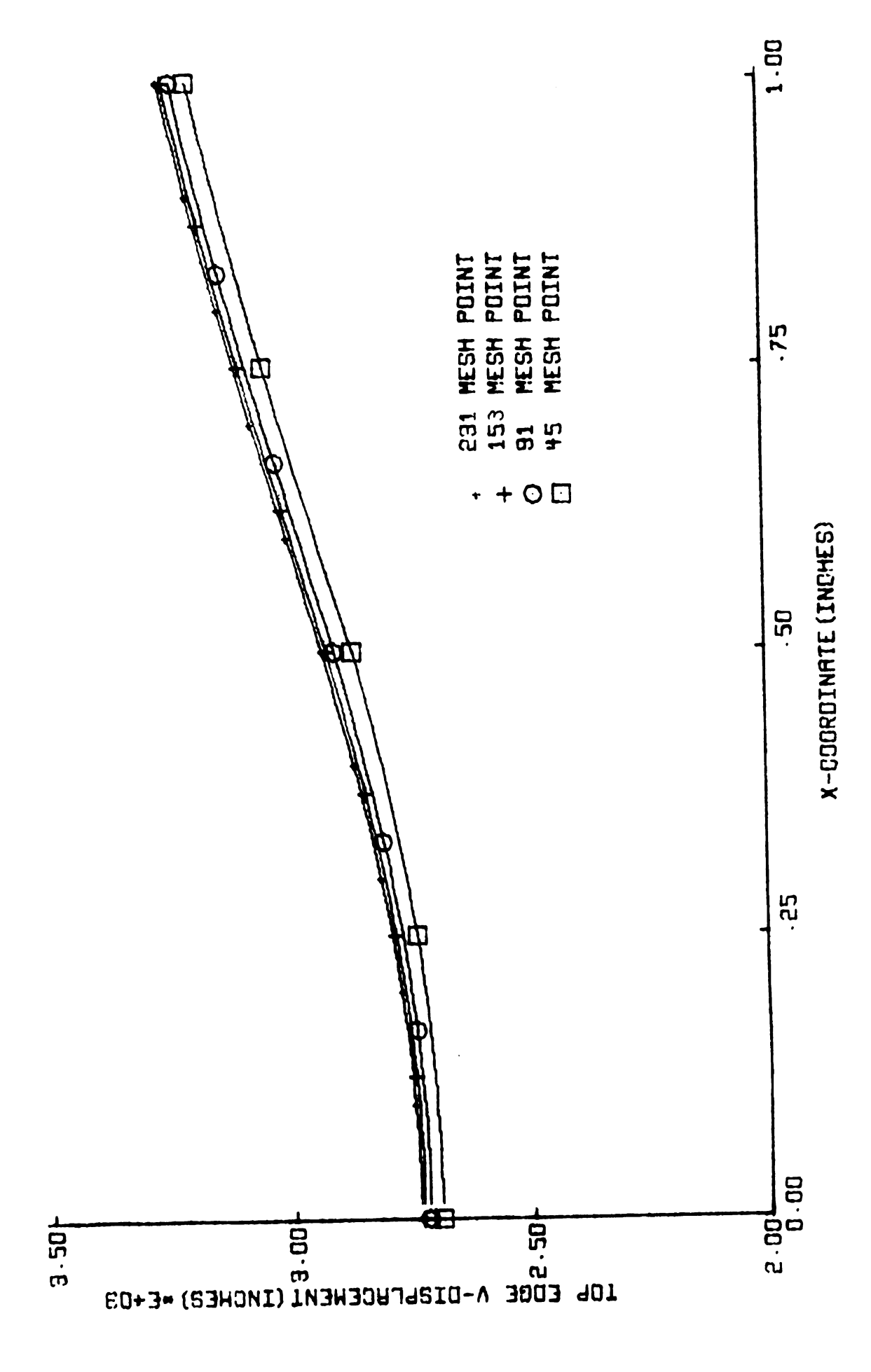


Figure 4.18, FD Top Edge v-Displacements

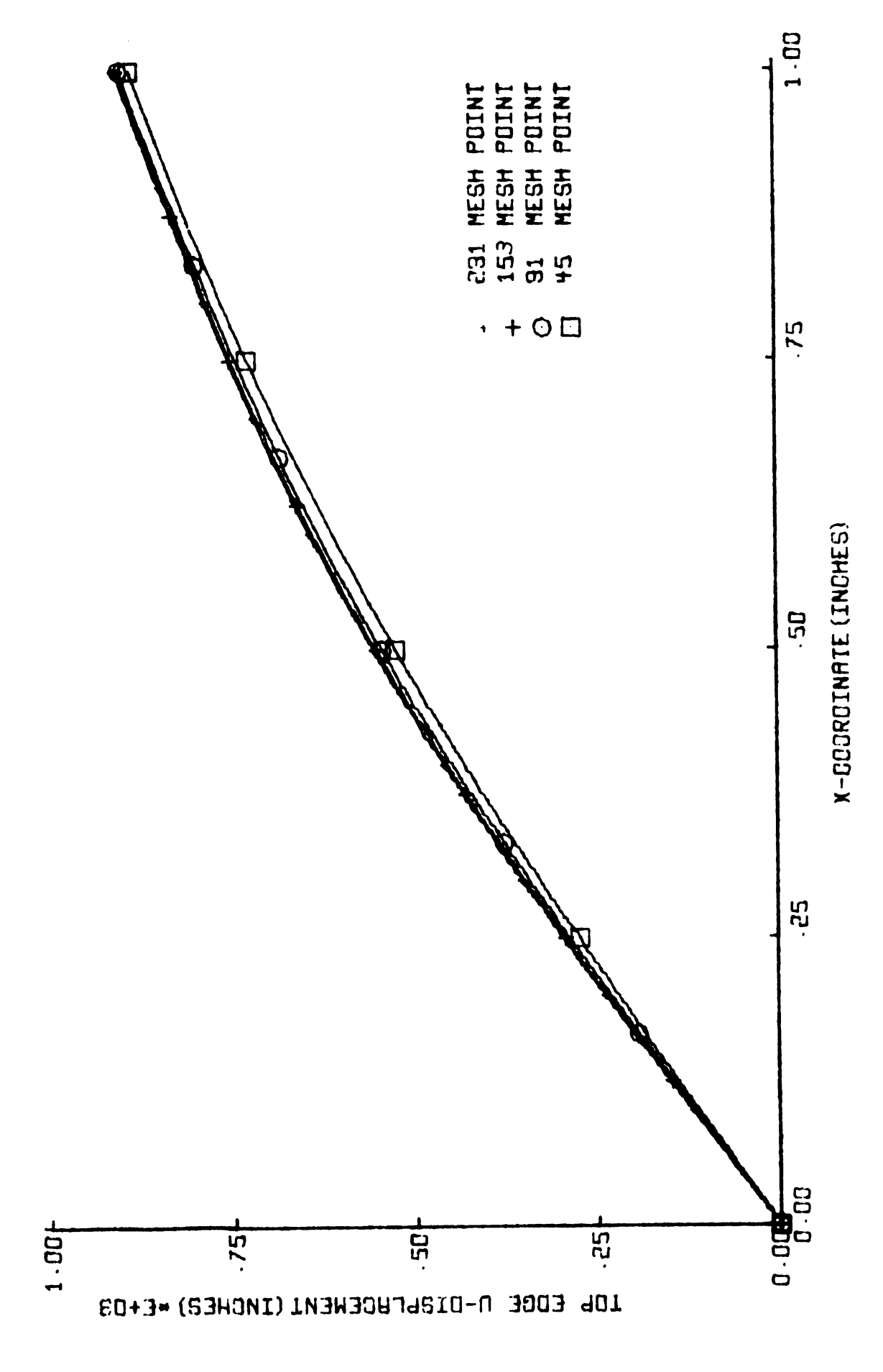


Figure 4.19, FD Top Edge u-Displacements

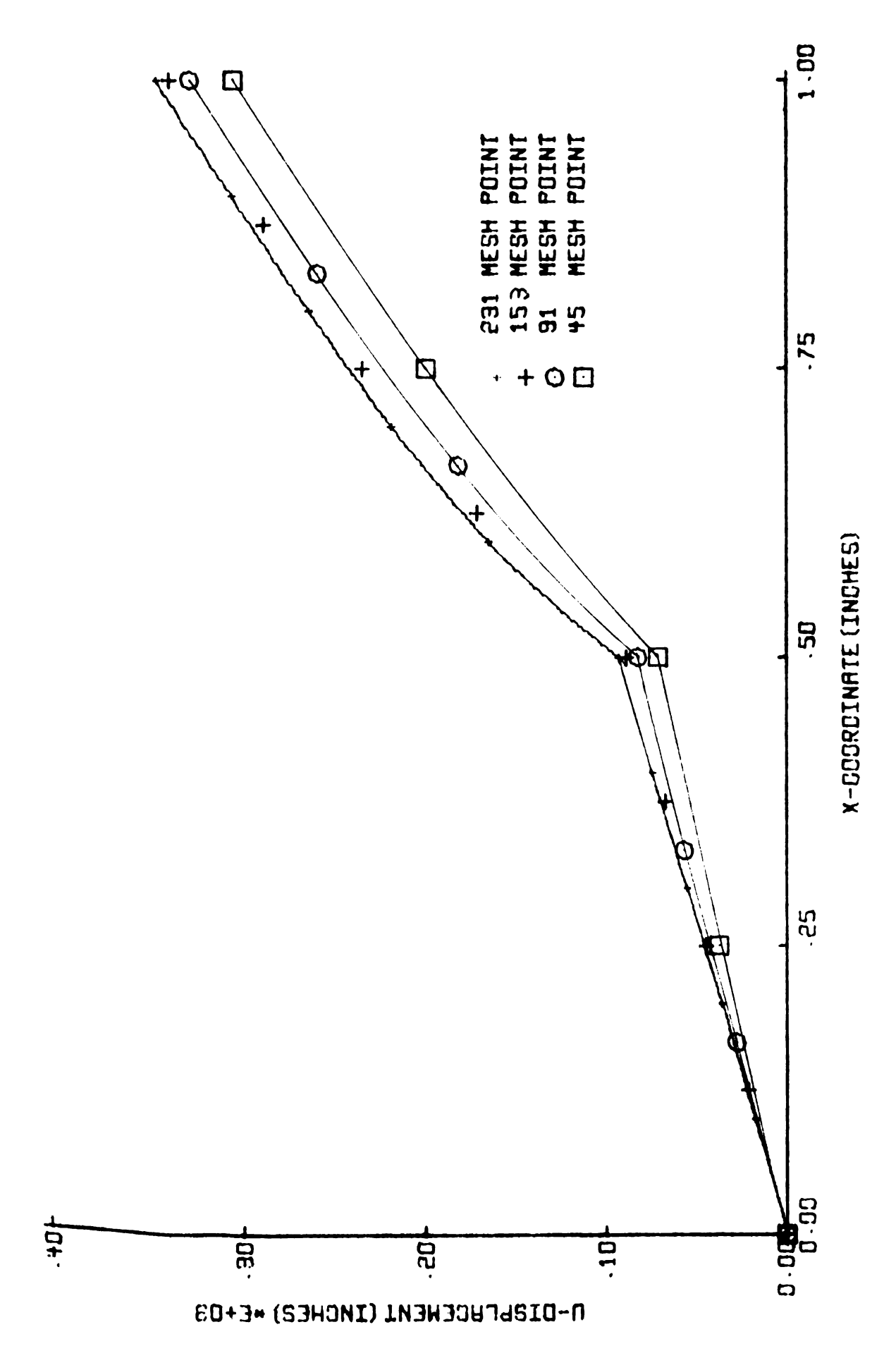


Figure 4.20, FD Horizontal Interface v-Displacements

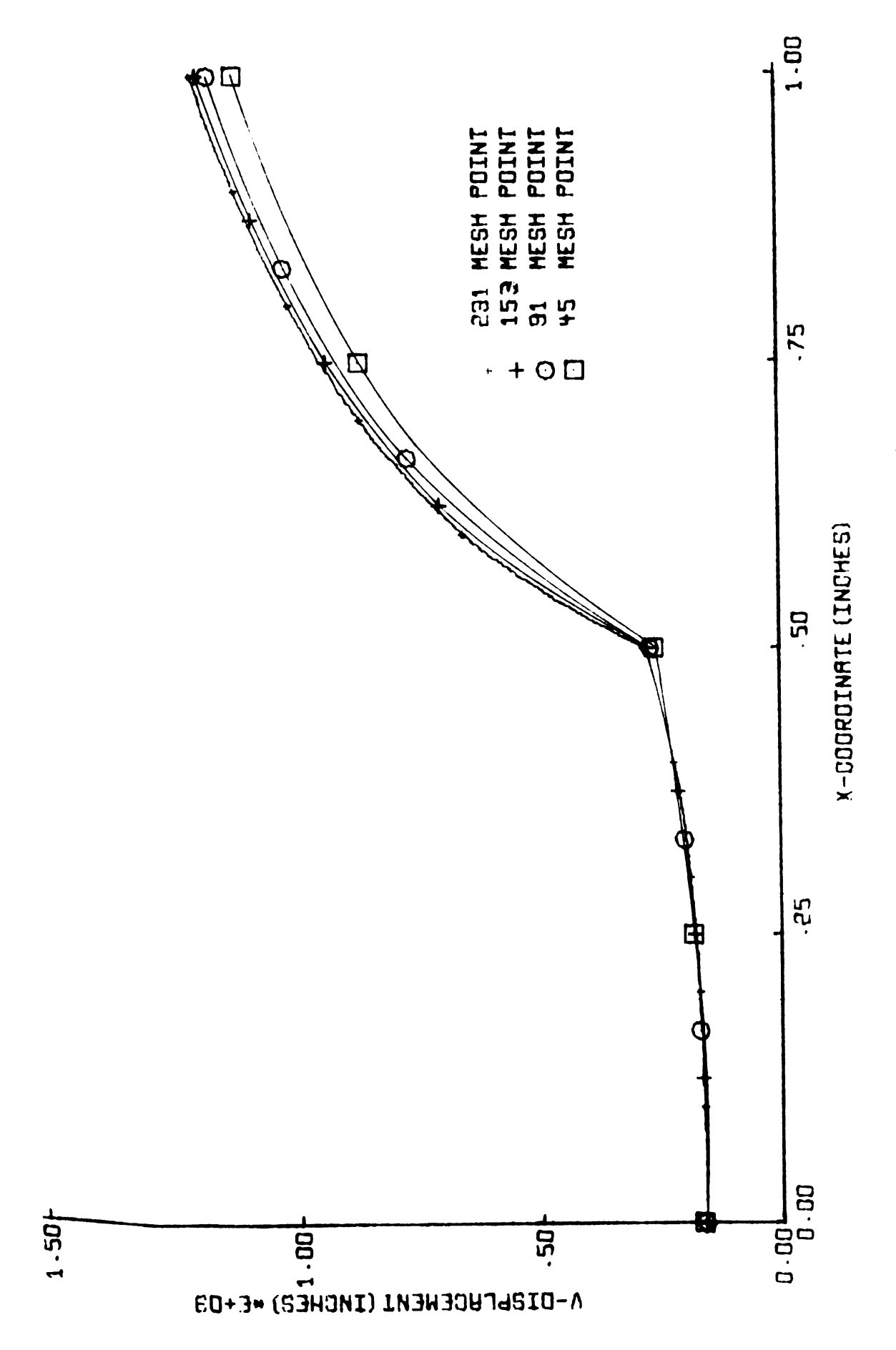


Figure 4.21, FD Horizontal Interface u-Displacements

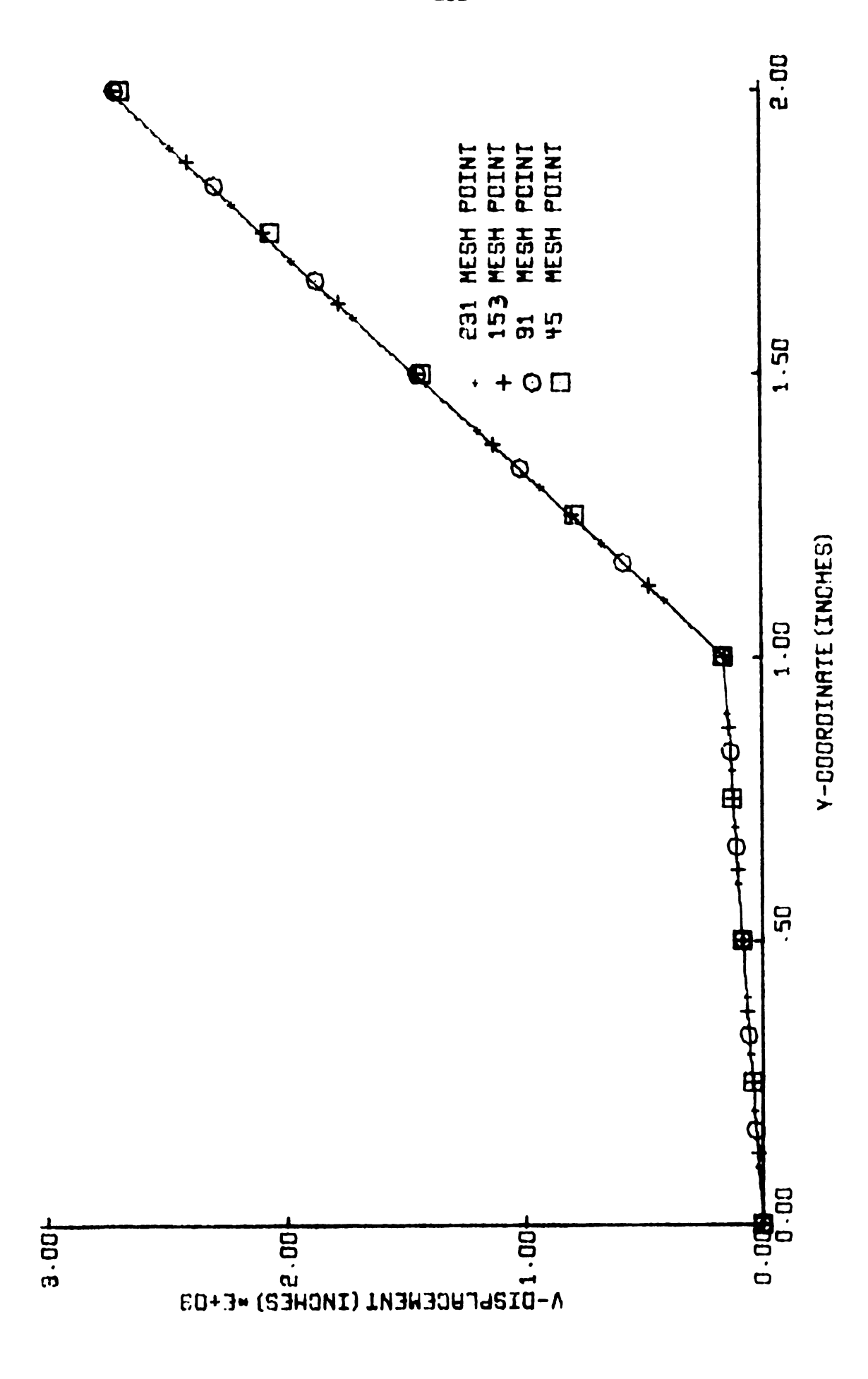


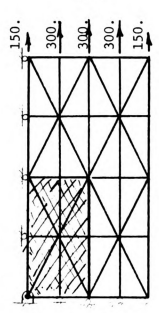
Figure 4.22, FD Vertical Symmetry Axis v-Displacements

CST Solution. The analysis with CST elements was carried out using the three layouts of Figure 4.23 on the following page. The location of nodal points is not generally the same as that used in the FD solution. However, the nodal point system is identical to that used in the LST analysis.

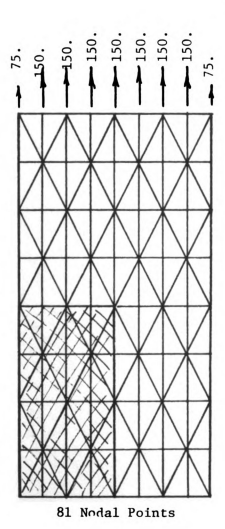
The convergence of displacements for the CST solutions to an apparent true solution is illustrated in Figures 4.24 through 4.28 which follow. The 25 point nodal point solution is a rather low order approximation and evidently gives very poor results. There is not an appreciable difference between the 81 and 169 point solutions indicating fairly rapid convergence beyond this point. The maximum extension derived from the 169 point solution is 3.2551×10^{-3} in. The best FD solution gave 3.260×10^{-3} in.

LST Solution. The three LST arrangements are illustrated in Figure 4.29, page 140. As mentioned earlier, the corresponding nodal point systems are identical with those used in the CST analysis.

The top edge displacements are given in Figures 4.30 and 4.31. These results demonstrate that convergence to the true solution occurs from below. It is interesting to note that at certain points, the 25 nodal point CST solution is better than the 25 point LST solution insofar as horizontal displacements are concerned. However, in general, these LST displacements are higher than both FD and CST displacements and thus apparently more satisfactory. The maximum extension for the 169 point LST solution is 3.2745×10^{-3} in. The comparable displacements for the best CST and FD solutions are 3.2551×10^{-3} in. and 3.260×10^{-3} in. respectively.



25 Nodal Points



y Control of the second of the

Figure 4.23

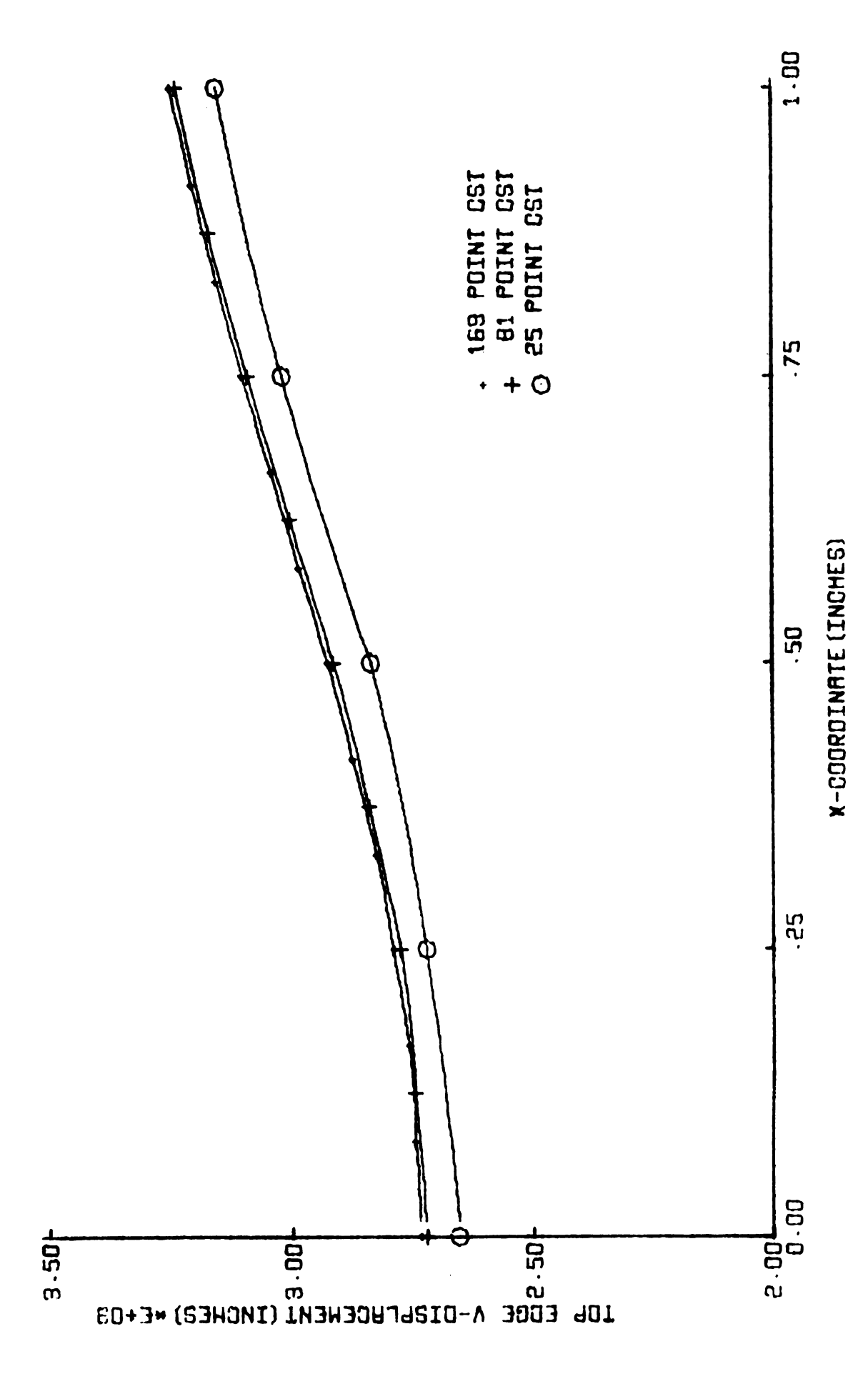


Figure 4.24, CST Top Edge v-Displacements

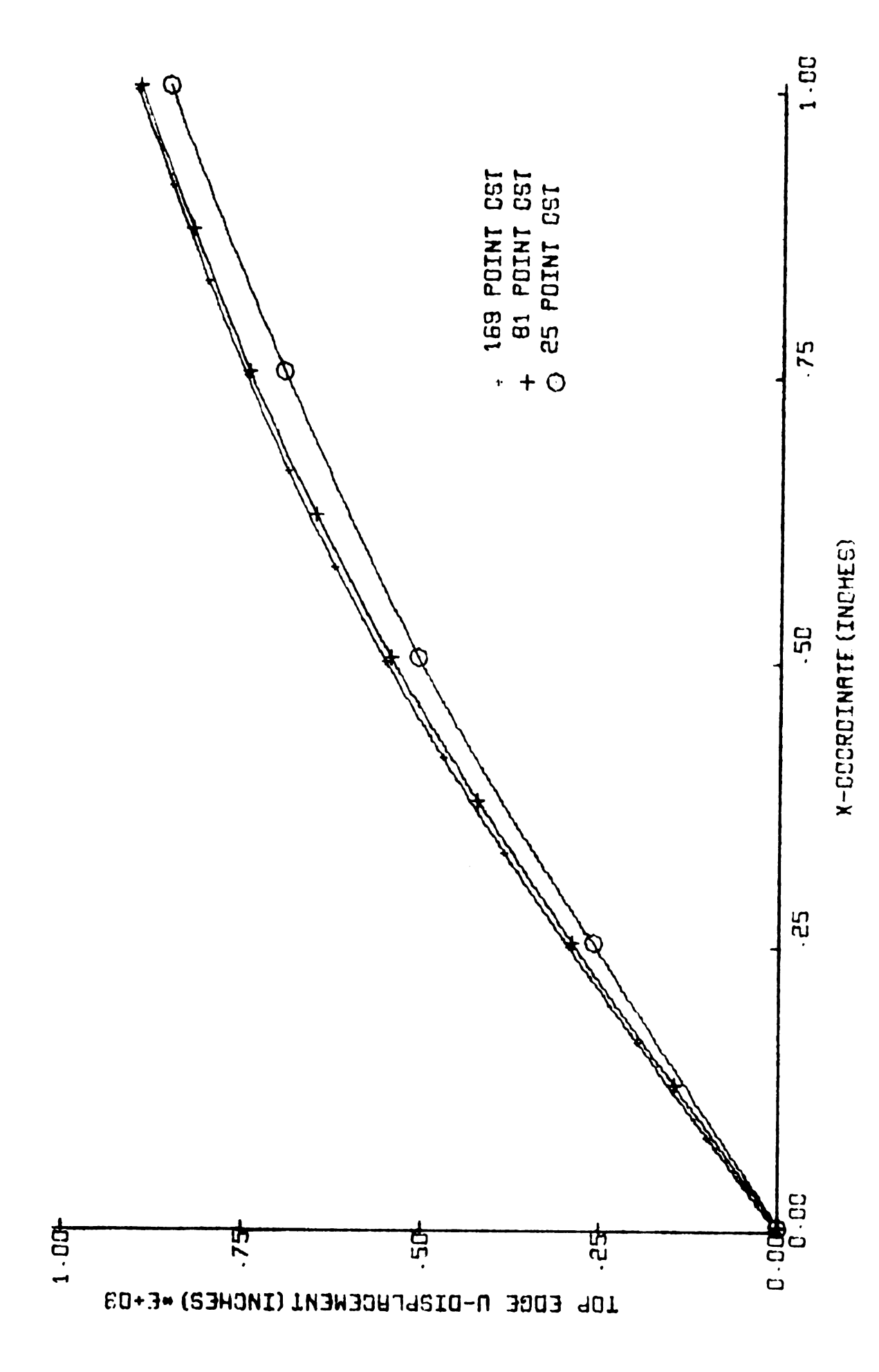


Figure 4.25, CST Top Edge u-Displacements

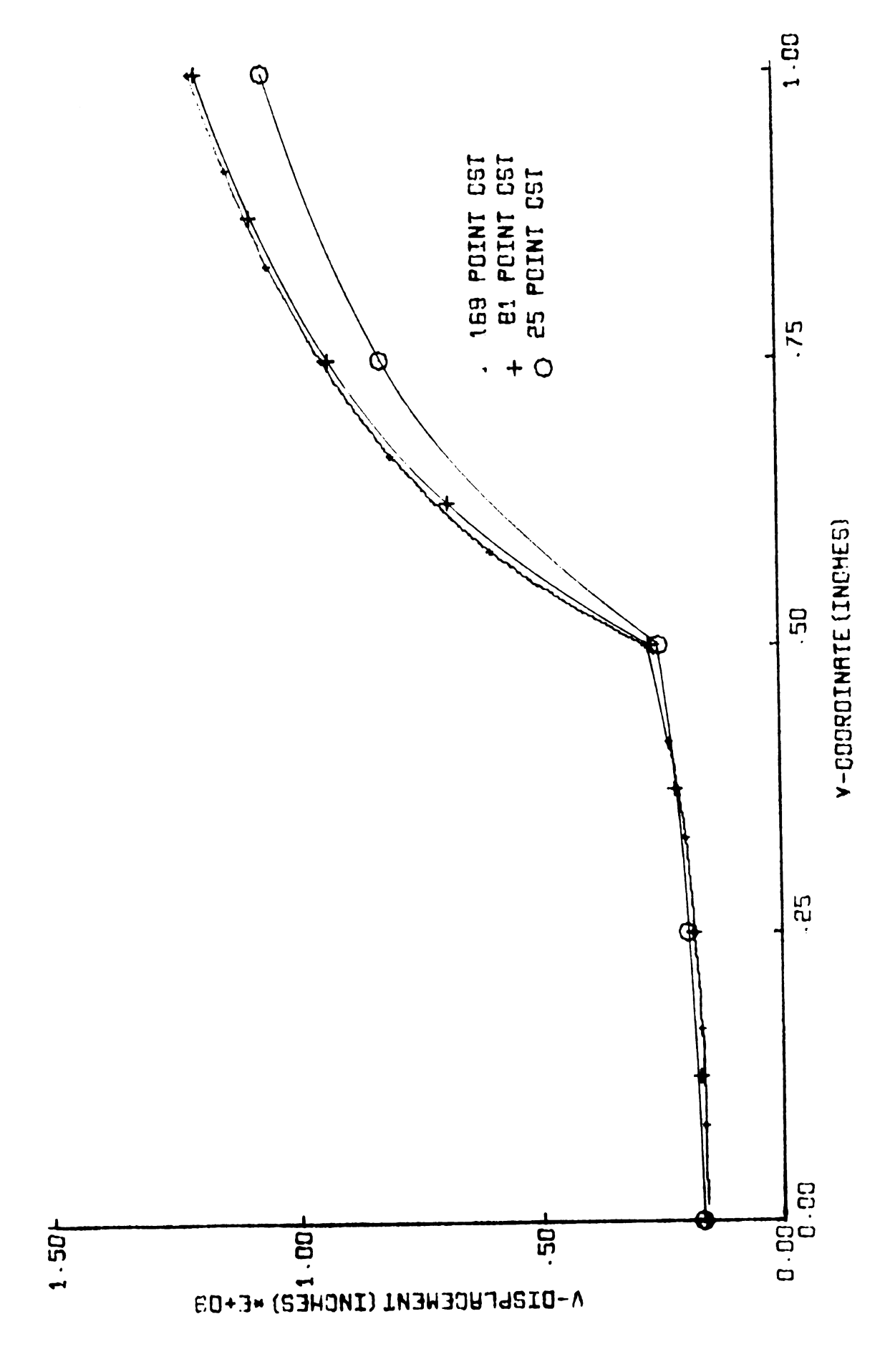


Figure 4.26, CST Horizontal Interface v-Displacements

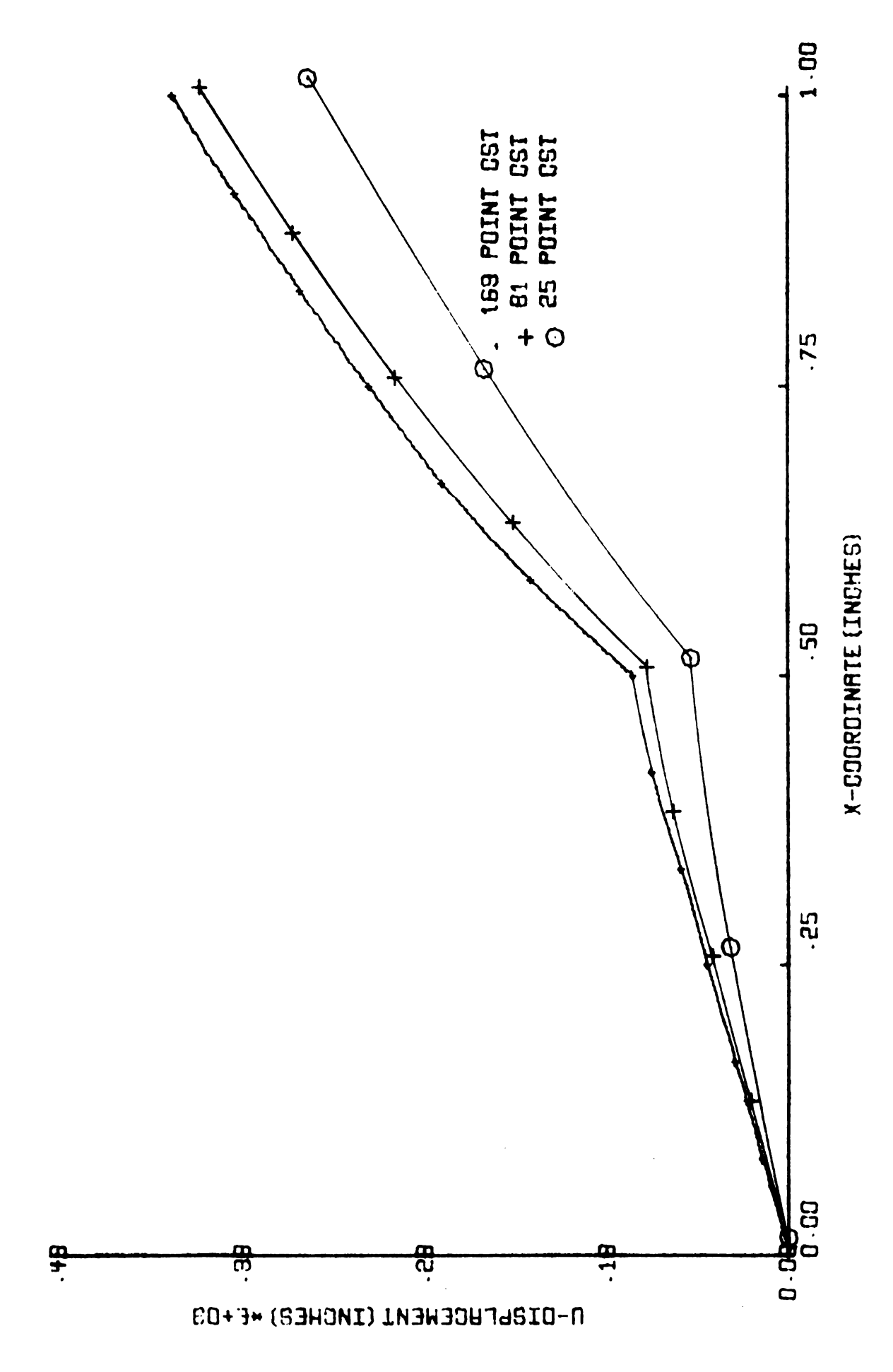


Figure 4.27, CST Horizontal Interface u-Displacements

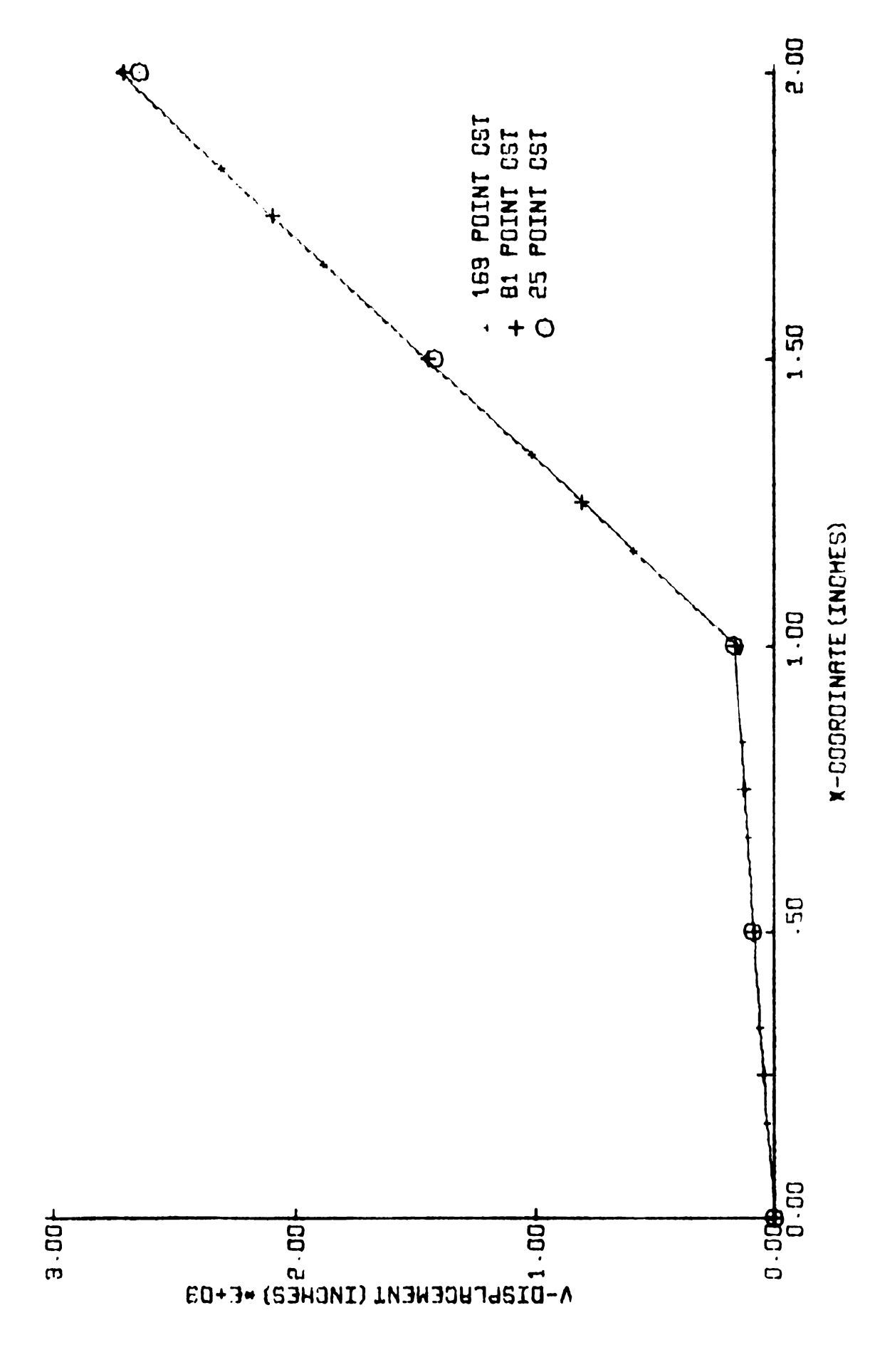


Figure 4.28, CST Vertical Symmetry Axis v-Displacements

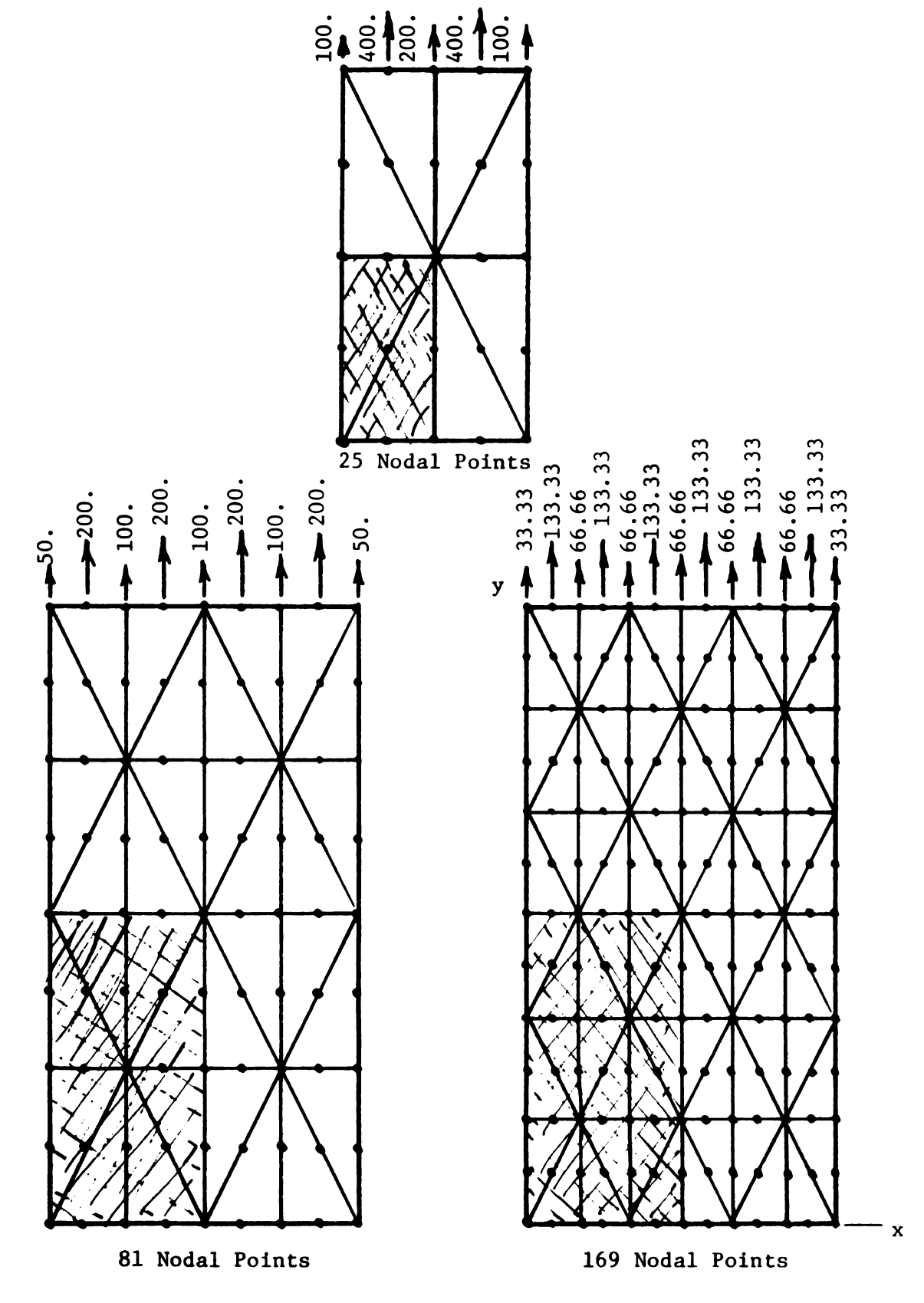


Figure 4.29
Composite Plate - LST Configurations

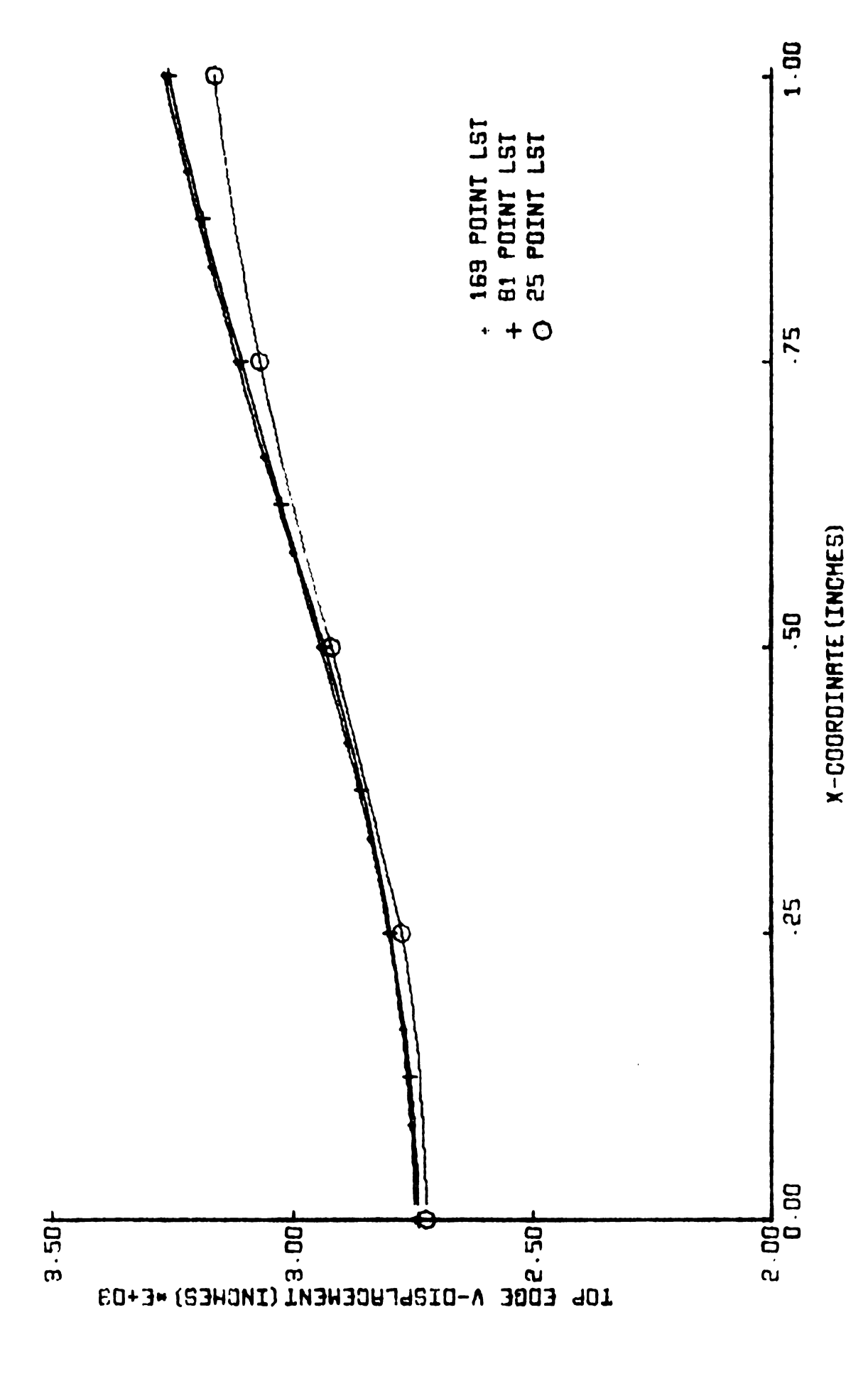


Figure 4.30, LST Top Edge v-Displacements

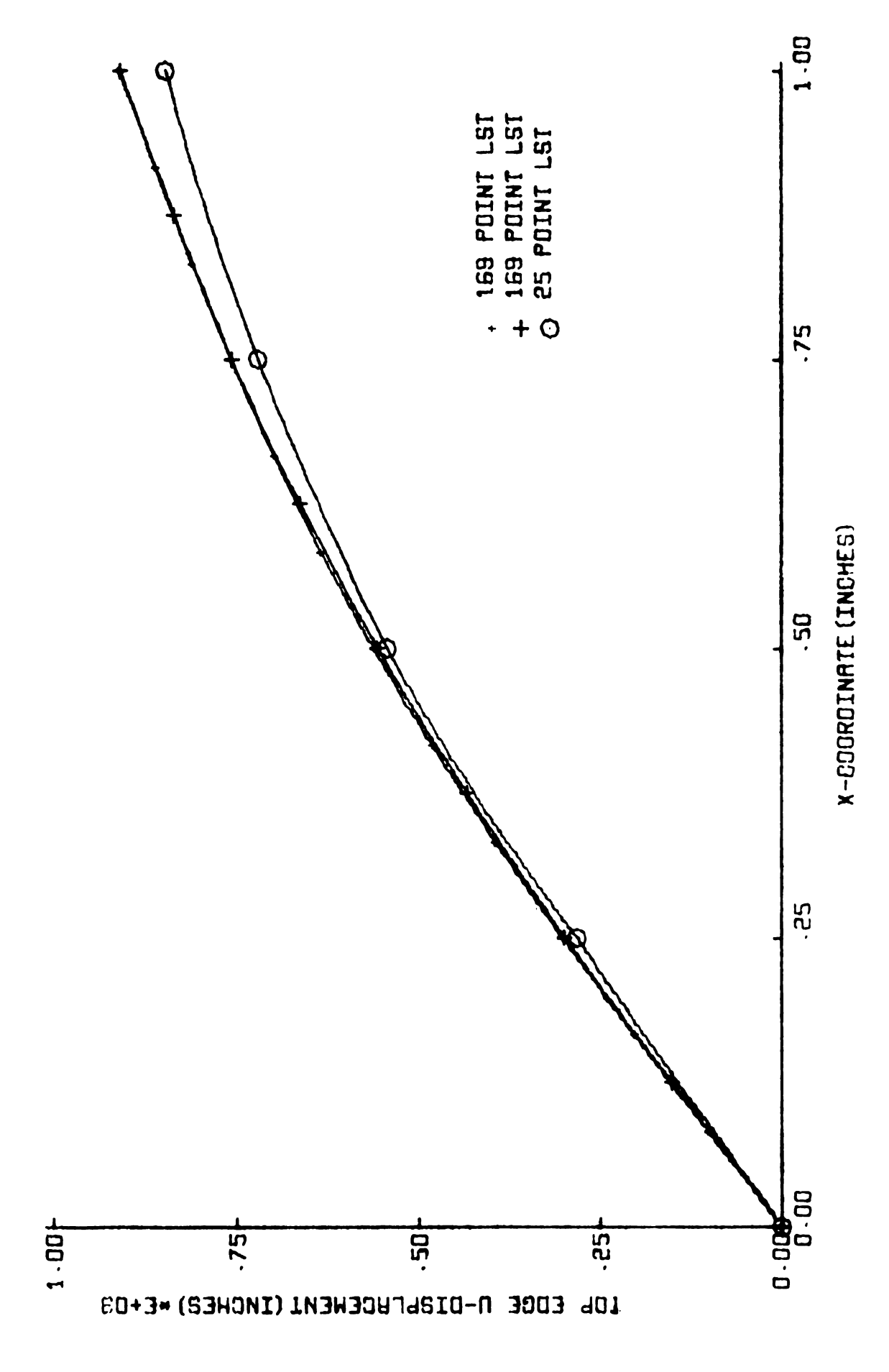


Figure 4.31, LST Top Edge u-Displacements

The horizontal interface displacements are displayed in Figures 4.32 and 4.33. The lowest order solution involving 25 nodal points is quite poor. The 81 and 169 point solutions are much more comparable. The vertical symmetry axis displacements are seen on page 146, Figure 4.34. These do not vary appreciably from the lower to the higher order approximations.

Comparison of the Solutions. For further comparison of the solutions already discussed, the displacements and stresses corresponding to the highest order approximations are considered next. Stresses at the lower order approximations are not likely to be as meaningful and are consequently not examined here. The stresses which are used for this purpose are nodal point stresses obtained by averaging appropriate element stresses. It was pointed out earlier that these may not always be accurate on boundary surfaces. The comparisons, however, are nevertheless felt to be largely meaningful.

Beginning with displacements, the plotted information of pages 147 through 151 pertain to displacements of points on the top edge, the horizontal interface and the vertical symmetry axis. These results are also listed in Tables 4.7 to 4.11 beginning on page 152. The top edge displacements, Figures 4.35 and 4.36, are essentially the same for the three solutions with the LST results slightly higher in each case. This is also the case insofar as the vertical symmetry axis displacements are concerned (Figure 4.39). Noticeable variations between the three solutions are apparent with regard to the horizontal interface displacements. The largest variations are seen to occur for the vertical displacement component (Figure 4.37). The LST

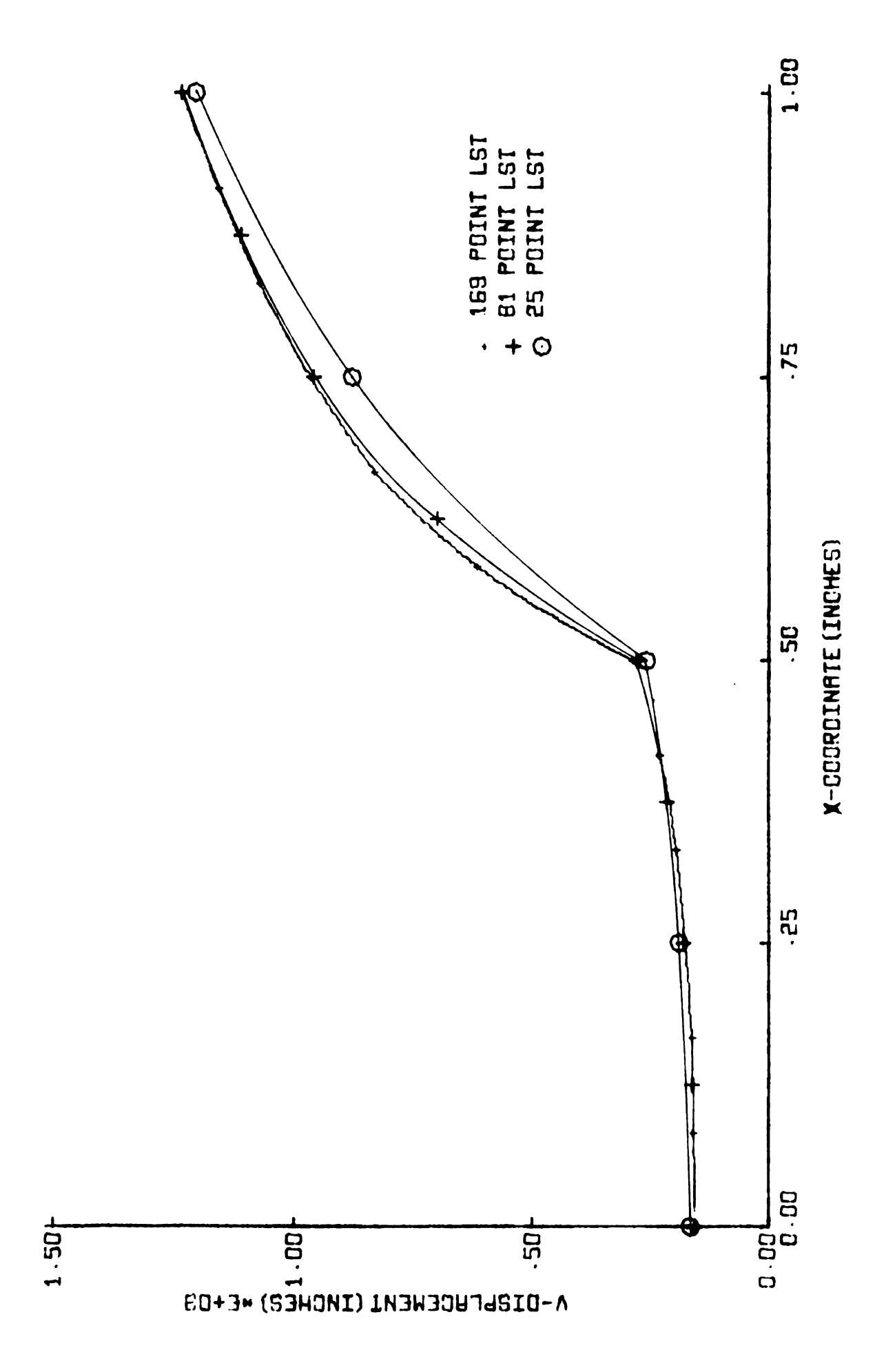


Figure 4.32, LST Horizontal Interface v-Displacements

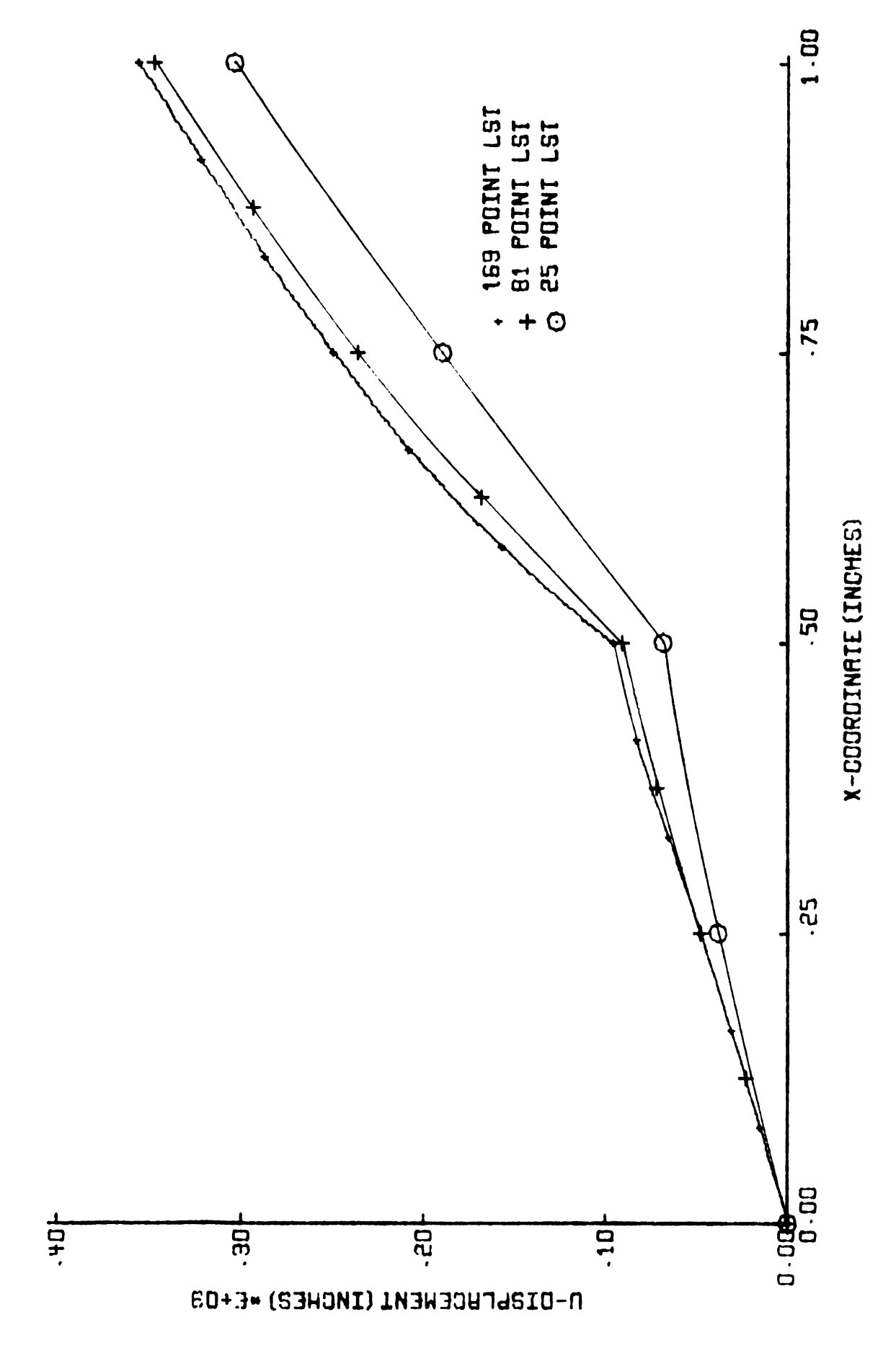


Figure 4.33, LST Horizontal Interface u-Displacements

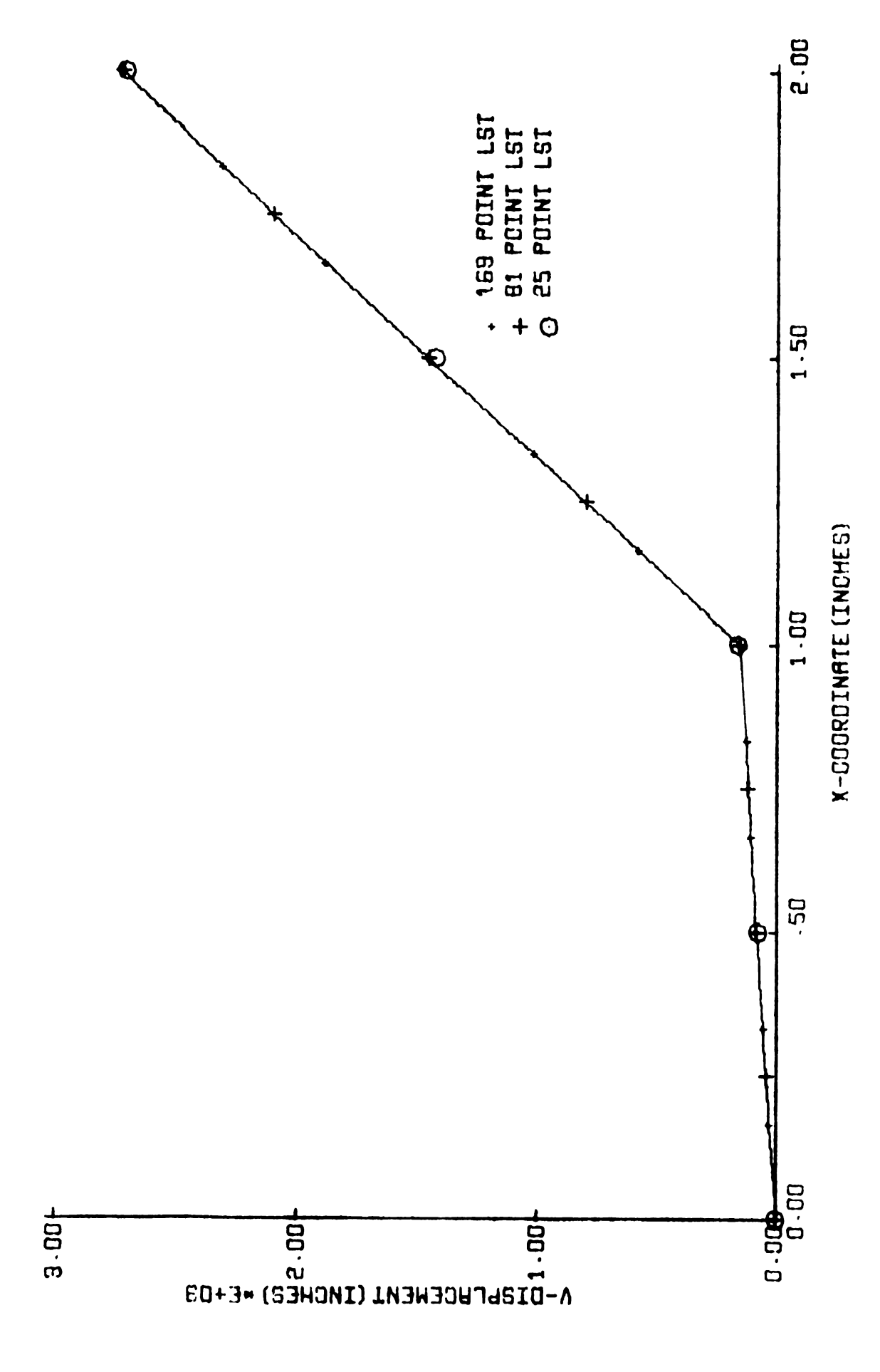


Figure 4.34, LST Vertical Symmetry Axis v-Displacements

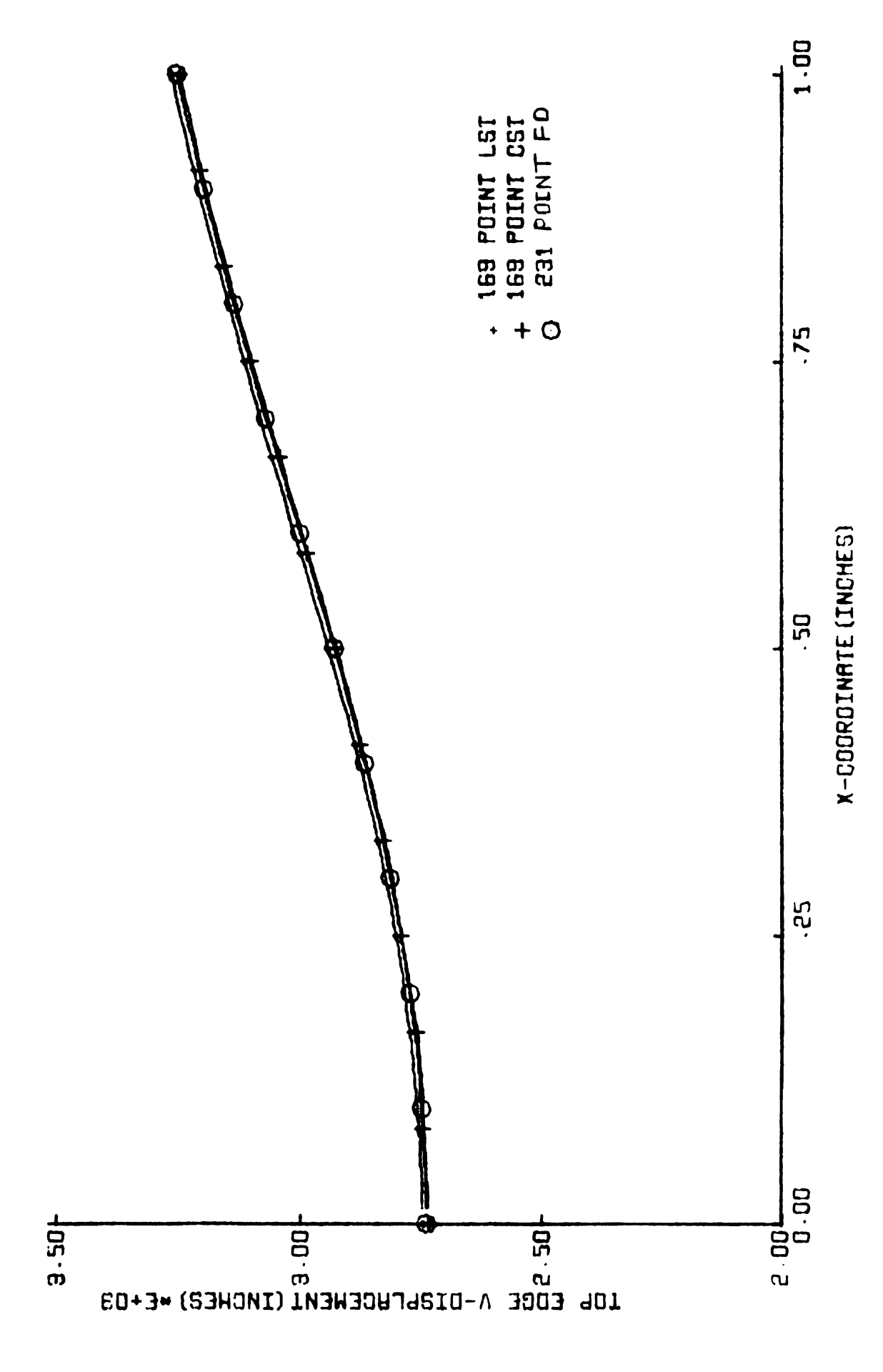


Figure 4.35, FD, CST, LST Top Edge v

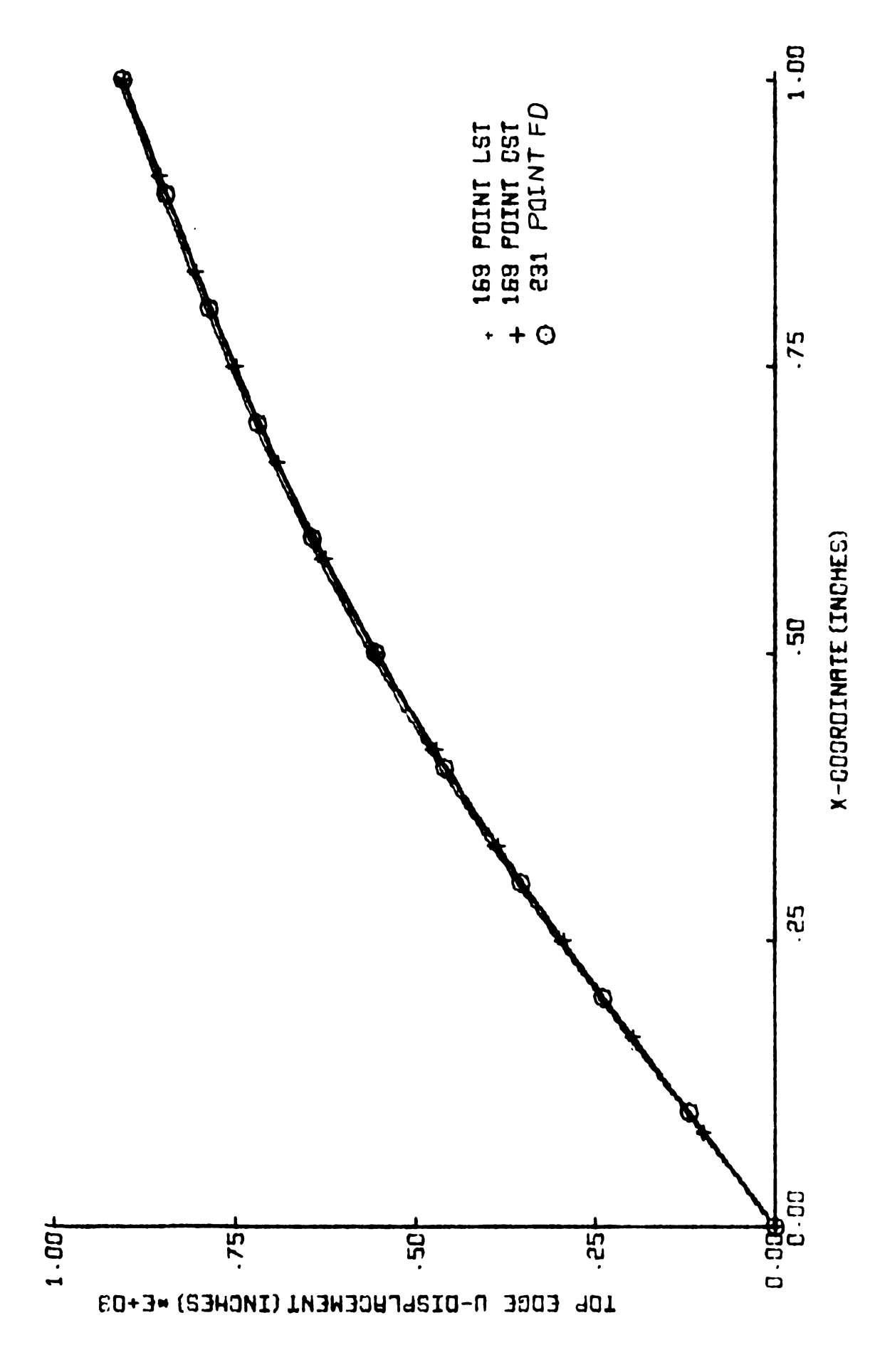


Figure 4.36, FD, CST, LST Top Edge u

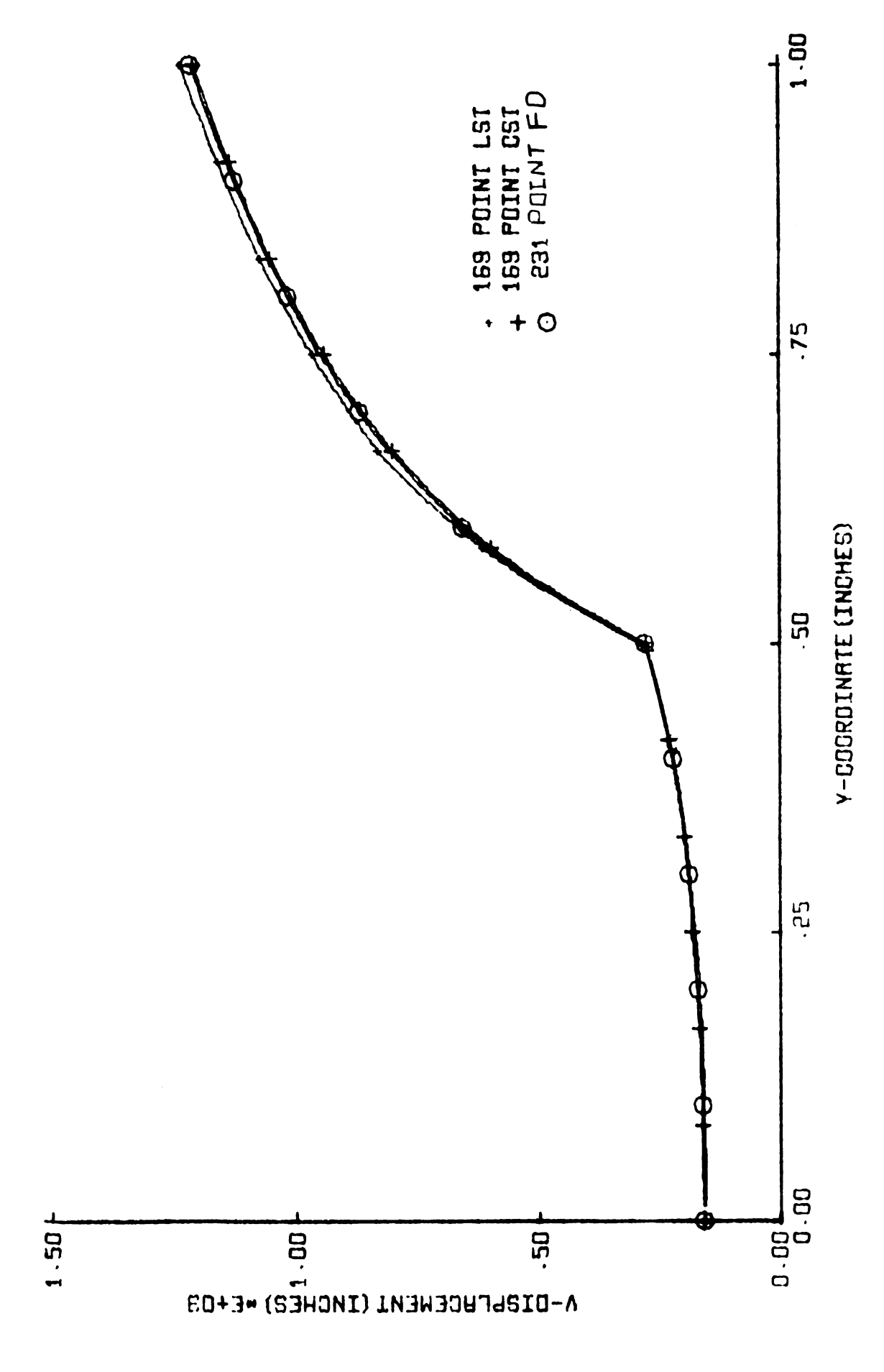


Figure 4.37, FD, CST, LST, Horizontal Interface v

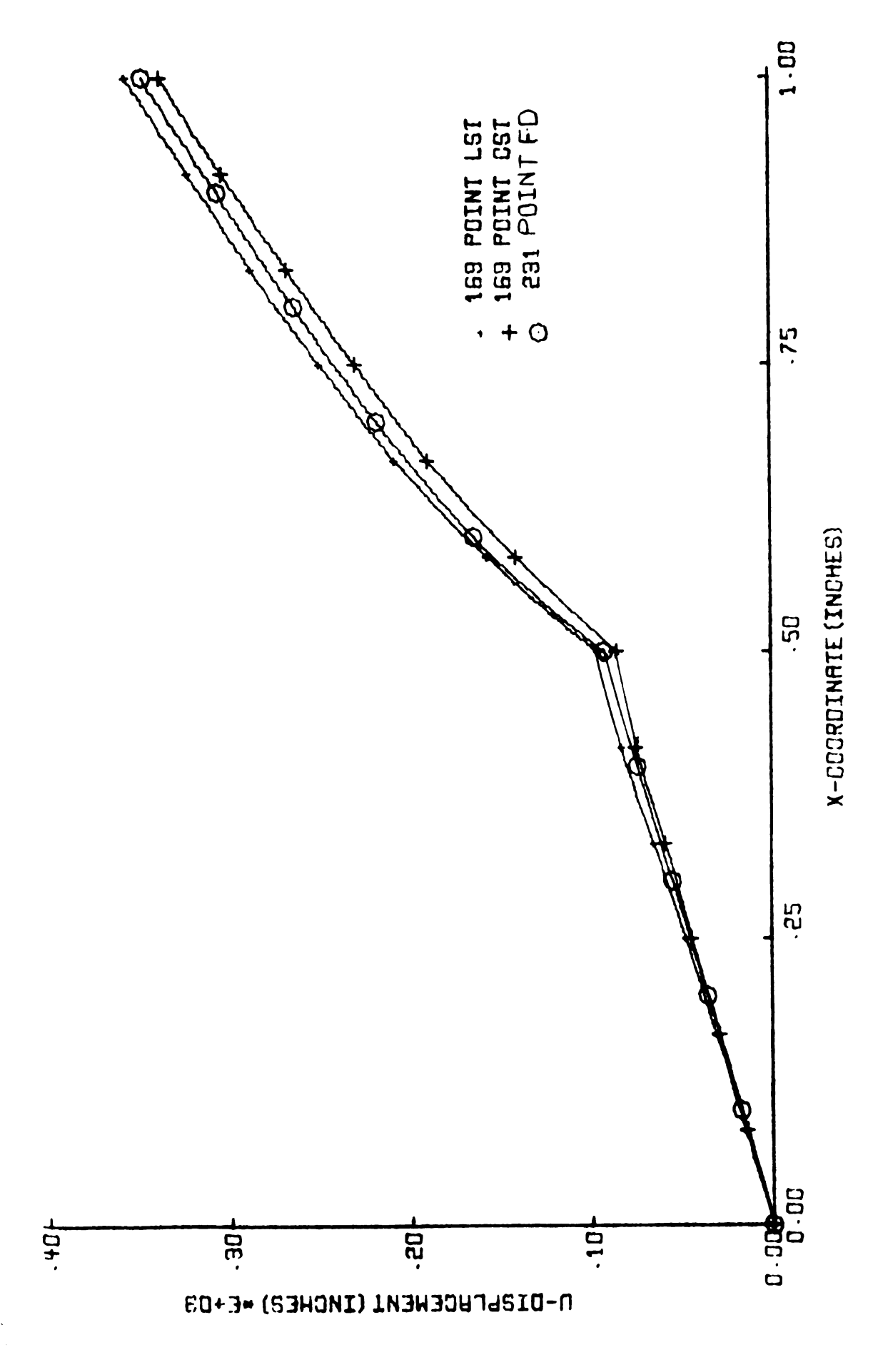


Figure 4.38, FD, CST, LST Horizontal Interface u

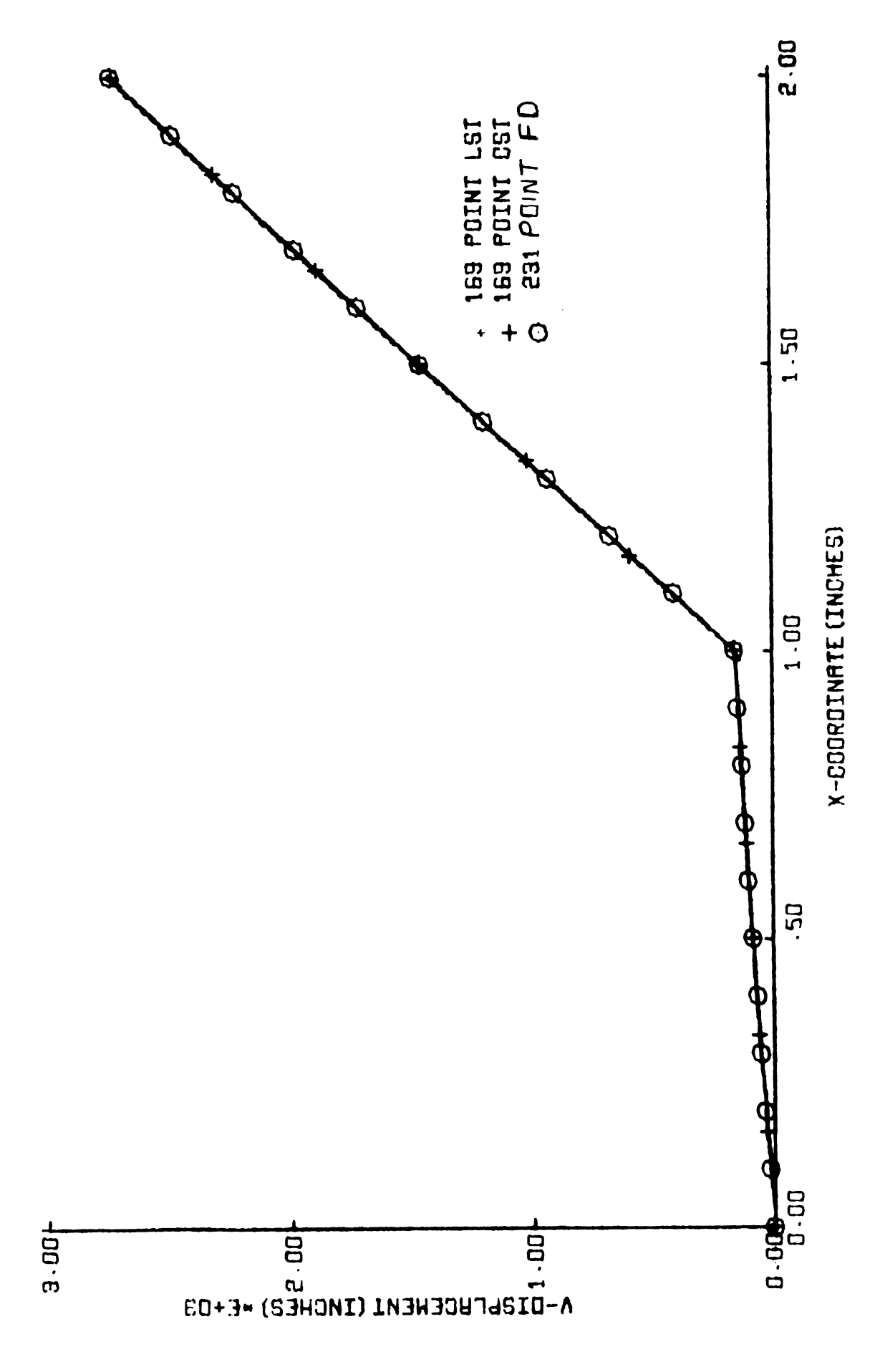


Figure 4.39, FD, CST, LST Vertical Symmetry Axis v

Table 4.7

Composite Plate Top Edge v-Displacements \times 10^{+3}

x-Coord.	231 Point Finite Diff.	x-Coord.	169 Point C.S.T.	169 Point L.S.T.
0.	2.7391	0.	2.7342	2.7469
.1	2.7477	.08333	2.7446	2.7546
.2	2.7730	.16666	2.7581	2.7736
.3	2.8139	.25	2.7909	2.8024
.4	2.8681	.33333	2.8264	2.8414
.5	2.9324	.41666	2.8767	2.8906
.6	3.0027	.5	2.9284	2.9454
.7	3.0741	.58333	2.9876	3.0035
.8	3.1424	.66666	3.0462	3.0633
.9	3.2043	.75	3.1045	3.1208
1.	3.2600	.83333	3.1594	3.1747
		.91666	3.2093	3.2264
		1.	3.2551	3.2745

Table 4.8

Composite Plate Top Edge

u-Displacements × 10⁺³

x-Coord.	231 Point Finite Diff.	x-Coord.	169 Point C.S.T.	169 Point L.S.T.
0.	0.	0.	0.	0.
.1	1214	.08333	1004	1030
.2	2402	.16666	1996	2046
.3	3541	.25	2954	3024
.4	4605	.33333	3876	3961
.5	5576	.41666	4736	4831
.6	6443	.5	5540	5639
.7	7206	.58333	6264	6360
.8	7880	.66666	6928	7014
.9	8495	.75	 7517	7601
1.	9093	.83333	8063	8141
		.91666	8570	8649
		1.	9065	9143



x-Coord.	231 Point Finite Diff.	x-coord.	169 Point C.S.T.	169 Point L.S.T.
0.	.1604	0.	.1603	.1579
.1	.1634	.08333	.1648	.1596
.2	.1729	.16666	.1689	.1649
.3	.1909	.25	.1830	.1782
.4	.2222	.33333	.1992	.1979
.5	.2818	.41666	.2318	.2318
.6	.6577	.5	.2776	.2870
.7	.8720	.58333	.5994	.6168
.8	1.0194	.66666	.8018	.8316
.9	1.1294	.75	.9442	.9679
1.	1.2186	.83333	1.0537	1.0769
		.91666	1.1399	1.1630
		1.	1.2125	1.2403

x-Coord.	231 Point Finite Diff.	x-Coord.	169 Point C.S.T.	169 Point L.S.T.
0.	0.	0.	0.	0.
.1	0180	.08333	0149	0158
.2	0365	.16666	0296	0317
.3	0556	.25	0449	0484
.4	0751	.33333	0595	0659
.5	0933	.41666	0756	0836
.6	1654	.5	0861	0985
.7	2189	.58333	1418	1580
.8	2646	.66666	1905	2089
.9	3071	.75	2310	2504
1.	3487	.83333	2687	2887
		.91666	3045	3232
		1.0	3389	 3577

y-Coord.	231 Point Finite Diff.	y-Coord.	169 Point C.S.T.	169 Point L.S.T.
0.	О.	0.	0.	0.
.1	.0186	.16666	.0309	.0305
.2	.0370	.33333	.0607	.0596
.3	.0548	.5	.0880	.0865
.4	.0717	.66666	.1123	.1102
.5	.0877	.83333	.1367	.1318
.6	.1027	1.	.1603	.1579
.7	.1167	1.16666	.5884	.5860
.8	.1304	1.33333	1.0189	1.0248
.9	.1446	1.5	1.4585	1.4659
1.	.1604	1.66666	1.8871	1.8988
1.1	.4140	1.83333	2.3148	2.3250
1.2	.6727	2.	2.7342	2.7469
1.3	.9349			
1.4	1.1981			
1.5	1.4603			
1.6	1.7202			
1.8	2.2316			
1.9	2.4849			
2.	2.7391			

displacements are generally the largest for the 3 sets of results. The exception to this observation occurs in the stiffener where displacements are apparently overestimated in general.

Regarding the horizontal interface $y=\frac{b}{2}$, the LST solution gives a maximum vertical displacement of 1.2404 \times 10⁻³ in. The CST and FD difference values for this same displacement component are 1.2125 \times 10⁻³ in. and 1.2186 \times 10⁻³ in. respectively. In this connection, the LST solution is apparently best.

As a final observation, it should be noticed that FD displacements generally represent a slight improvement over the CST displacements. However, not to be overlooked is the fact that considerably more points (231) have been employed as opposed to 169 for the CST solution.

In any stress analysis, the location of regions of maximum stress and the determination of these stresses is of primary concern. For the present problem, these regions correspond to the material interface. The overall stress distribution obtained from the best solution for each of the methods is presented in Figures 4.40 through 4.42 on page 158 through 160. Two sets of stresses are shown for interface points because some stress components are not continuous across the interface. It is evident from these results that maximum stresses indeed occur in the interface regions. In fact, compared to the 1200 psi applied stress—very large values of σ_y occur in the stiffener. Along the vertical interface, the methods indicate σ_y stresses in excess of 3600 psi, or a stress concentration factor greater than 3. The maximum σ_y in the matrix is nearly 2300 along the horizontal interface near the corner. The stress concentration factor is approximately 1.9.

i				15	•						
-309 1203 10	-302 1203	-283 1203	-252 1203	-210 1202	-160 1200 26	-108 1199	- 60 1197	- 23 1195	-4 1195	120]	
-234 1209 12	-230 1209	-217 1209 22	18 -196 1207 32	-167 1205 40	-133 1202 45	26 -97 1198 45	-62 -1193 -39	- 33 1188 27	-13 1187 13	-1 -5 1196	
-180 1224	-177 1224	-169 1223	-154 1220	-135 1215	11 <u>1)</u>	83 1194	-15 1162	31 1171	-12 1166	-5 11/7	σ
14 -137	-135	36 -13	-122	-108	75	76	68	51	28	14	σ
1244 15	1244	1243	1238	1229 86	1213 99	1191 102	1167 93	-25 1148 71	-10 1136 41	1140 23	τ
-98 1268 15	-98 1268 24	-97 1267 49	-94 1262 75	-86 1249 99	1224 118	-54 T187 123	-34 1150 112	-18 1119 - 87	-6 1097 51	-2 1087 29	
- <u>58</u> 1291 15	-60 1292 23	-64 1293 48	-67 1290 76		- <u>56</u> 1241 134	-39 1184 143	-20 1130 129	1086 99	1052 57	-1 1026 32	
-14 1311 13	-18 1313 18	-26 1319 40	-38 1322 69	- 4 6 1311 108	-41 1269 148	-22 1180 163	- <u>5</u> 1102 143	1045 105	1003 58	2 962 31	
39 1324 11	35 1329 10	21 1341 25	-1 1357 52	-22 1360 98	-24 1319 162	-3 1169 188	16 1064 154	17 998 104	952 52	4 903 25	
103 1328	99 1335	83 1356	53 1389	14 1423	-4 1413 173	1740 1740 219	38 1007 158	30 941 93	903	6 859	
175 1324	172 1332 -8	162 1358 -14	139 1406 -14	88 1486	34 1602 167	35 1068 254	45 929 150	29 881 76	39 12 859 25	15 5 837	
243 1319	245 1328	250 1356	264 1410	304 1514	12	, 234	130	"			
0 -1500 1295	-10 -1519 1306	-26 -1564 1346	-41 -1583 1464	-49 -1361 -1141 1884 3740	318	102 849 362	-42 823 166	-16 816 75	-5 818 -21	-2 830 0	
-793 1291	- 30 - 766 1306	-46 -674 1367	-499 1534	325 537 -270 -154 2019 369	-70 1 148	-79 589	-72 698	-41 741	-16 773	-7 817	
-268 1314	-1 -238 1342	-153 1443	- 33 1689	51 7 2249 348	1 40 3 163	358 	-37 584	99 - 30 - 662	35 -14 718	-6 782	
58 71 1393	87 1431	145 128 1563	283 166 1839	157 13 2342 317	5 56	320	-1	121	52	-3	
75	105	224	356	450 66	316	273	495 202	586 129	656	727 30	
257 1506 72	260 1549 123	261 1688 344	244 1947 351	192 15 2349 289 391 37	3 157	60 312 228	25 431 180	522 123	595 64	- 0 661 33	
341 1627 63	335 1669 118	313 1798 226	268 2018 305	200 16 2321 267 318 29	7 151	279 185	- 1384 152	18 470 109	6 538 59	- 2 594 31	
_366 1738 50	355 1775 100	322 1885 186	267 2062 243	197 16 2285 254 249 22	1 <u>105</u> 0 146 4 155	85 257 145	50 350 122	24 428 89	8 490 50	3 535 27	
362 1828 37	350 1859 76	313 1950 140	256 2089 178	190 15 225 3 241 176 16	7 306 1 141 0 113	87 242 107	53 326 91	27 397 68	9 451 38	3 486 20	
349 1893 24	336 1920 50	299 1994 92	244 2105 116	183 15 2229 234 113 10	1138	, 88 232 70	54 310 60	28 374 45	10 424 25	3 451 14	
337 1932 12	324 1955 25	288 2020 46	236 2114 57	2215 230	9 105 2 137 0 37	87 226 35	54 300 30	28 362 23	10 407 13	3 430 7	
332 1945 3	320 1967 6	284 2029	232 2117 18	2211 229	8 104 0 136 7 9	87 224 8	54 297 8	28 358 6	10 401 3	3 423 1	

Figure 4.40

Figure 4.41

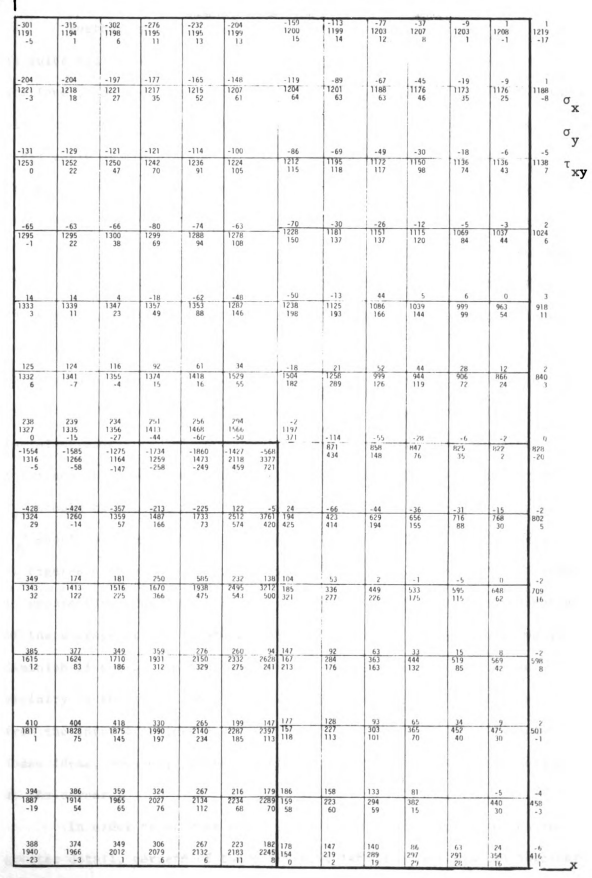


Figure 4.42

Further examination of these stress results indicates that $\sigma_{\rm X}$ is quite small (less than 400 psi) throughout the matrix. In the stiffener, however, large compressive values as great as 1860 psi arise along the horizontal interface. This is clearly the result of the large ratio of elastic moduli for the two materials. Maximum shear stresses also occur along the material interface. The indicated values are approximately 700 psi for the stiffener and 500 psi for the matrix.

It is well to recall that due to the sharp corner corresponding to the intersection of the vertical and horizontal material interfaces, the theoretical stress components at the corner are undefined. Since the nodal point stresses represent the average stresses in the neighborhood of any point, they clearly would not reflect this situation.

A second point of clarification is in order. Regarding interfacial stresses, certain components should be continuous across the interface in view of equilibrium considerations. For instance, $\sigma_{\mathbf{y}}$ and $\tau_{\mathbf{y}\mathbf{x}}$ should be continuous across the horizontal interface whereas $\sigma_{\mathbf{x}}$ and $\tau_{\mathbf{x}\mathbf{y}}$ should be continuous across the vertical interface. The results in Figures 4.40 through 4.42, however, do not reflect this. The difference is apparently due to the fact that nodal point stresses are indicative of the average stress around a given point. These discrepancies would diminish if smaller spacing and smaller triangles were used in the vicinity of the interface. Along with this, one could extrapolate from the interior points and this should further improve the results. These ideas, however, probably would not greatly improve the situation at the corner.

In order to examine and compare these interfacial stresses in greater detail, certain of these are next tabulated and plotted together.

The normal stress component σ_y is listed for the three solutions in Tables 4.15 through 4.18. The first two tables pertain to the horizontal interface whereas the others pertain to the vertical interface. These same results are graphically presented in Figures 4.44 and 4.45 on pages 168 and 171. It is apparent from these figures that the three solutions are more comparable than they were for the σ_x stress. The finite element σ_y stresses display a much smoother variation than σ_x . In Figure 4.44, the largest deviations in σ_y across the horizontal interface obviously take place at the corner. In fact these deviations

x-Coord.	Finite Diff.	x-Coord.	C.S.T.	L.S.T.
0.	243	0.	187	238
.1	245	.08333	244	239
.2	250	.16666	185	234
.3	264	.25	256	251
.4	304	.33333	179	256
.5	12	.41666	302	294
.6	-102	.5	24	-2
.7	- 42	.58333	-105	-114
.8	-16	.66666	- 28	- 55
.9	- 5	.75	- 32	- 28
1.	- 2	.83333	- 7	- 6
		.91666	- 6	- 2
		1.	0	0

x-Coord.	Finite Diff.	x-Coord.	C.S.T.	L.S.T.
0.	-1500	0.	-930	-1554
.1	-1519	.08333	-1452	-1585
.2	-1564	.16666	-896	-1275
.3	- 1583	.25	-1432	-1734
.4	-1361	.33333	- 751	-1860
.5	-1147	.41666	-1049	-1427
		.5	- 411	- 586

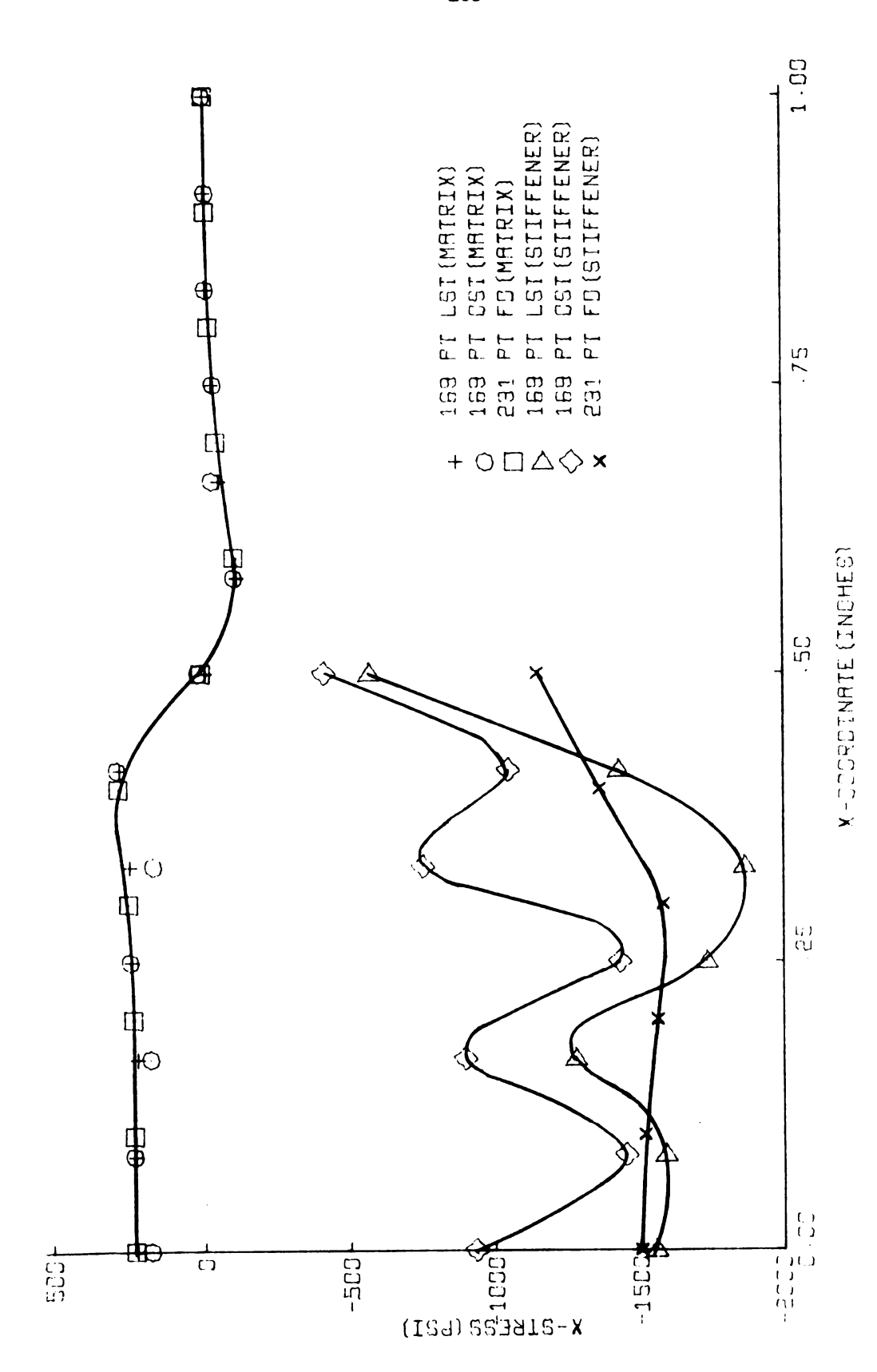


Figure 4.43, Composite Plate Horizontal Interface $\sigma_{\mathbf{x}}$

A

x-Coord.	Finite Diff.	x-Coord.	C.S.T.	L.S.T.
0.	1319	0.	1323	1327
.1	1328	.08333	1329	1335
.2	1356	.16666	1347	1356
.3	1410	.25	1381	1413
. 4	1514	.33333	1435	1468
.5	1198	.41666	1525	1566
.6	849	.5	1103	1197
.7	823	.58333	834	871
.8	816	.66666	826	858
.9	818	. 75	812	847
1.	830	.82222	816	825
		.91666	820	822
		1.0	827	828

Table 4.15
Composite Plate

Horizontal Interface Stress

 $\sigma_{\mathbf{y}}$ (Stiffener)

y-Coord.	Finite Diff.	y-Coord.	C.S.T.	L.S.T.
0.	1295	0.	1308	1316
.1	1306	.08333	1304	1266
.2	1346	.16666	1367	1164
.3	1464	.25	1438	1259
. 4	1864	.33333	1726	1473
.5	3740	.41666	2188	2118
		.5	2889	3377

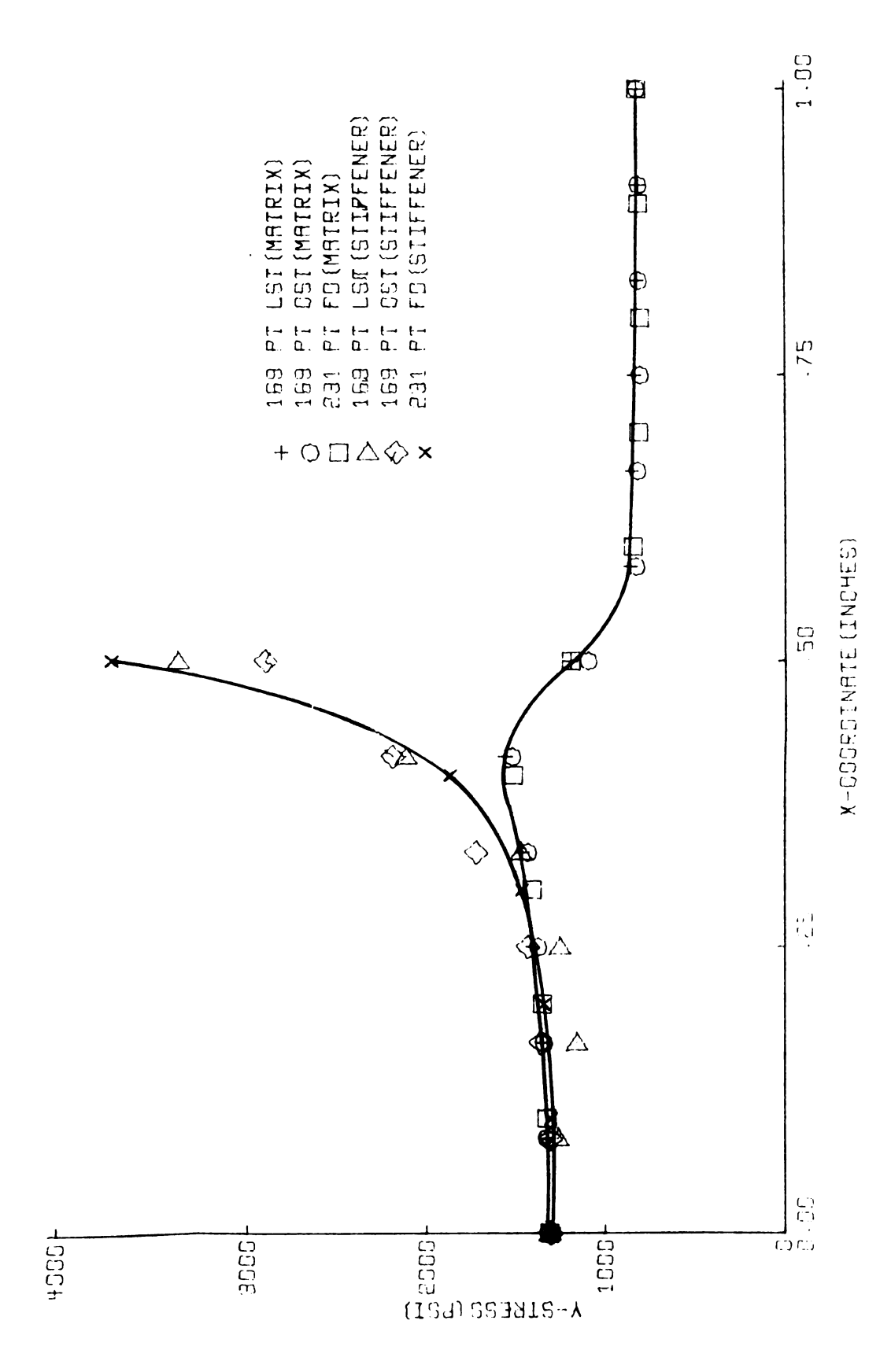


Figure 4.44, Composite Plate Horizontal Interface $_{
m y}$

		y (Matrix)		
y-Coord.	Finite Diff.	y-Coord.	C.S.T.	L.S.T.
0.	136	0.	177	154
.1	137	.16666	144	159
. 2	138	.33333	190	157
.3	141	.5	160	167
.4	146	.66666	244	185
.5	151	.8333	180	194
.6	157	1.	1103	1197
. 7	162	1.16666	1484	1504
.8	163	1.3333	1285	1238
.9	148	1.5	1240	1228
1.	1198	1.66666	1215	1212
1.1	1602	1.8333	1205	1204
1.2	1413	2.	1201	1200
1.3	1319			
1.4	1269			
1.5	1241			
1.6	1224			
1.7	1213			
1.8	1206			
1.9	1202			

2.0

y-Coord.	Finite Diff.	y-Coord.	C.S.T.	L.S.T.
0.	2290	0.	2255	2245
.1	2302	.16666	2319	2289
.2	2341	.33333	2365	2397
.3	2411	.5	2657	2628
. 4	2540	.66666	2734	3212
.5	2677	.83333	3368	3761
.6	2893	1.	2889	3377
.7	3171			
.8	3483			
.9	3691			
1.	3740			

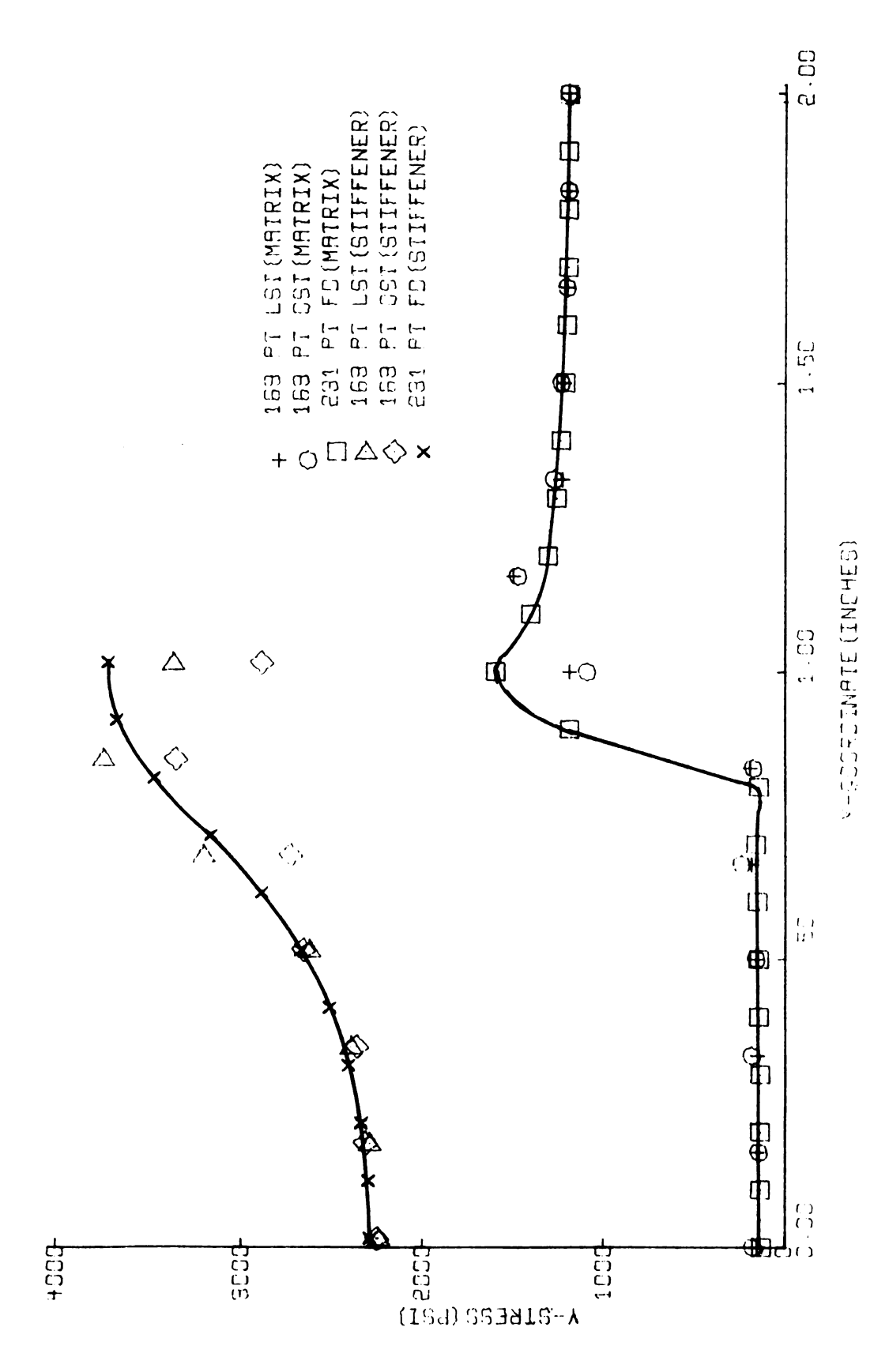


Figure 4.45, Composite Plate Vertical Interface $_{
m y}$

become very apparent as the corner is approached. In Figure 4.45, the stress σ_y is different in the matrix and stiffener due to the difference in elastic properties.

The interfacial shear stresses on the vertical interface are shown in Table 4.18 for the matrix and in Table 4.19 for the stiffener. These are also plotted in Figure 4.46. The results are again quite comparable for the three solutions. The largest deviations occur at the corner where stresses in the stiffener are indicated to 532, 551, and 721 psi respectively for the FD, CST, and LST solutions respectively.

Concluding Remarks. The three solutions seem to have comparable capability for predicting displacements in a simple composite. The maximum overall extension did not vary appreciable for the three solutions. The situation insofar as stress is concerned is somewhat different, however. The finite element solutions in general and the CST solutions more specifically display erratic tendencies. The finite difference stresses vary in a much smoother fashion and consequently seem more realistic. It is well to recall in this connection that the best FD solution employed 231 points whereas the best finite element solutions used only 169 points.

An additional remark is in order at this point. For truly accurate analysis, one would use an arrangement of elements whereby many more smaller elements would be placed along the interface. In this way a better indication of the complicated state of stress would be achieved. This is a very easy thing to do within the framework of the Finite Element Theory. A similar concept in the finite difference

Table 4.18

Composite Plate Vertical Interface Stress

τ_{xy} (Matrix)

y-Coord.	Finite Diff.	y-Coord.	C.S.T.	L.S.T.
0.	9	0.	34	0
.1	37	.16666	61	58
.2	75	.33333	128	118
.3	113	.5	197	213
.4	155	.66666	293	321
.5	200	.83333	398	425
.6	251	1.	295	371
.7	310	1.16666	162	371
.8	383	1.33333	162	198
.9	476	1.5	131	150
1.	318	1.66666	105	115
		1.83333	64	64
1.1	167	2.	42	15
1.2	173		/	
1.3	162			
1.4	148			
1.5	134			
1.6	118			
1.7	99			
1.8	75			
1.9	45			
2.0	26			

Table 4.19

Composite Plate Vertical Interface Stress

 τ_{xy} (Stiffener)

y-Coord.	Finite Diff.	y-Coord.	C.S.T.	L.S.T.
0.	17	0.	39	8
.1	50	.16666	79	70
.2	103	.33333	183	113
.3	160	.5	273	241
. 4	224	.66666	468	500
.5	297	.83333	468	420
.6	379	1.	551	721
.7	667			
.8	532			
.9	448			
1.	532			

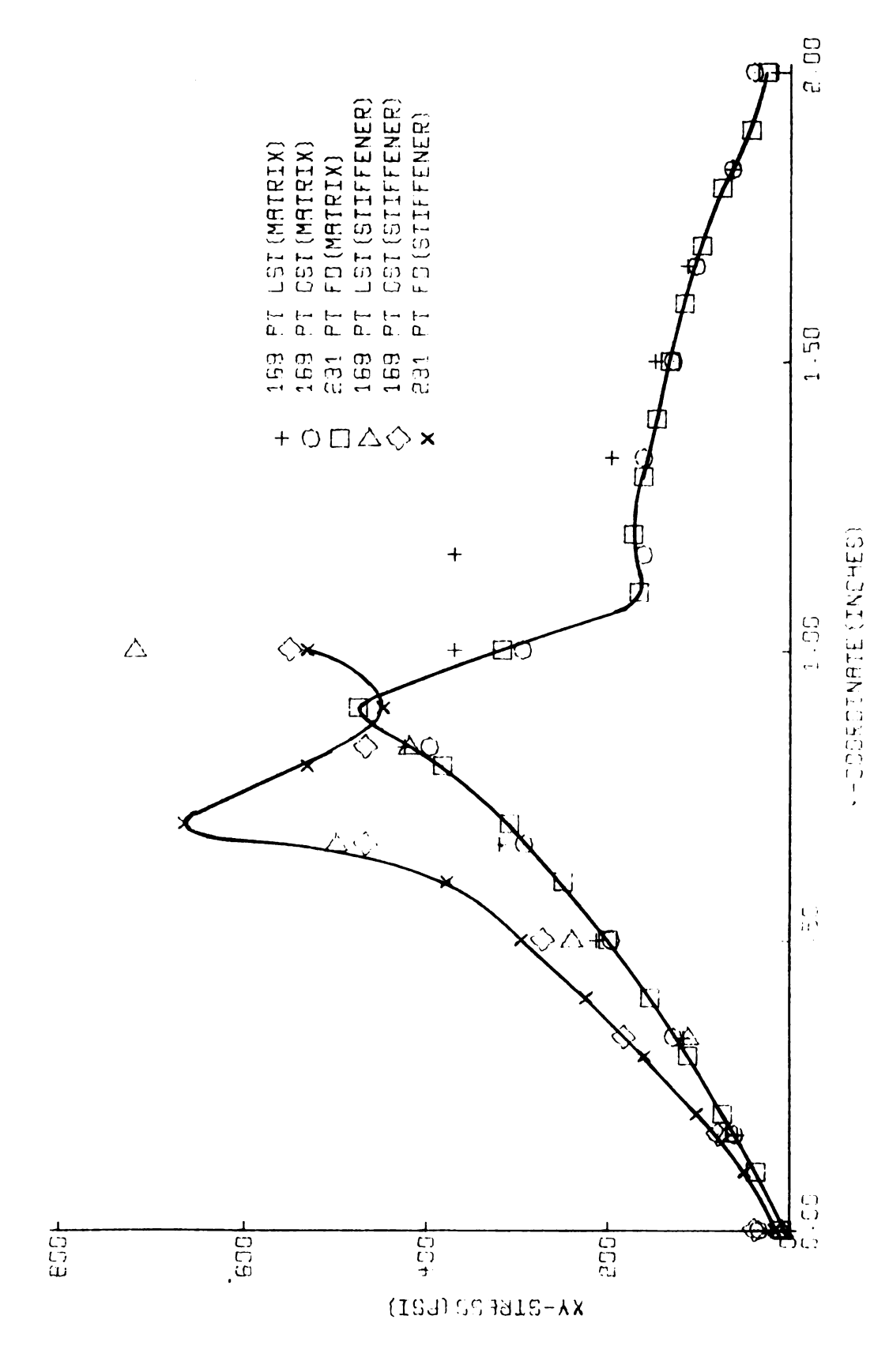


Figure 4.46, Composite Plate Vertical Interface τ

analysis would involve a transition region whereby the mesh spacing would accordingly be diminished. This effect is not as readily achieved as the comparable concept in the finite element method. No attempt has been made to develop the idea in this research.

V. AXIALLY SYMMETRIC APPLICATIONS

The finite element methods are not limited to two dimensional problems, and for that matter neither are the finite difference methods. Three dimensional analysis, however, is considerably more involved and generally requires significantly more computer memory. Consequently, most of the applications have involved plane stress or plane strain.

The axially symmetric applications generally involve a triaxial state of stress. The special character of such situations results in a two dimensional displacement field. As a result, the axially symmetric elasticity problem is almost as readily formulated as the true two dimensional problem.

Two axially symmetric applications are treated in this section.

Included are a thick hollow cylinder subjected to internal and external pressure and a composite solid cylinder uniformly stressed at its ends. Both finite element and finite difference solutions are included for each example. The finite element solutions employ the constant strain triangular ring (CSTR) and the linearly varying strain triangular ring (LSTR) discussed in Chapter III. The finite difference solution involves the axially symmetric Navier equations; however, the particular equations used correspond to the alternate derivation of section 2.9. The primary emphasis here as in Chapter IV is on the comparison of the methods involved. In the case of the thick cylinder, comparison is also made with the known elasticity solution.

5.1 Thick Cylinder

The thick cylinder under internal and external pressure is a fundamental problem of the Theory of Elasticity. A portion of such a cylinder is shown in Figure 5.1, page 179. The numerical properties pertinent to this application are also shown. These include outside and inside radii which are 10 in. and 5 in. respectively. The material is assumed to have a Young's modulus $E = 10^7$ psi and a Poisson's ratio $v = \frac{1}{4}$. The external pressure designated by P_0 is 15,000 psi. The internal pressure P_1 is 9000 psi. The finite element solution for a similar thick cylinder has been considered by a number of other writers. For example, Wilson [25] reports very excellent results using the constant strain triangular ring element.

Elasticity Solution. The general elasticity solution for the thick cylinder is presented in the text by Timoshenko and Goodier [39]. Using the notation of Figure 5.1, the stresses are

$$\sigma_{\mathbf{r}} = \frac{a^{2}b^{2}(p_{o} - p_{i})}{b^{2} - a^{2}} \cdot \frac{1}{r^{2}} + \frac{p_{i}a^{2} - p_{o}b^{2}}{b^{2} - a^{2}}$$

$$\sigma_{\theta} = -\frac{a^{2}b^{2}(p_{o} - p_{i})}{b^{2} - a^{2}} \cdot \frac{1}{r^{2}} + \frac{p_{i}a^{2} - p_{o}b^{2}}{b^{2} - a^{2}}$$

$$\sigma_{\mathbf{z}} = \tau_{\mathbf{rz}} = 0$$

The radial strain is

$$\varepsilon_r = \frac{1}{F} (\sigma_r - v\sigma_\theta)$$

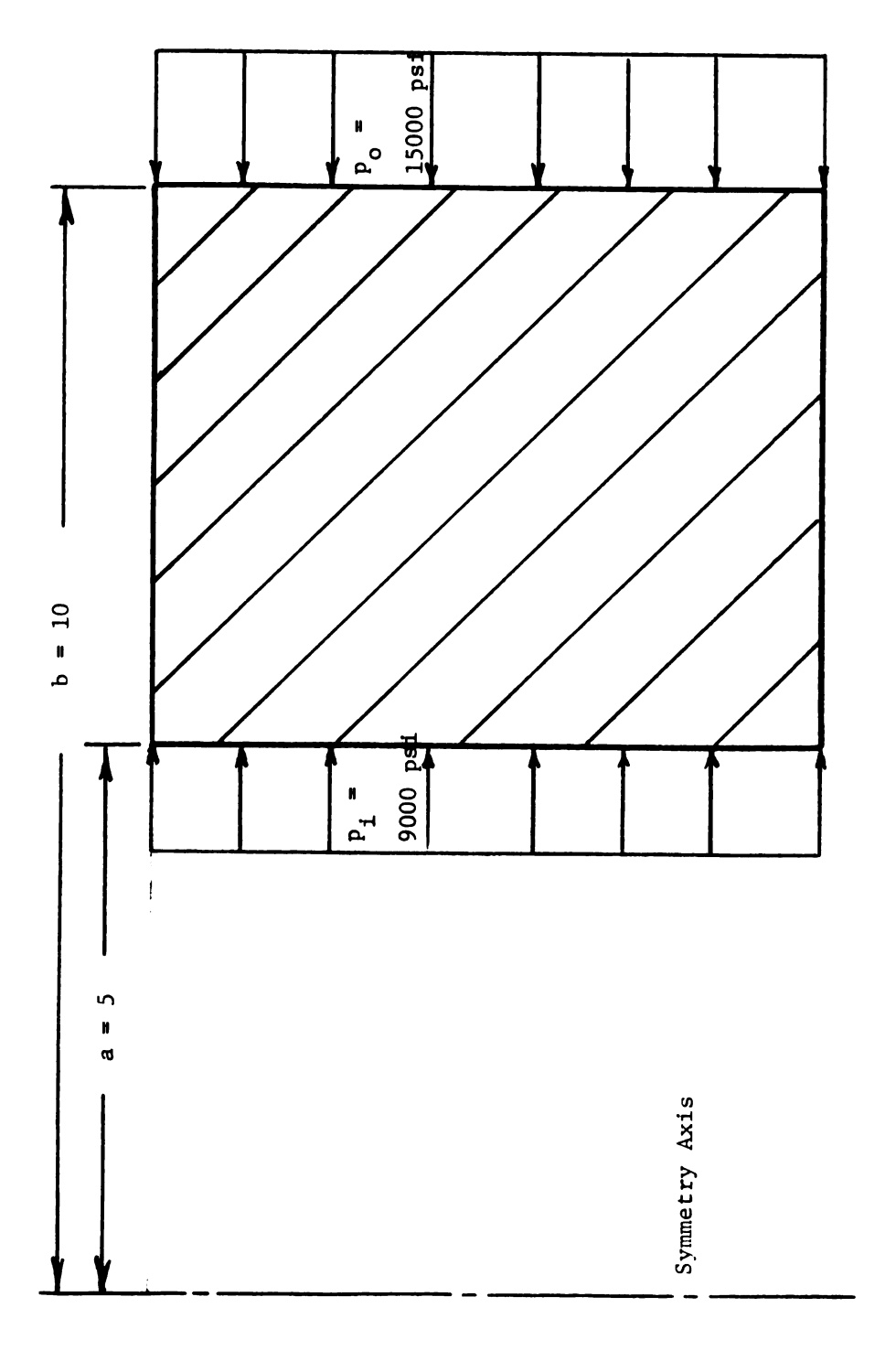


Figure 5.1 Pressurized Thick Cylinder

Eliminating the stresses, one obtains

$$\varepsilon_{\mathbf{r}} = \frac{1}{E} \left[\frac{a^2 b^2 (p_0 - p_1)}{b^2 - a^2} \cdot \frac{(1 + v)}{r^2} + \frac{p_1 a^2 - p_0 b^2}{b^2 - a^2} \cdot (1 - v) \right]$$

Similarly

$$\varepsilon_z = \frac{-v}{E} (\sigma_r + \sigma_\theta) = \frac{-2v}{E} \left[\frac{p_i a^2 - p_o b^2}{b^2 - a^2} \right]$$

The displacements are obtained by integrating the strain displacement equations. Thus from the relationships

$$\varepsilon_{\mathbf{r}} = \frac{\partial \mathbf{u}}{\partial \mathbf{r}}$$

$$\varepsilon_z = \frac{\partial w}{\partial z}$$

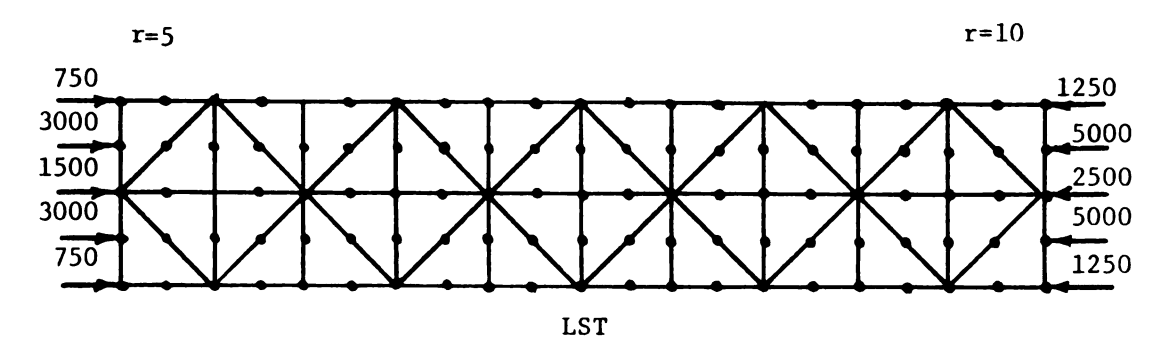
one can derive

$$u = \frac{1}{E} \left[-\frac{a^2b^2(p_0 - p_1)}{b^2 - a^2} \cdot \frac{(1 + v)}{r} + \frac{p_1a^2 - p_0b^2}{b^2 - a^2} \cdot (1 - v)r \right]$$

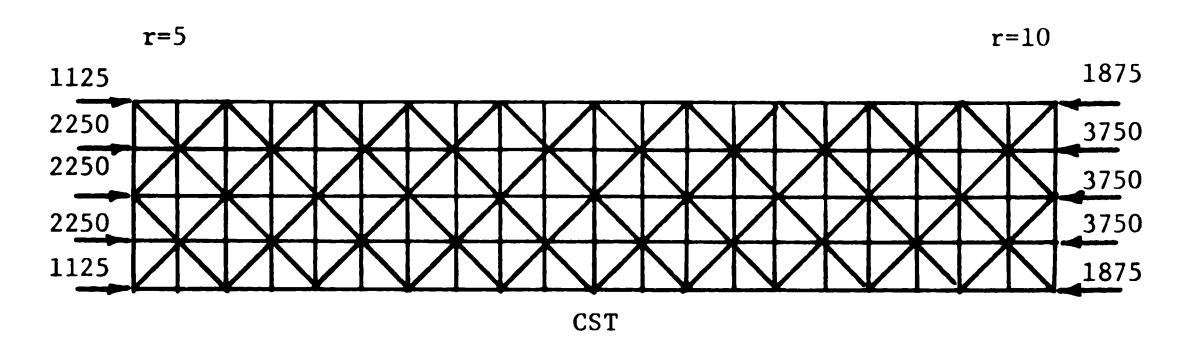
$$w = -\frac{2v}{E} \left[\frac{p_1a^2 - p_0b^2}{b^2 - a^2} \right] \cdot r$$

The approximate solutions of the finite element and finite difference methods follow. The results are exceedingly good in each case and thus only one solution for each method is presented.

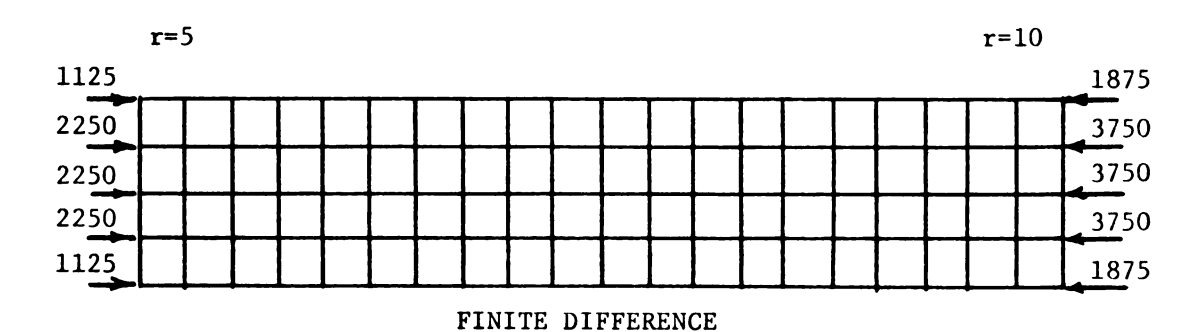
Numerical Solutions. In analyzing the thick cylinder, the configurations of Figure 5.2 on the following page were used. As can be seen, a small axial segment is involved using a total of 105 points in each case. Half of the segment is above the $r-\theta$ plane and half of it



105 Nodal Points



105 Nodal Points



105 Mesh Points

Figure 5.2

Thick Cylinder
Finite Element and Finite Difference Configurations

is below the r - 0 plane. The nodal circle force intensities associated with the external and internal pressures are shown. In the finite element method, these must be multiplied by corresponding nodal circle radii before they can be used in the equilibrium equations. The LSTR solution uses 40 triangular ring elements as shown in the figure. The CSTR solution employs 160 triangular ring elements.

As typical indications of the accuracy of the approximate solutions, the radial displacement, radial stress and circumferential stress are summarized and compared with exact results. The specific values used in this comparison correspond to the cylinder mid-plane and are specified as u(r,0), $\sigma_r(r,0)$ and $\sigma_{\theta}(r,0)$.

Beginning with the radial displacements, these are tabulated on page 183. The same information is plotted on the following page, Figure 5.3. The solid curve represents the exact solution. The approximate solutions are shown with appropriate characters as noted in the figure. Clearly, there are no significant deviations from the exact solution for any of the approximate solutions.

The radial stress is plotted in Figure 5.4 and tabulated on page 185. The radial stress is compressive throughout the body and ranges from 9000 psi on the inside surface to 15,000 psi on the outside surface. It is apparent that each approximate solution is excellent at the interior points. Noticeable deviations from the exact stresses occur at the inner and outer surfaces for the FD and CSTR solutions. Thus on the inside surface, the error is 4.37% for the FD solution and 6.43% for the CSTR solution. The error in the LSTR solution is only 0.46%. All of these are higher than the exact stress. On the outside surface, the errors are less than 0.5% for all solutions.

TABLE 5.1 Thick Cylinder Radial Displacement $u(\textbf{r,0}) \times 10^{-3}$

r-Coord.	Finite Diff.	C.S.T.R.	Elasticity	L.S.T.R.
5.00	-1.1364	-1.1365	-1.1375	-1.1372
5.25	-1.1445	-1.1448	-1.1455	-1.1452
5.50	-1.1548	-1.1548	-1.1557	-1.1555
5.75	-1.1669	-1.1672	-1.1679	-1.1675
6.00	-1.1807	-1.1808	-1.1816	-1.1814
6.25	-1.1959	-1.1962	-1.1968	-1.1965
6.50	-1.2124	-1.2125	-1.2133	-1.2131
6.75	-1.2301	-1.2303	-1.2309	-1.2306
7.00	-1.2488	-1.2489	-1.2496	-1.2494
7.25	-1.2683	-1.2685	-1.2692	-1.2689
7.50	-1.2887	-1.2888	-1.2895	-1.2893
7.75	-1.3099	-1.3101	-1.3107	-1.3104
8.00	-1.3317	-1.3318	-1.3325	-1.3323
8.25	-1.3541	-1.3543	-1.3549	-1.3546
8.50	-1.3771	-1.3772	-1.3778	-1.3776
8.75	-1.4005	-1.4007	-1.4013	-1.4010
9.00	-1.4245	-1.4246	-1.4252	-1.4251
9.25	-1.4489	-1.4491	-1.4496	-1.4493
9.50	-1.4737	-1.4738	-1.4744	-1.4742
9.75	-1.4988	-1.4990	-1.4995	-1.4992
10.00	-1.5243	-1.5244	-1.5250	-1.5248

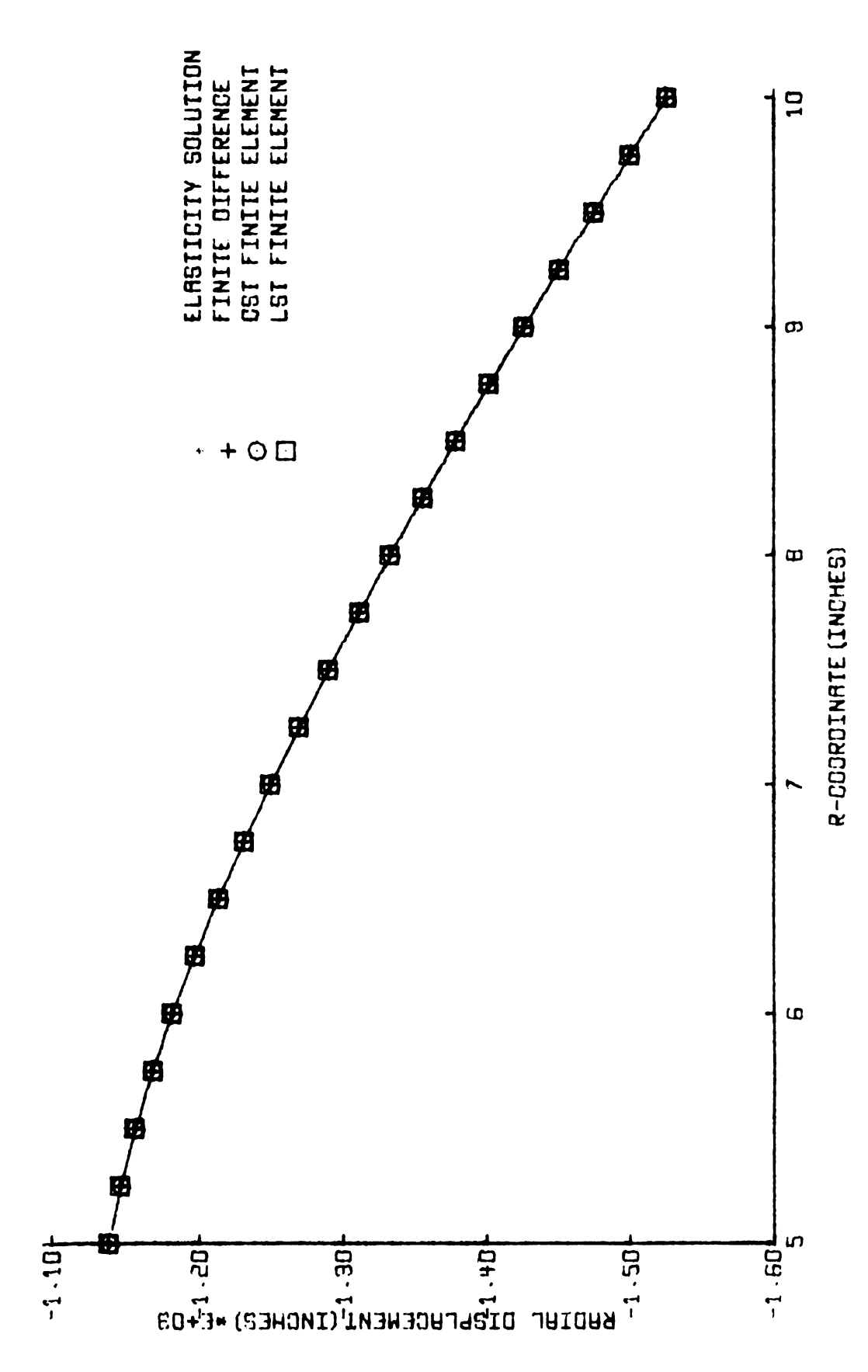


Figure 5.3, Thick Cylinder Radial Displacements

Table .5.2 Thick Cylinder Radial Stress $\boldsymbol{\sigma}_{r}(r,0)$

r-Coord.	Finite Diff.	C.S.T.R.	Elasticity	L.S.T.R.
5.00	- 9392.1	- 9578.4	- 9000.0	- 9040.9
5.25	- 9735.2	- 9738.3	- 9743.7	- 9725.1
5.50	-10379.5	-10375.2	-10388.4	-10410.1
5.75	-10944.9	-10948.9	-10950.8	-10937.3
6.00	-11441.2	-11434.5	-11444.4	-11477.6
6.25	-11878.5	11877.4	-11880.0	-11867.7
6.50	-12265.6	-12259.1	-12266.0	-12275.8
6.75	-12610.3	-12608.6	-12610.4	-12604.0
7.00	-12918.5	-12913.3	-12918.3	-12934.2
7.25	-13195.3	-13194.0	-13195.0	-13187.3
7. 50	-13444.9	-13440.9	-13444.4	-13448.9
7.75	-13670.7	-13669.7	-13670.1	-13667.8
8.00	-13875.6	-13872.6	-13875.0	-13883.0
8.25	-14062.3	-14061.3	-14061.5	-14056.4
8.50	-14232.8	-14230.5	-14231.8	-14234.1
8.75	-14389.1	-14388.1	-14387.7	-14387.7
9.00	-14532.8	-14530.0	-14530.8	-14534.5
9.25	-14665.3	-14663.0	-14662.5	-14658.3
9.50	-14787.7	-14783.4	-14783.9	-14784.1
9.75	-14899.6	-14896.7	-14896.1	-14897.3
10.00	-14952.8	-14925.1	-15000.0	-15071.6

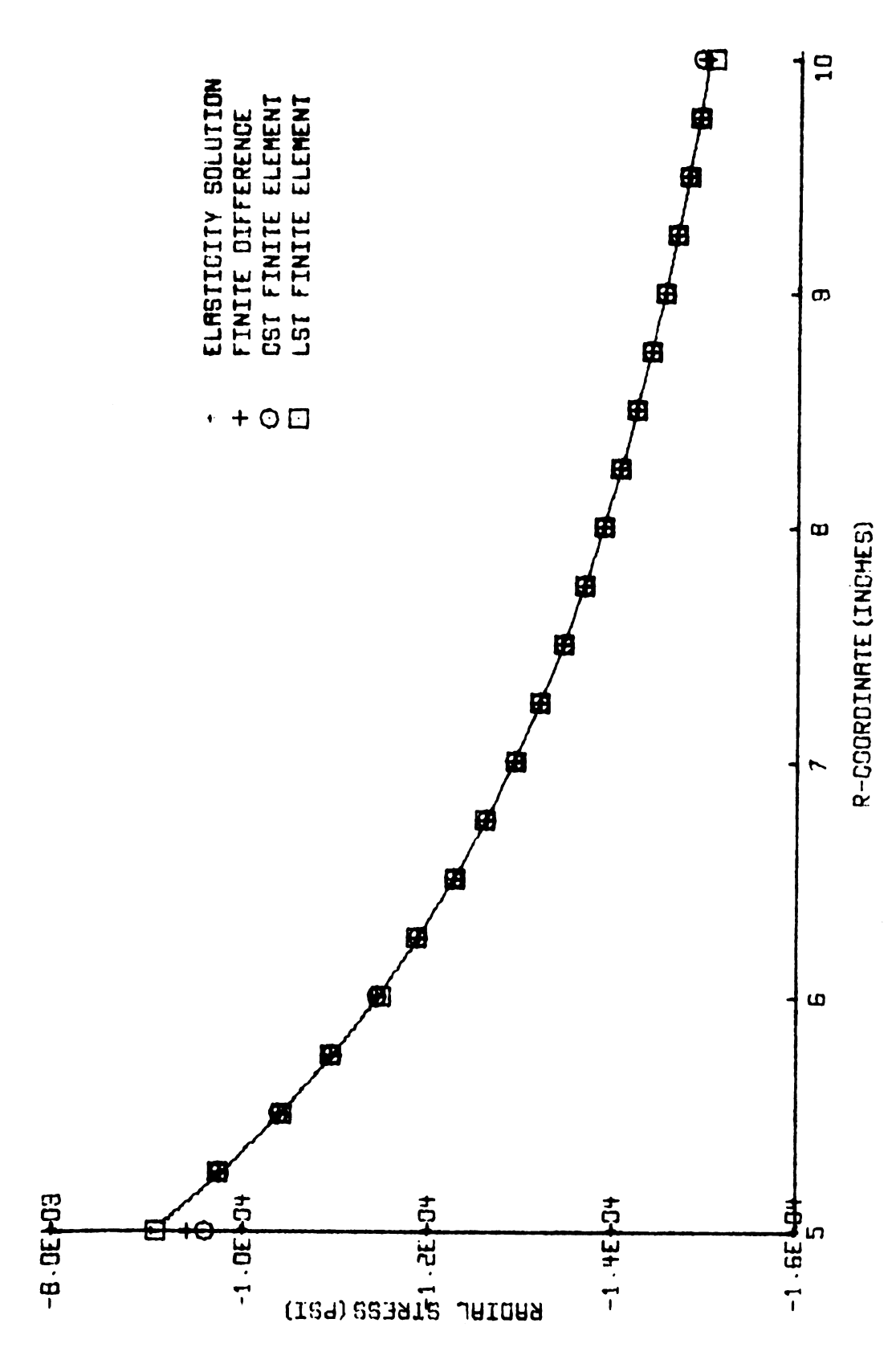


Figure 5.4, Thick Cylinder Radial Stress

The circumferential stresses are also compressive throughout the body. They are considerably higher than the radial stresses and range from 19,000 psi on the outside surface to 25,000 psi on the inside surface. The numerical and exact results are listed in Table 5.3 and plotted in Figure 5.5. Once again, the agreement of the numerical results with the exact theory is excellent. The largest deviation occurs with the FD and CSTR solutions on the inside surface. The errors here are 0.43% and 0.7% for the two solutions respectively. The largest error for the LSTR solution is a mere 0.1% on the outside surface.

Concluding Remarks. In the preceding discussion, axially symmetric finite difference and finite element solutions for a pressurized thick cylinder were compared with the exact solution from the theory of elasticity. Remarkably good results were obtained by each method for both displacements and stresses. The finite element solution employing linearly varying strain triangles gave slightly better results than the other solutions. The differences in this example, however, were generally very insignificant.

5.2 Composite Solid Cylinder

The second axially symmetric problem treated in this work involves a solid cylinder which is subjected to a uniform axial end load. Such a cylinder is displayed in Figure 5.6. In this application, the outer cylinder (matrix) is reinforced with a relatively large concentric cylinder(stiffener) of a much stiffer material. The particular case considered here assumes a 1 inch radius for the outer cylinder and a length of 4 inches. The stiffener has a radius of $\frac{1}{2}$ inch and its length

Table 5.3 $\label{eq:table_final} \mbox{Thick Cylinder Circumferential Stress } \sigma_{\theta}(\mbox{r,0})$

r-Coord.	Finite Diff.	C.S.T.R.	Elasticity	L.S.T.R.
5.00	-25149.7	-25173.9	-25000.0	-25007.2
5.25	-24225.3	-24241.3	-24256.2	-24245.1
5.50	-23586.6	-23589.1	-23611.5	-23614.5
5.75	-23027.5	-23035.1	-23049.1	-23037.0
6.00	-22536.1	-22536.7	-22555.5	-22561.6
6.25	-22102.3	-22107.7	-22120.0	-22112.6
6.50	-21717.4	-21718.1	-21733.7	-21733.4
6.75	-21374.4	-21378.8	-21389.5	-21380.4
7.00	-21067.5	-21068.4	-21081.6	-21083.4
7.25	-20791.7	-20795.4	-20804.9	-20800.3
7.50	-20543.1	-20544.2	-20555.5	-20554.0
7.75	-20318.1	-20321.3	-20329.8	-20322.2
8.00	-20113.9	-20115.0	-20125.0	-20125.0
8.25	-19928.0	-19930.7	-19938.4	-19935.5
8.50	-19758.2	-19759.4	-19768.1	-19766.3
8.75	-19602.8	-19605.2	-19612.2	-19605.3
9.00	-19460.3	-19461.3	-19469.1	-19468.4
9.25	-19329.3	-19331.1	-19337.4	-19335.8
9.50	-19208.9	-19208.9	-19216.0	-19213.9
9.75	-19098.4	-19097.8	-19103.8	-19096.5
10.00	-18975.2	-18968.2	-19000.0	-19019.3

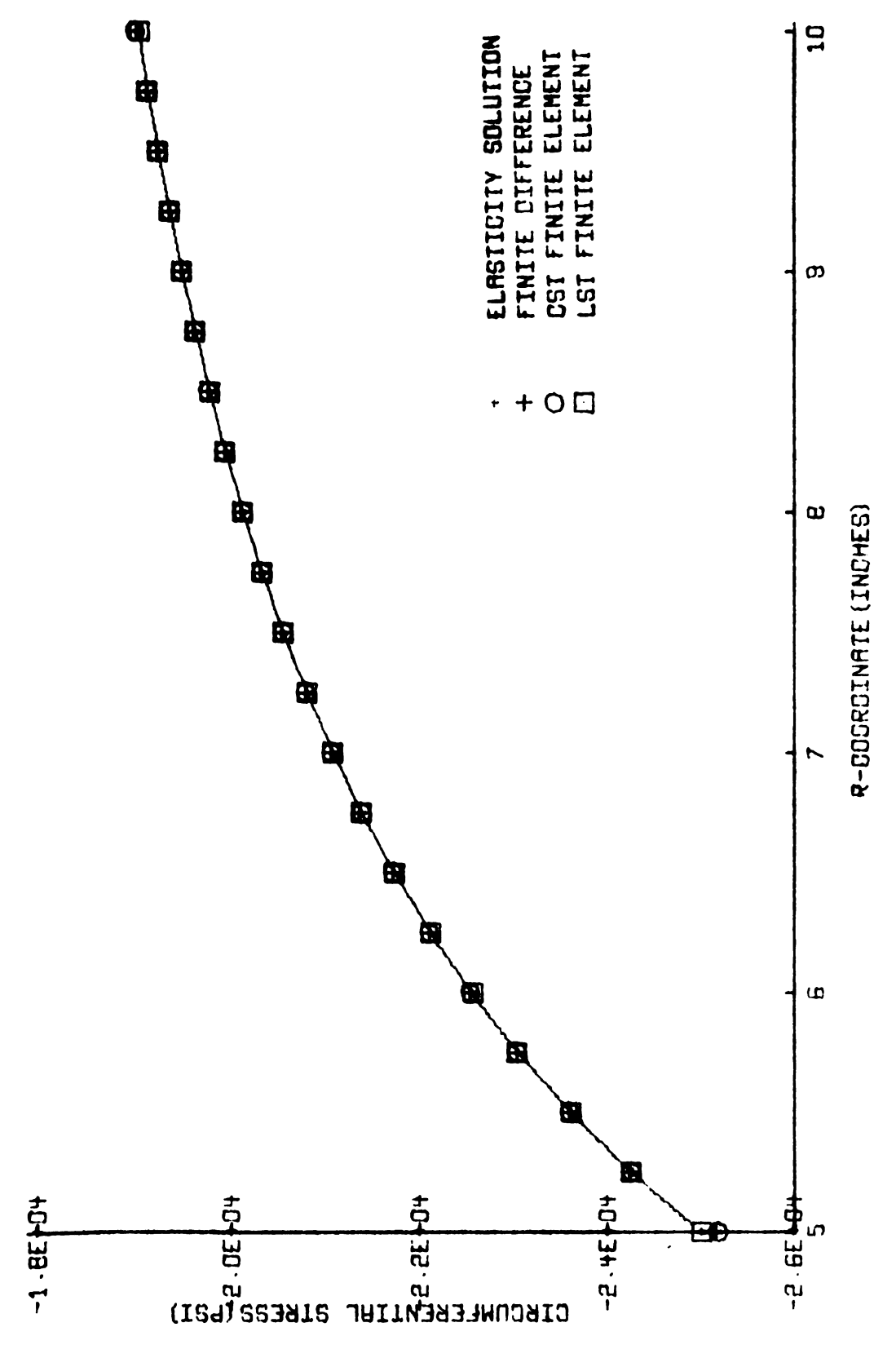


Figure 5.5, Thick Cylinder Circumferential Stress

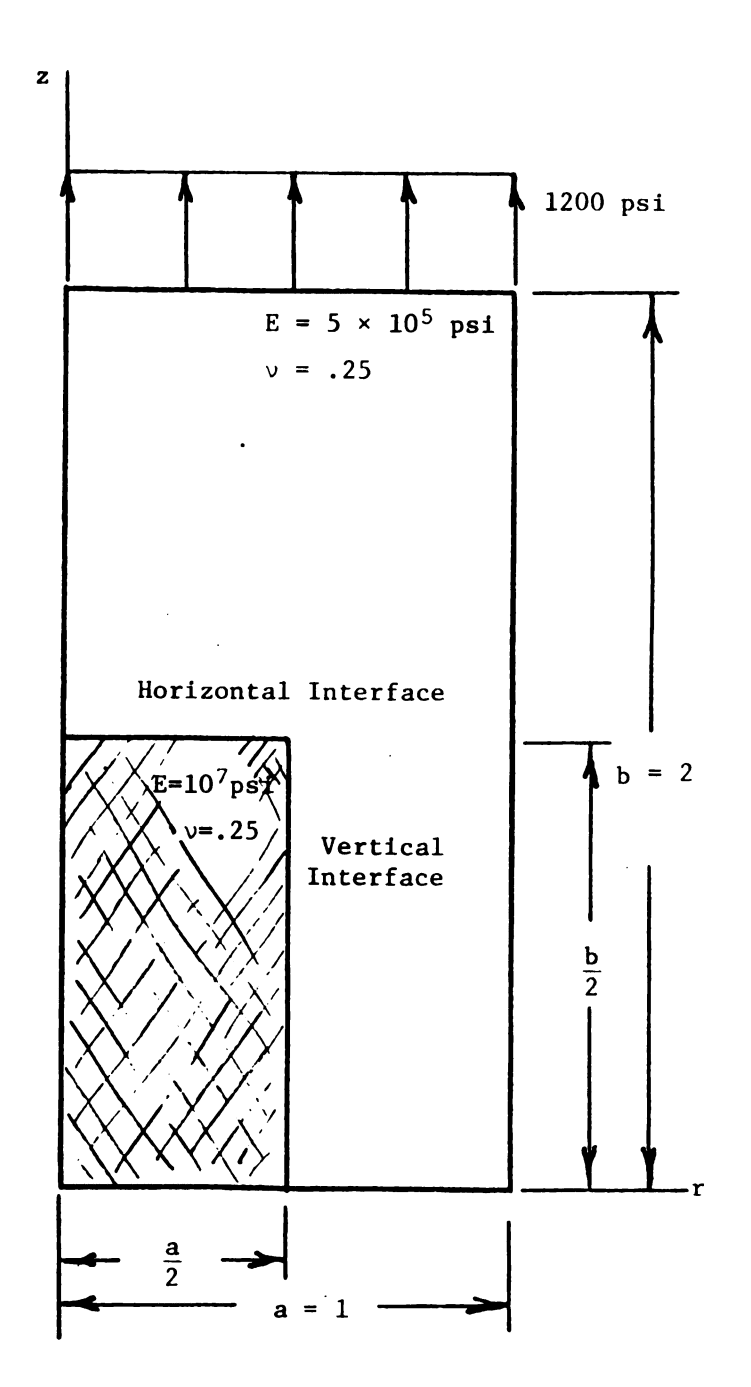


Figure 5.6 Composite Cylinder

is 2 inches. The material properties are $E=5\times 10^6$ psi and $\nu=\frac{1}{4}$ for the matrix and $E=10^7$ psi with $\nu=\frac{1}{4}$ for the stiffener. The magnitude of the applied stress is 1200 psi. The materials are assumed to be perfectly bonded throughout the analysis so that complete displacement continuity is maintained across the material interface.

Referring once again to Figure 5.6, it can be seen that the stiffener does not extend throughout the length of the matrix. For this situation, there is no exact solution available. Accordingly, only approximate solutions are considered here. As was true for earlier applications, both finite difference and finite element solutions are included in the analysis. Convergence of the various solutions is demonstrated using several approximations for each method.

Finite Difference Solution. Four difference solutions were employed in the analysis of the above mentioned problem. The mesh point arrangements used are displayed in Figure 5.7 where $\frac{1}{4}$ of the cylinder cross section is shown. The 4 approximations involve 45, 91, 153, and 231 mesh points. The geometry for each case is identical to that used in the similar plane problem treated in Chapter IV. The difference equations of this analysis utilize nodal circle force intensities (1b/in). The force intensities which correspond to the 1200 psi applied stress are also shown in the figure. The intensity at the symmetry axis is undefined since at this location r = 0. For the purpose of numerical calculations, it is reasonable to use a small finite value of r, say r = .001. The particular equations programmed in this work involve a numerical factor of 5 on the right hand sides. Therefore in preparing data, the intensities of Figure 5.7 must be multiplied by 5.

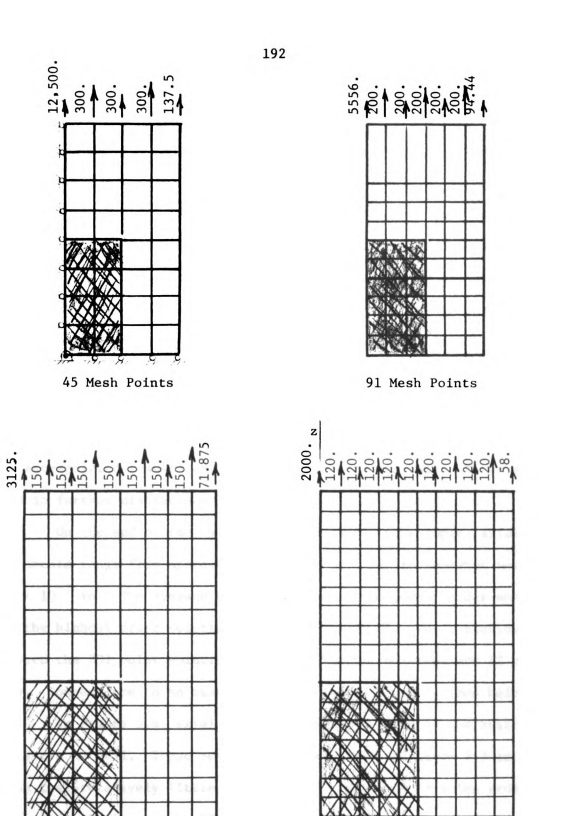


Figure 5.7

153 Mesh Points

231 Mesh Points

The character of the FD solution is demonstrated in Figures 5.8 and 5.9. These illustrations pertain to axial displacements which occur at the cylinder end and along the horizontal material interface. Additional displacement results are presented in Appendix A, beginning on page 247. In Figures A1 and A2 radial displacements for these regions are plotted. In Figures A3 and A4, axial and radial displacements are presented for selected points. Referring to Figure A3, page 249 it should be observed that the axial displacements at r = 0 on the cylinder end seem unrealistic. These are greater than displacements for the point immediately to the right. This discrepancy is believed to be the result of the sigularity at the symmetry axis. Extrapolation from the interior results in a more realistic symmetry axis displacement. The extrapolated results are shown in Figure A3 as well. These are used in further displacement discussions.

On the end of the cylinder, Figure 5.8, for example, axial displacements range from approximately 3.0×10^{-3} in. to somewhat more than 3.4×10^{-3} in. The average deviation between the lowest order solution and the highest order solution is approximately 6%. The variations between the 231 point solution and the 153 point solution are 1% and less. Convergence to an exact solution evidently occurs from below.

In Figure 5.9, axial displacements for points in the stiffener are shown as well. These results are comparable to Figure 5.8 in the sense that relatively little improvement is realized in going from the 153 point solution to the 231 point solution. Noticeable deviations occur, however, with regard to the lower order solutions, especially for the 45 point solution. The tendency for displacements to be under estimated in the matrix and over estimated in the stiffener is

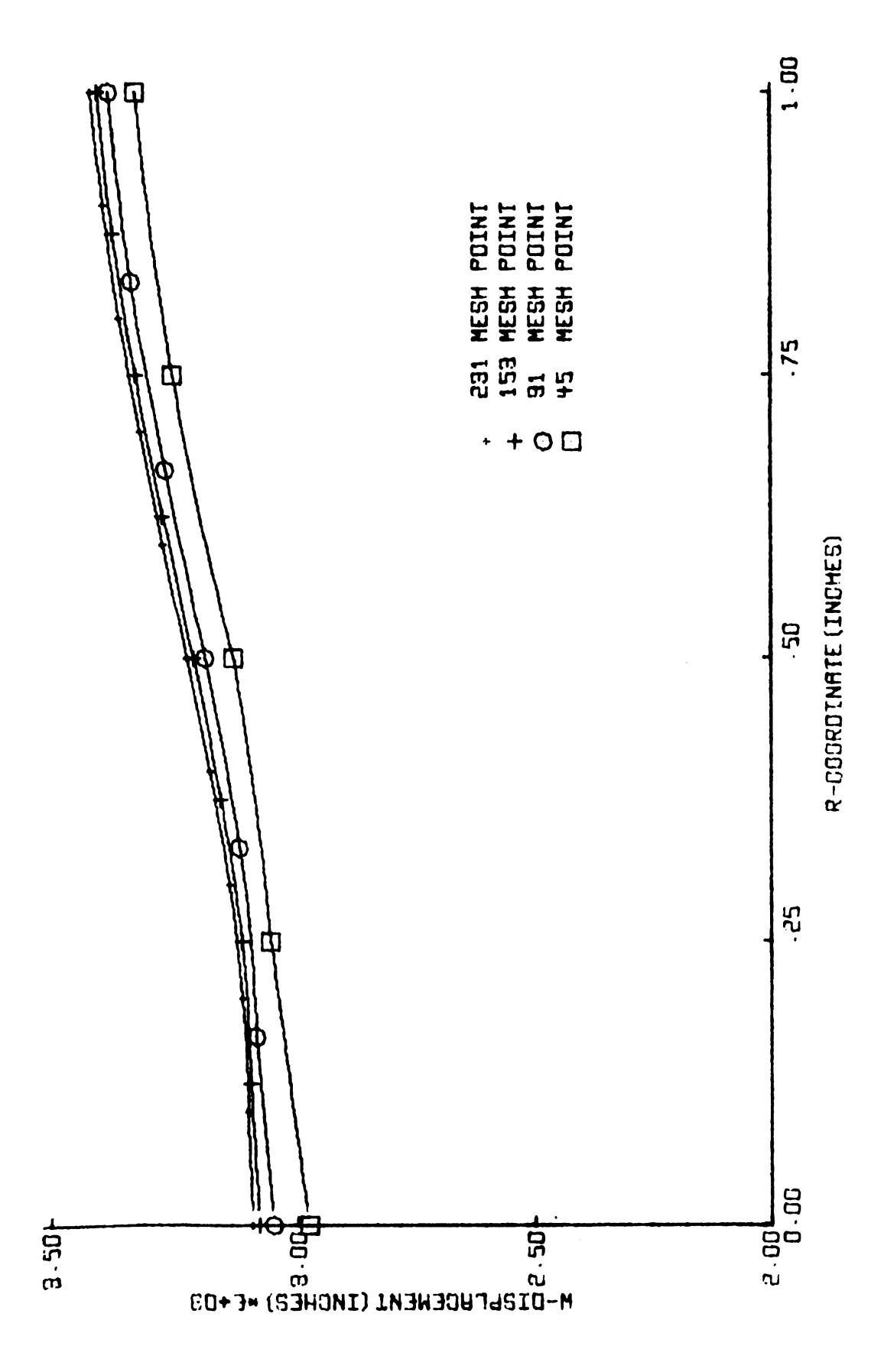


Figure 5.8, FD Cylinder End Axial Displacements

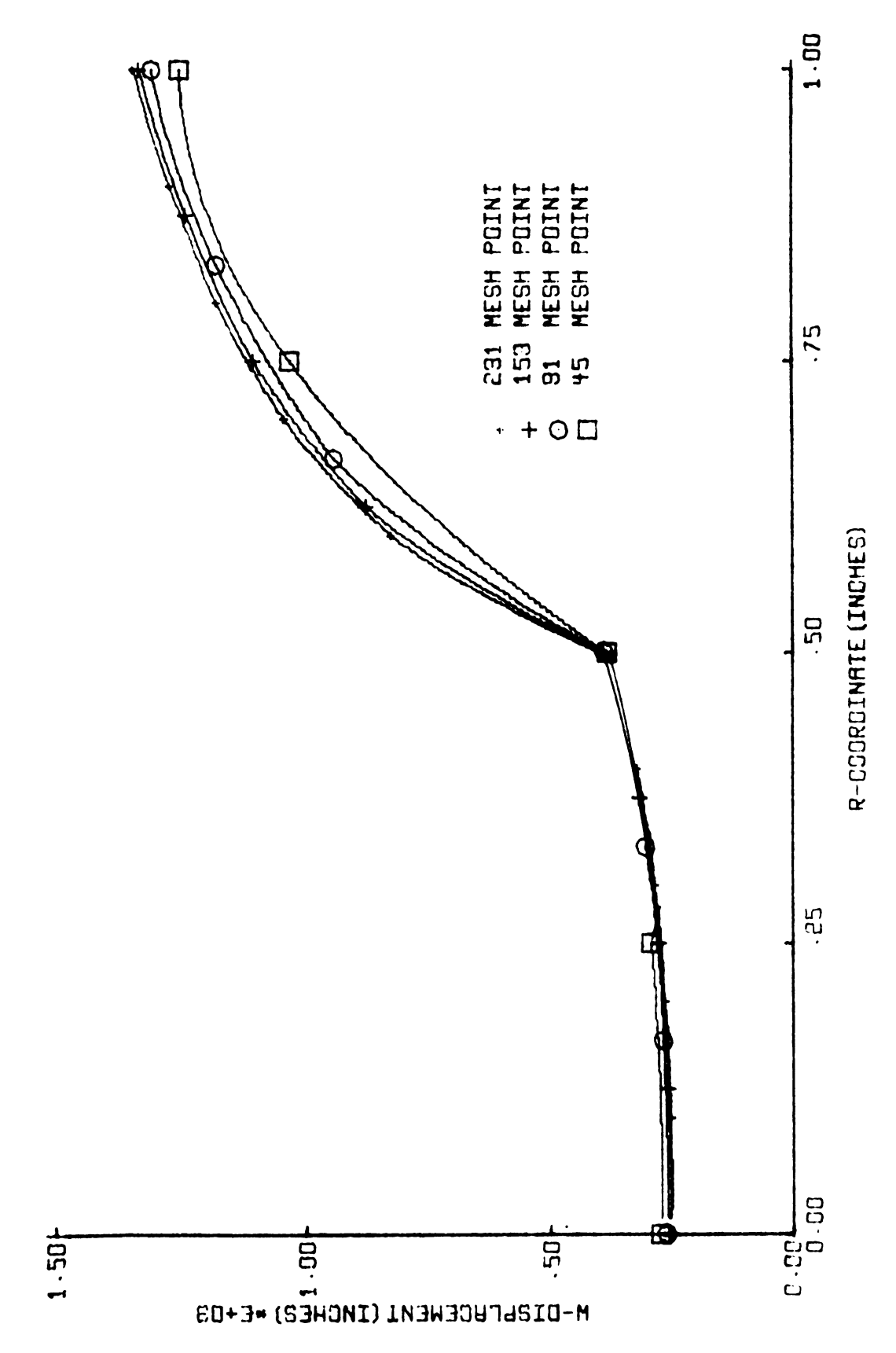


Figure 5.9, FD Horizontal Interface Axial Displacements

apparent from Figure 5.9.

It is of interest to consider the effect of extrapolation on certain of these results. To this end, the Richardson Formula [40] is applied.

$$I = I_2 + \frac{m_1^2}{m_2^2 - m_1^2} (I_2 - I_1)$$

In the above formula, I_1 and I_2 are approximations to some function corresponding to nodal point systems whose numbers are m_1 and m_2 . I is the extrapolated value of the function.

The result of applying this formula to selected FD displacements is shown in Figure 5.10, page 197. Both axial and radial displacements are shown. It is evident that the extrapolated results generally represent some improvement. In fact extrapolating between the 91 and 153 point solutions gives displacements which are a slight improvement over results derived from the 231 point solution. A peculiar situation occurs at the upper right hand corner point of Figure 5.10. The radial displacement apparently increases when the number of mesh points is increased. The extrapolations, however, appear to decrease.

The stress distribution for the highest order FD solution (231 mesh points) is presented in Figure 5.11. The stresses shown were obtained by averaging the stresses for the material regions around the mesh point. At each point, the stresses are listed vertically in the order $\sigma_{\bf r}$, $\sigma_{\bf z}$, σ_{θ} , and $\tau_{\bf rz}$. Two sets of stresses are given for the mesh points on the material interface. Those to the right and above the interface were computed from the matrix stresses. Those to the left and below the interface were obtained from stresses in the

y	7	v	_	v	
2.9778(45)	0.0751(7)	3.1360(45)	2 0127/7)	3.3417(45)	2 /1// (7)
3.0513(91)	3.0751(E)	3.1947(91)	3.2137(E)	3.3983(91)	3.4166(E)
3.0811(153)	3.0974(E)	3.2207(153)	3.2349(E)	3.4237(153)	3.4376(E)
	3.1071(E)	3.2345(231)	3.2453(E)	3.4374(231)	3.4481(E)
3.0957(231)			1	3.43/4(231)	u
		4372(45)	-	7451(45)	
		4477(91)	4511(E)	7503(91)	7520(E)
		•	4537(E)		7515(E)
		4516(153)	4548(E)	7511(153)	7511(E)
		4534(231)		7511(231)	
v			,		v
.2654(45)	.2570(E)	.3834(45)	.3886(E)	1.2591(45)	1.3347(E)
.2573(91)		.3873(91)		1.3162(91)	
.2530(153)	.2525(E)	.3909(153)	.3929(E)	1.3410(153)	1.3546(E)
.2510(231)	.2493(E)	.3937(231)	.3977(E)	1.3540(231)	1.3723(E)
(231)			u		u
		0874(45)	1006(E)	3649(45)	3960(E)
		0974(91)	1075(E)	3884(91)	4067(E)
		1039(153)		4002(153)	
		1082(231)	1143(E)	4068(231)	4161(E)
		, , , , , , , , , , , , , , , , , , , ,		, , , , , , , , , , , , , , , , , , , ,	
			(45) - 45 Po	oints	
			(91) - 91 Po	oints	
			(153) - 153 (231) - 231		
			(E) - Extra		
			L		J

Figure 5.10 Extrapolated FD Displacements

263	-277	-245	-208	-165	-118	-70	-30	1196 1 -103	6	5
315 21	1202 -285 17	1207 -263 21	1207 -241 24	1205 -215 30	1203 -187 30	1201 -157 29	1196 -128 24	1196 -103 15	1194	1194 -77 -3
-168 1101 341	-188 1218 -190	-175 1220	-152 1218	-124	-94 1209	-63 1202	-37	-17	-5	1190
341	-190 21	1220 -182 32	1218 -171 41	1214 -156 48	1209 -139 52	1202 -122 50	1196 -103 42	1190 -90 29	1186 -77 12	7
-118 1157 360	-138 1260 -139	-130 1255 -135	-116 1249 -129	-97 1239 -120	-75 1224 -110	-53 1207 -100	-32 1190 -89	-16 1175 -79	-5 1166 -69	1174
360 20	-139 29	-135 49	-129 67	-120 80	-110 87	84	-89 72	-79 52	-69 27	-58 13
-82 1220 381	-103 1315 -103	-98 1305 -101	-89 1293	-75 1275 -95	-58 1248	-40 1215 -85 112	-23 1183	-10 1157 -73	-3 1139 -66	1139
20	33	60	1293 -99 84	103	1248 -90 114		1183 -79 97	72	40	-58 21
-51 1288 404 21	-72 1379 -73	-70 1365 -73	7-66 1349 -73	-56 1321 -73	-42 1279 -74	-25 1225 -74	-11 1175	1135 -70	1106 -66	1091
	35	66	96	122	137	136	118	88	50	-62 27
-17 1357 4 27 21	-39 1445 -39	1431 -41	1413 -44	-38 1379 -49	-25 1321 -35	-8 1237 -63	1165 -66 137	1109	1066 -67	1034
21	35	67	102	135	160	161		100	55	-68 30
442	1506 6 30	1497	1485	1451 -16 141	1379 -29	1248	23 1147 -57	1077	1023	974 -71 30
20	30 65	60	98	141	182	188	153	106	56	
468 17	1553	1555	1558	1541 36 133	1465	1251	1117	1036	979	920 -68 24
17	20	132	78	133	204	218	165	104	50	24
481 11	1575	1591	1621	1646	1609	1232	1067	987	937	- 882 -53 14
274	5 260	13	38	97	218 95	255 84	167 75	91	36 17	1 7
503 489 4	1566 265 -9	1593 262 -18	1648 256 -17	1739 241 15	1871 247 196	1162 30 288	995	933 -6 68	900 -15 19	866
388	387 1555	401	427		34	288	151		19	1
506 506	386	1585 399	1650 422	485 1776 471	1399 265. 360	-146	-55 904	-20 974	-6 947	1 -2
-2 1319 1325 161	-18 -2451 1555 -2468	-35 -2477 1565 -2467	-55 -2445 1724 -2447	-69 -2103 -1 2265 4 -2271 -1	803 831 401	939 23 406	896 19 165	876 16 65	867 14 13	-2 868 12 -3
15	-64	-56	19	365	706					
1112 1332 385	-1147 1556 -1189	-1021 1613 -1100	-782 1852 -935	2514 4	335 - 163 802 140 -70 -80	-152 673	-109 777 40	-57 809	-22 830 43	865 49 5
68	10	58	184	475	633 596	412	204	90	27	
-373 1465 465	-383 1673 -406	-289 1810 -331	-153 2168 -197	-58 2928 4	-34 -66 600 175 441 -23	-79 525	-80 668	-52 738 64	-23 785 67	-10 842 75
109	118	251	101	659	748 471	376	-42	-34	-17	
766	1951	2135	2522	3184 4	267 187 503 5	443	583	670	733 82	-8 799 90 25
117	176	344 225	518	628	641 387	324	214	123	-10	١.,
122 691 104	2291	2477 268 343	2819 308 476	3323 3 362	1998 192 471 20 503 315	395 71 271	523 81 191	614 85 119	681	744 94 28
340	183	274	223	157	123 60	39	7	-5	-5	-3 688
794 83	2615 320 159	2773 327 292	3044 341 387	3401 3 359 403	820 195 398 26 380 253	365 73 221	83 IA2	568 87 106	633 89 54	688 92 27
352	313	276	222	161	131 73	52	19	2	-2	
723 878 61	2883 327 124	3004 326 224	3206 327 290	3451 3 326 296	719 134 337 29 270 196	347 73 173	452 82 130	532 86 87	592 88 46	637 86 23
338	296	261	212	159	133 80	59	25	7	0	1
922 939 42	3084 309 88	3172 304 158	3318 298 202	3487 3 290 205	667 198 288 30 193 144	335 72 128	80 97	506 83 67	560 83 35	595 80 18
319	275	245	201	155	122 02	61	28	9		1
979 26	3219 286 55	3283 280 99	3391 272 126	3512 3 260 128	646 198 253 29 89 94	328 70 84	418 77 65	80 45	536 79 24	565 75 12
304 132 003	260	232	194	152	131 83	62	29	10	1	١,
A88	3297 270 27	263	3432 254 60	3528 3 242 61	638 199 233 29 59 47	324 69 42	410 76 32	176 178 22	521 76 12	547
12	27	48	00	01	37 4/					

Figure 5.11, Finite Difference Stress Distribution

stiffener.

In analyzing the data of Figure 5.11, the rather large axial stress in the stiffener is a significant feature. The axial stress is seen to exceed 4800 psi and thus indicates a stress concentration factor of more than 4. Axial stress in the matrix is as high as 1871 psi or more than 50% higher than the applied stress. The presence of the rather rigid inclusion gives rise to large radial and circumferential stresses in the stiffener. These are compressive stresses near the interface which exceed 2400 psi. The corresponding stresses in the matrix are 500 psi tension and less. The shear stresses are greatest in the stiffener and do not appear to exceed 800 psi.

As was true for the similar plane problem of Chapter IV, the stresses are undefined at the corner of the stiffener and the matrix. Obviously, neither the difference method nor the finite element method is able to predict such stresses. In view of this, it is instructive to examine in greater detail the corner stresses which were used to obtain the nodal point stresses of Figure 5.11. These stresses are shown below in Figure 5.12

in the order σ_r , σ_z , σ_θ , and τ_{rz} . It is significant that the low axial stress in the lower right region results in the smaller average for the three unshaded regions. The axial stresses in particular are large compared to the applied stress (1200 psi) but are certainly finite.

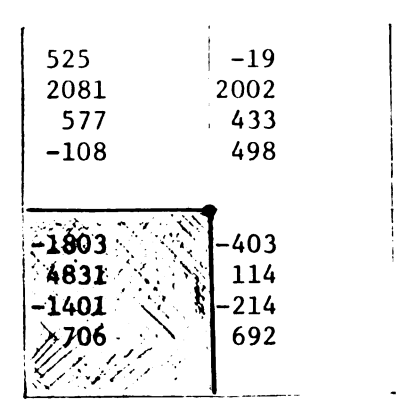


Figure 5.12
FD Corner Stresses

Referring once again to Figure 5.11, two other points are significant. First of all, the stress components for points on the symmetry axis are generally quite unrealistic. The lack of agreement between radial and circumferential stresses is an apparent discrepancy. Much better results are obtained using a quadratic extrapolation from the interior. The second point relates to interfacial stresses. From equilibrium considerations certain of these, as indicated in Chapter IV, should be continuous across the interface. Thus in this case, $\sigma_{\rm z}$ and $\tau_{\rm rz}$ should be continuous across the horizontal interface whereas $\sigma_{\rm r}$ and $\tau_{\rm rz}$ should be continuous across the vertical interface. This is apparently not the case. The discrepancies are greatest near the corner.

CSTR Solution. Three CSTR finite element solutions used in this analysis are shown in Figure 5.13. These include a 32 element layout with 25 nodal points, a 128 element layout with 81 nodal points, and a 288 element layout with 169 nodal points. The nodal circle force intensities associated with a uniform axial stress of 1200 psi are shown for each case. These have been multiplied by appropriate radii.

Typical displacement curves for the CSTR solutions are plotted in Figures 5.14 and 5.15. The end displacements are shown in Figure 5.14. These displacements range from 3.06×10^{-3} in. to 3.43×10^{-3} in. for the highest order solution. The lower order displacements are consistently less than these. There is not an appreciable difference between the 81 and 169 point solutions indicating reasonably good convergence of displacements.

The axial displacement variation along the horizontal interface is shown in Figure 5.15. The trend in these curves is much the

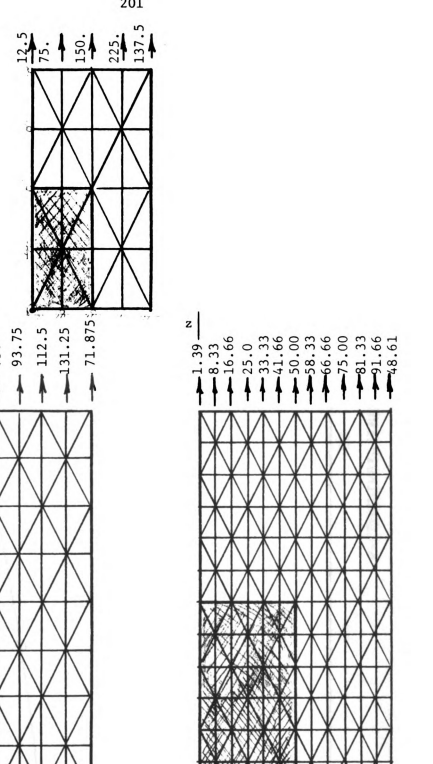


Figure 5.13 Composite Cylinder - CSTR Configurations

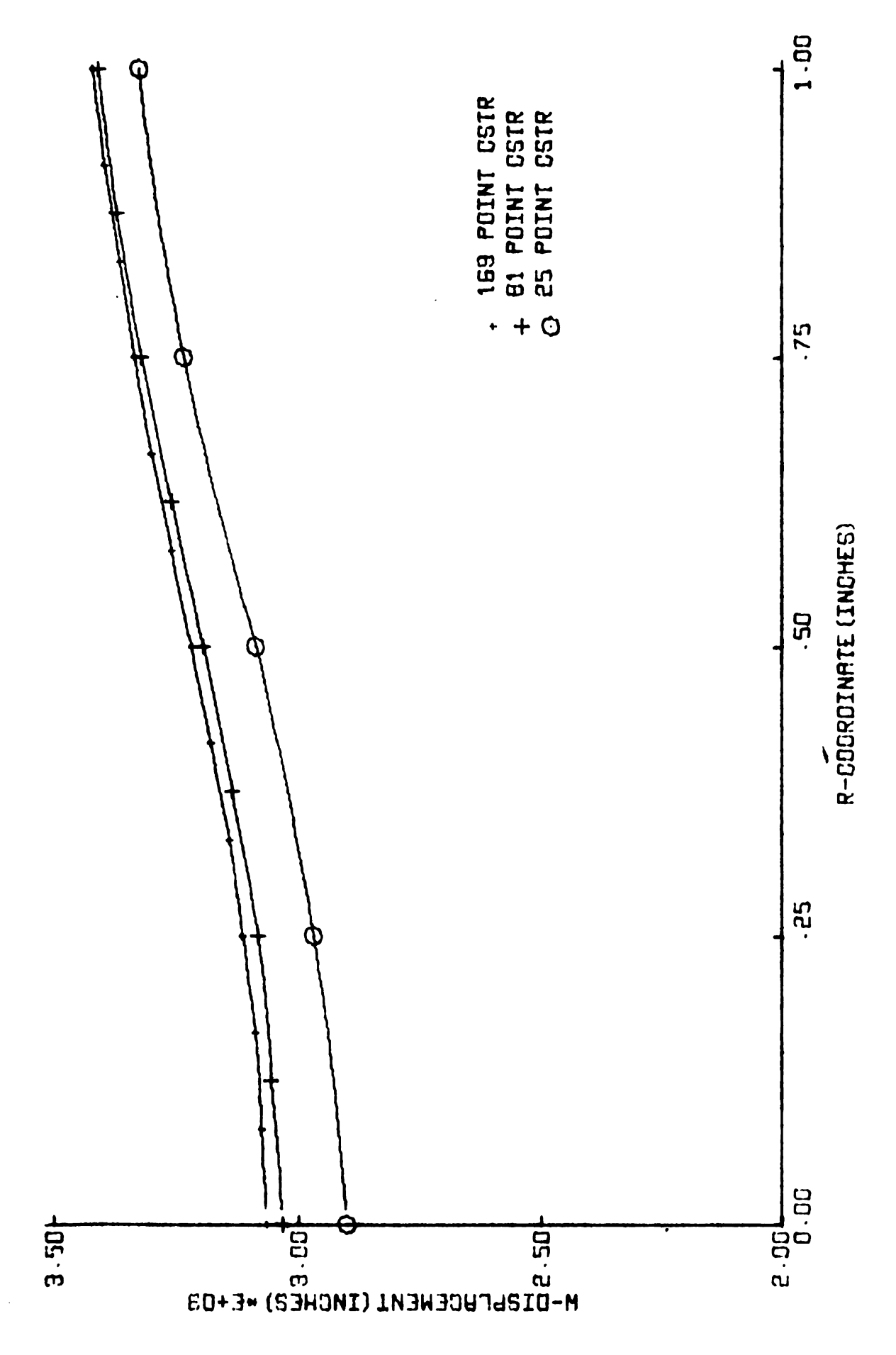


Figure 5.14, CSTR Cylinder End Axial Displacements

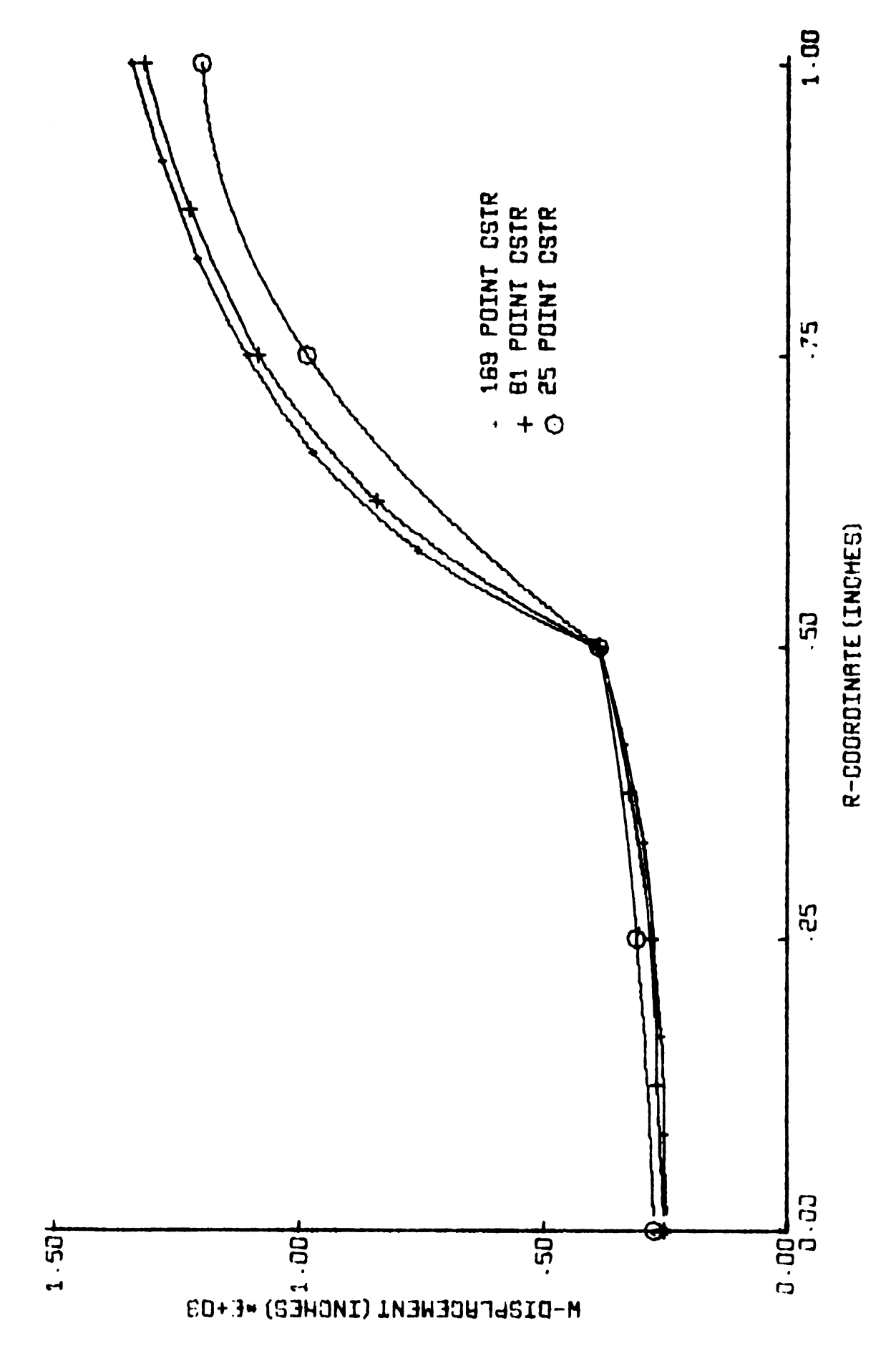


Figure 5.15, CSTR Horizontal Interface Axial Displacements

same as in Figure 5.14. The tendency for displacements to be overestimated in the stiffener is apparent.

Additional displacement results are presented in Appendix A.

Radial displacements are plotted in Figures A5 and A6 for points on the end horizontal interface respectively. In Figures A7 and A8, displacements for various points are listed on cross sectional diagrams. Of particular interest are certain radial end displacements which are apparently underestimated by the method.

Extrapolated displacements corresponding to selected points are listed in Figure 5.16, page 205. Both axial and radial displacements are shown. In the case of the maximum axial displacement for example, the best extrapolated result is a .16% improvement over the 169 point approximation. As was true for the FD results, extrapolation between the two lower order solutions gives results which are comparable to the 169 point solution.

The stress distribution for the 169 nodal point CSTR solution is displayed in Figure 5.16. The stresses are listed in the order $\sigma_{\mathbf{r}}$, $\sigma_{\mathbf{z}}$, $\sigma_{\mathbf{0}}$, and $\tau_{\mathbf{rz}}$ for each point. These are nodal point stresses obtained by averaging appropriate element stresses. As was explained in the earlier FD solution, two sets of stresses are shown along the material interface, one set corresponding to the matrix and the other to the stiffener.

The overall situation is quite similar to the FD solution.

Axial stresses in the stiffener as large as 4547 psi are observed. Compressive radial and circumferential stresses exceed 2600 psi along the horizontal material interface. The maximum observed shear stress is 896 psi.

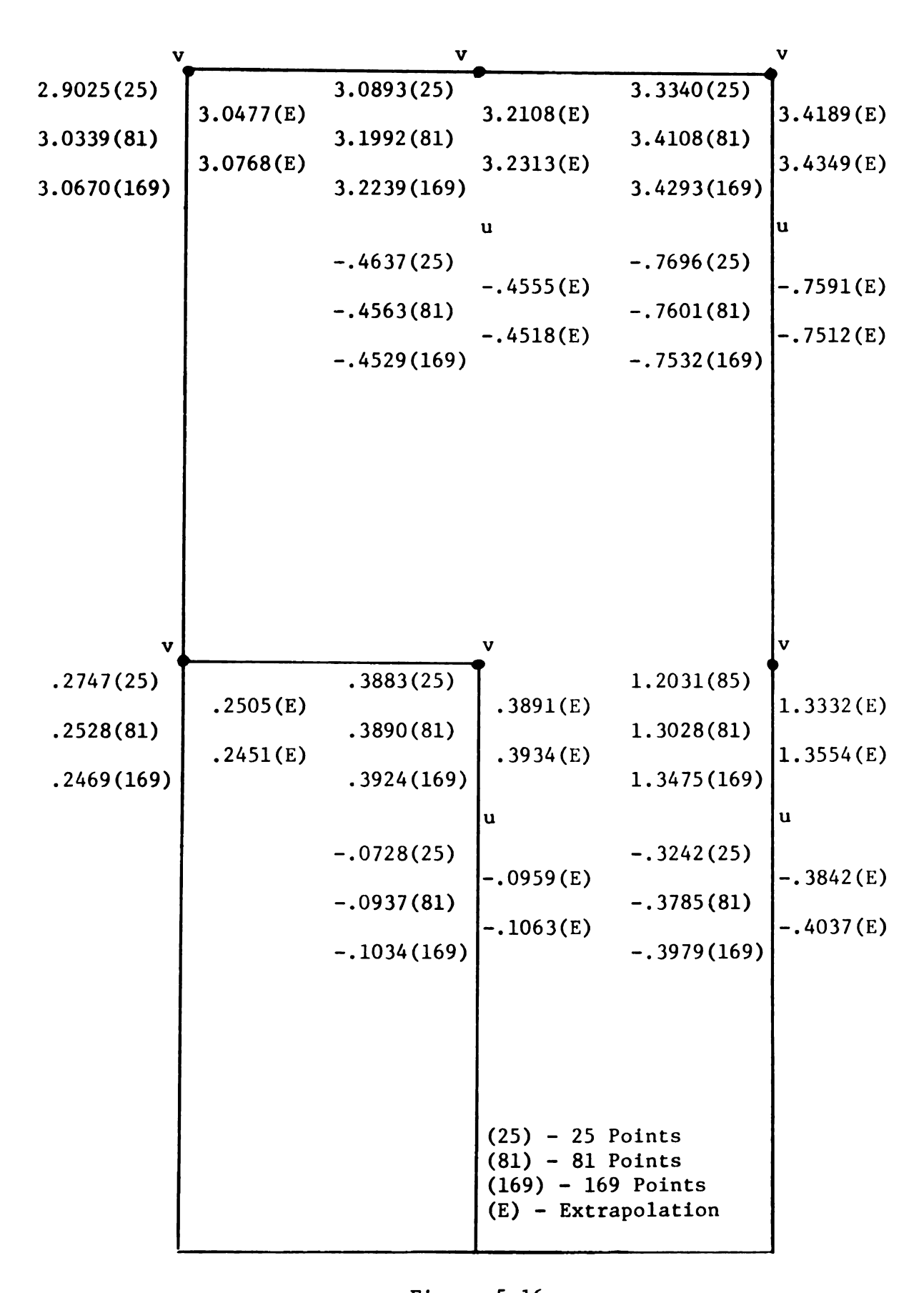


Figure 5.16
CSTR Extrapolated Displacements

38	330 258 471	379 920 190 60	381 579 466 117	73 86 54 54	132 113 248 -16	196 137 137 125 121 177 26	212 565 267 -9	100 350 174 8	4 174 90 19	-51 381 40 15	103 306 -8 11	-167 1266 -83 11
77	286 3277 34 47	317 2985 318 92	306 2602 348 148	179 2069 177 156	-791 1739 -583 50	378 1584 376 -12 -2616 1164 -2654 -16	196 1550 191 -1	44 1513 45 18	-32 1432 -36 27	-91 1335 -91 28	-163 1256 -152 19	- 270 1197 -273 11
73	240 3772 267 73	300 3062 337 169	309 2690 332 253	69 2238 194 286	-479 1834 -506 137	310 1604 367 -18 -1752 1305 -2352 -27	179 1559 184 2	54 1520 49 32	-40 1431 -38 53	-91 1331 -92 51	-143 1256 -146 34	-213 1201 -253 21
103	230 3354 275 103	254 3193 314 212	268 2916 372 367	194 2437 779 425	-643 2067 -458 216	409 1649 404 -40 -2351 1414 -2444 73	188 1593 192	25 1526 38 60	-37 1421 -41 -79	-85 1324 -90 74	-141 1250 -145 46	-219 1201 -344 27
106	174 3441 251 106	210 3354 325 255	213 3158 354 401	145 2903 335 558	-179 2431 -264 398	319 1709 399 -26 -1491 1845 -2078 157	137 1614 172 30	27 1521 32 87	-43 1408 -45 110	-81 1307 -91 96	-118 1244 -135 40	-168 1201 -221 30
108 9	143 10 3527 360 245 22 108 9	157 10: 3517 357 305 277 223 224	170 54 3488 378 394 36 426 35	171 9: 3404 379: 382 47: 551 647	-340 -27: 3349 454; -25 171 606 64;	481 1828 468 -51 -1750 -956 2481 3526 -2001 -1422 896 703	165 1672 183 56	-9 1509 15 142	-43 1366 -55 142	-66 1286 -86 110	-103 1234 -129 70	-152 1199 -204 39
*	95 210 41 79	80 266 34 164	78 214 43 255	14 309 54 370	(-1	l	35 1682 134 202	-12 1403 -19 204	-25 1316 -55 157	-54 1256 -86 122	-80 1222 -117 72	-108 1196 -181 44
73	70 306 88 73	70 321 67 147	41 339 71 232	6 398 52 317	-95 409 47 427	-151 921 43 517	16 1306 14 288	29 1268 -29 203	-8 1248 -63 164	-37 1724 -41 117	-57 1209 -107 72	-79 1193 -159 39
38	33 385 72 38	29 402 77 120	10 444 77 179	-38 513 71 240	-112 671 55 266	-37 905 41 212	104 1092 4 178	46 1166 -42 180	3 1184 -63 142	-21 1191 -78 110	-41 1195 -78 43	-50 1187 -137 39
44 74	10	14 478 81 90	524 64 133	-31 614 80 162	-52 731 65 149	-40 874 22 121	37 1004 -25 109	40 1076 -51 129	12 1133 -63 120	-11 1161 -74 89	-18 1162 -87 -51	-34 1183 -120 22
499 77 31	3 499	530 83 63	592 87 86	-22 672 84 97	-43 772 61 83	971 23 47	43 955 -24 58	24 1027 -57 83	9 1088 -66 82	-1 1139 -69 68	-10 1166 -79 36	-13 1174 -108 -20
130 78 17	-2 530	-2 576 83 31	-5 640 89 45	-10 724 87 47	-10 808 68 78	-7 865 18 14	7 914 -37 18	11 961 -61 -42	5 1056 -67 -48	1 1121 -65 36	2 1171 -67 21	118] 11
",	-5 552 72	-5 588 76 18	-6 678 87 23	-2 748 85 23	-13 839 66 14	0 867 18 -6	13 883 -37 8	958 -63 22	7 1029 -65 25	1120 -57 23	-2 1175 -60 10	

Figure 5.17, CSTR Stress Distribution

The symmetry axis stresses, though more reasonable than the FD stresses, are also apparently incorrect. The radial and circumferential stresses should be the same here but are not. The CSTR solution like the FD solution exhibits discrepancies with regard to certain stress components which should be continuous across the material interface. These discrepancies are more pronounced at the corner.

The element stresses which were averaged to obtain the corner nodal point stresses are shown in Figure 5.18. The shaded region is part of the stiffener and the unshaded region is the matrix. The element stresses corresponding to the two materials are averaged to obtain the nodal point stresses of Figure 5.17. These averages are considerably smaller than the maximum element stresses. In view of larger stress predicted to the left and below the corner, the average stresses for the corner in Figure 5.17 seem quite unrealistic.

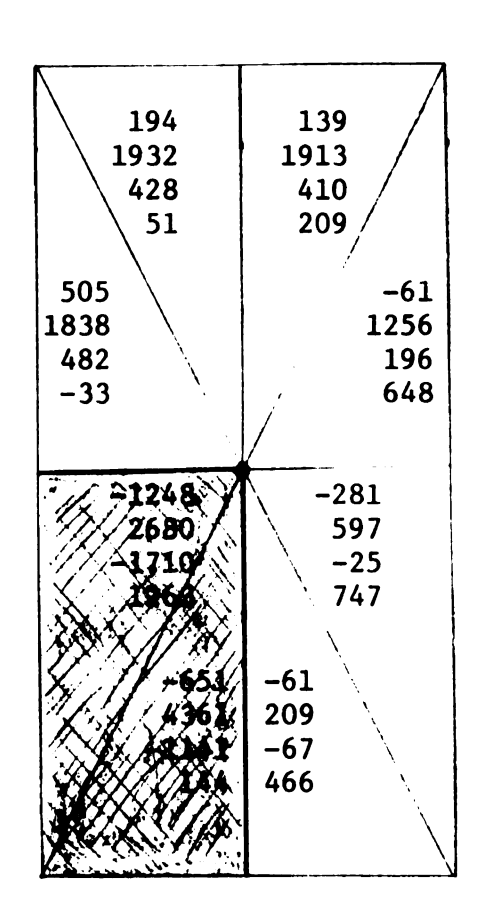
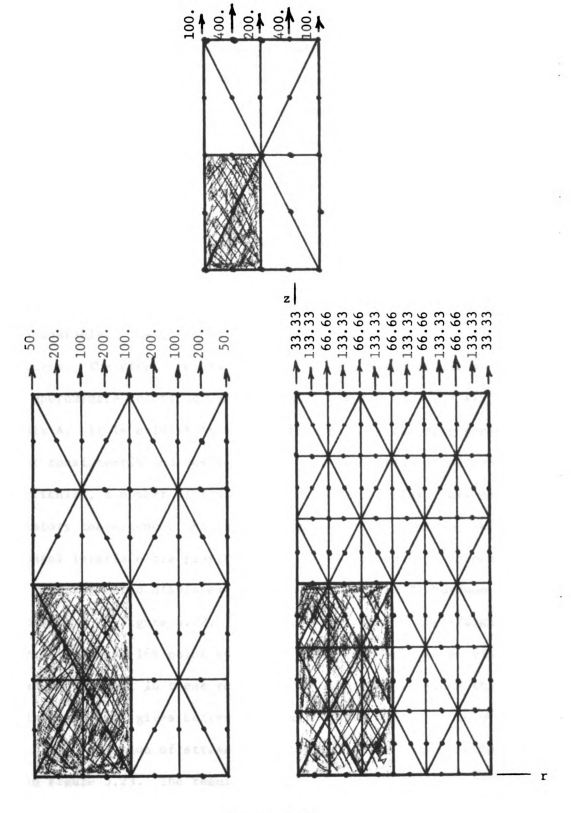


Figure 5.18
CSTR Corner Stresses

LSTR Solution. The finite element analysis with LSTR elements employed the three configurations of Figure 5.19. Involved are 25, 81, and 169 nodal point systems comparable to those used in the CSTR solutions. The 25 point layout utilizes 8 elements, the 81 point



 $\label{eq:Figure 5.19}$ Composite Cylinder - LSTR Configurations

layout 32, and the 169 point layout 72. The axial nodal circle force intensities are shown for each case. They must be multiplied by corresponding nodal circle radii for use in the equilibrium equations.

The variation of axial displacements for the cylinder end is shown in Figure 5.20. In the illustration, the displacements range from 3.1×10^{-3} in. at the symmetry axis to 3.47×10^{-3} in. at the cylinder periphery. As was true for the previous FD and CSTR solutions, convergence to the exact solutions apparently occurs from below.

Horizontal interface axial displacements are plotted in Figure 5.21. In this figure, the 81 and 169 point solutions are seen to be very comparable. The 25 point solution is significantly different from the others. The displacements of selected points, as predicted by the three approximate solutions, are listed in Figures A9 and A10 in Appendix A. It is evident from these figures that all displacements are not consistently underestimated or over estimated by the procedure. In particular, a number of radial displacements display somewhat of an oscillatory convergence. Radial displacements for points on the end and horizontal interface are plotted in Figures A11 and A12 respectively.

Extrapolated displacements obtained from the Richardson Formula are presented in Figure 5.22. Although these are not significantly different from the 169 point solutions, they evidently do provide a further improvement in these results. Extrapolation between the 25 and 81 point solutions gives better results than the 169 point solution.

The variation of stresses for the 169 point LSTR solution is seen in Figure 5.23. The results presented are nodal point stresses which were obtained by averaging element stresses. The axial stress in the stiffener exceeds 5000 psi. Compressive radial stresses in excess

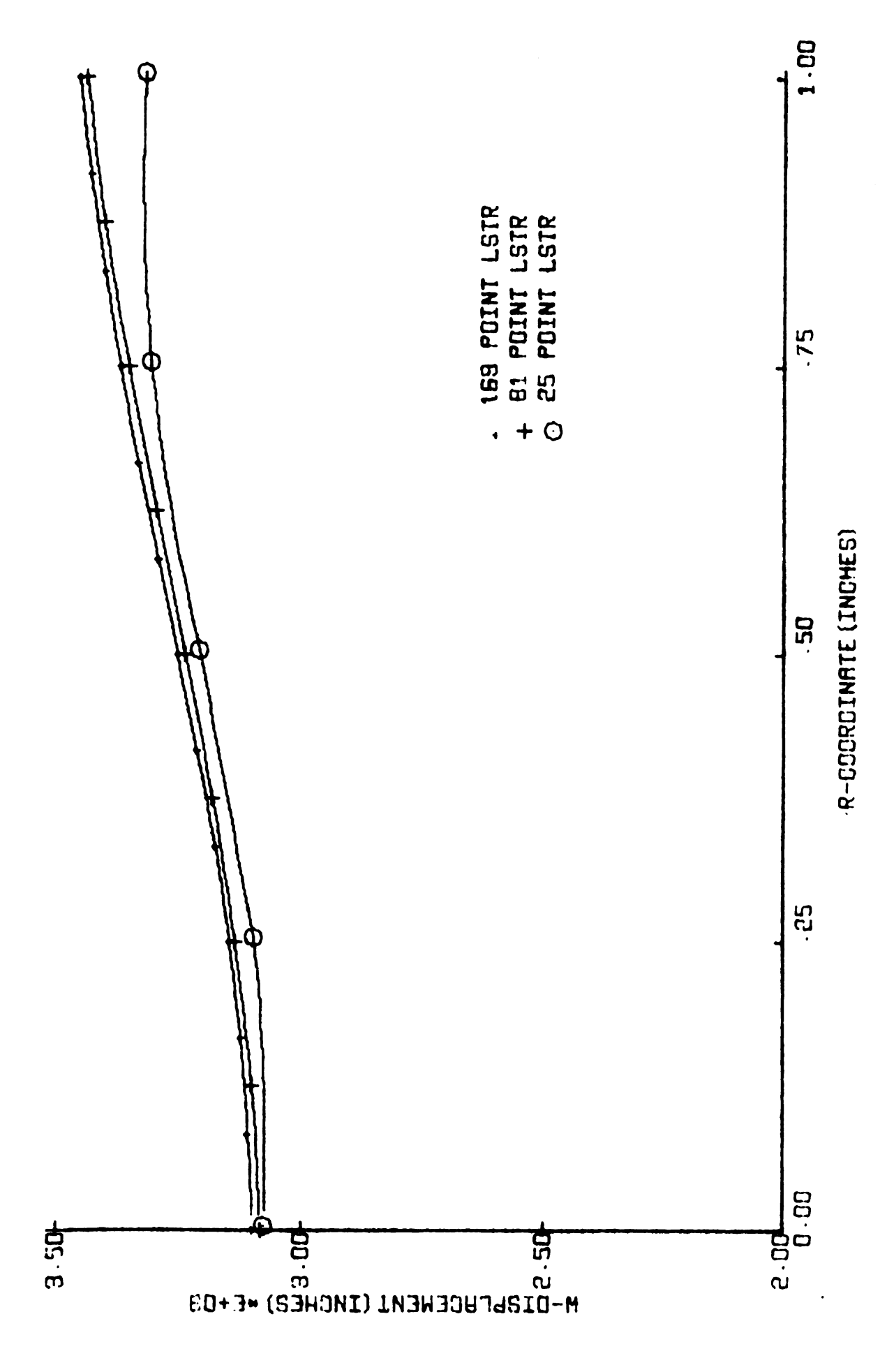


Figure 5.20, LSTR Cylinder End Axial Displacements

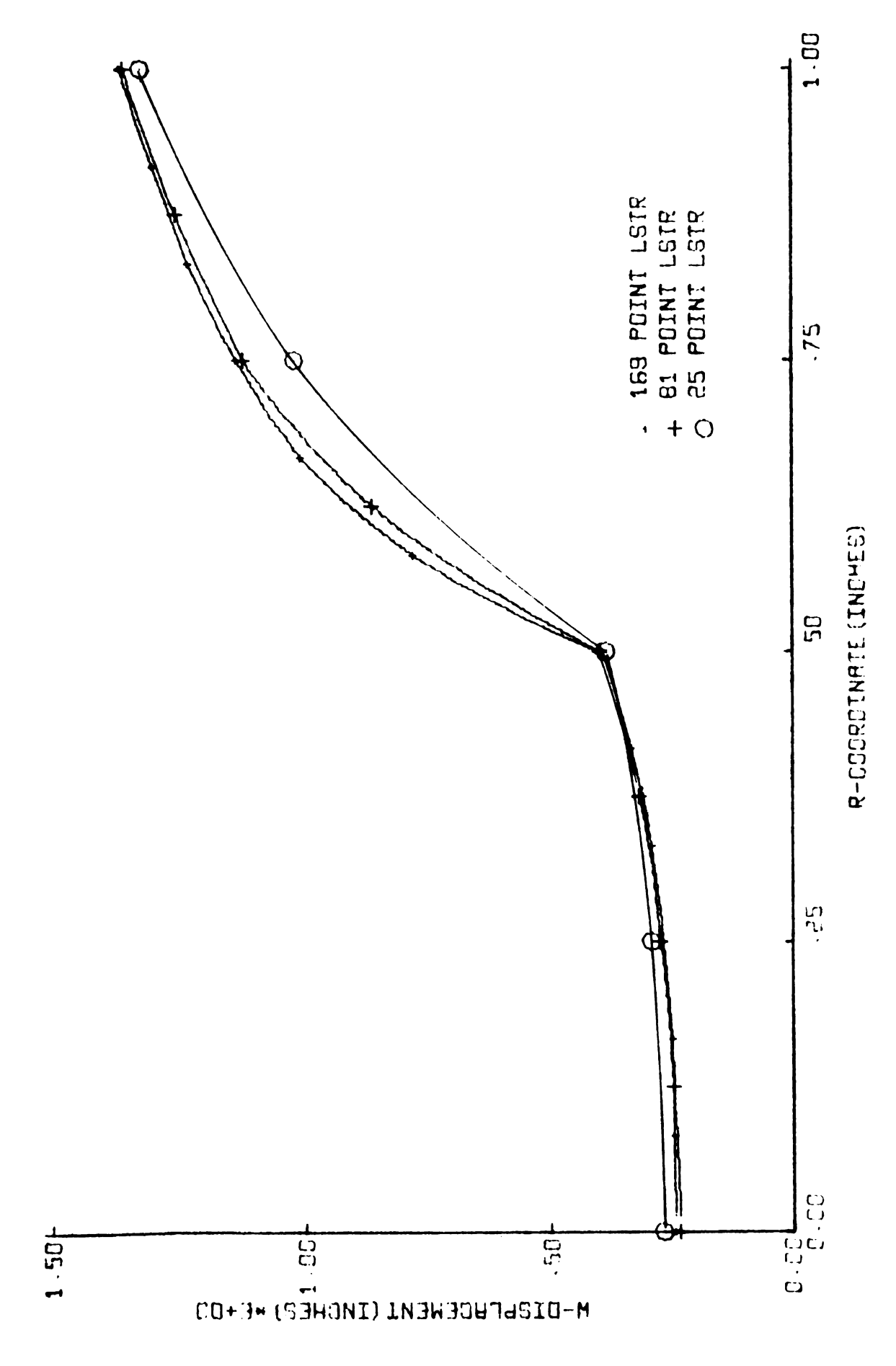


Figure 5.21, LSTR Horizontal Interface Axial Displacements

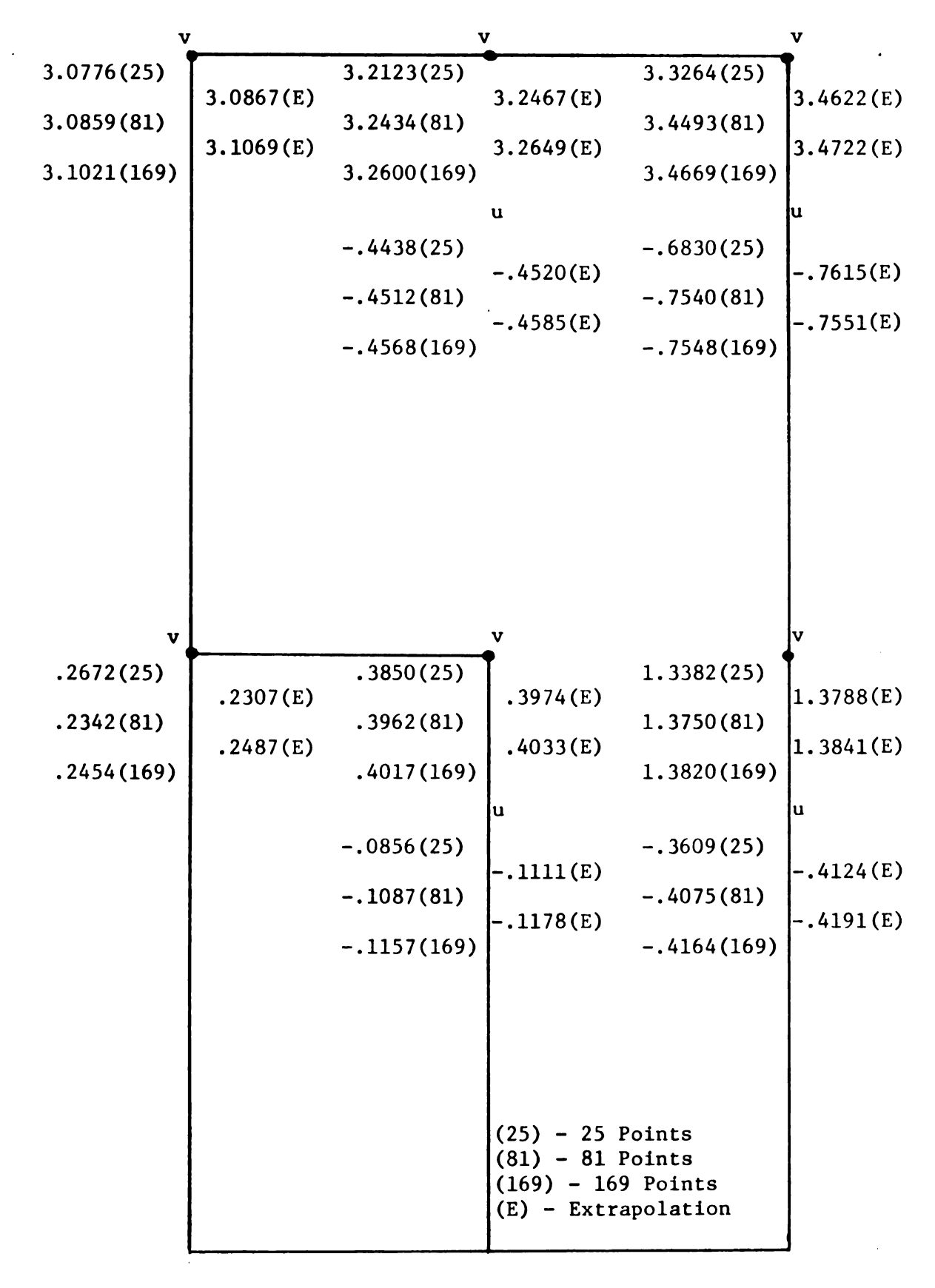


Figure 5.22
LSTR Extrapolated Displacements

250 171 250 -12 151 258 151 -10	-281 1173 -287 2 2 -157 1207 -154 -22	-150 1255 -151 35	-230 1184 -235 11 11 -134 1247 -146 45	-180 1161 -215 115 -121 1240 -140 43	-160 1191 -212 17 -104 -1225 -132 70 -68 1268 -95	-117 1195 -187 18 -80 1221 -119 73	-74 1194 -161 15 15 -28 1215 -107 70	-50 1198 -139 14 -40 11197 -96 67	-15 1205 -114 10 -23 1181 -89 0	120 120 120 120 1177 177 177 15	1200 -50 -4 1178 -68 25	3 1217 -73 -16 2 1189 -57 -7
-51 450 -51 -3	-44 -1452 -48 -30	-43 1454 -45 53	-55 1439 -52 96	-45 1411 -54 124	-34 1389 -53 135	-39 1305 -69 183	8 1234 -65 151	3 1195 -65 146	11 1149 -64 125	77 1091 -70 82	42 1051 -71 42	1 1032 -69 5
33 576 33 9	50 1581 53 19	35 1582 46 37	1586 32 76	-49 1564 2 129	-18 1453 -20 195	-14 1369 -38 258	26 1210 -57 233	107 1149 -34 181	31 1084 -56 151	20 1035 -60 98	8 989 -65 52	7 935 -72 11
185 569 185 18	190 1592 191 -4	180 1599 187 -2	155 1620 179 24	116 1660 170 26	94 1794 179 78	43 1727 127 228	66 1386 38 337	98 1076 -16 124	77 1002 -23 118	41 953 -34 64	15 900 -45 19	3 864 -52 3
364 553 364 1 537 637 636 36	369 1577 370 -20 -2660 1393 -2646 -149	360 1619 378 -38 -2173 959 -2651 -272	405 1681 405 -60 -2735 1151 -2723 -365	414 1742 422 -81 -2843 1509 -2678 -383	473 1874 469 -62 -2227 -1101 2420 4204 -2317 -1546 532 934		-160 968 38 492	-71 943 28 137	-35 919 21 62	-4 882 14 19	-2 869 10 -5	0 865 8 -20
509 676 509 186	-651 1410 -629 15	-527 1659 -551 113	-387 -387 -1834 -451 270	-393 -336 -336 143	51 -49 3329 5047 61 391 819 609	231 -2	-158 492 22 490	-87 716 65 201	-69 731 52 155	-45 786 57 76	-18 833 64 22	-2 859 67 4
467 747 467 116	48 1795 42 204	114 1994 116 372	155 2209 172 598	557 2591 361 720	154 53 3296 4198 403 522 755 693	43 223 39 441	-6 406 67 346	-60 536 68 246	-38 620 77 179	-25 677 80 106	-11 726 	-7 784 89 12
377 555 378 16	328 2543 352 102	303 2637 348 240	286 2958 389 417	198 3220 374 422	231 -11 3420 3676 380 333 366 305	94 215 48 304	42 366 74 219	10 458 90 184	-13 537 83 151	-7 608 89 88	0 656 97 46	-4 686 88 4
327 1016 327 -2	312 3046 320 93	317 3104 325 166	257 3205 320 320 220	195 3369 314 265	141 89 3520 3622 299 272 224 149	222	71 317 70 150	33 409 79 122	12 492 86 99	1 548 86 78	-1 546 76 41	-1 586 77 2
275 1200 275 -41	265 3240 272 51	246 3276 266 71	227 3335 260 83	175 3431 252 123	135 112 3532 3577 241 223 84 90	115 215 48 79	75 305 67 80	38 389 76 54	17 466 83 40	-1 514 80 22	2 568 86 38	587 83 -19
258 1353 258 -47	269 2357 281	245 3396 249	212 2400 259 5	173 3499 238 0	147 115 3534 3590 222 201	105 213 44 0	83 204 22 2	33 345 45 -3	24 373 61 0	450	-18 572 83 0	-10 620 86 -20

Figure 5.23, LSTR Stress Distribution

of 2800 psi and compressive circumferential stresses in excess of 2700 psi exist along the material interface. The maximum shear stress is 934 psi.

The results in Figure 5.23 seem very plausible. The only questionable stresses occur at the corner where the two materials join. The decreases in radial and circumferential stresses in the stiffener do not seem realistic. These decreases are the result of averaging carried out over elements around the corner. Evidence of this point is apparent in Figure 5.24 where element 540 2009 1447 522 226

Referring once again
to Figure 5.23, the agreement of
radial and circumferential stresses
at the symmetry axis is significant.
There is essentially no difference
in these stress components for any
of the points on the symmetry axis.
Certainly, this is further evidence of
the excellence of the LSTR solution.
There are, however, discrepancies

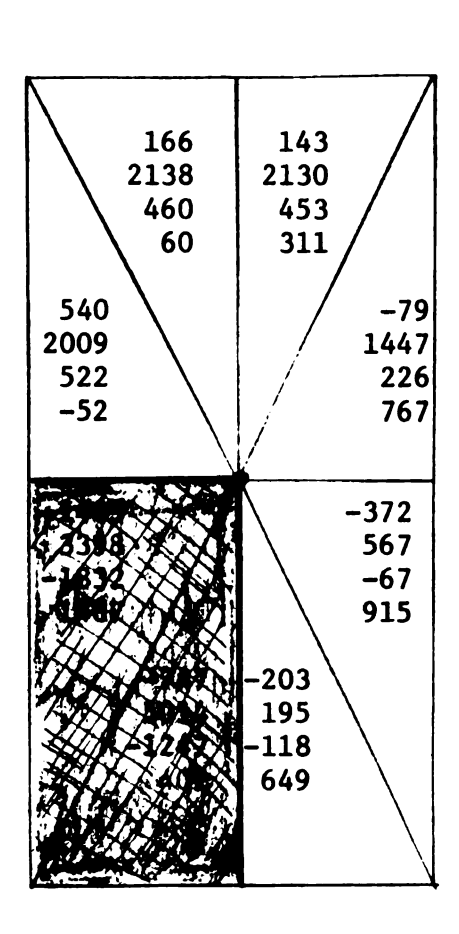


Figure 5.24
LSTR Corner Stresses

in certain interfacial stresses. The axial stress should be continuous across the material interface but it apparently is not.

Comparison of Solutions. In the preceding discussion of displacement solutions, the FD, CSTR, and LSTR results were seen to display similar trends as the number of points was increased. In order to compare these results in more detail, a number of displacement and stress curves are included here corresponding to the highest order approximation used for each method. The same displacements discussed earlier are used. The stress comparisons are made in terms of interfacial stresses which are generally the largest stresses for the various regions of the body.

Axial displacements for the 3 solutions are listed in Tables 5.4 and 5.5. These same results, presented graphically in Figures 5.25 and 5.26, need little additional explanation. Axial displacements for the 3 solutions are very comparable. The LSTR solution is consistently better than the other solutions. The CSTR solution falls short of both the LSTR and FD solutions. It should again be noted that the axial displacements ar r = 0 for the difference solution are extrapolated results.

Radial displacements are plotted in Figures 5.27 and 5.28. The end displacements are practically identical for the 3 solutions. Radial displacements along the horizontal interface differ only slightly. The LSTR solution is again best and the FD solution next best.

The stress variation along the material interface is of particular interest. This is the region of maximum stress for both the matrix and the stiffener. Consequently, stress comparisons are made in terms of these regions.

The interfacial stresses corresponding to the various solutions are tabulated on pages which follow. These same results are presented

Table 5.4

Composite Cylinder End

w-Displacement × 10⁺³

r-Coord.	231 Point Finite Diff.	r-Coord.	169 Point CSTR	169 Point LSTR
0.	3.06009	0.	3.06694	3.10207
.1	3.07403	.08333	3.07794	3.11008
.2	3.10145	.16666	3.08960	3.12732
.3	3.19698	.25	3.11678	3.15033
.4	3.18106	.33333	3.12577	3.18033
.5	3.23094	.41666	3.18456	3.21873
.6	3.28273	.5	3.22391	3.25999
.7	3.33222	.58333	3.26598	3.30169
.8	3.37573	.66666	3.30623	3.34268
.9	3.41084	.75	3.34236	3.37960
1.0	3.43700	.83333	3.37264	3.41214
		.91666	3.40430	3.44154
		1.0	3.42934	3.46693

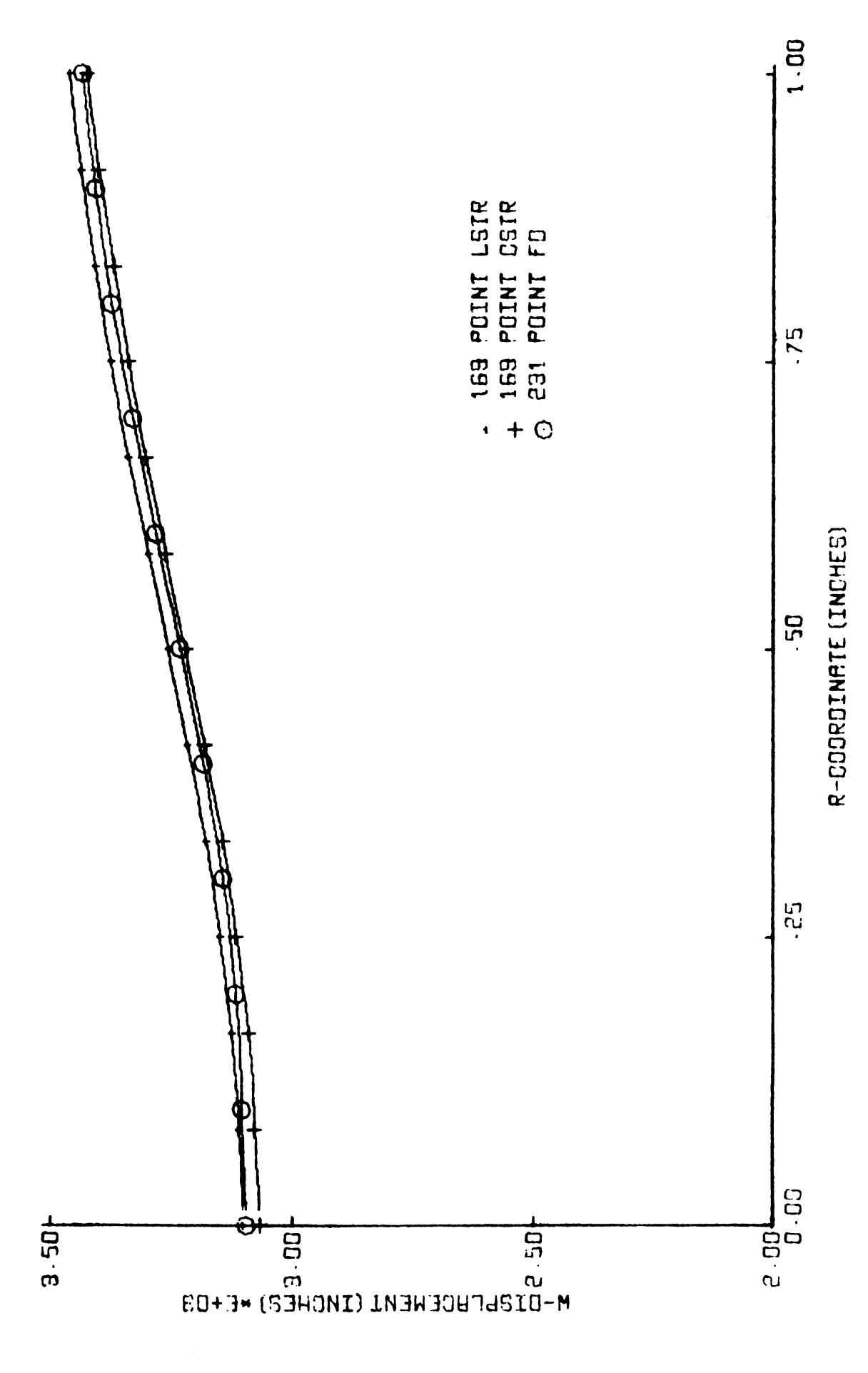


Figure 5.25, Comparison of End Axial Displacements

r-Coord.	231 Point Finite Diff.	r-Coord.	169 Point CSTR	169 Point LSTR
0.	.25098	0.	.24688	.24535
.1	.25308	.08333	.25439	.24533
.2	.26456	.16666	.25847	.25171
.3	.28617	.25	.27776	.26938
.4	.32339	.33333	.29641	.29399
.5	.39318	.41666	.33674	.33452
.6	.82465	.5	.39235	.40165
.7	1.04466	.58333	.76011	.78139
.8	1.18220	.66666	.97726	1.01132
.9	1.27788	.75	1.11206	1.14399
1.0	1.35295	.83333	1.21204	1.24273
		.91666	1.28542	1.31620
		1.0	1.34747	1.38196

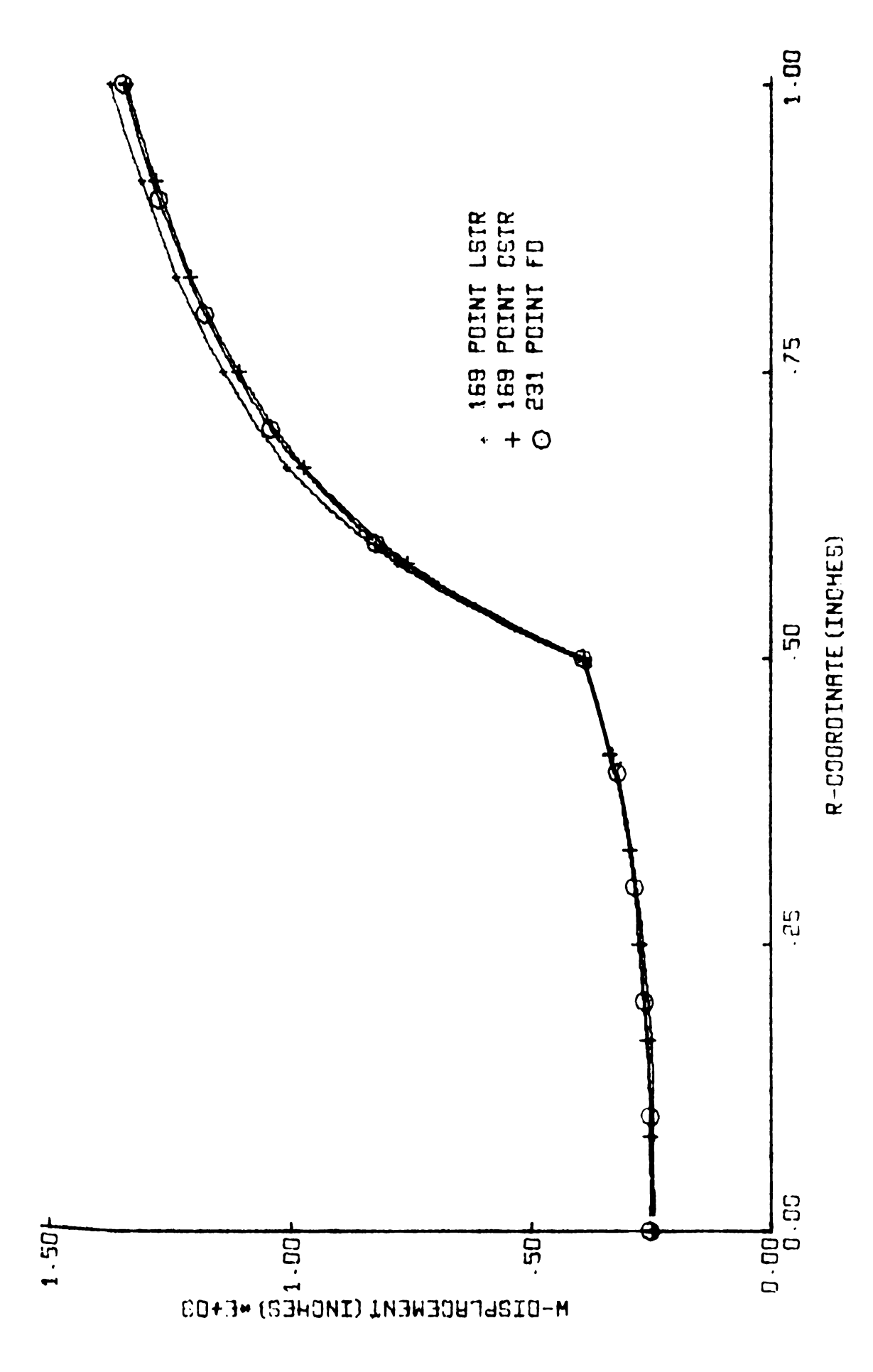


Figure 5.26, Comparison of Horizontal Interface Axial Displacements

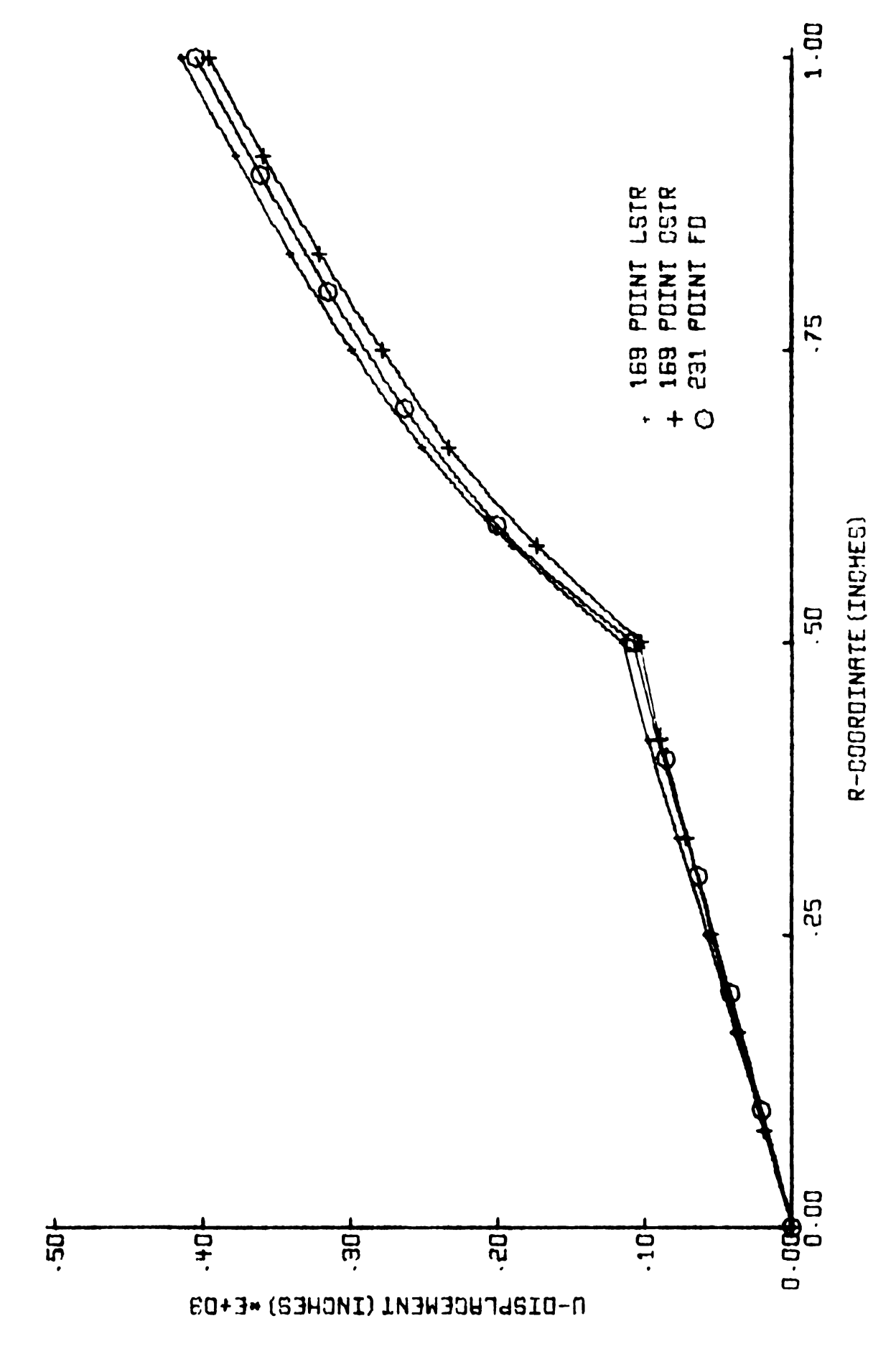


Figure 5.27, Comparison of End Radial Displacements

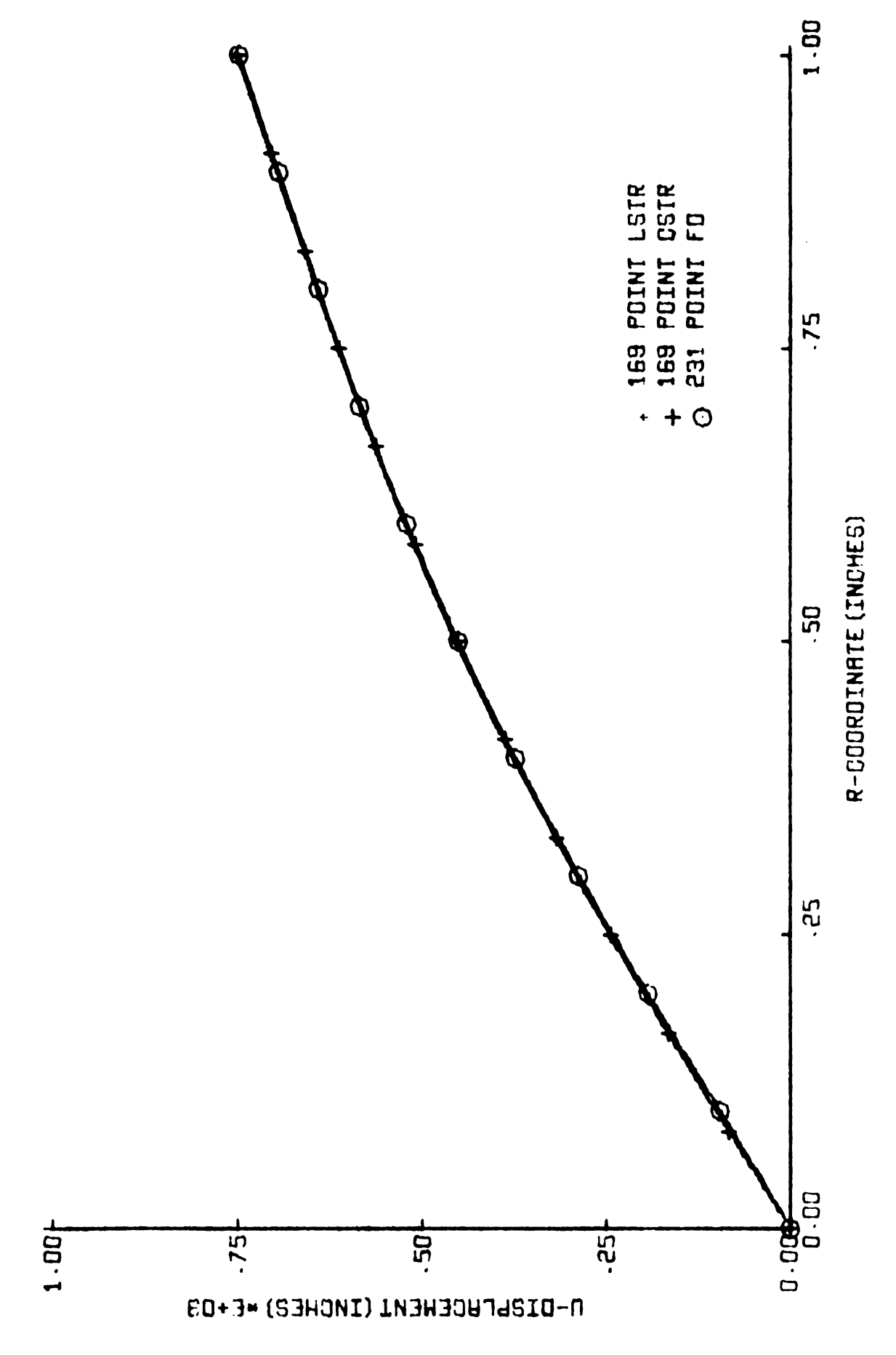


Figure 5.28, Comparison of Horizontal Interface Radial Displacements

graphically as well. In Tables 5.6 and 5.7 and in Figure 5.29, radial stresses along the horizontal interface are shown. The three methods give very comparable radial stress in the matrix where the stress level is quite low. In the stiffener, the radial stress variation is quite different. The finite element solutions are very erratic and seem less reasonable than the finite difference stresses. Much the same behavior was observed in Chapter 4 with regard to the composite plate example. It was noted there that this behavior depends to some extent on the finite element configurations. Also, one could use smaller triangles around the interface to improve the situation.

The axial stress variation along the horizontal interface is given in tables on pages 227 and 228. These results, which are also plotted in Figure 5.30, are more comparable than radial stresses in the same region. The methods predict axial stresses of more than 3500 psi in the stiffener and 1800 psi in the matrix. Axial stress variations along the vertical interface are given in Tables 5.10 and 5.11. In Figure 5.31, this same information is seen to display a similar trend for the three methods. Fairly significant variations in axial stress occur near the corner of the stiffener. Typical of this is the maximum axial stress which is 4831 psi for the FD solution, 4547 psi for the CSTR solution, and 5047 psi for the LSTR solution.

The final comparison here pertains to the circumferential stress along the horizontal interface. These stresses are shown in Tables 5.13 and 5.14. The plotted results in Figure 5.32 are more comparable in the matrix, where stresses are tensile and relatively small, than in the stiffener where stresses are compressive and rather large. It has previously been mentioned that FD stresses along the

Table 5.6
Horizontal Interface Stress

σ_r (Matrix)

r-Coord.	231 Point Finite Diff.	r-Coord.	169 Point CSTR	169 Point LSTR
.0	388	.0	296	364
.1	387	.08333	378	369
.2	401	.16666	310	360
.3	427	.25	409	405
.4	485	.33333	319	414
.5	34	.41666	481	473
.6	-146	.5	73	32
.7	- 55	.58333	-151	-160
.8	- 20	.66666	- 37	- 71
.9	- 6	.75	- 40	- 35
1.0	- 2	.83333	- 8	- 4
		.91666	- 7	- 2
		1.0	0	0

Table 5.7
Horizontal Interface Stress

 $\sigma_{\mathbf{r}}$ (Stiffener)

r-Coord.	231 Point Finite Diff.	r-Coord.	169 Point CSTR	169 Point LSTR
.0	-2319	.0	-1425	-2537
.1	-2451	.08333	-2616	-2660
.2	-2477	.16666	-1752	-2173
.3	-2445	.25	-2351	-2735
.4	-2103	.33333	-1491	-2843
.5	-1803	.41666	-1750	-2227
		.5	- 950	-1108

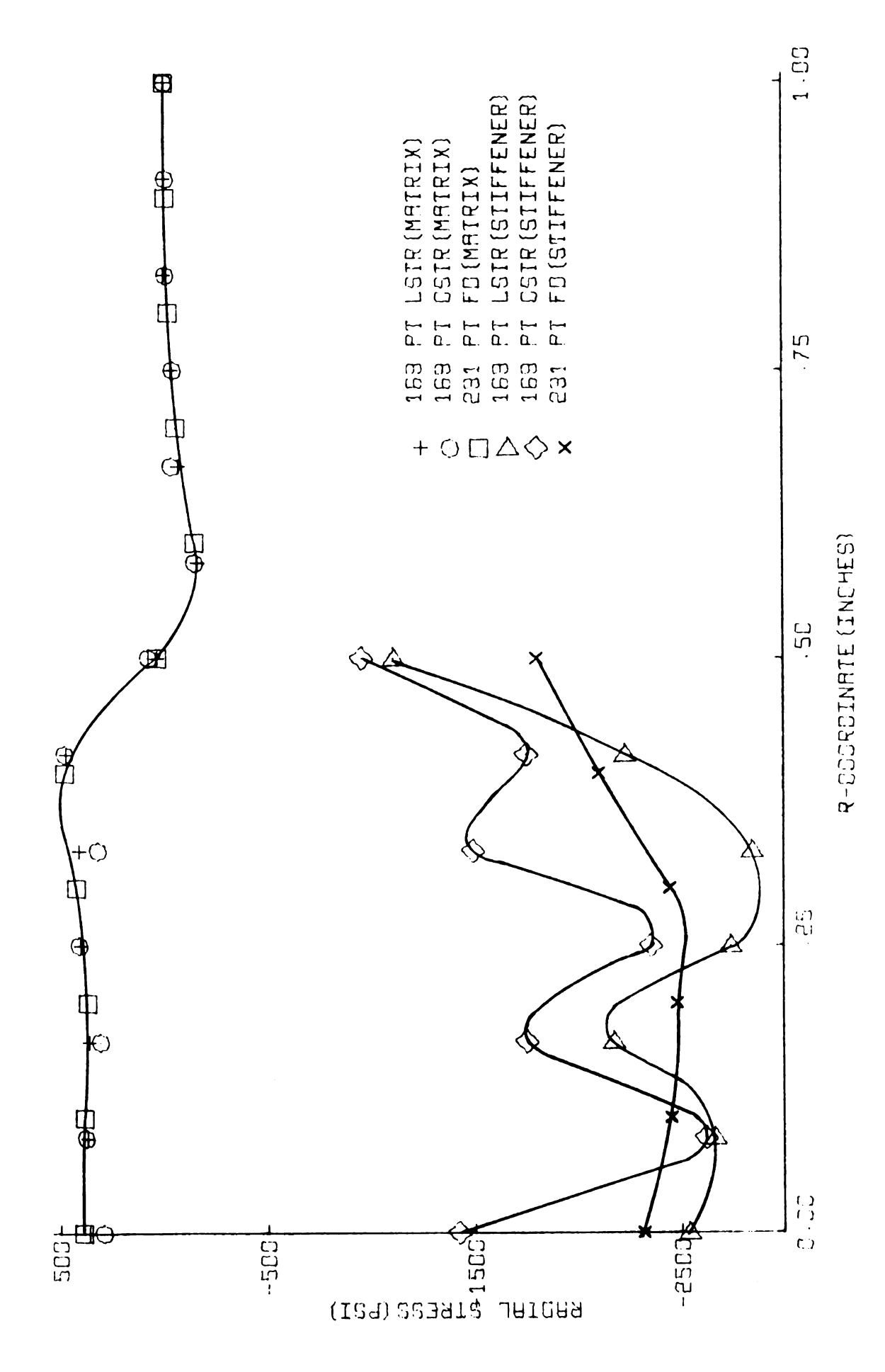


Figure 5.29, Horizontal Interface $\sigma_{\mathbf{r}}$

Table 5.8
Horizontal Interface Stress

 $\sigma_{\mathbf{z}}$ (Matrix)

r-Coord.	231 Point Finite Diff.	r-Coord.	169 Point CSTR	169 Point LSTR
0.	1496	.0	1571	1553
.1	1555	.08333	1584	1577
.2	1585	.166666	1604	1619
.3	1650	.25	1649	1681
.4	1776	.33333	1709	1742
.5	1399	.41666	1828	1874
.6	939	.5	1291	1415
.7	896	.58333	921	968
.8	876	.66666	905	943
.9	867	.75	874	919
1.0	868	.83333	871	882
		.91666	865	869
		1.0	867	865

Table 5.9
Horizontal Interface Stress

 $\sigma_{\mathbf{z}}$ (Stiffener)

r-Coord.	231 Point Finite Diff.	r-Coord.	169 Point CSTR	169 Point LSTR
0.	1325	.0	1621	1637
.1	1555	.08333	1164	1393
.2	1565	.16666	1305	959
.3	1724	.25	1414	1151
. 4	2265	.3333	1845	1509
.5	4831	.41666	2481	2420
		.5	3520	4206

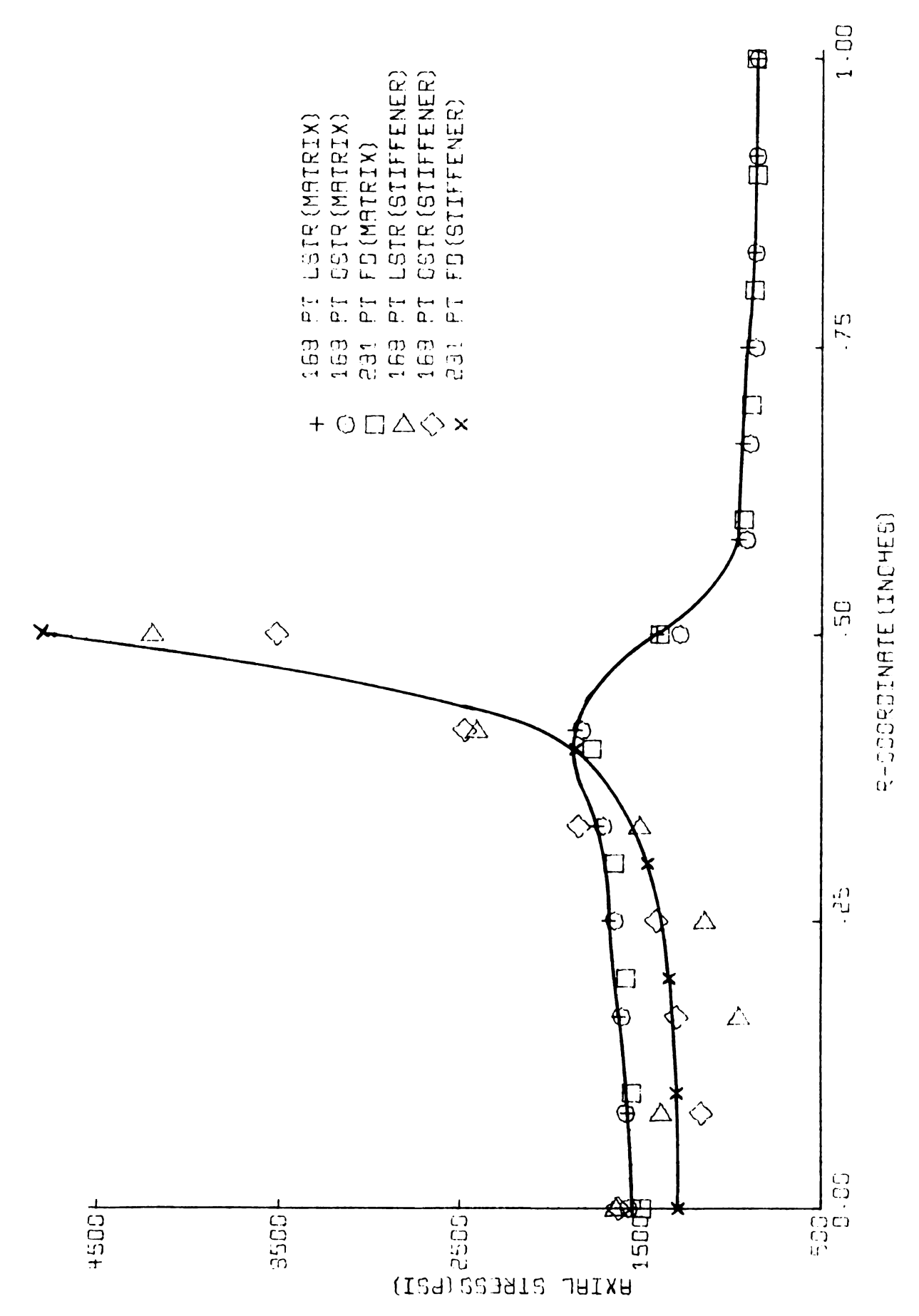


Figure 5.30, Horizontal Interface $\sigma_{\mathbf{z}}$

Table 5.10

Vertical Interface Stress

 $\sigma_{\mathbf{z}}$ (Matrix)

z-Coord.	231 Point Finite Diff.	z-Coord.	169 Point CSTR	169 Point LSTR
0.	199	0.0	259	213
.1	199	.16666	210	215
. 2	198	.33333	266	222
.3	198	.5	314	215
.4	134	.66666	309	223
.5	195	.83333	218	231
.6	192	1.0	1291	1415
.7	187	1.16666	1682	1727
.8	175	1.33333	1403	1369
.9	140	1.5	1316	1305
1.0	1399	1.66666	1256	1246
1.1	1871	1.83333	1222	1221
1.2	1609	2.0	1196	1195
1.3	1465			
1.4	1379			
1.5	1321			
1.6	1279			
1.7	1248			
1.8	1224			
1.9	1209			
2.0	1203			

Table 5.11
Vertical Interface Stress

 $\sigma_{\mathbf{z}}$ (Stiffener)

z-Coord.	231 Point Finite Diff.	z-Coord.	169 Point CSTR	169 Point LSTR
0.	3637	0.	356 5	3590
.1	3638	.166666	3600	3577
.2	3646	.33333	3572	3622
.3	3667	.5	3785	3676
.4	3719	.66666	3792	4198
.5	3820	.83333	4547	5047
.6	3998	1.0	3520	4206
.7	4267			
.8	4600			
.9	4802			
1.0	4831			•

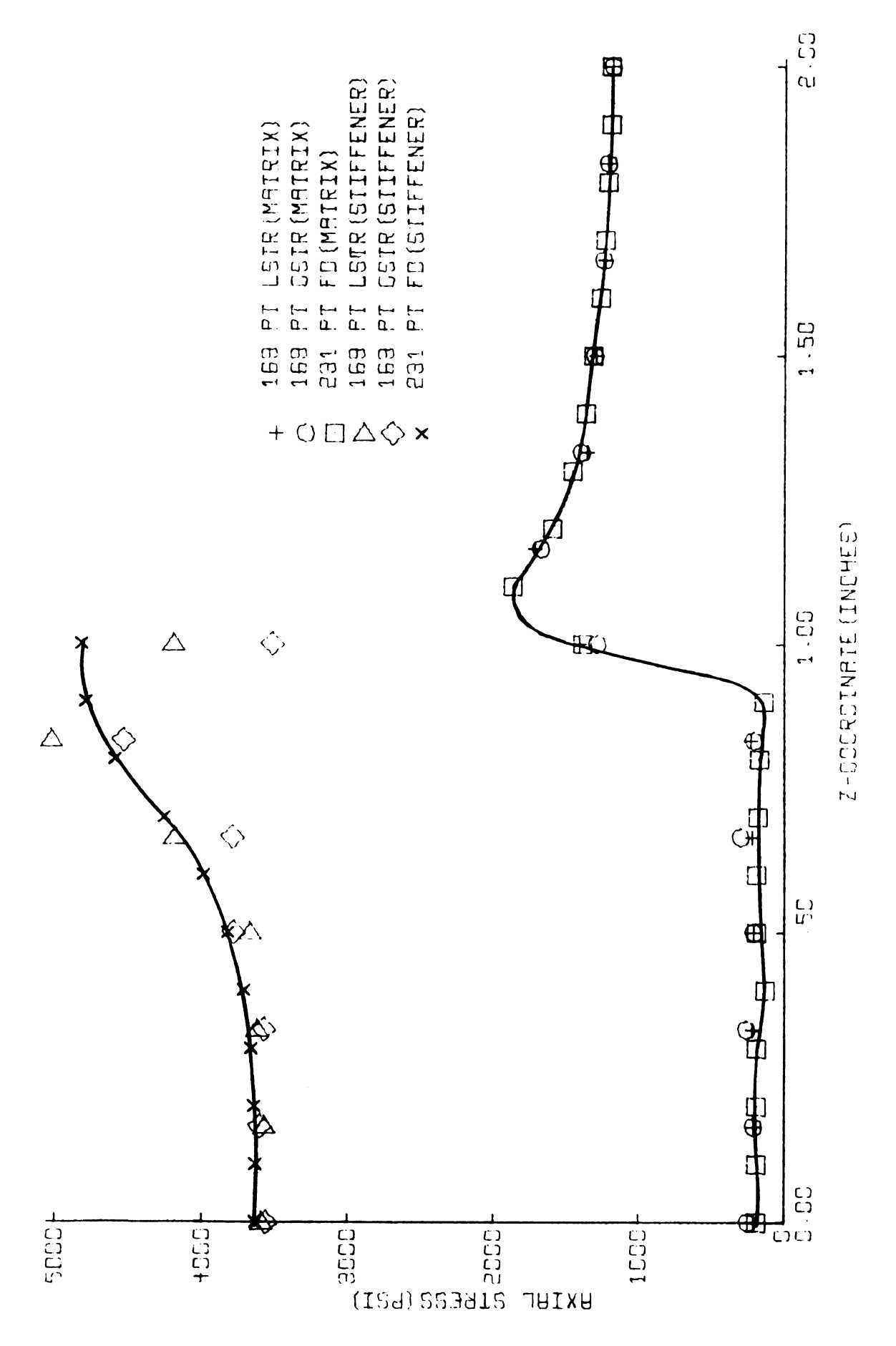


Figure 5.31, Vertical Interface $\sigma_{\mathbf{z}}$

symmetry axis are unlikely to be valid, and thus extrapolation from the interior is desirable. In Figure 5.32, the FD stress at r=0 is an extrapolated result. The CSTR stresses in the stiffener exhibit to some extent the erratic behavior of the radial stresses in this same region.

Concluding Remarks. The axially symmetric finite difference and finite element formulations are apparently equally acceptable in their ability to predict displacements in simple composite solids. Although no numerical comparisons have been employed, convergence to exact displacements is quite comparable for the three methods.

The formulations, however, lead to somewhat different solutions insofar as stress is concerned. Certain stress components are very similar, for example, the axial stress in the axially loaded composite solid. Other stresses, however, tend to be very much different. The radial stresses and circumferential stresses displayed different variations along the material interface. The finite element stresses were more erratic. In this connection, best fit curves seem to be more realistic.

Table 5.12
Horizontal Interface Stress

 σ_{θ} (Matrix)

r-Coord.	231 Point Finite Diff.	r-Coord.	169 Point CSTR	169 Point LSTR
0.	506	0.	337	364
.1	386	.08333	376	370
.2	399	.16666	367	378
.3	422	.25	404	405
. 4	471	.33333	399	422
.5	265	.41666	468	469
.6	23	.5	238	246
.7	19	.58333	43	38
.8	16	.66666	41	28
.9	14	.75	22	21
1.0	12	.8333	23	14
		.91666	18	10
		1.0	18	8

Table 5.13
Horizontal Interface Stress

 σ_{θ} (Stiffener)

r-Coord.	231 Point Finite Diff.	r-Coord.	169 Point CSTR	169 Point LSTR
0.	161 (-2508)*	0.	-1077	-2536
.1	-2488	.08333	-2654	-2646
.2	-2467	.16666	-2352	-2651
.3	-2447	.25	-2444	-2723
. 4	-2271	.33333	-2078	-2678
.5	-1401	.41666	-2001	-2317
		.5	-1425	-1540

*Extrapolated

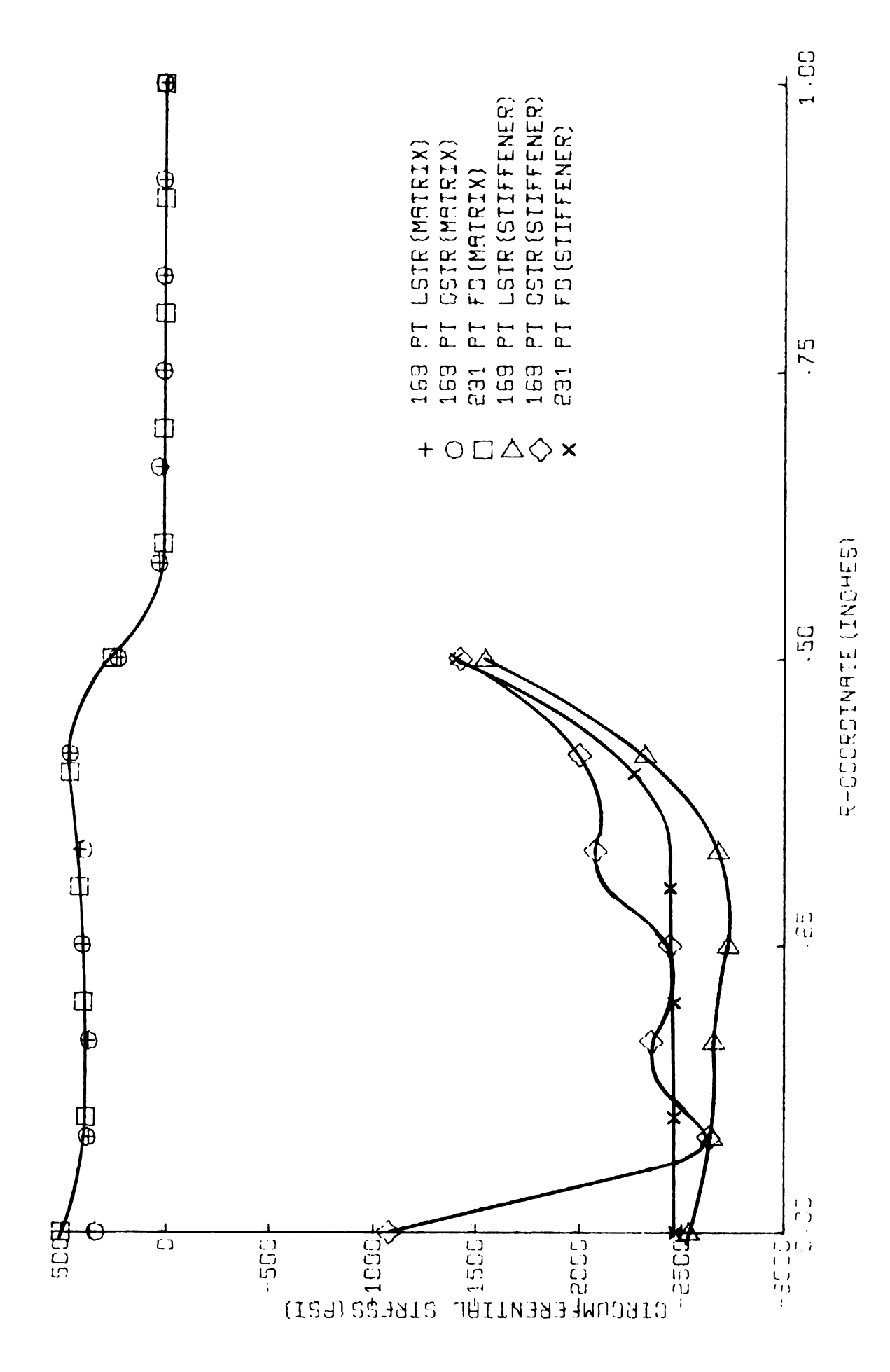


Figure 5.32, Horizontal Interface σ_{θ}

VI. CONCLUSIONS AND RECOMMENDATIONS

Finite element and finite difference methods have been formulated for plane and axially symmetric stress analysis. Stiffness influence coefficient matrices for the direct stiffness method have been discussed. These relate to the constant and linearly varying strain triangle and triangular ring elements. Nodal point forces associated with arbitrary distributed boundary loads were treated for each case. The formulation of the difference method was done in terms of the Navier equations of Classical Elasticity Theory. Difference equations were derived by expressing the equilibrium of a material element. Involved are assumptions of strains in terms of displacement differences.

The methods were applied to both plane stress and axially symmetric elastostatic problems. Two examples with well known elasticity solutions provided an excellent basis for comparison for both stress and deformation analysis.

6.1 Conclusions

The finite difference and finite element methods have proved to be very capable in the deformation analysis of elastic solids. The finite element solutions employing linear strain triangular elements (LST) were consistently better than either the finite difference

solutions or the finite element solutions which employed constant strain triangular elements (CST). The improvement was not excessive in every case when a comparable number of points was utilized. In the cantilever beam problem, however, the LST solution for deflections was significantly better. The finite difference (FD) solutions were comparable to the CST solutions but generally gave somewhat better results.

In the analysis of stress, nodal point stresses, obtained by averaging element stresses, were employed. A similar concept was employed with regard to the difference method whereby nodal point stresses were obtained by averaging the stresses for the regions around the mesh point. In this connection, the LST formulations were significantly better than the CST and FD formulations. This was particularly true along free boundaries. The FD solutions were generally better than the CST solutions and in some cases were comparable to the LST solution. It should be mentioned, however, that in regard to certain interfacial stresses associated with composite materials, both finite element methods exhibited erratic stress variations suggesting the desirability of using best fit curves in interpreting these results. The finite difference method, on the other hand, gave much smoother stress variations and consequently appeared to be more realistic.

6.2 Recommendations

The capabilities of the finite element and finite difference methods, in the analysis of elastostatic problems, have been demonstrated for a limited class of applications. The presentation of the difference method in particular was limited to special geometrical situations. In view of this as well as results obtained in this

investigation, a number of recommendations are advanced. These follow immediately.

Difference Method. The scope of the finite difference method, as presented in this work, included both plane and axially symmetric analysis. The formulation of boundary equations, however, was limited to surfaces parallel to the coordinate surfaces of the problem. It is possible to approximate other situations within the framework of this analysis by treating arbitrary boundaries as a series of broken lines as in Figure 6.1a for example. This technique has not been investigated here. To achieve any degree of accuracy, it would no doubt be necessary to utilize a variable mesh spacing. This last point has not been developed here either. A more suitable approach from a geometric stand point would eliminate the ragged edge as in Figure 6.1b. The development of boundary equations for such situations has not been pursued here and appears at first glance to present difficulties if considered from the equilibrium point of view as in sections 2.8 and 2.9.

The method requires further development and application in addition to that discussed above. The possibility of treating 3-dimensional problems with simple boundaries presents no difficulties. The procedure of section 2.8 would be applied to the 3-dimensional Navier Equations. Computationally, however, there may arise problems associated with computer memory capability. For example, where each plane stress or axially symmetric equation involves 18 non-zero coefficients, the 3-dimensional equations involve 57 non-zero coefficients. Thus for problems with comparable numbers of mesh points,

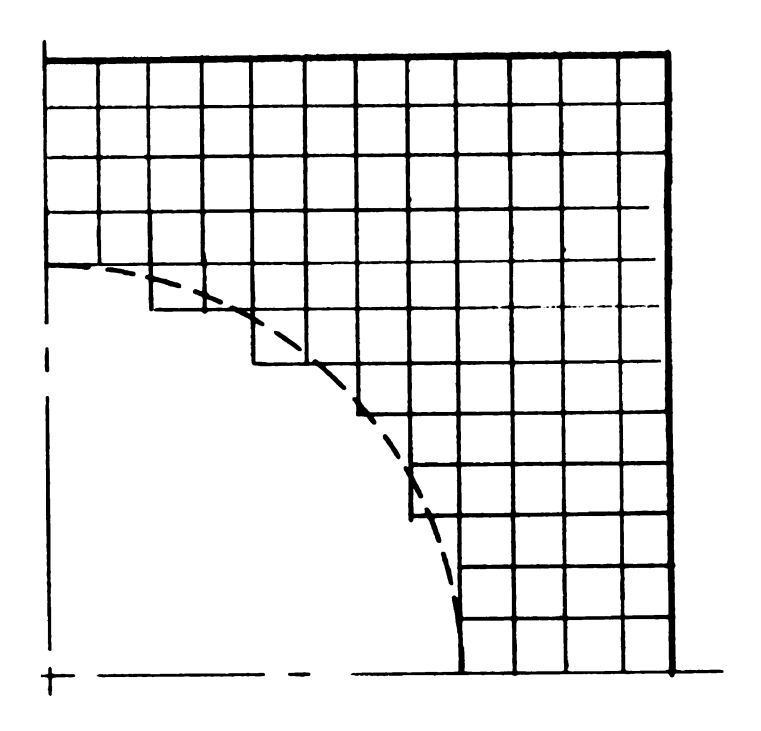


Figure 6.1a

Finite Difference Approximation for Present Analysis

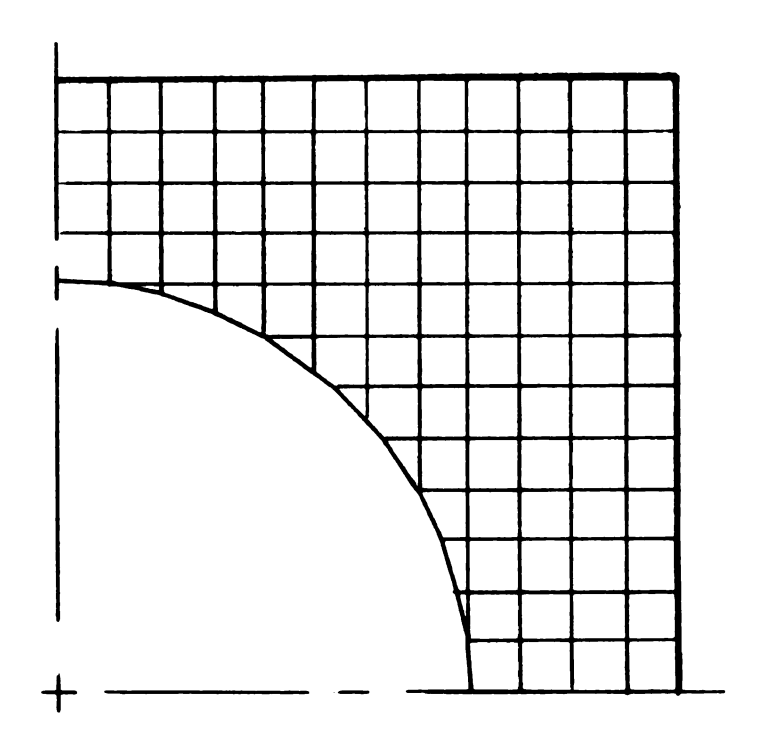


Figure 6.1b

Possible Finite Difference Approximation Square Plate with a Circular Hole

approximately 4.22 times as much memory capability is required.

Stiffness Method. The plane stress triangle utilizing either constant or linear strain variation has been rather thoroughly investigated by various authors. The constant strain triangular ring has been used extensively as well. From the limited scope of this research, the linear strain triangular ring appears to give the same degree of improvement in axially symmetric problems that the linear strain triangle gives in plane stress analysis. It is therefore recommended that additional applications of this element be treated to indicate its full capability.

BIBLIOGRAPHY

- Runge, C., "Über eine Methode die partielle Differentialgleichung
 Δu = Constans numerish zu integrieren," Z. Math. Phys., Vol. 56,
 1908, p. 225.
- Richardson, L. F., "The Approximate Arithmetical Solution by Finite Differences of Physical Problems Involving Differential Equations, with an Application to the Stresses in a Masonry Dam," Trans. Roy. Soc., London, Series A, Vol. 210, 1910, p. 307.
- 3. Marcus, H., "Die Theorie Elastischer Gewebe Und Ihre Anwendung Auf Die Berechnung Elastischer Platten," Armierter Beton, 1919, p. 107.
- 4. Hencky, H., "Die Berechnung dunner rechteckiger Platten mit verschwindender Biegungsteifigkeit," Z. Agnew, Math. Mech., Vol., 1921, p.81, and Vol. 2, 1922, p. 58
- 5. Southwell, R. V., Relaxation Methods, Vols. I, II, III.
- 6. Langefors, B., "Analysis of Elastic Structures by Matrix Transformation with Special Regard to Monocoque Structures," Journal of the Aeronautical Sciences, Vol. 19, No. 7, 1952, pp. 451-458.
- 7. Argyris, J. H. and Kelsey, S., <u>Energy Theorems and Structural</u> Analysis, Butterworth, London, 1960.
- Hrennikoff, A., "Solution of Problems in Elasticity by the Framework Method," Journal Appl. Mech., Vol. 8, No. 4., December 1941.
- 9. McHenry, D., "A Lattice Analogy for the Solution of Plane Stress Problems," Journal Inst. Civil Eng., December 1943.
- 10. Parikh, K. S., and Norris, C. H., "Analysis of Shells using Framework Analogy," World Conference on Shell Structures, October 1962, pp. 213-222.
- 11. Turner, M. J., Clough, R. W., Martin, H. C. and Topp, L. J.,
 "Stiffness and Deflection Analysis of Complex Structures,"
 J. Aeron, Science, 23, No. 9, September 1956.

- 12. Argyris, J. H., Kelsey, S., and Kamel, H., <u>Matrix Methods of Structural Analysis</u>. A Precis of Recent Developments, AGARDograph 72, Ed. de Veubeke, Permagon Press, 1964.
- 13. Argyris, J. H., Kelsey, S., "Initial Strains in the Matrix Force Method of Structural Analysis," Journal of the Royal Aeronautical Society, August 1960, pp. 493-495.
- 14. Turner, M. J., Dill, E. H., Martin, H. C., and Melosh, R. J., "Large Deflections of Structures Subjected to Heating and External Loads," Journal of Aero/Space Science, Vol. 27, No. 2, February 1960.
- 15. Argyris, J. H., "Reinforced Fields of Triangular Elements with Linearly Varying Strain; Effect of Initial Strains," Journal of the Royal Aeronautical Society, November 1965, pp. 799-801.
- 16. Fraeijs de Veubeke, B. M., "Upper and Lower Bounds in Matrix Structural Analysis," A Precis of Recent Developments, AGARDograph 72, Ed. de Veubeke, Permagon Press, 1964.
- 17. Argyris, J. H., "Triangular Elements with Linearly Varying Strain for the Matrix Displacement Method," Journal of the Royal Aeronautical Society, October 1965, pp. 711-713.
- 18. Fellippa, C. A., "Refined Finite Element Analysis of Linear and Non-Linear Two Dimensional Structures," Ph.D., Dissertation, California Univ., Berkeley, 1966.
- 19. Melosh, R. J., "A Stiffness Matrix for the Analysis of Thin Plates in Bending," Journal of Aerospace Sciences, January 1961, pp. 44-43.
- 20. Argyris, J. H., "Matrix Displacement Analysis of Plates and Shells," Ingenieur Archiv., Vol. 35, No. 2, 1965.
- 21. Bogner, F. K., Fox, R. L., Schmit, L. A., "A Cylindrical Shell Discrete Element," AIAA Journal, Vol. 5, No. 4, April 1967.
- 22. Clough, R. W., and Tocher, J. L., "Finite Element Stiffness Matrices for Analysis of Plate Bending," Proceedings of Conference on Matrix Methods in Structural Mechanics, Wright Patterson Air Force Base, Ohio, 1965.
- 23. Zienkiewicz, O. C., "Finite Element Procedures in the Solution of Plate and Shell Problems," <u>Stress Analysis</u>, edited by O. C. Zienkiewicz, and G. S. Holister, John Wiley and Sons, 1965.
- 24. Argyris, J. H., "Three-Dimensional Anistropic and Inhomogeneous Elastic Media Matrix Analysis for Small and Large Displacements," Ingenieur Archiv., Vol. 34, No. 1, January 1966, pp. 33-55.

- 25. Wilson, E. L., "Structural Analysis of Axisymmetric Solids," AIAA Journal, Vol. 3, No. 12, December 1965.
- 26. Clough, R. W., and Rashid, Y., "Finite Element Analysis of Axi-Symmetric Solids," Journal Eng. Mech. Div., ASCE, 91, February 1965, pp. 73-85.
- 27. Argyris, J. H., "Matrix Analysis of Three-Dimensional Elastic Media Small and Large Displacements," AIAA Journal, Vol. 3, No. 1, January 1965, pp. 45-51.
- 28. Klein, Bertram, "Application of a New Matrix Method to Vibration Analysis of Structures," Journal of Aerospace Sciences, March 1962, pp. 350-351.
- 29. Flower, M., Severn, R. T., and Taylor, P. R., "Static and Dynamic Analysis of Plates and Shells Using the Finite Element Method," Paper presented at the International Symposium on the use of Digital Computers in Structural Engineering.
- 30. Dawe, D. J., "A Finite Element Approach to Plate Vibration Problems," Journal of Mechanical Engineering Science, Vol. 7, No. 1, 1965.
- 31. Taylor, R. L. and Chang, T. Y., "An Approximate Method of Thermoviscoelastic Stress Analysis," Nucl. Eng. and Des. 4, 1966, pp. 21-28.
- 32. Taylor, R. L., "Methods of Thermoviscoelastic Stress Analysis in Concrete Reactor Vessels," Nucl. Struct. Eng. 1, 1965, pp. 385-594.
- 33. Sokolnikoff, I. S., "Mathematical Theory of Elasticity," McGraw-Hill Book Company, Inc., New York, 1956.
- 34. Fraeijs de Veubeke, B. M., "Displacement and Equilibrium Models in the Finite Element Method," <u>Stress Analysis</u>, edited by O. C. Zienkiewicz and G. S. Holister, John Wiley and Sons, 1965.
- 35. Clough, R. W., "The Finite Element in Structural Mechanics,"

 Stress Analysis, edited by O. C. Zienkiewicz and G. S. Holister,

 John Wiley and Sons, 1965.
- 36. Archer, J. S., "Consistent Matrix Formulations for Structural Analysis using Finite Element Techniques," AIAA Journal, Vol. 3, No. 10, October 1965, pp. 1910-1918.
- 37. Tocher, J. L., "Selective Inversion of Stiffness Matrices," Journal Struct. Div., ASEE, 92, February 1966, pp. 75-87.
- 38. Wilson, E. L., "Finite Element Analysis of Two Dimensional Structures," Ph.D., Dissertation, California Univ., Berkley, 1963.

- 39. Timoshenko, S. and Goodier, J. W., <u>Theory of Elasticity</u>, McGraw-Hill Book Company, Inc., New York, 1951.
- 40. Ralston, A., A First Course in Numerical Analysis, McGraw-Hill Book Company, Inc., New York, 1965.
- 41. Denke, P. H., "The Matrix Solution of Certain Nonlinear Problems in Structural Analysis," Journal of Aeronautical Sciences, Vol. 23, No. 3, March 1956, pp. 231-236.
- 42. Melosh, R. J., "Basis for Derivation of Matrices of the Direct Stiffness Method," AIAA Journal, Vol. 1, No. 7, July 1963, pp. 1631-1637.
- 43. Martin, H. C., "Plane Elasticity Problems and the Direct Stiffness Method," Trend in Engineering, Vol. 13, January 1961, pp. 5-8, 19.
- 44. Allen, D. N. de G., and Wendle, D. W., "The Finite Difference Approach," <u>Stress Analysis</u>, edited by O. C. Zienkiewicz and G. S. Holister, John Wiley and Sons, 1965.
- 45. Melosh, R. J., "Structural Analysis of Solids," J. Struct. Div., ASEE, 89, August 1963, pp. 205-223.
- 46. Clough, R. W., "The Finite Element Method in Plane Stress Analysis," Proceedings, ASEE 2nd Conference on Electronic Computation, Pittsburgh, Pa., September 1960.
- 47. Turner, M. J., Martin, H. C., and Weikel, R. C., "Further Developments and Applications of the Stiffness Method," Matrix Methods of Structural Analysis. A Precise of Recent Developments, AGARDograph 72, Ed. deVeubeke, Pergamon Press, 1964.
- 48. Davis, C. L., "Iterative Solutions of Plane Elastostatic Problems," Ph.D., Dissertation, Michigan State Univ., 1965.
- 49. Wilson, E. L., "Matrix Analysis of Non-Linear Structures,"
 Proceeding, ASEE 2nd Conference on Electronic Computation,
 Pittsburgh, Pa., September 1960.
- 50. Martin, H. C., "Truss Analysis by Stiffness Considerations," Journal of Engineering, Mech. Div., ASCE, October 1956.
- 51. Przemieniecki, J. S., "Triangular Plate Elements in the Matrix Force Method of Structural Analysis," (TN), AIAA Journal, Vol. 1, No. 8, August 1963.
- 52. Irons, B. M., "Engineering Applications of Numerical Integration in Stiffness Methods," AIAA Journal, Vol. 4, No. 11, November, 1966, pp. 2035-2037.

- 53. Lasker, G. L., "Derivation of an Arbitrary Triangular Plate Bending Stiffness Matrix and its Application to Large Deflection Shell Problems," Ph.D., Dissertation, Michigan State Univ., 1966.
- 54. Argyris, J. H., "On the Analysis of Complex Elastic Structures," Applied Mechanics Reviews, Vol. II, No. 7, July, 1958.
- 55. Gallagher, R. H. Padlog, J., Bijlaard, B. P., "Stress Analysis of Heated Complex Shapes," ARS Journal, 32, May 1962, pp. 700-707.
- 56. Pian, T. H. H., "Derivation of Element Stiffness Matrices," AIAA Journal, Vol. 2, 1964, pp. 576-577.
- 57. Przemieniecki, J. S., "Tetrahedron Elements in the Matrix Force Method of Structural Analysis," AIAA Journal, Vol. 2, No. 6, June 1964.
- 58. Pian, T. H. H., "Derivation of Element Stiffness Matrices by Assumed Stress Distributions," AIAA Journal, (TN), Vol. II, No. 7, July 1964, pp. 1333-1336.
- 59. Holister, G. S., and Thomas, C., <u>Fibre Reinforced Materials</u>, Elsevier Publishing Co., New York 1966.
- 60. Love, A. E. H., A Treatise on the Mathematical Theory of Elasticity, Dover Publications, New York, 1944.



Appendix A

ADDITIONAL RESULTS

Additional results were made reference to in Chapter V with regard to displacements for the composite cylinder problem. These results follow immediately.

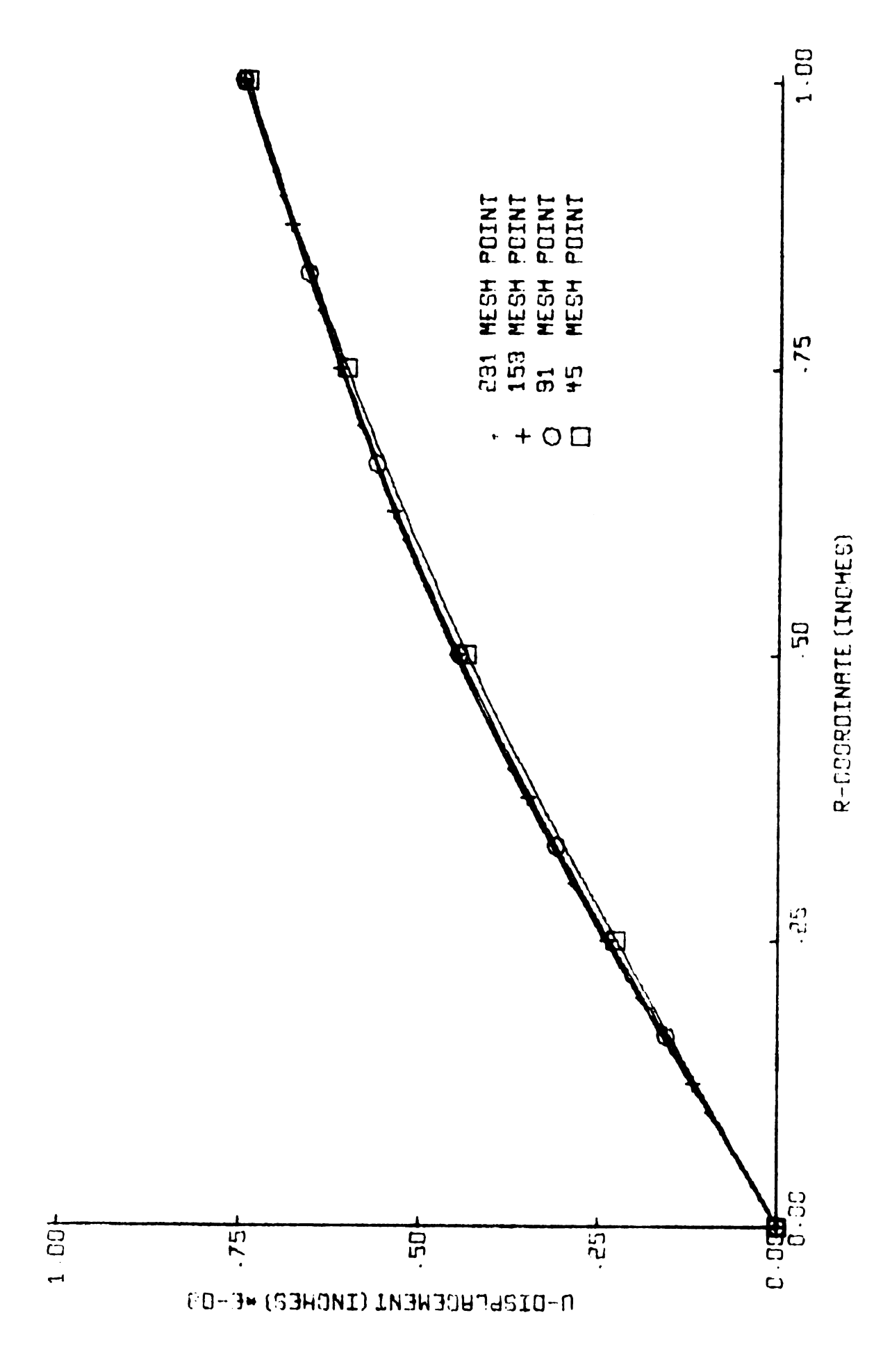


Figure Al., FD Cylinder End u-Displacements

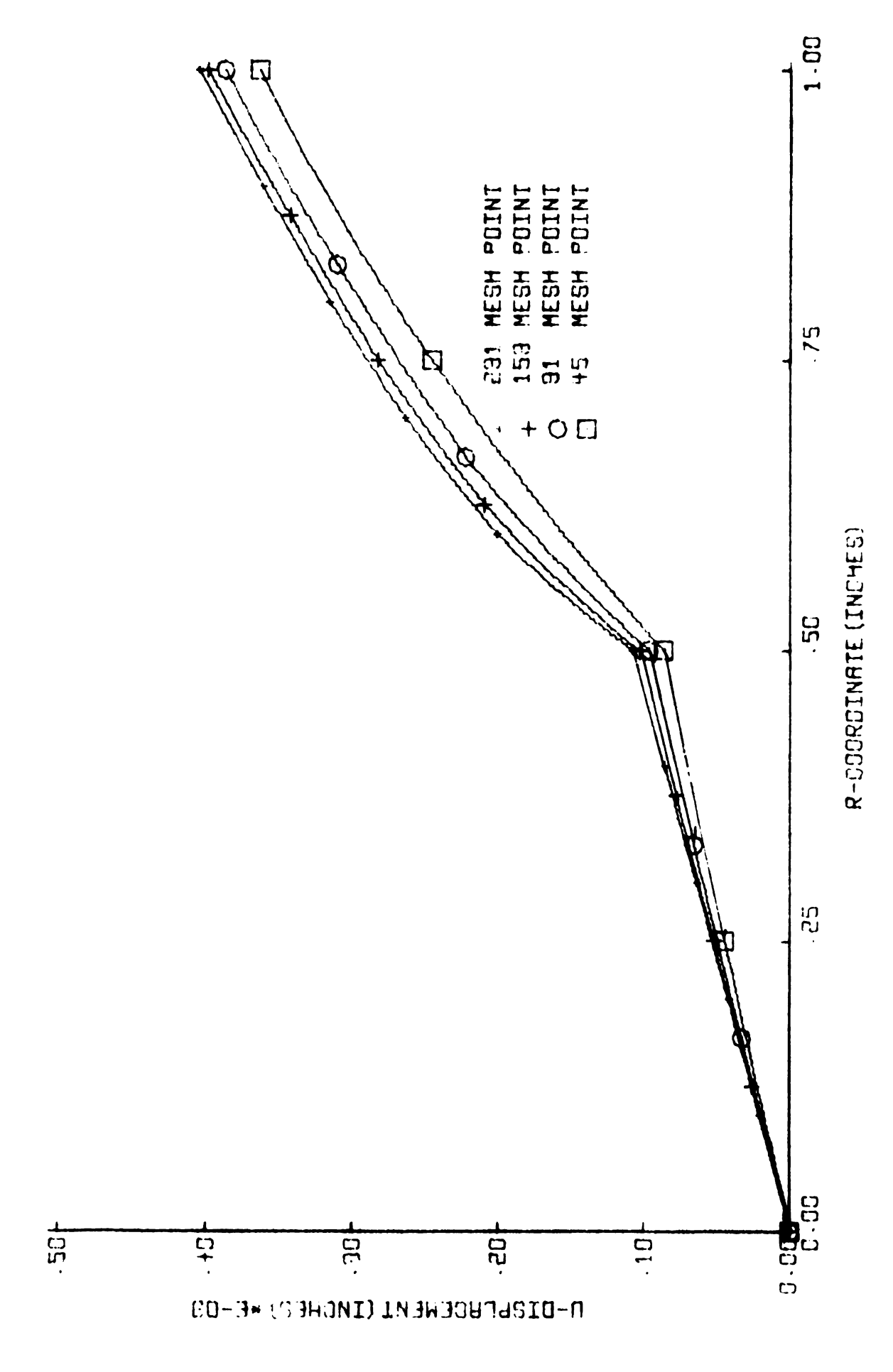


Figure A2., FD Horizontal Interface u-Displacements

3.1833(45) 3.1775(91) 3.1694(153) 3.1622(231)	3.0569(45) 3.1177(153)	3.1360(45) 3.1947(91) 3.2207(153) 3.2345(231)	3.2643(45) 3.3432(153)	3.3417 (45) 3.3983 (91) 3.4237 (153) 3.4374 (231)
2.9778(E) 3.0513(E) 3.0811(E) 3.0957(E)				
1.6724 1.6965 1.7111 1.7202	1.7076 1.7675	1.8414 1.9034 1.9327 1.9486	2.0729 2.1458	2.2049 2.2507 2.2701 2.2803
.2735	.2932	.3834	1.0338	1.2591
.2610 .2555 .2528	.2772	.3873 .3909 .3937	1.1083	1.3162 1.3410 1.3540
.1499 .1474 .1465 .1459	.1595 .1567	.1835 .1804 .1785 .1774	.4212 .4419	.5288 .5509 .5610 .5665
		(45) - 45 Poi (91) - 91 Poi (153) - 153 I	int FD Point FD	
		(231) - 231 H (E) - Extrapo		

Figure A3.

FD Axial Displacements

	2260(45) 2398(153)	4372(45) 4477(91) 4516(153) 4534(231)	6057(45) 6145(153)	7451(45) 7503(91) 7511(153) 7511(231)
	1850 1934	3639 3743 3785 3806	5130 5261	6371 6459 6497 6516
	0453 0528	0874 0974 1039 1082	2465 2832	3649 3884 4002 4068
(45) - 45 Point (91) - 91 Point (153) - 153 Poi (231) - 231 Poi	FD nt FD	0338 0313 0304 0300	0706 0714	1523 1578 1603 1617
(231) - 231 POI	0162 0162	0361 0358 0357 0357	0590 0588	1233 1265 1280 1287

Figure A4.

FD Radial Displacements

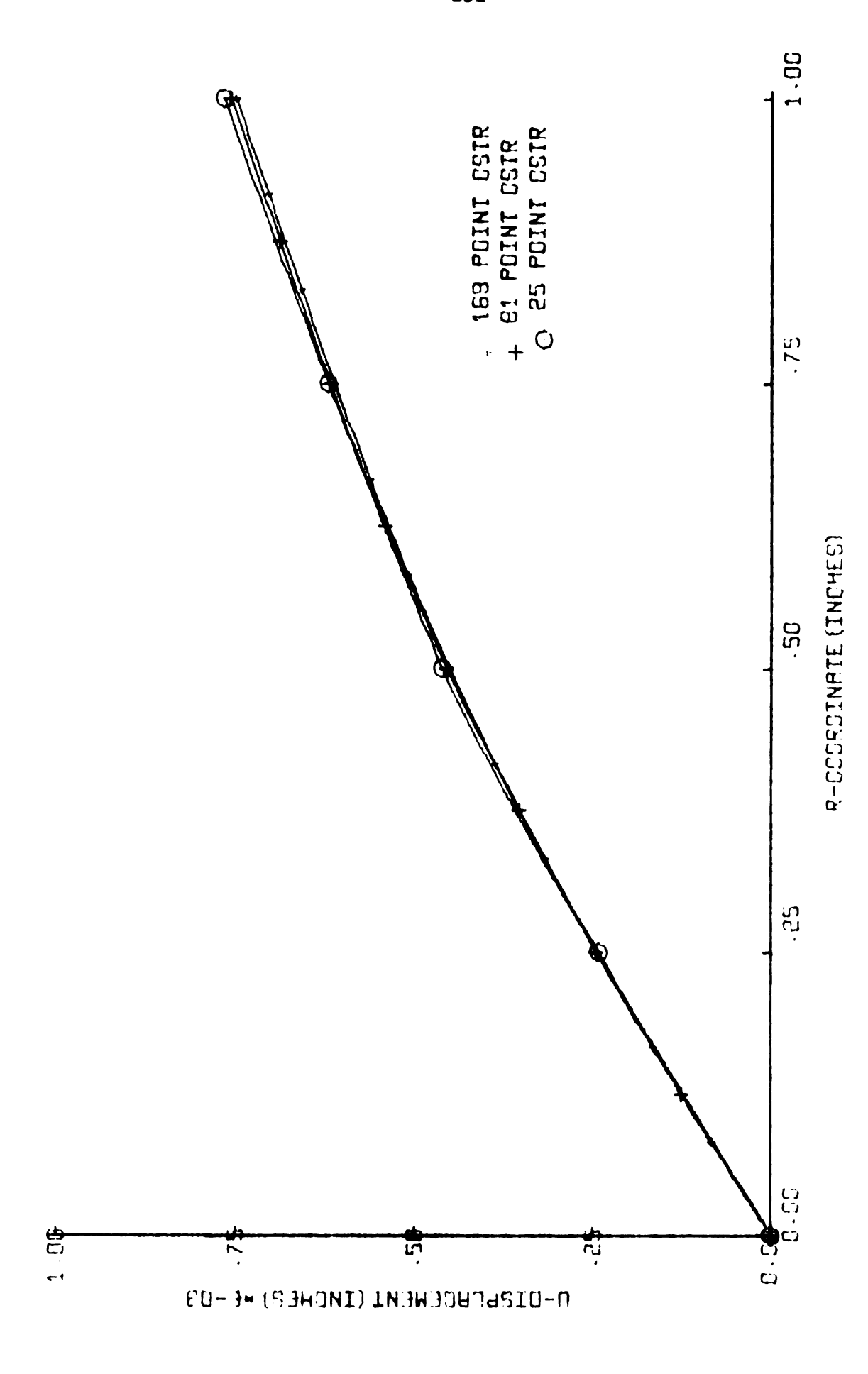


Figure A5., CSTR Cylinder End u-Displacements

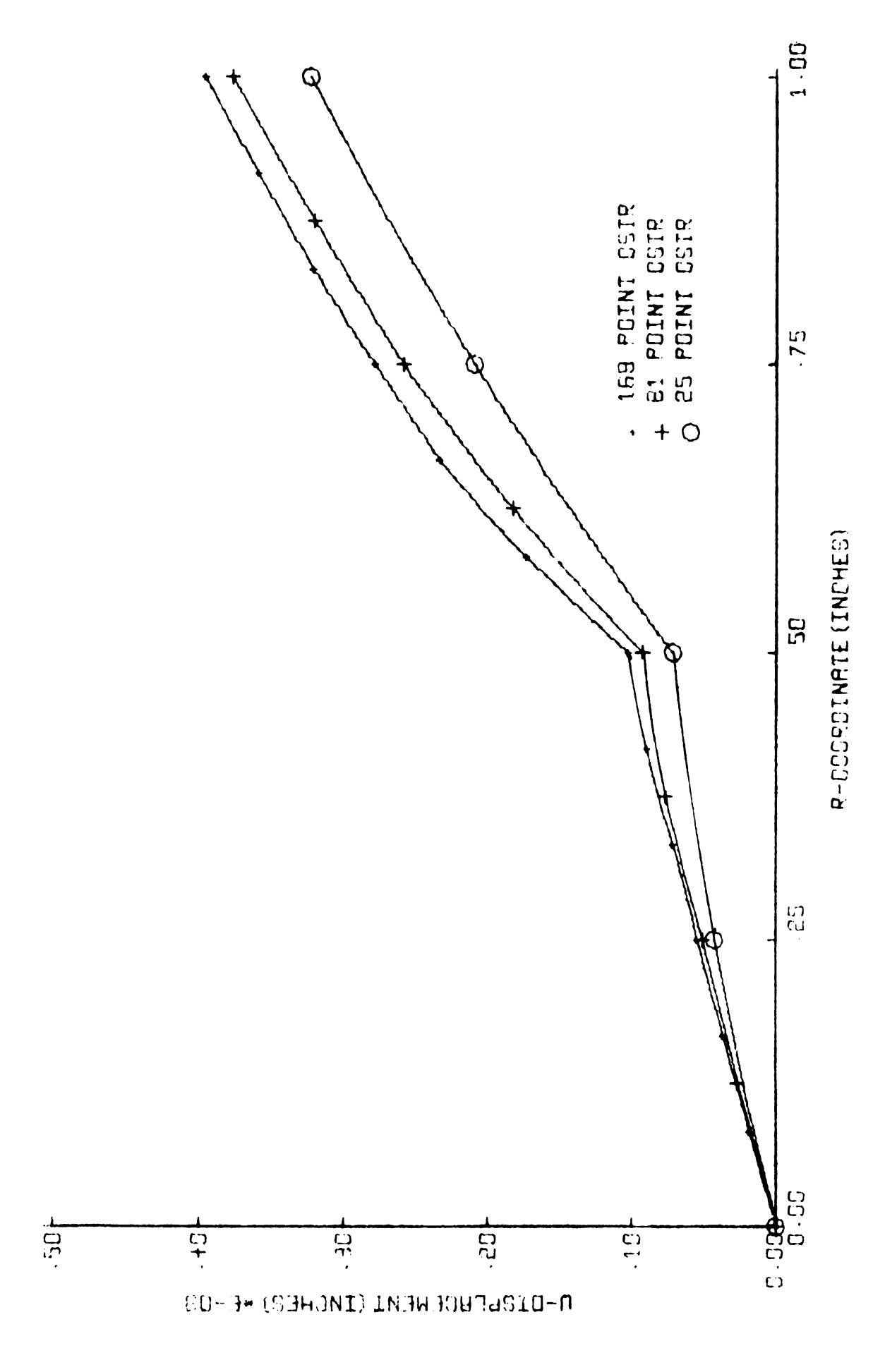


Figure A6., CSTR Horizontal Interface u-Displacements

2.9025(25)	2.9702(25)	3.0893(25)	3.2400(25)	3.3340(25)
3.0339(81)	3.0848(81)	3.1992(81)	3.3272(81)	3.4171(81)
3.0669(169)	3.1168(169)	3.2239(169)	3.3424(169)	3.4293(169)
1.6038	1.6149	1.7894	2.0349	2.1929
1.6767	1.7359	1.9117	2.1264	2.2594
1.7052	1.7666	1.9396	2.1482	2.2731
.2747	.3114	.3883	.9873	1.2031
.2528	.2806	.3890	1.0877	1.3208
.2469	.2778	.3924	1.1121	1.3475
.1508	.1609	.1881	.4018	.5139
.1468	.1582	.1798	.4336	.5505
.1446	.1565	.1770	.4418	.5635
		(25) - 25 Pos (81) - 81 Pos (169) - 169 I	int CSTR	

Figure A7.
CSTR Axial Displacements

 .2434(25)	4637(25)	6228(25)	7696(25)
.2464(81)	4563(81)	6213(81)	7601(81)
.2445(169)	4529(169)	6143(169)	7532(169)
 .1684	3417	5230	6393
.1883	3802	5253	6480
.1937	3779	5272	6484
 .0434	0728	2102	3242
.0517	0937	2556	3785
.0554	1034	2796	3979
 STR	0379 0278 0299	0369 0666 0679	1354 1555 1606
 .0158 .0159 .0164	0317 0355 0355	0752 0565 0601	

Figure A8.

CSTR Radial Displacements

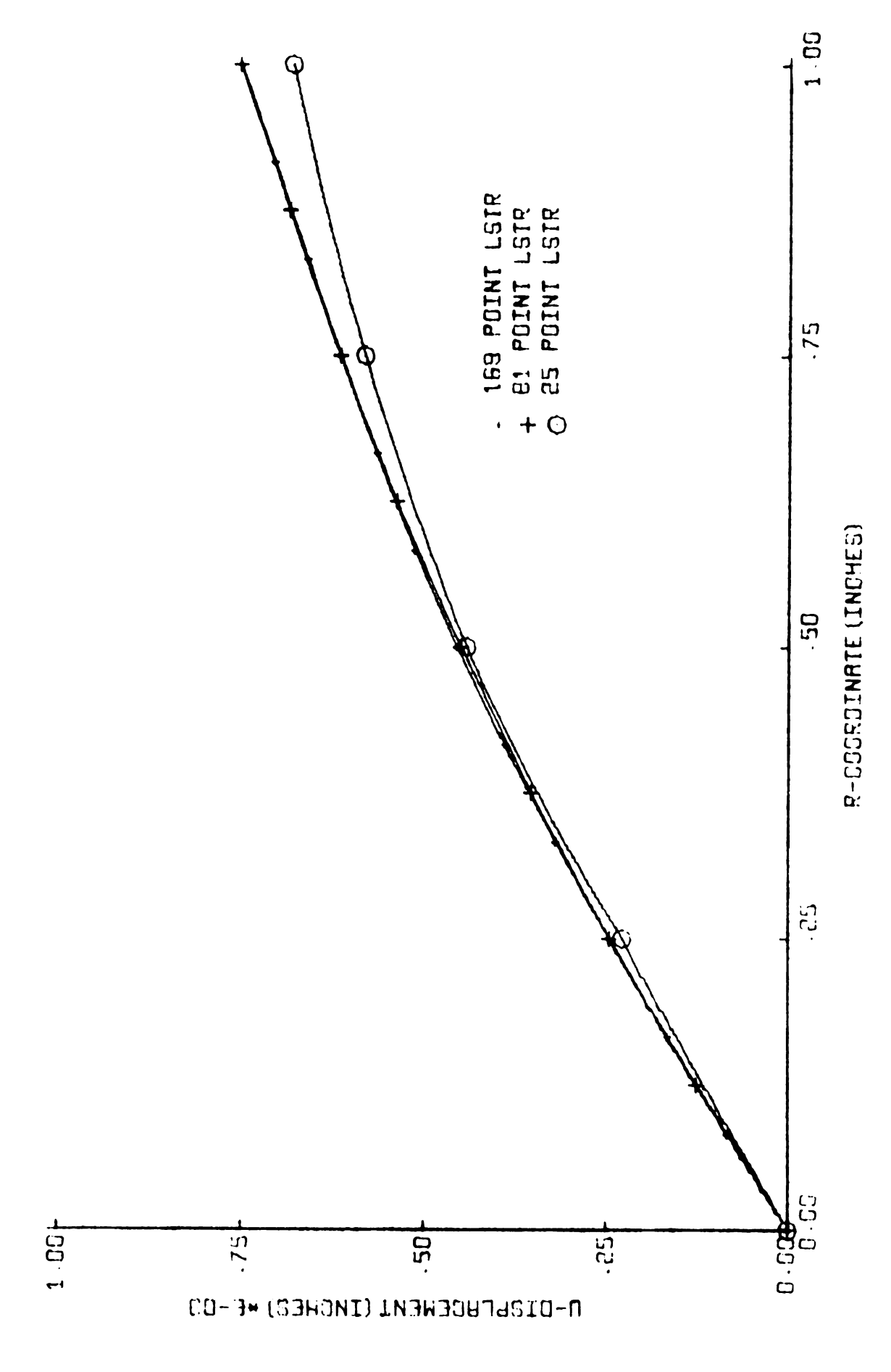


Figure A9., LSTR Cylinder End u-Displacements

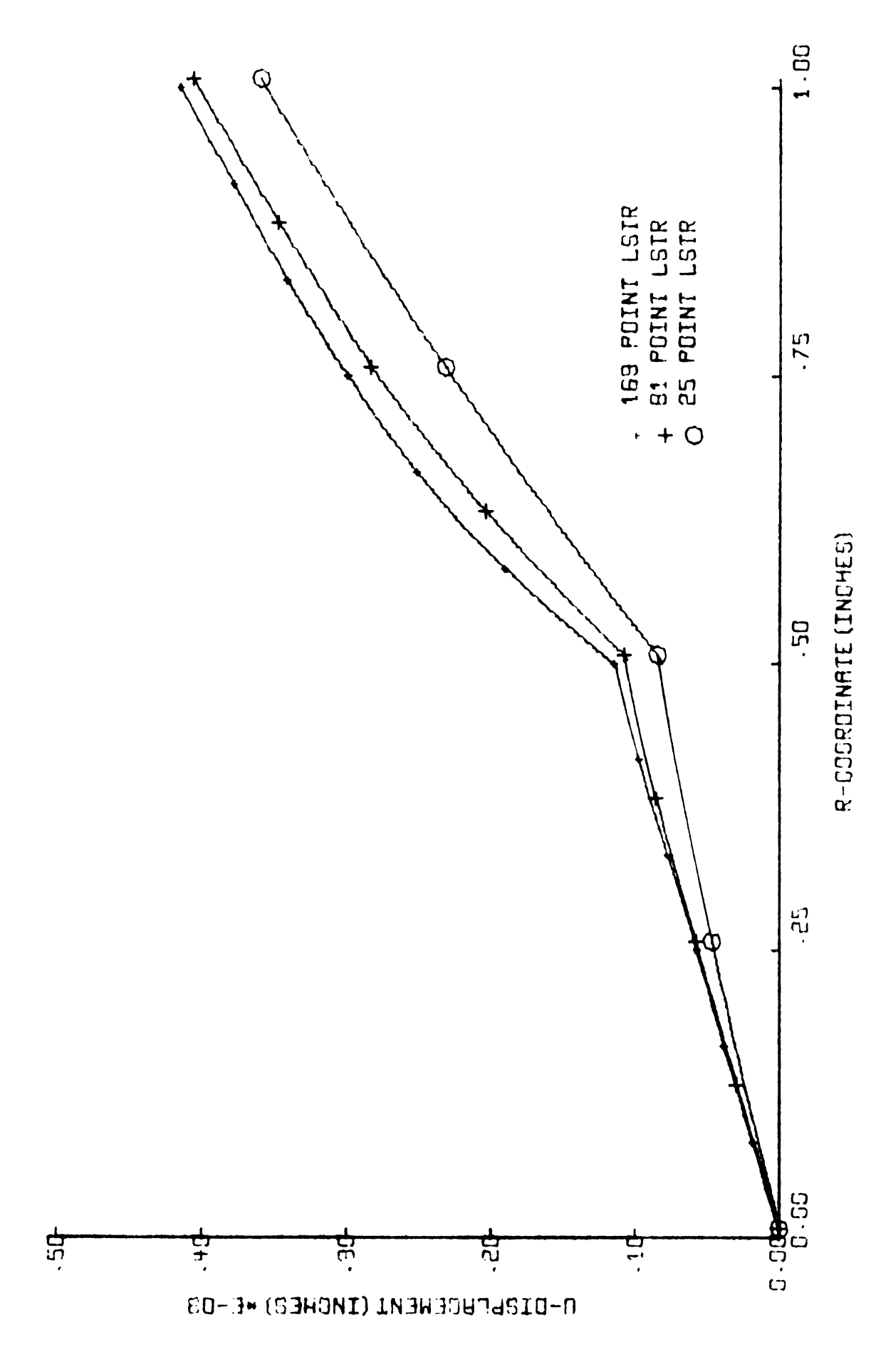


Figure AlO., LSTR Horizontal Interface u-Displacements

3.0776(25)	3.0990(25)	3.2123(25)	3.3144(25)	3.3264(25)
3.0859(81)	3.1389(81)	3.2434(81)	3.3615(81)	3.4493(81)
3.1024(169)	3.1503(169)	3.2600(169)	3.3796(169)	3.4669(169)
1.6273	1.7008	1.8652	2.1016	2.2481
1.7140	1.7871	1.9631	2.1611	2.2837
1.7358	1.7985	1.9759	2.1804	2.3002
.2672	.2928	.3850	1.0248	1.3382
.2342	.2733	.3962	1.1290	1.3750
.2454	.2694	.4017	1.1440	1.3820
.1397	.1497	.1836	.4192	.5496
.1450	.1608	.1732	.4462	.5676
.1456	.1561	.1755	.4520	.5828
		(25) - 25 Poi (81) - 81 Poi (169) - 169 P	nt LSTR	

Figure All.

LSTR Axial Displacements

	2297(25) 2463(81) 2467(169)	4438(25) 4512(81) 4568(169)	5831(25) 6180(81) 6169(169)	6830(25) 7540(81) 7548(169)
	1857 2007	3721 3873	5503 5253	6729 6497
	 1991	3860	 5314	6540
	0476	0856	2328	3609
	0588 0582	1087 1157	2482 3004	4075 4164
	0108	0331	 0555	1419
	0115 0105	0277 0291	0704 0726	1620 1648
(25) - 25 Point (81) - 81 Point (169) - 169 Poi	t LSTR			
	0145 0164	0330 0365	0575 0588	1514 1306
	0165	0359	 0579	1 340

Figure Al2.

LSTR Radial Displacements

Appendix B

COMPUTER PROGRAMS

The computer programs which were used in the analysis of axially symmetric problems by the difference method and by the LSTR finite element method are presented on the following pages. Included is a brief description of each program, the program itself, and sample data. The output of each program tends to be excessive and consequently is not presented.

FINITE DIFFERENCE PROGRAM

FOR AXIALLY SYMMETRIC ANALYSIS

The axially symmetric finite difference analysis involves 3 main steps: (1) generate equilibrium equations, (2) solve the system of algebraic equations for displacements, and (3) calculate stresses. It is possible to obtain mesh point loads directly as part of the computer analysis, but this is not a feature of the present program. Mesh point loads must be computed outside the program and are thus handled as input information.

The equations of section 2.9, namely (2.62), are the equilibrium equations related to the first step in the analysis. In the original program (included here), these were coded in a more simplified form with h = k and $\nu = \frac{1}{4}$. It is not difficult to remove these restrictions. The coding of the equations is accomplished in terms of 4 subroutines called COFNE, COFNW, COFSW, and COFSE. Then for each mesh point, one or more of these routines is executed depending on whether the point is an interior point or any of a number of types of boundary points. This necessitates the classification of mesh points and the assignment of a coding number for each type. The classification used here is presented in Table B1 on pages 262 and 263. In certain applications involving symmetry with respect to the r - θ plane, equilibrium equations for points in the r - θ plane are obtained from two additional subroutines called SYMNSE and SYMNSW.

The input information to the computer consists of mesh point identification numbers and material properties. Generally speaking, it is also necessary to provide information indicating which points are immediately around a given mesh point. For rectangular applications, this is done automatically in a subroutine called COORD.

The coefficient matrix for the system is very sparesely populated. In fact, no row of the matrix has more than 18 non-zero entries. The equations are solved by a modified Gauss Seidel Iterative procedure in which only non-zero coefficients are stored in the computer memory. A location array is also required to identify the displacement associated with a given coefficient of the matrix.

The final step in the analysis involves the computation of stresses. For each interior point, for example, 4 sets of stresses are computed corresponding to equations (259). The stresses for the mesh point are taken to be the average of these sets of stresses.

The simplified computer program for this analysis follows beginning on page 264. A list of Fortran Symbols used is given on pages 274 and 275. Sample data for the program is presented on page 276 and 277.

Table B-1
Finite Difference Mesh Point Coding

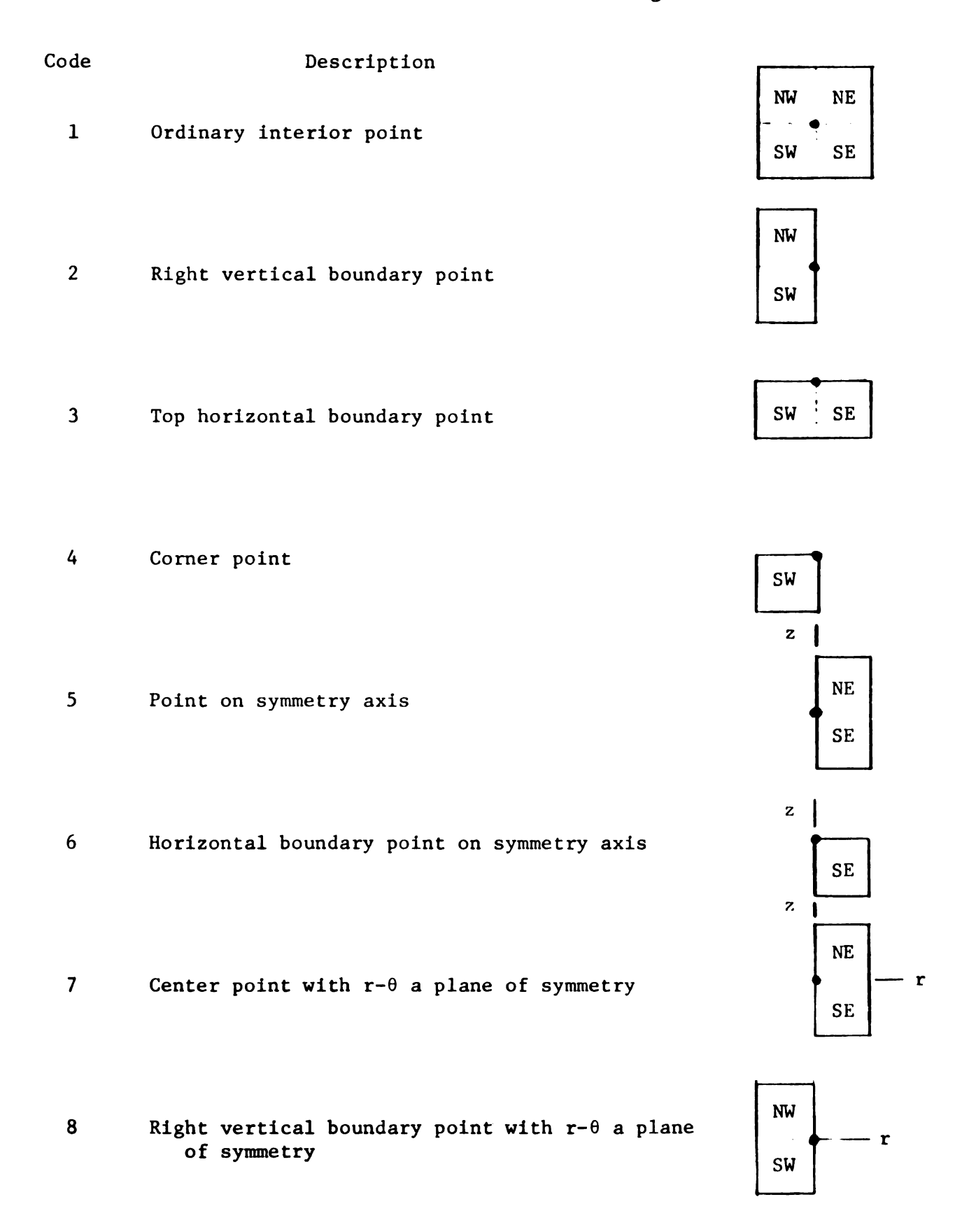
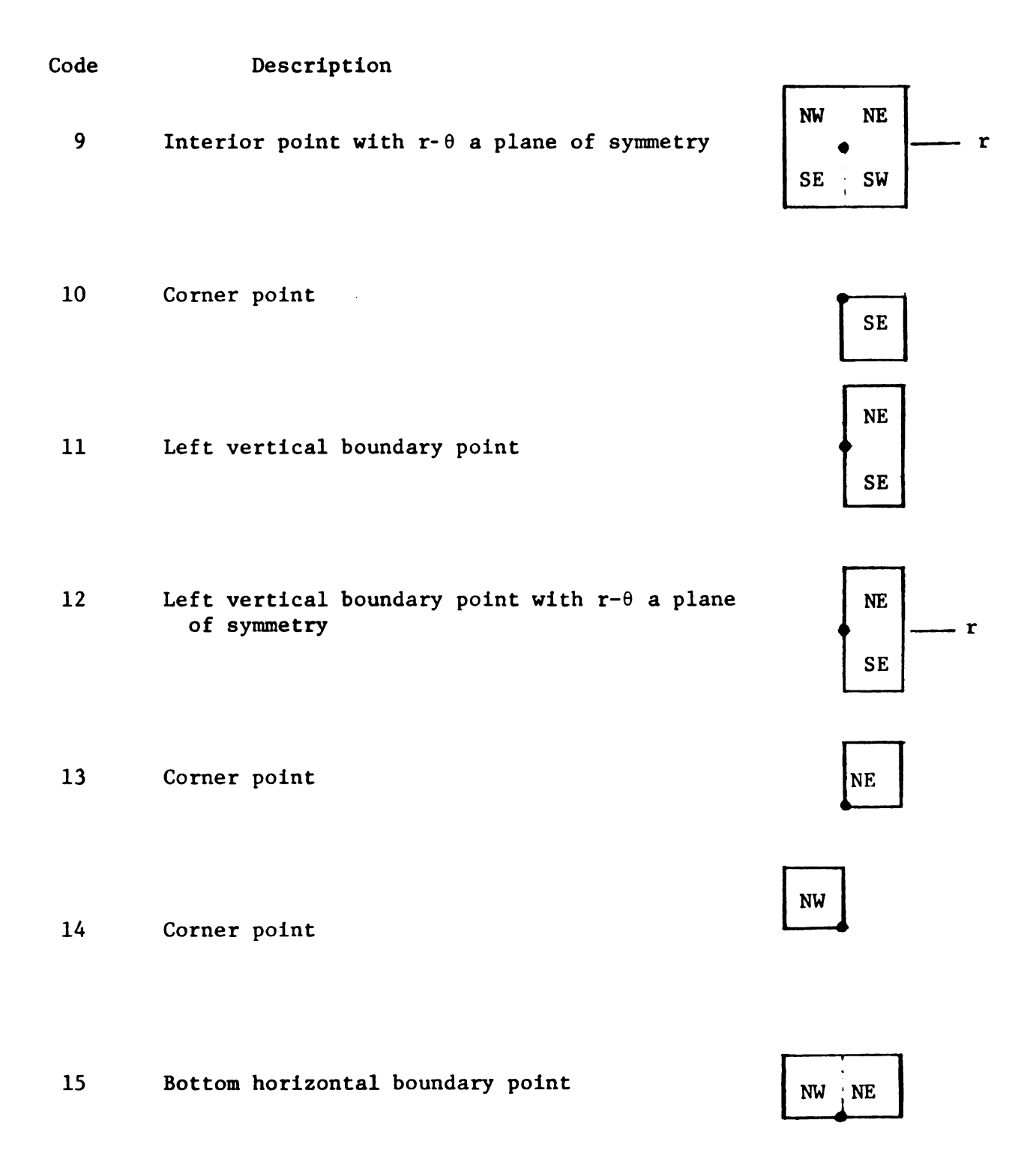


Table B-1 (Continued)



AXIALLY SYMMETRIC FINITE DIFFERENCE PROGRAM

```
PROGRAM AXSFD
C
      FINITE DIFFERENCE PROGRAM FOR AXISYMMETRIC
C
      ELASTOSTATIC PROBLEMS
      DIMENSION RR(231), E(231,4)
      COMMON S(462,18),NC(231,9),NTYP(231),U(462),N,N2,H,C1,
     1SRR(231),SZZ(231),STT(231),SRZ(231),KAD(231),SZR(231)
C
      FORMAT STATEMENTS
  100 FORMAT(8F10.1)
   51 FORMAT(915,4E18.6)
   47 FORMAT(8F10.6)
   41 FORMAT (915,4F8,5)
   36 FORMAT(1615)
C
      READ IN DATA
   74 READ 36.N.NOUT.KDAT
      IF(EDF,60)71,70
   70 READ 47.H.C1
      PRINT 36,N,NOUT,KDAT
      PRINT 47.H.C1
      N2=2*N
      READ 36, (NTYP(I), I=1, N)
      PRINT 36, (NTYP(I), I=1,N)
      GO TO(87,88)KDAT
C
      GENERATE MESH POINT DATA
   88 CALL COORD
      READ 100,((E(I,J), J=1,4), I=1,N)
      GO TO 89
   87 DO 39 I=1.N
   39 READ 41, (NC(I,J), J=1,9), (E(I,J), J=1,4)
   89 DO 99 I=1.N
   99 PRINT 51, (NC(I,J),J=1,9), (E(I,J),J=1,4)
      READ 47 \cdot (RR(I) \cdot I=1 \cdot N)
      PRINT 47, (RR(I), I=1,N)
C
       INITIALIZE COEFFICIENT ARRAY
      DO 31 I=1,N2
      DO 31 J=1,18
   31 S(I,J)=0.
C
      DEFINE COEFFICIENTS
      DO 60 J=1,N
      KEY=NTYP(J)
      I=2*J-1
      I1=2*J
      R = RR(J)
      GO TO(1,2,3,3,1,4,5,6,5,4,1,5,1,2,1),KEY
  IF X<1
    1 \text{ EM} = \text{E}(J \cdot 1)
      CALL COFNE(I, I1, EM, R)
      GO TO(2,60,60,60,4,60,60,60,60,4,60,60,60,2),KEY
    2 EM=E(J,2)
      CALL COFNW(I, II, EM, R)
      3 \text{ EM}=E(J,3)
      CALL COFSW(I, I1, EM, R)
```

```
GO TO (4,60,4,60,60,60),KEY
  4 EM=E(J,4)
    CALL COFSE(I, II, EM, R)
    GO TO 60
 5 EM=E(J.1)
    CALL SYMNSE(I, II, EM, R)
    GD TD(60,60,60,60,60,60,60,60,60,60,60),KEY
  6 EM=E(J,2)
    CALL SYMNSW(I, II, EM, R)
 60 CONTINUE
    IF(NOUT)77,78,77
 77 NO 75 I=1.N
    PRINT 36, (NC(I,J),J=1,9)
    PRINT 76, (S(2*I-1,J),J=1,18)
 75 PRINT 76, (S(2*I,J), J=1,18)
 76 FORMAT(4E20.8)
    GAUSS SEIDEL OVER RELAXATION PROCEDURE
 78 CALL FDIFF
    STRESS CALCULATIONS
    DO 90 I=1.N
    SRR(I)=0.
    SZZ(I)=0.
    STT(I)=0.
    SRZ(I)=0.
    SZR(I)=0.
90 KAD(I)=0
    00.50 I = 1.N
    KEY=NTYP(I)
    60 \ TO \ (101,102,103,103,101,104,101,102,101,104,101,101
   1,101,102,101),KEY
101 CALLSTNE(I, E(I, 1), RR(I))
    GO TO (102,50,50,50,104,50,50,102,50,104,104,50,50,
   1102) • KEY
102 CALLSTNW(I, E(I, 2), RR(I))
    GO TO (103,103,50,50,50,50,50, 50,50,50,50,50,50,50,50,
   150) • KEY
103 CALLSTSW(I, E(I, 3), RR(I))
    GO TO (104,50,104,50,50,50,50,50,50,50,50,50),KEY
104 CALLSTSE(I, E(I, 4), RR(I))
 50 CONTINUE
    COMPUTE AVERAGE STRESSES
    DO 91 I=1.N
    SAD=KAD(I)
    SRR(I) = SRR(I) / SAD
    SZZ(I) = SZZ(I)/SAD
    STT(I) = STT(I) / SAD
    SRZ(I) = SRZ(I)/SAD
 91 SZR(I)=SZR(I)/SAD
    PRINT 94
 94 FORMAT(///17H AVERAGE STRESSES)
    DO 92 I=1.N
 93 FORMAT(15,4E15.3)
    SHEAR=(SRZ(I)+SZR(I))/2.
 92 PRINT 93, I, SRR(I), SZZ(I), STT(I), SHEAR
```

C

C

C

```
GO TO 74
71 STOP
   END
   SUBROUTINE COORD
   DIMENSION RR(231), E(231,4)
   COMMON S(462,18),NC(231,9),NTYP(231),U(462),N,N2,H,C1,
  1SRR(231), SZZ(231), STT(231), SRZ(231), KAD(231), SZR(231)
   READ 41,KX
41 FORMAT (615)
   PRINT 41.KX
   DO 90 I=1.N
   NC(I \cdot I) = I
   KEY=NTYP(I)
   D0 64 J=2.9
64 NC(I_{*}J_{*}=0
   GD TD (91,92,93,94,99,95,96,97,98,95,99,96,96,97,98)
  1,KEY
94 NC(I,4)=I-1
   NC(I,5) = I + KX
   NC(I,8) = I + KX - 1
   GO TO 90
91 NC(I,2) = I+1
   NC(I,3) = I - KX
   NC(I.4) = I-1
   NC(I,5) = I + KX
   NC(I,6)=I-KX+1
   NC(I,7) = I - KX - 1
   NC(I,8) = I + KX - 1
   NC(I,9) = I + KX + 1
   GO TO 90
92 NC(I,3) = I - KX
   NC(1,4)=1-1
   NC(I,5) = I + KX
   NC(I,7) = I - KX - 1
   NC(I,8) = I + KX - 1
   GO TO 90
93 NC(I \cdot 2) = I + 1
   NC(I,4) = I-1
   NC(I,5) = I + KX
   NC(I,8) = I + KX - 1
   NC(I,9) = I + KX + I
   GO TO 90
95 NC(I_{1}2)=I+1
   NC(I,5) = I + KX
   NC(I,9) = I + KX + 1
   GO TO 90
96 NC(I_{1}2)=I+1
   NC(I.3) = I - KX
   NC(I,6) = I - KX + 1
   GO TO 90
98 NC(I_{+}2)=I+1
   NC(I,3) = I - KX
   NC(I,4) = I-1
   NC(I,6) = I - KX + 1
   NC(I,7)=I-KX-1
```

```
GO TO 90
99 NC(I,2)=I+1
   NC(I,3) = I - KX
   NC(I,5)=I+KX
   NC(I,6) = I - KX + 1
   NC(I,9) = I + KX + 1
   GO TO 90
97 \text{ NC}(I.3) = I-KX
   NC(I,4) = I-1
   NC(I,7) = I - KX - 1
90 CONTINUE
   RETURN
   END
   SUBROUTINE COFNE(I, II, E, R)
   COMMON S(462,18),NC(231,9),NTYP(231),U(462),N,N2,H,C1,
  1SRR(231),SZZ(231),STT(231),SRZ(231),KAD(231),SZR(231)
   Q=H/R
   S(I_{\bullet}I) = S(I_{\bullet}I) + (4_{\bullet} + {\bullet} 75 * Q + 1_{\bullet}5 * Q * * 2) * E
   S(I,2)=S(I,2)+(1.-.125*Q)*E
   S(I,3)=S(I,3)-(3.+1.5*0)*E
   S(I,4)=S(I,4)+.125*Q*E
   S(I,5)=S(I,5)-(1.+.25*Q)*E
   S(I,6)=S(I,6)+.375*Q*E
   S(I,12)=S(I,12)-(1.+.375*Q)*E
   S(11,1)=S(11,1)+(1.+.125*Q)*E
   S(I1,2)=S(I1,2)+(4.+1.25*Q)*E
   S(I1,3)=S(I1,3)-.125*Q*E
   S(I1,4)=S(I1,4)-(1.+.5*Q)*E
   S(I1,5)=S(I1,5)-.375*Q*E
   S(I1,6)=S(I1,6)-(3.+.75*Q)*E
   S(I1,11)=S(I1,11)-(1.+.625*Q)*E
   RETURN
   END
   SUBROUTINE COFNW(I, I1, E,R)
   COMMON S(462,18),NC(231,9),NTYP(231),U(462),N,N2,H,C1,
  1SRR(231),SZZ(231),STT(231),SRZ(231),KAD(231),SZR(231)
   S(I,1)=S(I,1)+(4.-.75*Q+1.5*Q**2)*E
   S(1,2)=S(1,2)-(1.+.125*Q)*E
   S(I,5)=S(I,5)-(1.-.25*0)*E
   S(I,6)=S(I,6)+.375*Q*E
   S(I,7)=S(I,7)-(3.-1.5*Q)*E
   S(I.8)=S(I.8)+.125*Q*E
   S(I_{1}14)=S(I_{1}14)+(1_{0}-375*Q)*E
   S(I1,1)=S(I1,1)-(1.-.125*Q)*E
   S(I1,2)=S(I1,2)+(4,-1,25*Q)*E
   S(I1,5)=S(I1,5)-.375*Q*E
   S(I1,6)=S(I1,6)-(3.-.75*0)*E
   S(I1,7)=S(I1,7)-.125*Q*E
   S(I1,8)=S(I1,8)-(1.-.5*Q)*E
   S(11.13)=S(11.13)+(1.-.625*Q)*E
   RETURN
   END
   SUBROUTINE COFSW(I, II, E,R)
```

```
CDMMON S(462,18),NC(231,9),NTYP(231),U(462),N,N2,H,Cl,
1SRR(231),SZZ(231),STT(231),SRZ(231),KAD(231),SZR(231)
 Q=H/R
 S(I,1)=S(I,1)+(4.-.75*Q+1.5*Q**2)*E
 S(I,2)=S(I,2)+(1.+.125*Q)*E
 S(I,7)=S(I,7)-(3,-1,5*Q)*E
 S(I,8)=S(I,8)-.125*Q*E
 S(I,9)=S(I,9)-(1.-.25*Q)*E
 S(I \cdot 10) = S(I \cdot 10) - .375 * 0 * E
 S(I_{\bullet}16) = S(I_{\bullet}16) - (1_{\bullet} - {\bullet}375*Q)*E
 S(I1,1)=S(I1,1)+(1.-.125*Q)*E
 S(I1,2)=S(I1,2)+(4.-1.25*Q)*E
 S(I1,7)=S(I1,7)+.125*Q*E
 S(I1.8)=S(I1.8)-(1.-.5*Q)*E
 S(I1.9)=S(I1.9)+.375*Q*E
 S(I1.10)=S(I1.10)-(3.-.75*0)*E
 S(I1,15)=S(I1,15)-(1.-.625*Q)*E
 RETURN
 END
 SUBROUTINE COFSE(I, II, E, R)
 COMMON S(462,18),NC(231,9),NTYP(231),U(462),N,N2,H,C1,
1SRR(231),SZZ(231),STT(231),SRZ(231),KAD(231),SZR(231)
 Q=H/R
 S(I_{\bullet}I) = S(I_{\bullet}I) + (4_{\bullet} + {\bullet} 75 * Q + 1_{\bullet} 5 * Q * * 2) * E
 S(I,2)=S(I,2)-(1,-.125*Q)*E
 S(I,3)=S(I,3)-(3.+1.5*Q)*E
 S(I,4)=S(I,4)-.125*Q*E
 S(I,9)=S(I,9)-(I_0+0.25*Q)*E
 S(I,10)=S(I,10)-.375*Q*E
 S(I,18)=S(I,18)+(1.+.375*Q)*E
 S(I1,1)=S(I1,1)-(1.+.125*Q)*E
 S(I1,2)=S(I1,2)+(4.+1.25*Q)*E
 S(I1,3)=S(I1,3)+.125*Q*E
 S(I1.4)=S(I1.4)-(1.4.5*Q)*E
 S(I1.9)=S(I1.9)+.375*Q*E
 S(I1.10)=S(I1.10)-(3.+.75*0)*E
 S(I1,I7)=S(I1,I7)+(I.+.625*Q)*E
 RETURN
 END
 SUBROUTINE SYMNSE (I, II, E, R)
 COMMON S(462,18),NC(231,9),NTYP(231),U(462),N,N2,H,C1,
1SRR(231),SZZ(231),STT(231),SRZ(231),KAD(231),SZR(231)
 Q=H/R
 S(I,1)=S(I,1)+(8.+1.5*Q+3.*Q**2)*E
 S(I,3)=S(I,3)-(6.+3.*Q)*E
 S(I,5)=S(I,5)-(2.+.5*Q)*E
 S(I,12)=S(I,12)-(2.+.75*Q)*E
 S(I,6)=S(I,6)+.75*Q*E
 S(I1,2)=S(I1,2)+(8.+2.5*Q)*E
 S(I1,4)=S(I1,4)-(2.+Q)*E
 RETURN
 END
 SUBROUTINE SYMNSW (I, II, E, R)
 COMMON S(462,18),NC(231,9),NTYP(231),U(462),N,N2,H,C1,
1SRR(231),SZZ(231),STT(231),SRZ(231),KAD(231),SZR(231)
```

```
Q=H/R
      S(I,1)=S(I,1)+(8,-1,5*Q+3,*Q**2)*E
      S(1,7)=S(1,7)-(6.-3.*Q)*E
      S(I_{\bullet}5)=S(I_{\bullet}5)-(2_{\bullet}-.5*0)*E
      S(I,6)=S(I,6)+.75*Q*E
      S(I,14)=S(I,14)+(2.-.75*Q)*E
      S(I1,2)=S(I1,2)+(8,-2,5*Q)*E
      S(I1.8) = S(I1.8) - (2.-0) *E
      RETURN
      FND
      SUBROUTINE FDIFF
      DIMENSION F(462), LL(462)
      COMMON S(462,18),NC(231,9),NTYP(231),U(462),N,N2,H,C1,
     1SRR(231),SZZ(231),STT(231),SRZ(231),KAD(231),SZR(231)
C
       SIMULTANEOUS EQUATIONS
C
      GAUSS SEIDEL OVER RELAXATION METHOD
C.
      THIS PROGRAM IS INTENDED FOR FINITE DIFFERENCE EQUATIONS
      READ 47, BETA, CON
      READ 47.(F(I).I=1.N2)
      PRINT47, (F(I), I=1, N2)
   47 FURMAT(8F10.0)
   46 FORMAT(4012)
      READ 46, (LL(I), I=1,N2)
      PRINT46,(LL(I), I=1,N2)
      KK = 0
      READ 200, INIT, KIT
  200 FORMAT(1615)
      IF(INIT)201,202,201
  201 READ 899, (U(I), I=1,N2)
      GO TO 32
  202 DO 2 I=1,N2
    2 U(I) = 0.
   32 DIFF=0.0
      KK = KK + 1
      DO 30 I=1.N
      10=2*1-1
      IE=2*I
      UBAR=F(IO)
      VBAR=F(IE)
      DO 28 J=1.9
      J0 = 2 * J - 1
      JE=2*J
      K=NC(I,J)
      IF( K ) 29,28,29
   29 KO=2*K-1
      KE=2*K
      IF(IO-KO)41,40,41
   41 UBAR=UBAR-S(IO,JO)*U(KO)
   40 UBAR=UBAR-S(IO,JE)*U(KE)
      IF(IE-KE)43,42,43
   43 VBAR=VBAR-S(IE, JE)*U(KE)
   42 VBAR=VBAR-S(IE,JO)*U(KO)
   28 CONTINUE
      UBAR=UBAR/S(IO,1)
```

```
VBAR=VBAR/S(IE,2)
    IF(LL(IO))60,61,60
 61 U1=U(I0)+BETA*(UBAR-U(I0))
    GO TO 62
60 U1=0.
62 IF(LL(IE))63,64,63
 64 V1=U(IE)+BETA*(VBAR-U(IE))
    GO TO 65
 63 V1=0.
 65 UDMAX=ABS (U1-U(IO))
    VDMAX=ABS (V1-U(IE))
    U(10) = U1
    U(IE)=V1
    IF(VDMAX-UDMAX)50,50,51
 51 DMAX=VDMAX
    GO TO 52
 50 DMAX=UDMAX
 52 IF( DMAX-DIFF)30,36,36
 36 DIFF=DMAX
 30 CONTINUE
    KTEN=KK/KIT
    IF(KK-KIT*KTEN)4,8,4
  8 PRINT 58,KK
 58 FORMAT(I10)
    PRINT 54, (U(I), I=1, N2)
 15 FORMAT(17H ITERATION COUNT=110//)
 54 FORMAT (6E20.8)
    PUNCH 899 \cdot (U(I), I=1,N2)
    TEST FOR CONVERGENCE
  4 IF(DIFF-CON) 33,32,32
33 PRINT 35,KK
 35 FORMAT (25H THE NUMBER OF ITERATIONS, //(I10))
    PRINT 34
 34 FORMAT(42H NODAL POINT R-DISPLACEMENT Z-DISPLACEMENT)
    DO 37 I=1,N
    10=2*1-1
    IE=2*I
 37 PRINT 38, I, U(IO), U(IE)
38 FORMAT(112.2E15.6)
    PUNCH 899 (U(I) . I=1,N2)
899 FURMAT (4E20.8)
    PRINT 12
                                         AXIAL STRESS
                        RADIAL STRESS
 12 FORMAT(40H POINT
                                  SHEAR STRESS)
   137HCIRCUMFERENTIAL STRESS
    RETURN
    END
    SUBROUTINE STNE(I, E, R)
    COMMON S(462,18),NC(231,9),NTYP(231),U(462),N,N2,H,Cl,
   1SRR(231), SZZ(231), STT(231), SRZ(231), KAD(231), SZR(231)
    B=H
  1 D=E/((1.+C1)*(1.-2.*C1))
    D1=E/(2.*(1.+C1))
    J\Omega = NC(I,1)*2
    JE=NC(I,2)*2
    JN=NC(I \cdot 3)*2
```

C

```
JNE=NC(1.6)*2
       10 = 10 - 1
        IE=JE-1
        IN=JN-1
       INE=JNE-1
       RR = D*((1.-C1)*(U(IE)-U(IO))/H+C1*(U(IE)+U(IO))/
     1(2.*(R+H/2.))+C1*(U(JN)-U(JO)+U(JNE)-U(JE))/(2.*8))
       TT=D*((1.-C1)*U(ID)/R+C1*(U(IE)-U(ID))/H+
     1C1*(U(JN)-U(JO))/B)
       ZZ=D*((1.-C1)*(U(JN)-U(JO))/B+C1*(U(INE)-
     1U(IN)+U(IE)-U(IO))/(2.*H)+C1*(U(INE)+U(IN)+
     2U(IE)+U(IO))/(4.*(R+.25*H)))
       RZ=D1*((U(JE)-U(JO))/H+(U(INE)-U(IE)+U(IN)-U(IE)+U(IN)-U(IE)+U(IN)-U(IE)+U(IN)-U(IE)+U(IN)-U(IE)+U(IN)-U(INE)-U(IE)+U(IN)-U(INE)-U(IE)+U(INE)-U(INE)-U(INE)-U(INE)-U(INE)-U(INE)-U(INE)-U(INE)-U(INE)-U(INE)-U(INE)-U(INE)-U(INE)-U(INE)-U(INE)-U(INE)-U(INE)-U(INE)-U(INE)-U(INE)-U(INE)-U(INE)-U(INE)-U(INE)-U(INE)-U(INE)-U(INE)-U(INE)-U(INE)-U(INE)-U(INE)-U(INE)-U(INE)-U(INE)-U(INE)-U(INE)-U(INE)-U(INE)-U(INE)-U(INE)-U(INE)-U(INE)-U(INE)-U(INE)-U(INE)-U(INE)-U(INE)-U(INE)-U(INE)-U(INE)-U(INE)-U(INE)-U(INE)-U(INE)-U(INE)-U(INE)-U(INE)-U(INE)-U(INE)-U(INE)-U(INE)-U(INE)-U(INE)-U(INE)-U(INE)-U(INE)-U(INE)-U(INE)-U(INE)-U(INE)-U(INE)-U(INE)-U(INE)-U(INE)-U(INE)-U(INE)-U(INE)-U(INE)-U(INE)-U(INE)-U(INE)-U(INE)-U(INE)-U(INE)-U(INE)-U(INE)-U(INE)-U(INE)-U(INE)-U(INE)-U(INE)-U(INE)-U(INE)-U(INE)-U(INE)-U(INE)-U(INE)-U(INE)-U(INE)-U(INE)-U(INE)-U(INE)-U(INE)-U(INE)-U(INE)-U(INE)-U(INE)-U(INE)-U(INE)-U(INE)-U(INE)-U(INE)-U(INE)-U(INE)-U(INE)-U(INE)-U(INE)-U(INE)-U(INE)-U(INE)-U(INE)-U(INE)-U(INE)-U(INE)-U(INE)-U(INE)-U(INE)-U(INE)-U(INE)-U(INE)-U(INE)-U(INE)-U(INE)-U(INE)-U(INE)-U(INE)-U(INE)-U(INE)-U(INE)-U(INE)-U(INE)-U(INE)-U(INE)-U(INE)-U(INE)-U(INE)-U(INE)-U(INE)-U(INE)-U(INE)-U(INE)-U(INE)-U(INE)-U(INE)-U(INE)-U(INE)-U(INE)-U(INE)-U(INE)-U(INE)-U(INE)-U(INE)-U(INE)-U(INE)-U(INE)-U(INE)-U(INE)-U(INE)-U(INE)-U(INE)-U(INE)-U(INE)-U(INE)-U(INE)-U(INE)-U(INE)-U(INE)-U(INE)-U(INE)-U(INE)-U(INE)-U(INE)-U(INE)-U(INE)-U(INE)-U(INE)-U(INE)-U(INE)-U(INE)-U(INE)-U(INE)-U(INE)-U(INE)-U(INE)-U(INE)-U(INE)-U(INE)-U(INE)-U(INE)-U(INE)-U(INE)-U(INE)-U(INE)-U(INE)-U(INE)-U(INE)-U(INE)-U(INE)-U(INE)-U(INE)-U(INE)-U(INE)-U(INE)-U(INE)-U(INE)-U(INE)-U(INE)-U(INE)-U(INE)-U(INE)-U(INE)-U(INE)-U(INE)-U(INE)-U(INE)-U(INE)-U(INE)-U(INE)-U(INE)-U(INE)-U(INE)-U(INE)-U(INE)-U(INE)-U(INE)-U(INE)-U(INE)-U(INE)-U(INE)-U(INE)-U(INE)-U(INE)-U(INE)-U(INE)-U(INE)-U(INE)-U(INE)-U(INE)-U(INE)-U(INE)-U(INE)-U(INE)-U(INE)-U(INE)-U(INE)-U(INE)-U(INE)-U(INE)-U(INE)-U(INE)-U(INE)-U(INE)-U(INE)-U(INE)-U(INE)-U(INE)-U(INE)-U(INE)-U(INE)-U(INE)-U(INE)-U(INE)-U(INE
     1U(IO))/(2.*B))
       ZR = D1 * ((U(IN) - U(IO))/B + (U(JNE) - U(JN) + U(JE) -
     1U(JO))/(2.*H))
       TA=(RZ+ZR)/2.
       SRR(I) = SRR(I) + RR
       SZZ(I)=SZZ(I)+ZZ
       STT(I) = STT(I) + TT
       SZR(I) = SZR(I) + ZR
       SRZ(I) = SRZ(I) + RZ
       KAD(I) = KAD(I) + 1
       PRINT 10, I, RR, ZZ, TT, TA
10 FORMAT(14,3F15.2,10X,F15.2,6X,5H STNE)
       RETURN
       END
       SUBROUTINE STNW(I, E, R)
       COMMON S(462,18),NC(231,9),NTYP(231),U(462),N,N2,H,C1,
     1SRR(231).SZZ(231).STT(231).SRZ(231).KAD(231).SZR(231)
       B=H
       D=E/((1.+C1)*(1.-2.*C1))
       D1=E/(2.*(1.+C1))
       JO=NC(I,1)*2
       JW=NC(I,4)*2
       JN=NC(I,3)*2
       JNW=NC(I,7)*2
       IO=JO-1
       IN=JN-1
       IW=JW-1
       INW=JNW-1
       RR=D*((1.-C1)*(U(IU)-U(IW))/H+C1*(U(IW)+U(IO))/
     1(2.*(R-H/2.))+C1*(U(JN)-U(JO)+U(JNW)-U(JW))/(2.*B))
       TT=D*((1.-C1)*U(ID)/R+C1*(U(IO)-U(IW))/H+
     1C1*(U(JN)-U(JO))/B)
       ZZ=D*((1.-C1)*(U(JN)-U(JO))/B+C1*(U(IN)-U(JO))/B+C1*(U(IN))
     1U(INW)+U(IO)-U(IW))/(2.*H)+C1*(U(INW)+U(IN)+
     2U(IW)+U(IO))/(4.*(R-.25*H)))
       RZ=D1*((U(J\Omega)-U(JW))/H+(U(INW)-U(IW)+U(IN)-
     1U(IO))/(2.*B))
       ZR=D1*((U(IN)-U(ID))/B+(U(JN))-U(JNW)+U(JD)-
     1U(JW))/(2.*H))
       TA = (RZ + ZR)/2
       SRR(I) = SRR(I) + RR
```

```
SZZ(I)=SZZ(I)+ZZ
   STT(I) = STT(I) + TT
   SZR(I) = SZR(I) + ZR
   SRZ(I) = SRZ(I) + RZ
   KAD(I) = KAD(I) + 1
   PRINT 10, I, RR, ZZ, TT, TA
10 FORMAT(14,3F15.2,10X,F15.2,6X,5H STNW)
   RETURN
   END
   SUBROUTINE STSW(I,E,R)
   COMMON S(462,18),NC(231,9),NTYP(231),U(462),N,N2,H,C1,
  1SRR(231),SZZ(231),STT(231),SRZ(231),KAD(231),SZR(231)
   D=E/((1.+C1)*(1.-2.*C1))
   D1=E/(2.*(1.+C1))
   JO=NC(I,1)*2
   JW=NC(I,4)*2
   JS=NC(I,5)*2
   JSW=NC(I.8)*2
   10 = 10 - 1
   IW=JW-1
   IS=JS-1
   ISW=JSW-1
   RR=D*((1.-C1)*(U(I0)-U(IW))/H+C1*(U(IW)+U(I0))/
  1(2.*(R-H/2.))+C1*(U(JO)-U(JS)+U(JW)-U(JSW))/(2.*B))
   TT=D*((1.-C1)*U(IO)/R+C1*(U(IO)-U(IW))/H+
  1C1*(U(J0)-U(JS))/B)
   ZZ=D*((1.-C1)*(U(JO)-U(JS))/B+C1*(U(IS)-
  1U(ISW)+U(IO)-U(IW))/(2.*H)+C1*(U(ISW)+U(IS)+
 2U(IW)+U(ID))/(4.*(R-.25*H)))
   RZ=D1*((U(JO)-U(JW))/H+(U(IO))-U(IS)+U(IW)-
  1U(ISW))/(2.*B))
   ZR=D1*((U(IO)~U(IS))/B+(U(JO )~U(JW)+U(JS)~
  1U(JSW))/(2.*H))
   TA=(RZ+ZR)/2
   SRR(I) = SRR(I) + RR
   SZZ(I) = SZZ(I) + ZZ
   STT(I) = STT(I) + TT
   SZR(I) = SZR(I) + ZR
   SRZ(I) = SRZ(I) + RZ
   KAD(I) = KAD(I) + 1
   PRINT 10.I.RR.ZZ.TT.TA
10 FORMAT(14,3F15.2,10X,F15.2,6X,5H STSW)
   RETURN
   END
   SUBROUTINE STSE(I, E, R)
   COMMON S(462,18),NC(231,9),NTYP(231),U(462),N,N2,H,C1,
  1SRR(231),SZZ(231),STT(231),SRZ(231),KAD(231),SZR(231)
   B=H
   D=E/((1.+C1)*(1.-2.*C1))
   D1=E/(2.*(1.+C1))
   JO=NC(I,1)*2
   JS=NC(I,5)*2
   JE=NC(I,2)*2
   JSE=NC(I,9)*2
```

```
10 = 10 - 1
   IS=JS-1
   IE=JE-1
   ISE=JSE-1
   RR=D*((1.-C1)*(U(IE)-U(IO))/H+C1*(U(IE)+U(IO))/
  1(2.*(R+H/2.))+C1*(U(JD)-U(JS)+U(JE )-U(JSF))/(2.*B))
   TT=D*((1.-C1)*U(IO)/R+C1*(U(IE)-U(IO))/H+
  1C1*(U(JO)-U(JS))/B)
   ZZ=D*((1.-C1)*(U(JO)-U(JS))/B+C1*(U(ISE)-
  1U(IS)+U(IE)-U(IO))/(2.*H)+C1*(U(ISE)+U(IS)+
  2U(IE)+U(IO))/(4.*(R+.25*H)))
   RZ=D1*((U(JE)-U(JO))/H+(U(IE)-U(ISE)+U(IO)-
  1U(IS))/(2.*B))
   ZR=D1*((U(IO)-U(IS))/B+(U(JSE)-U(JS)+U(JE)-U(JS))
  1U(JO))/(2.*H))
   TA = (RZ + ZR)/2.
   SRR(I) = SRR(I) + RR
   SZZ(I) = SZZ(I) + ZZ
   STT(I) = STT(I) + TT
   SZR(I) = SZR(I) + ZR
   SRZ(I) = SRZ(I) + RZ
   KAD(I) = KAD(I) + 1
   PRINT 10, I, RR, ZZ, TT, TA
10 FORMAT(14,3F15.2,10X,F15.2,6X,5H STSE)
   RETURN
   END
```

FORTRAN PROGRAM SYMBOLS

AXIALLY SYMMETRIC FINITE DIFFERENCE PROGRAM

RR(I)	Mesh Point Radius Array
E(I,J)	Elastic Modulus Array
S(I,J)	Equilibrium Equation Coefficient Array
NC(I,J)	Location Array for Equilibrium Coefficients
NTYP(I)	Mesh Point Identification Array (see Table B1)
U(I)	Displacement Array
N	Number of Mesh Points
Н	Mesh Point Spacing
C1	Poisson's Ratio (used as 1/4 in the equilibrium equations of this program but could be generalized)
SRR(I)	Mesh Point Radial Stress Array
SZZ(I)	Mesh Point Axial Stress Array
STT(I)	Mesh Point Circumferential Stress Array
SRZ(I)	Mesh Point Shear Stress
SZR(I)	Mesh Point Shear Stress
NOUT	Indicator to surpress printing equilibrium equations. If NOUT is non-zero, equations are printed.
KDAT	Indicates that mesh point data (N, E, W, etc.) will be read into the program or generated by COORD routine. IF KDAT is 2, the data is generated. IF KADT is 1, the data is read in.
	When data is generated, it is necessary to indicate the number of mesh points in the radial direction (KX).

KX	Indicates the number of mesh points in the radial direction for rectangular cross sections.
F(I)	Array of Mesh Point Force Intensities
LL(I)	Displacement Boundary Condition Λ rray $LL(I)$ is non-zero for restrained displacements.
BETA	Relaxation Factor
CON	Convergence Criterion
NCY	Number of Cycles Allowed for Iterative Solution
KIT	Cycle Print Interval Indicator
INIT	Initial Displacement Indicator If INIT is zero, initial displacements are set to zero. Otherwise, displacements are read in.

⋖
-
۷
C
L.
_
Q.
2
⋖
S

	'n	-																															
	2	'n																															
	-	7		•																										•	• 5	ċ	• 5
	-		4							O					0										0		5.	•	5.	5.	٠ د	٠5	• 0
	-	-	e																														
	₽.	-	n	°	10.	10.	٠. بر	2.	ċ	10.	10.	•	٠ د	•	0	10.		٠ د	ċ	10.	10.	٠.	5	•	.	• 5	٠,			2.	٠,	• 5	ċ
	7	ς,	6		0	S			Č					0			°.		O										• ~	• ~	.5	•0	• 5
	-	2	9	0	0	0	C	0	C 1	۲,	4	'n	0	^	œ	6	10														52		
	-	-	7	0	0	0	0	0	0	-	2	m	4	0	9	7	c o	6	c												23		
	~	-	-	0	9	_	œ	O-	c																						ر. د ا		c
	'n	-	~	7	6 0	0																									35		
	∞	S	-	0	0	0	C	0	_	2	~ ,	4	ιC,	9	7	∞	0														77		
	6	7	ď	0	_	2	(C.	4	C	9	^	c	σ	0			13														28		
•25	0	_	7	9	^	c	σ																								34		
	6	-	~	7	m	4	₽	O	^	∞	0	0					15		17							54		72			06		35
25		-	-	-	2	((1)	4	ď	9	^	c o	Φ																			53		

	c c
	CC
	cc
νο	CC
	c c
	CC
	c c
	СC
W 01	c c
4 000000000	СС
	CC
	CO
· · · · O · · · · · O O O O O O O O O O	cc
O P O V U V .	((
H 00 0000000	CC
~ · · O · · · • O O O O O O	c c
	cc
$\begin{array}{cccccccccccccccccccccccccccccccccccc$	
W O F V	CC
- CO 00000CCC	
0000	CC
	CC
0 C B C C C C C C C C C C C C C C C C C	CC
LOI NOL wwww 4444 NN ON	CC
- 00 00000000 - 00 00000000	C
ww4 4444 @ \$ 0 0 0 0 4 4 6 C 0 0 0 0 0	c c
	CC
	CO
	c c
	F- C O
	c
	r (C O
	ددد
N WULUO	-00
4400 00000000 00 0000000 00 0000000 00 0	c 0 0 0
<i>~~~~~~~~~~~~~~~~~~~~~~~~~~~~~~~~~~~~~</i>	~00~
	C C C
<pre></pre>	- ' C ' O O
H HCC 000000000000000000000000000000000	P P P

AXIALLY SYMMETRIC FINITE ELEMENT PROGRAM USING LINEAR STRAIN TRIANGULAR RINGS

Like the finite difference program, the finite element program has 3 main parts: (1) generate stiffness coefficients, (2) solve the system of equilibrium equations, and (3) compute stresses. Nodal forces are determined outside of the program and thus become part of the input data.

The computer program consists of the main program and several subroutines. The main program is essentially involved with reading in the element and nodal point data and initialization. An array (LOC) of location elements is also defined in the main program. The location array indicates the position of non-zero elements in the stiffness matrix. This is necessary in this procedure since only non-zero stiffness coefficients are stored.

The subroutine STIF1 generates the stiffness coefficients. The subroutine makes use of several other routines in the process.

The quanties in equation (3.99) are formed in the subroutine

Form B. The integration of these expressions over the volume is per
formed numerically in the subroutine NUMINT. A quintic formula discussed

by Felippa [18] is used in this connection.

The displacement transformation matrix of equation (3.96) is then generated. The inversion of (3.97) is accomplished by calling a standard matrix inversion subroutine. Since such routines are available on all modern systems, the program is not listed here. The routine STIF2 is then executed many times to complete the formulation of the overall stiffness.

The equations of the system are solved iteratively in the subroutine GSORP. Involved is a modification of the Gauss-Seidel over
relaxation procedure. Relaxation factors of 1.6 to 1.9 seem to give the
most rapid convergence for such problems.

The final step in the analysis involves the determination of stresses. Element nodal point stresses are calculated in the subroutine STRSA. The strains are obtained first from the product of the matrix [D] in equation (3.98) and the column matrix [α] of (3.97). The matrix [D] is generated in still another program called FORM G. Element nodal point stresses follow from the stress-strain law. Nodal point stresses for the overall structure are obtained by simply averaging the element nodal point stresses.

The finite element program including the above mentioned subroutines is presented next. A listing of Fortran program symbols used begins on page 290. A sample data set is shown on page 292.

AXIALLY SYMMETRIC FINITE ELEMENT PROGRAM LINEAR STRAIN TRIANGULAR RING ELEMENTS

```
PROGRAM LST
C
      FINITE ELEMENT PROGRAM-LINEAR STRAIN ELEMENTS
C.
      AXISYMMETRIC ELASTOSTATIC PROBLEMS
      COMMON R(169).Z(169).E(72).PR(72).N1(72).N2(72).N3(72)
     1,N4(72),N5(72),N6(72),NMAT(72),F(338),LL(338),LI(12),
     2S(338,50),LOC(169,50),SIGZ(169,2),SIGT(169,2),
     3,LT(338),KEY(338),U(338),KAD(169,2),SIGR(169,2),
     4SIGRZ(169,2),T(2,338),CON,KEX,NCY,BETA,M,MP,M2,KIT
C
      FORMAT STATEMENTS
  301 FORMAT(55H
  102 FORMAT(8110)
  104 FORMAT(8F10.6)
  151 FORMAT(1215)
  149 FORMAT(8F10.1)
  152 FORMAT(4012)
      INPUT ELEMENT AND NODAL POINT DATA
C
    1 READ 301
      IF(EOF,60)100,600
  600 READ 102, M, MP, IP
      PRINT 301
      M2 = 2 * MP
      READ 104, BETA
      PRINT 104.BETA
      READ 102, KEX, NCY, KIT
      PRINT 102, KEX, NCY, KIT
      READ 104 \cdot (R(I) \cdot I = 1 \cdot MP)
      PRINT 104,(R(I),I=1,MP)
      READ 104,(Z(I),I=1,MP)
      PRINT 104.(Z(I).I=1.MP)
      READ 151,(N1(1),N2(1),N3(1),N4(1),N5(1),N6(1),I=1,M)
      PRINT 151, (N1(I), N2(I), N3(I), N4(I), N5(I), N6(I), I=1, M)
      READ 104 \cdot (F(I), I=1,M2)
      PRINT 104, (F(I), I=1,M2)
      READ 152, (NMAT(I), I=1, M)
      PRINT 152 \cdot (NMAT(I) \cdot I = 1 \cdot M)
      READ 149, (E(I), PR(I), I=1, M)
      PRINT 149, (E(I), PR(I), I=1, M)
  150 READ 152, (LL(I), I=1, M2)
      PRINT 152,(LL(I), I=1,M2)
       INITIALIZE STIFFNESS AND LOCATION ARRAYS
C
  113 DO 201 IA=1,M2
      DO 201 JA=1,50
  201 S(IA,JA)=0.0
      DO 202 IA=1,MP
      DO 202 JA=1.50
  202 LOC(IA,JA)=0
C
       INITIALIZE NODAL POINT STRESS ARRAYS
      DO 107 I=1.MP
      00 107 J=1,2
      KAD(I,J)=0
```

```
SIGR(I \cdot J) = 0
      SIGT(I,J)=0.
      SIGZ(I,J)=0.
  107 SIGRZ(I,J)=0.
C
      DEFINE LOCATION ARRAY
      DO 212 I=1,MP
      DO 209 J=1.M2
  209 LT(J) = 0
      DO 211 N=1,M
      I1=N1(N)
      I2=N2(N)
      I3=N3(N)
      I4=N4(N)
      15=N5(N)
      I6=N6(N)
      LI(1)=2*I1-1
      LI(2)=2*I2-1
      LI(3) = 2 * I3 - 1
      LI(4)=2*I4-1
      LI(5)=2*15-1
      LI(6)=2*I6-1
      LI(7)=2*I1
      LI(8)=2*I2
      LI(9) = 2 * 13
      LI(10)=2*I4
      LI(11)=2*I5
      LI(12) = 2 * I6
      IF(I1-I) 210,220,210
  210 IF (I2-I) 230,220,230
  230 IF (13-1) 250,220,250
  250 IF (I4-I) 270,220,270
  270 IF (15-I) 290,220,290
  290 IF (I6-I) 211,220,211
  220 DO 224 IS=1,12
      L1=LI(IS)
  224 LT(L1)=1
  211 CONTINUE
      KEY(I)=0
      DO 278 JA=1,M2
      IF(LT(JA))278,278,288
  288 KEY(I)=KEY(I)+1
      K1=KEY(I)
      LOC(I,K1)=JA
  278 CONTINUE
  212 CONTINUE
C
      PRINT OUT LOCATION ARRAY
      IF(IP)285,284,285
  285 DO 311 JA=1,MP
      KK=KEY(JA)
      PRINT 279, KK
  279 FORMAT (6110)
      PRINT 279, (LOC(JA, IT), IT=1,KK)
  311 CONTINUE
C
       DEFINE STIFFNESS ARRAY
  284 CALL STIF1
```

```
С
       PRINT OUT STIFFNESS ARRAY
       IF(IP)121,122,121
  121 DO 111 I=1.M2
  111 PRINT 110, (S(I,J), J=1.50)
  110 FORMAT(8F15.5)
C
      GAUSS SEIDEL OVER RELAXATION PROCEDURE
  122 CALL GSORP
C
       CALCULATE STRESSES
       CALL STRSA
      GO TO 1
  100 STOP
      END
       SUBROUTINE STIF1
       DIMENSION SEE(3,7), MT(4,3), L(6), RN(6), ZN(6), XI(15),
      1A(6,6),D(6,6),B(12,12),LIP(6),NIP(6)
      COMMON R(169), Z(169), E(72), PR(72), N1(72), N2(72), N3(72)
      1,N4(72),N5(72),N6(72),NMAT(72),F(338),LL(338),LI(12),
     2S(338,50),LOC(169,50),SIGZ(169,2),SIGT(169,2),
      3,LT(338),KEY(338),U(338),KAD(169,2),SIGR(169,2),
     4SIGRZ(169,2),T(2,338),CON,KEX,NCY,BETA,M,MP,M2,KIT
       READ 12 \cdot ((SEE(I \cdot J) \cdot I = 1 \cdot 3) \cdot J = 1 \cdot 7)
   12 FORMAT (6F13.8)
      READ 10 \cdot ((MT(I \cdot J) \cdot J = 1 \cdot 3) \cdot I = 1 \cdot 4)
   10 FORMAT(1215)
      DO 400 N=1.M
       I1=N1(N)
       I2=N2(N)
       I3=N3(N)
       14=N4(N)
       I5=N5(N)
       I6=N6(N)
      C11=E(N)*(1.-PR(N))/(1.-PR(N)-2.*PR(N)**2)
      C12=E(N)*PR(N)/(1.-PR(N)-2.*PR(N)**2)
      C44=E(N)/(2.+2.*PR(N))
      C=C11+C12
      L(1)=N1(N)
      L(2)=N2(N)
      L(3) = N3(N)
      L(4) = N4(N)
      L(5) = N5(N)
      L(6) = N6(N)
      DO 15 I=1.6
       J=L(I)
      ZN(I)=Z(J)
   15 RN(I)=R(J)
C
      PERFORM NUMERICAL INTEGRATION
      CALL NUMINT (RN, ZN, XI, SEE, MT)
      CALL FORMB(B, XI, C, C11, C12, C44)
C
       FORM DISPLACEMENT TRANSFORMATION MATRIX
      DO 72 I=1.6
       A(I \cdot 1) = 1.
      A(I,2)=RN(I)
       A(I,3) = ZN(I)
      A(I,4)=RN(I)*RN(I)
```

```
A(I,5)=RN(I)*ZN(I)
   72 A(I,6)=ZN(I)*ZN(I)
      DO 291 JG=1,6
      DO 291 KG=1,6
  291 D(JG,KG)=A(JG,KG)
      CALL MINV(D,6,DET,LIP,NIP)
C
      D IS NOW THE INVERSE OF A
C
      FORM DT*B*D
      LI(1) = 2 \times I1 - 1
      LI(2) = 2 \times I2 - 1
      LI(3) = 2 * I3 - 1
      LI(4)=2*I4-1
      LI(5) = 2 \times I5 - 1
      LI(6)=2*I6-1
      LI(7)=2*I1
      LI(8)=2*I2
      LI(9) = 2 \times I3
      LI(10) = 2 * I4
      LI(11)=2*15
      LI(12)=2*I6
      DO 411 JA=1,6
      JT=L(JA)
      DO 833 I=1,MP
      IF(JT-I)833,421,833
  421 CALL STIF2(JA,I,D,B)
      GO TO 411
  833 CONTINUE
  411 CONTINUE
  400 CONTINUE
      RETURN
      END
      SUBROUTINE NUMINT(X1,Y1,XI,SEE,MT)
      DIMENSION X1(6),Y1(6),X(15),Y(15),XM(15),XI(15),XX(15)
      DIMENSION SEE (3,7), MT (4,3)
      COEF = X1(2) * (Y1(3) - Y1(1)) + X1(1) * (Y1(2) - Y1(3)) + X1(3) *
     1(Y1(1)-Y1(2))
      COEF=COEF/8.
      XX(1) = .225
      XX(2) = .13239415
      XX(3)=XX(2)
      XX(4) = XX(2)
      XX(5) = .12593918
      XX(6) = XX(5)
      XX(7) = XX(5)
      DO 50 I=1,15
   50 XI(I)=0.
      DO 75 K=1.4
      L=MT(K.1)
      M=MT(K,2)
      N=MT(K,3)
      DO 2 I=1.7
      X(I)=X1(L)*SEE(1,I)+X1(M)*SEE(2,I)+X1(N)*SEE(3,I)
    2 Y(I)=Y1(L)*SEE(1,I)+Y1(M)*SEE(2,I)+Y1(N)*SEE(3,I)
      00 35 I=1.7
   35 XM(I)=XX(I)*X(I)
```

```
DO 100 I = 1.7
    XI(1)=XI(1)+XM(I)
    XI(2)=XI(2)+XM(I)/X(I)
    XI(3)=XI(3)+XM(I)/(X(I)**2)
    XI(4)=XI(4)+XM(I)*Y(I)/X(I)
    XI(5)=XI(5)+XM(I)*Y(I)/(X(I)**2)
    XI(6)=XI(6)+XM(I)+Y(I)+*2/(X(I)+*2)
    XI(7)=XI(7)+XM(I)*X(I)
    XI(8)=XI(8)+XM(I)*Y(I)
    XI(9) = XI(9) + XM(I) + X(I) + 2
    XI(10) = XI(10) + XM(I) + X(I) + Y(I)
    XI(11) = XI(11) + XM(I) + Y(I) + 4/X(I) + 2
    XI(12)=XI(12)+XM(I)*Y(I)**2/X(I)
    XI(13) = XI(13) + XM(I) * Y(I) * * 3/X(I) * * 2
    XI(14)=XI(14)+XM(I)*Y(I)**3/X(I)
    XI(15)=XI(15)+XM(I)*Y(I)**2
100 CONTINUE
 75 CONTINUE
    DO 150 I=1,15
150 XI(I)=XI(I)*COEF
    RETURN
    END
    SUBROUTINE FORMB(B, XI, C, C11, C12, C44)
    DIMENSION B(12,12), XI(15)
    DO 60 I=1,12
    00 60 J=1,12
60 B(I,J)=0.
    B(1,1)=C11*XI(3)
    B(1,2)=C*XI(2)
    B(1,3)=C11*XI(5)
    B(1,4)=(2.*C12+C11)*XI(1)
    B(1,5)=C*XI(4)
    B(1,6) = C11 * XI(6)
    B(1,9)=C12*XI(2)
    B(1,11) = C12 * XI(1)
    B(1,12)=2.*C12*XI(4)
    B(2,2)=2.*C*XI(1)
    B(2,3)=C*XI(4)
    B(2,4)=3.*C*XI(7)
    B(2,5)=2.*C*XI(8)
    B(2,6)=C*XI(12)
    B(2,9)=2.*C12*XI(1)
    B(2,11)=2.*C12*XI(7)
    B(2,12)=4.*C12*XI(8)
    B(3,3)=C44*XI(1)+C11*XI(6)
    B(3,4)=(2.*C12+C11)*XI(8)
    B(3.5)=C44*XI(7)+C*XI(12)
    B(3.6)=2.*C44*XI(8)+C11*XI(13)
    B(3,8)=C44*XI(1)
    B(3,9)=C12*XI(4)
    B(3,10)=2.*C44*XI(7)
    B(3,11) = (C12+C44)*XI(8)
    B(3,12)=2.*C12*XI(12)
    B(4,4)=(5.*C11+4.*C12)*XI(9)
```

```
B(4.5)=3.*C*XI(10)
    B(4.6)=(2.*C12+C11)*XI(15)
    B(4,9)=3.*C12*XI(7)
    B(4,11)=3.*C12*XI(9)
    B(4,12)=6.*C12*XI(10)
    B(5,5)=2.*C*XI(15)+C44*XI(9)
    B(5,6)=C*XI(14)+2.*C44*XI(10)
    B(5,8)=C44*XI(7)
    B(5,9)=2.*C12*XI(8)
    B(5,10)=2.*C44*XI(9)
    B(5,11)=(2.*C12+C44)*XI(10)
    B(5,12)=4.*C12*XI(15)
    B(6,6)=C11*XI(11)+4.*C44*XI(15)
    B(6,8)=2.*C44*XI(8)
    B(6.9)=C12*XI(12)
    B(6,10)=4.*C44*XI(10)
    B(6,11) = (C12+2.*C44)*XI(15)
    B(6,12)=2.*C12*XI(14)
    B(8,8)=C44*XI(1)
    B(8,10)=2.*C44*XI(7)
    B(8,11)=C44*XI(8)
    B(9,9)=C11*XI(1)
    B(9,11)=C11*XI(7)
    B(9.12)=2.*C11*XI(8)
    B(10,10)=4.*C44*XI(9)
    B(10,11)=2.*C44*XI(10)
    B(11 \cdot 11) = C11 \times XI(9) + C44 \times XI(15)
    B(11,12)=2.*C11*XI(10)
    B(12,12)=4.*C11*XI(15)
    DO 66 I=1.11
    J1=I+1
    DO 66 J=J1,12
 66 B(J,I)=B(I,J)
    RETURN
    END
    SUBROUTINE STIF2(M9,I,D,B)
    DIMENSION D(6,6),B(12,12)
    COMMON R(169), Z(169), E(72), PR(72), N1(72), N2(72), N3(72)
   1,N4(72),N5(72),N6(72),NMAT(72),F(338),LL(338),LI(12),
   2S(338,50),LOC(169,50),SIGZ(169,2),SIGT(169,2),
   3,LT(338),KEY(338),U(338),KAD(169,2),SIGR(169,2),
   4SIGRZ(169,2),T(2,338),CON,KEX,NCY,BETA,M,MP,M2,KIT
    DO 221 J=1,M2
    DO 221 KP=1,2
221 T(KP,J)=0.
    DO 222 J=1,6
    J6=J+6
    K=L1(J6)
    L=LI(J)
    DO 222 KI=1,6
    K16=K1+6
    DO 222 KJ=1,6
    KJ6=KJ+6
    T(1,L)=T(1,L)+D(KI,M9)*B(KI,KJ)*D(KJ,J)
    T(1,K)=T(1,K)+D(KI,M9)*B(KI,KJ6)*D(KJ,J)
```

```
T(2,L)=T(2,L)+D(KI,M9)*B(KI6,KJ)*D(KJ,J)
222 T(2,K)=T(2,K)+D(KI,M9)*B(KI6,KJ6)*D(KJ,J)
    J2=2*I
    J1 = J2 - 1
    DO 240 K=1,50
    K1=LOC(I,K)
    IF(K1)1.2.1
  1 S(J1,K)=S(J1,K)+T(1,K1)
240 S(J2,K)=S(J2,K)+T(2,K1)
  2 RETURN
    END
    SUBROUTINE GSORP
    COMMON R(169),Z(169),E(72),PR(72),N1(72),N2(72),N3(72)
   1,N4(72),N5(72),N6(72),NMAT(72),F(338),LL(338),LI(12),
   2S(338.50).LOC(169.50).SIGZ(169.2).SIGT(169.2).
   3,LT(338),KEY(338),U(338),KAD(169,2),SIGR(169,2),
   4SIGRZ(169,2),T(2,338),CON,KEX,NCY,BETA,M,MP,M2,KIT
317 CON=1.0*(10.**(-KEX))
    PRINT 339. CON
339 FORMAT (23H CONVERGENCE CRITERION= E20.8)
    SEIDEL ITERATION
382 PRINT 386, BETA
386 FORMAT (19H RELAXATION FACTOR= E20.8)
    READ 10.INIT
 10 FORMAT(1015)
    IF(INIT) 11,377,11
 11 READ 12, (U(I), I=1,M2)
 12 FORMAT(4E20.8)
    GO TO 376
377 DO 314 I=1,M2
314 U(I) = 0.0
376 KK=0
332 DIFF=0.0
    KK = KK + 1
    IF(KK-NCY) 346,346,345
345 PRINT 347
347 FORMAT (21H CYCLE LIMIT EXCEEDED)
    PRINT 396
396 FORMAT(30H THE CURRENT DISPLACEMENTS ARE)
    PRINT 348,KK, (U(I), I=1,NM)
348 FORMAT (1H0, 15, (4E15.8))
    GO TO 1
346 DO 330 I=1,M2
    IF(LL(I))330,355,330
355 KJ=(I+1)/2
    UBAR=F(I)
    NUM=KEY(KJ)
    DO 328 J=1,NUM
    N=LOC(KJ,J)
    IF(N-1)329,394,329
394 DIAG=S(I.J)
    GO TO 328
329 UBAR=UBAR-S(I,J)*U(N)
328 CONTINUE
```

```
UBAR=UBAR/DIAG
      U1=U(I)+BETA*(UBAR-U(I))
      DMAX=ABS (U1-U(I))
      U(I)=U1
  364 IF(DMAX-DIFF) 330,336,336
  336 DIFF=DMAX
  330 CONTINUE
      KTEN=KK/KIT
      IF(KK-KIT*KTEN) 303,306,303
  306 PRINT 305.KK
  305 FORMAT(17H ITERATION COUNT=110//)
      PRINT 304 \cdot (U(I) \cdot I = 1 \cdot M2)
      PUNCH 304 \cdot (U(I) \cdot I = 1 \cdot M2)
  304 FORMAT(4E20.8)
  303 CONTINUE
C
      TEST FOR CONVERGENCE
      IF(DIFF-CON) 333,332,332
  333 PRINT 335.KK
  335 FORMAT (25H THE NUMBER OF ITERATIONS.//(I10))
      PRINT 334
  334 FORMAT(42H NODAL POINT R-DISPLACEMENT Z-DISPLACEMENT)
      DO 337 I=1,MP
      10=2*1-1
      1E=2*1
  337 PRINT 338, I, U(10), U(1E)
  338 FORMAT(I12,2E20.8)
      PUNCH 304,(U(I), I=1,M2)
    1 RETURN
      END
      SUBROUTINE STRSA
      DIMENSION LIP(6), NIP(6), L(6), A(6,6), G(4,12), B(12)
      DIMENSION EP(4), STR(4), CE(4,4)
      COMMON R(169),Z(169),E(72),PR(72),N1(72),N2(72),N3(72)
     1,N4(72),N5(72),N6(72),NMAT(72),F(338),LL(338),LI(12),
     2S(338,50),LOC(169,50),SIGZ(169,2),SIGT(169,2),
     3,LT(338),KEY(338),U(338),KAD(169,2),SIGR(169,2),
     4SIGRZ(169,2),T(2,338),CON,KEX,NCY,BETA,M,MP,M2,KIT
      PRINT 44
   44 FORMAT(17H ELEMENT STRESSES///)
      DO 926 I=1.M
      PRINT 100.I
  100 FORMAT(16H ELEMENT NUMBER=15)
      L(1)=N1(I)
      L(2) = N2(I)
      L(3)=N3(I)
      L(4) = N4(I)
      L(5)=N5(1)
      L(6)=N6(I)
    1 00 10 J=1,6
      LY=L(J)
      A(J,1)=1.
      A(J,2)=R(LY)
      A(J,3)=Z(LY)
      A(J,4)=R(LY)*R(LY)
      A(J_{+}5)=R(LY)+Z(LY)
```

```
10 A(J_{\bullet}6)=Z(LY)*Z(LY)
    CALL MINV(A,6,DET,LIP,NIP)
    DO 20 N=1,12
 20 B(N) = 0.
    DO 30 N=1.6
    DO 30 J=1,6
    LY=L(J)
    JE=2*LY
    J0=2*LY-1
    B(N)=B(N)+A(N,J)+U(JO)
    K=N+6
 30 B(K)=B(K)+A(N,J)+U(JE)
    DO 77 K=1.4
    DO 77 J=1,4
77 CE(K,J)=0.
    PO=PR(I)
    Y=E(I)
    CE(1,1)=Y*(1.-PO)/(1.-PO-2.*PO**2)
    CE(1,2)=Y*PO/(1.-PO-2.*PO**2)
    CE(2.1) = CE(1.2)
    CE(4,4)=Y/(2.+2.*PO)
    CE(2,2)=CE(1,1)
    CE(3,3)=CE(1,1)
    CE(2.3) = CE(1.2)
    CE(3,2)=CE(1,2)
    CE(1,3) = CE(1,2)
    CE(3,1)=CE(1,2)
    KAY=NMAT(I)
    DO 71 N=1,6
    LY=L(N)
    CALL FORMG(G.LY)
    DO 51 J=1.4
51 EP(J)=0.
    DO 52 J=1,4
    DO 52 K=1,12
52 EP(J)=EP(J)+G(J,K)*B(K)
    00 61 J=1,4
61 STR(J)=0.
    DO 62 J=1,4
    DO 62 K=1,4
62 STR(J) = STR(J) + CE(J,K) \times EP(K)
    GO TO (37,38),KAY
37 JZ=1
    GO TO 39
38 JZ=2
 39 SIGR(LY,JZ)=SIGR(LY,JZ)+STR(1)
    SIGZ(LY,JZ)=SIGZ(LY,JZ)+STR(2)
    SIGT(LY,JZ)=SIGT(LY,JZ)+STR(3)
    KAD(LY,JZ)=KAD(LY,JZ)+1
    SIGRZ(LY,JZ)=SIGRZ(LY,JZ)+STR(4)
    PRINT 17,LY,(STR(NK),NK=1,4)
 17 FORMAT(I10,4F20.2)
71 CONTINUE
926 CONTINUE
```

```
PRINT 461
461 FORMAT(21H NODAL POINT STRESSES///)
    DO 511 I=1.MP
    IF(KAD(I,1))325,326,325
325 SAD=KAD(I.1)
    SIGR(I,1)=SIGR(I,1)/SAD
    SIGZ(I,I)=SIGZ(I,I)/SAD
    SIGT(I,1)=SIGT(I,1)/SAD
    SIGRZ(I,1)=SIGRZ(I,1)/SAD
326 IF(KAD(I,2))327,328,327
327 SID=KAD(1.2)
    SIGR(I,2)=SIGR(I,2)/SID
    SIGZ(I,2)=SIGZ(I,2)/SID
    SIGT(I,2)=SIGT(I,2)/SID
    SIGRZ(I,2)=SIGRZ(I,2)/SID
328 PRINT 512,I,SIGR(I,1),SIGZ(I,1),SIGT(I,1),SIGRZ(I,1)
512 FORMAT(I5,4F20.2)
511 PRINT 513, SIGR(I, 2), SIGZ(I, 2), SIGT(I, 2), SIGRZ(I, 2)
513 FORMAT(11X.4F19.2)
    RETURN
    END
    SUBROUTINE FORMG(G,LY)
    DIMENSION G(4.12)
    COMMON R(169),Z(169),E(72),PR(72),N1(72),N2(72),N3(72)
   1,N4(72),N5(72),N6(72),NMAT(72),F(338),LL(338),LI(12),
   2S(338,50),LOC(169,50),SIGZ(169,2),SIGT(169,2),
   3.LT(338).KEY(338).U(338).KAD(169.2).SIGR(169.2).
   4SIGRZ(169,2),T(2,338),CON,KEX,NCY,BETA,M,MP,M2,KIT
    X=R(LY)
    Y=Z(LY)
    IF(X-.001)11.12.12
 11 X = .001
 12 DO 10 I=1,4
    DO 10 J=1,12
 10 G(I.J) = 0.
    G(1,2)=1.
    G(1,4)=2.*X
    G(1,5) = Y
    G(2,9)=1.
    G(2,11)=X
    G(2,12)=2.*Y
    G(3,1)=1./X
    G(3,2)=1.
    G(3,3)=Y/X
    G(3,4)=X
    G(3,5)=Y
    G(3,6)=Y*Y/X
    G(4,3)=1.
    G(4.5) = X
    G(4.6) = 2.4Y
    G(4.8)=1.
    G(4,10)=2.*X
    G(4,11) = Y
    RETURN
    END
```

FORTRAN PROGRAM SYMBOLS

AXIALLY SYMMETRIC FINITE ELEMENT PROGRAM

R(I)	Radial Coordinate
Z(I)	Axial Coordinate
N1(I)	
N2(I)	
N3(I)	Element Nodal Point Numbers
N4(I)	
N5(I)	
N6(I)	
PR(I)	Poisson's Ratio
E(I)	Elastic Modulus
NMAT(I)	Material Indicator for Composites
F(I)	Nodal Point Force Array
U(I)	Nodal Point Displacement Array
LL(I)	Displacement Boundary Condition Array
S(I,J)	Stiffness Coefficient Array
LOC(I,J)	Location Array
SIGR(I,J)	Radial Stress Array
SIGZ(I,J)	Axial Stress Array
SIGT(I,J)	Circumferential Stress Array
SIGRZ(I,J)	Shear Stress Array

M Number of Finite Elements

MP Number of Nodal Points

BETA Relaxation Factor

CON Convergence Criterion

NCY Number of Cycles Allowed for Iterative Solution

KIT Cycle Print Interval Indicator

A(I,J) Transformation Array from Generalized Displacements

[a] to Nodal Displacement [u]

C11,C12,C44 Elastic Constants

CE(J,J) Elastic Constants

SEE(I,J) Numerical Integration Coefficients

MT(I,J) Numerical Integration Nodal Point Numbers

T(I,J) Temporary Equilibrium Equation Array

EP(I) Element Strains

STR(I) Element Stresses

G(I,J) Displacement Gradient Matrix

IP Indicator to surpress printing stiffness coefficients.

If IP is non-zero, coefficients are printed.

INIT Initial Displacement Indicator

If INIT is zero, initial displacements are set to

zero. Otherwise, displacements are read in.

			• 5	•0	•75			۰ • ٥						300•	•	•0	•	•0	•0	•0	•0	•0	•		•25	• 25	0000000		701420	.05961587	012865		
			• 25	1.	·		1.5	• • • •		6 0	12	18	14	•	°	•0	•	•	•	•	•	•	•0		200	8	0 0 1 0 0		01420	.47014206	7974269		3
			•	•75	•25		1.5	• •		4	7	8	9	100.	•	•0	•	•0	•	•0	•	ċ	•		•2	•2	0 0 0 0		96158	014206	12865		9
SAMPLE DATA			1.	٠ د	•		2•	0. •		5	1	7	5 1	•	•	ċ	•	•0	•0	•	•0	•	•		200	200	0 0 1 0 0		333 .0	20	651 .1	69	2 5
SAM		40	•75		•	,	. 5	1 • •		9 13	7 1	7	9 1	100.	•	•	•	•	•	•	•	•	•		•25		0 0 0 0		.33333	7014	128	974	4
	25	500	• 5	•	• 75		5•	1. • 5.		14 10	&	-	8	•	•	•	•	•0	•0	•	•	•	•0		200	10000	0	0 1	3333	0596158	.10128651	1012865	
	6 0	7	•25	1.	٠ •		2•			15 5	m	7	3 2	•	100•	•	•	•0	•	•	•	•	•	12211	•2	•2	0 0 0 0	10101	33333	01420	426	12865	
	0	•	•	• 75	• 2	1.	2.	۱ پ س	• 0			13		•	•	°	•0	•	•	•	•	•	•		00	0000							-

